Laser Ablation of Polymer Waveguide and Embedded Mirror for Optically-Enabled Printed Circuit Boards (OEPCB)

by

Shefiu S. Zakariyah

Wolfson School of Mechanical and Manufacturing Engineering

Loughborough University

PhD Thesis

Submitted in partial fulfilment of the requirements

for the award of

Doctor of Philosophy of Loughborough University

September 2010

ABSTRACT

Due to their inherent BW capacity, optical interconnect (OI) offers a means of replacement to BW limited copper as bottlenecks begin to appear within the various interconnect levels of electronics systems. Low-cost optically enabled printed circuit boards are a key milestone on many electronics roadmaps, e.g. iNEMI. Current OI solutions found in industry are based upon optical fibres and are capable of providing a suitable platform for inter-board applications especially on the backplane. However, to allow component assembly onto high BW interconnects, an integral requirement for intra-board applications, optically enabled printed circuit boards containing waveguides are essential.

Major barriers to the deployment of optical printed circuit boards include the compatibility of the technique, the cost of acquiring OI and the optical power budget. The purpose of this PhD research programme is to explore suitable techniques to address these barriers, primarily by means of laser material processing using UV and IR source lasers namely 248 nm KrF Excimer, 355 nm UV Nd:YAG and 10.6 µm IR CO_2. The use of these three main lasers, the trio of which dominates most PCB production assembly, provides underpinning drive for the deployment of this technology into the industry at a very low cost without the need for any additional system or system modification. It further provides trade-offs among the suitable candidates in terms of processing speed, cost and quality of waveguides that could be achieved.

This thesis presents the context of the research and the underlying governing science, i.e. theoretical analysis, involving laser-matter interactions. Experimental investigation of thermal (or pyrolitic) and bond-breaking (or photolytic) nature of laser ablation was studied in relation to each of the chosen lasers with regression analysis used to explain the experimental results. Optimal parameters necessary for achieving minimum Heat Affected Zone (HAZ) and surface/wall roughness were explored, both of which are key to achieving low loss waveguides. While photochemical dominance – a function of wavelength and pulse duration – is desired in laser ablation of photopolymers, the author has been able to find out that photothermally-processed materials, for example at 10.6 µm, can also provide desirable waveguides.

Although there are literature information detailing the effect of certain parameters such as fluence, pulse repetition rate, pulse duration and wavelength among others, in relation to the etch rate of different materials, the machining of new materials requires new data to be obtained. In fact various models are available to try to explain the laser-matter interaction in a

mathematical way, but these cannot be taken universally as they are deficient to general applications. For this reason, experimental optimisation appears to be the logical way forward at this stage of the research and thus requiring material-system characterisation to be conducted for each case thereby forming an integral achievement of this research.

In this work, laser ablation of a single-layer optical polymer (Truemode™) multimode waveguides were successfully demonstrated using the aforementioned chosen lasers, thus providing opportunities for rapid deployment of OI to the PCB manufacturing industry. Truemode™ was chosen as it provides a very low absorption loss value < 0.04 dB/cm at 850 nm datacom wavelength used for VSR interconnections – a key to optical power budget – and its compatibility with current PCB fabrication processes. A wet-Truemode™ formulation was used which required that optical polymer layer on an FR4 substrate be formed using spin coating and then UV-cured in a nitrogen oxygen-free chamber. Layer thickness, chiefly influenced by spinning speed and duration, was studied in order to meet the optical layer thickness requirement for multimode (typically > 9 µm) waveguides. Two alternative polymers, namely polysiloxane-based photopolymer (OE4140 and OE 4141) from Dow Corning and PMMA, were sparingly utilized at some point in the research, mainly during laser machining using UV Nd:YAG and CO_2 lasers.

While Excimer laser was widely considered for polymer waveguide due to its high quality potential, the successful fabrication at 10.6 µm IR and 355 nm UV wavelengths and at relatively low propagation loss at datacom wavelength of 850 nm (estimated to be < 1.5 dB/cm) were unprecedented. The author considered further reduction in the optical loss by looking at the effect of fluence, power, pulse repetition rate, speed and optical density on the achievable propagation but found no direct relationship between these parameters; it is therefore concluded that process optimisation is the best practice. In addition, a novel in-plane 45-degree coupling mirror fabrication using Excimer laser ablation was demonstrated for the first time, which was considered to be vital for communication between chips (or other suitable components) at board-level.

Keywords: Laser Ablation, Optical Interconnect, Polymer Waveguide, OPCB, Micromachining, 2D 45-degree mirror, Metallisation , Excimer Laser, UV Nd:YAG Laser, CO_2 Laser.

ACKNOWLEDGEMENT

GLOSSARY

AFM   Atomic Force Microscope

BER   Bit Error Rate

BERT   Bit Error Rate Tester

BW   Bandwidth

CCD   Charged-coupled device

CVD   Chemical Vapour Deposition

CW   Continuous Wave

CTE   Coefficient of Thermal Expansion

DR   Direct Writing

EMI   Electromagnetic Interference

EOCB   Electro-Optical Circuit Board

FEGSEM   Field Emission Gun Scanning Electron Microscope

GRIN   GRaded INdex

HDI   High Density Interconnect

HAZ   Heat Affected Zone

IR   Infra-Red

LASER   Light Amplification by Stimulated Emission of Radiation

LED   Light Emitting Diode

LD   Laser Diode

LAN   Local Area Network

MASER   Microwave Amplification by Stimulated Emission of Radiation

MAN   Metropolitan Area Network

MM   Multimode

MPE   Maximum Permissible Exposure

NA   Numerical Aperture

OD   Optical Density

OI   Optical Interconnect

OPCB   Optical Printed Circuit Board

PCB   Printed Circuit Board

PRF   Pulse Repetition Frequency

PC   Polycarbonate

PD   Photo Diode/Detector

PET   Poly Ethylene Terephthalate

PI   Polyimide

PMMA   Polymethyl Methacrylate

PRR   Pulse Repetition Rate

PS   Polystyrene

PWB   Printed Wiring Board

RF   Radio Frequency

RI   Refractive Index

RIE   Reactive Ion Etching

SPD   Scanning Power Density

SEM   Scanning Electron Microscope

SMT   Surface Mount Technology

TEM   Transverse Electromagnetic Mode

TIR   Total Internal Reflection

UV   Ultraviolet

VCSEL   Vertical Cavity Surface Emitting Laser

VSR   Very Short Reach

WAN   Wide Area Network

YAG   Yttrium Aluminium Garnet

CONTENTS

LIST OF FIGURES

LIST OF TABLES

1   INTRODUCTION

1.1   Research Problem Definition

1.2   Introduction

This thesis and the research contained therein address the inherent bandwidth-limited copper interconnection and the possible deployment of optical interconnection at short range such that hybridisation of electrical and optical technologies can be featured on Printed Circuit Boards (PCB) for the next generation of consumer electronics where data rate, ~10 Gb/s, at reasonably cost is desired.

Limitation of conventional copper interconnection

Active (transistors and Integrated Circuits) and passive (resistors, capacitors and inductors) components which are used in electronic devices rely heavily on metallic tracks to ensure their functionalities. In other words they are connected by conventional copper transmission, which itself has seen dramatic changes from what used to be, 'big-sized wires', to thin short tracks of electrical lines. This change in size and architecture of Printed Wiring Technology (PWT) is mostly forced by an increase in the number of components. The rise in the demand for more features in electronics and the change in the manufacturing technology has caused an increase in the data rate on the micro-level such as backplane, board-to-board, rack-to-rack, box-to-box and chip-to-chip. Unfortunately, the bandwidth (BW) of electrical connection is limited by cross-sectional area and the length of the track given by $BW \ \alpha \ A/L^2$, where A and L are the area and length of the track respectively [1]. Of course, the area can be increased while the length reduced but it is not a technically-viable solution to the issue and, in fact, doing this, is at the expense of not only power dissipation (and power management) but also bit rate and size. In addition, there are many more parasitic or applied problems that could arise from this change alone. Furthermore, the frequency-dependence of metallic transmission line is another major area of concern in this miniaturized electronic world.

The aforementioned bottleneck for copper transmission in PCB with high interconnection density and high-frequency is more pronounced at the 10 Gb/s crossbar where problems such as crosstalk, radio frequency interference (RFI) [2], electromagnetic interference (EMI), power dissipation and signal loss among others cannot be tolerated. Detailed

accounts of copper limitations have been widely covered in the literature and some of the key investigations and demonstration for Optical Interconnects (OI) are shown later in this chapter.

Research has shown that the limitations in electrical transmission on board can be minimized using a number of approaches including minimizing conductor length, development of new dielectric material, and multi-level data coding which can allow up to 10 Gb/s transmission electrically, but these approaches are not cost-effective [3]. To overcome this bottleneck, optical interconnection at short distances – as it has been successfully used for long and medium range communication – has been widely suggested as the practical way forward. It is believed that optical interconnect will perform efficiently at this stage and at a low cost – lower than those incurred to overcome the copper limitations as cited above. The deployment suggested here is not to overhaul traditional copper technology – far from that – but to create a hybrid electric-optical interconnection where data processing is handled electrically while data routing is carried optically in order to meet the High Density Interconnection (HDI) trend while maintaining a balance between data transfer and cost.

To address the bottleneck caused by the inherent problems in the copper transmission used in backplanes and boards, the last decade has witnessed vigorous research input and output from researchers – academic and industry – around the world to deploy OI on PCB. Japan, EU and Asia-Pacific/North America, who led in the microvia technology, are also key figures in the OI deployment [2, 4].

Undoubtedly, the cost-effectiveness of OI is a major consideration if it is to be implemented on PCB [5]; Hopkins, K. and Pitwon, R. asserted [6] that, at higher BW for current and near future requirements for telecom and datacom systems, the application of OI at the backplane – where it is expected to be foremostly required – is unavoidable. It was argued that the cost of solving the bottleneck of copper transmission will surpass that of the implementation of the OI at ~ 6.25 Gb/s. Figure 1.1 depicts such an assertion from Hopkins, K. and Pitwon, R. where the cost of deployment and implementation of OI technology is expected to fall gradually when the date rate exceeds the 6.25 Gb/s 'threshold' with an increase in the electrical connection. This prediction is, by expectation, valid for higher level of interconnection such as backplane level but it might not be true, at least for the first phase of OI deployment, for the lower hierarchical level of interconnection e.g. chip-to-

chip.

Furthermore, the total power loss, commonly referred to as power budget, is also a consideration; and is currently being investigated. Uhlig and Robertson [7], while analysing the power-budget requirement, argued that optical amplification, at some point along the transmission, would be needed for a realistic OI on PCB to be implemented.
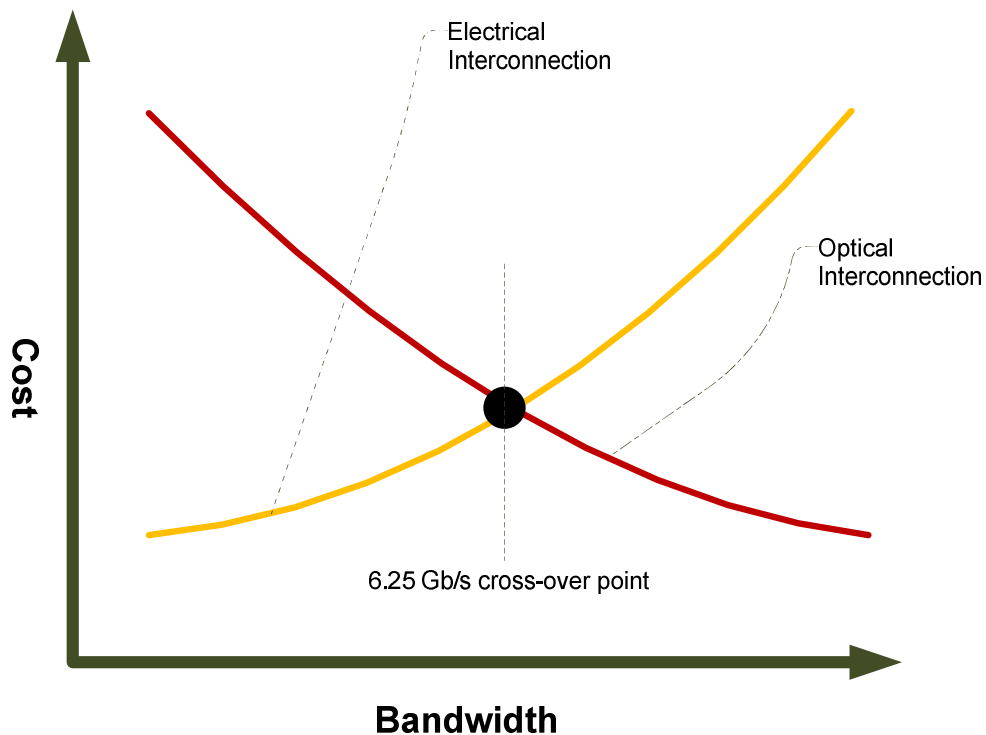
Figure 1-1: Relative cost of copper technologies as compared to optical technologies on PCB [6].

1.2.1 Optical interconnect on PCB as a solution

It is evident that today the question is not whether OI is required, rather it is a matter of when and how it would be implemented efficiently and at a reasonable cost. Table 1.1 is a list, though not exhaustive, of some of the key research– past and present – in the European Union that are geared towards OI technology and many more investigations are underway under EC-funded 'Framework Programme'. Varioprint AG – a PCB manufacturer – has taken the lead in the deployment of OI by opening a sister company, named Vario-Optics AG, in the last quarter of 2009 dedicated to the production and supply of hybrid optical-electrical PCBs. Other active candidates include Celestica, Intel Corporation, NTT Advanced Technology, VTT Technical Research Centre, Agilent technologies, Advanced

Interconnection Technology Inc. (AIT), DaimlerChrysler Research Centre at Ulm, and The University of Texas at Austin among others.

The two OI approaches under consideration are either unguided or guided; both have their pros and cons. The latter can be further divided into fibre- and polymer-based technologies. Current trends in electronic system architecture vis-a-vis miniaturization and literature reports suggest that polymer-waveguide is the favoured candidate. This is because : (i) polymers are relatively cheap, (ii) low acceptable loss is achievable with polymer, (iii) they are easily available, and (iv) most importantly, polymer waveguide fabrication which is being considered, is compatible with the standard processes employed in PCB manufacturing such as soldering temperature, Coefficient of Thermal Expansion (CTE) matching, thermal stability and stress during lamination.

Polymer waveguide fabrication for Optical-PCB application has been reported and/or demonstrated using a number of techniques, and more techniques are still emerging. These techniques include, photolithography, laser direct writing, hot/UV embossing, inkjet printing, microprinting, laser ablation, Reactive Ion Etching (RIE), electron beam writing , photolocking and selective polymerisation, photobleaching, photocrosslinking [8 - 14]. Each of these techniques has one or more advantages that make it of interest.

However, laser ablation of optical waveguides is a technique of choice in the research being reported here in this thesis. This is because laser ablation of polymers, which started in the early1980's [15], has been demonstrated [16 - 21] as a viable technique for a wide range of materials, more importantly, the class of polymers, i.e. photopolymers, required for the technology being reported. Furthermore, it is a technique that is currently used for the drilling of vias for blind, buried and through holes in PCB manufacturing making it a more suitable choice when compatibility issues are taken into consideration. Laser ablation is a non-contact micromachining technology that is based on a controlled and selective removal of materials with intense laser pulses giving high precision and repeatability, and a minimal heat-affected zone (HAZ) especially with ultraviolet (UV) laser source(s).

Table 1-1: A table showing some of the research conducted and reported on the deployment of OI on printed circuit board to overcome the inherent barriers with current copper transmission.

Project/Organisation	Research Activities and Collaboration Overview	Partners	Reference
OHIDA project (Optics on future printed circuit board in high speed data transmission applications)	It conducted a research project called, OHIDA (2002 – 2005). The main goal was to demonstrate ~10 Gb/s optical interconnection on circuit board. The research was a collaborative project mainly between Helsinki University of Technology (HUT), and VTT Technical Research Centre, Finland though with significant inputs from the industrial partners in the area of assembly and demonstration. HUT focused mainly on board side while VTT was looking at the transceiver. A 4-channel 10 Gb/s optical interconnect on Printed Wiring Board (PWB) was demonstrated at the end of the project with potential application in copper-limited electronic devices such as computers.	Helsinki University of Technology (Finland), VTT Electronics (Finland), Aplac Solutions, Asperation, Aspocomp, Elcoteq Network, Perlos Aspocomp.	22 , 23
PPC Electronic AG, Switzerland	It is a PCB manufacturer based in Switzerland. It has an optical technology product called Optoboard® which allows optical tracks to be sandwiched between electrical tracks in a multilayer PCB design.		24

Varioprint AG, Switzerland	It is a PCB manufacturer based in Switzerland. In 2004, it filed a patent on light coupling method for EOCB. It demonstrated what it called "electro-optical circuit board (EOCB)" at SMT 2005, Nuernberg, Germany. In the third quarter of 2009, the Optical Printed Circuit Board (OPCB) technologies and patents from Varioprint AG has led to the creation of a spinout company called "vario-optics ag" (http://www.vario-optics.ch/). This newly formed company will focus on optically-enabled printed circuit board due to the growing demands.	Varioprint AG and Vario-optics AG.	25,26
Optical Printed Circuit Board (OPCB)	OPCB was a 3-year UK EPSRC IeMRC funded Flagship project that drew partners from UK institutions and industries both in the UK and USA. Four different polymer waveguide manufacturing techniques were investigated and compared; they were photolithography, direct laser writing, laser ablation and inkjet printing.	University College London, UCL; Heriot-Watt University, Loughborough University, Xyratex Technology, BAE Systems, Renishaw, Dow Corning USA ; Exxelis; Stevenage Circuits Ltd, Cadence Design Systems, and National Physical	27,28

		Laboratory (NPL).	
The Storlite (Storage Systems Optical Networking) project	It is a UK DTI/EPSRC funded project; it is an academia-industrial project led by Xyratex. It investigated optical polymer waveguide fabrication using photolithography. During the project, a novel patented technique to align them with Vertical Cavity Surface Emitting Laser (VCSEL) was developed which was later licensed to US connector manufacturer Samtec. Partners of this project also participated in OPCB project.	Exxelis, Xyratex Technology, University College London (UCL) and Edinburgh University.	29
EOCB (Electrical/Optical Circuit Boards) project	It was an EU research consortium funded by the German government, department of Education and Research (1998 – 2001). It developed a packaging concept where optical layer is embedded in a typical PCB board. The optical layer is a multimode waveguide patterned using hot embossing.	Andus Electronics GmbH, Robert Bosch GmbH, FhG IZM Berlin, Mikropacks, Siemens AG C-Lab, OECA GmbH, ILFA GmbH, and among others.	30
Information Society Technologies (IST) EU funded projects	IST is a research funding body/organization that has been sponsoring projects in emerging technologies under its 'framework programme' such as FP4, FP5 , FP6 (2002 – 2006) and FP7(2007 – 2013) with Centre for Microsystems Technology, Ghent University as a key partner in optical		31, 32

	interconnection.		
IBM Zurich Research Laboratory, Switzerland	IBM Zurich is an active centre in OI; in 2006 it developed and demonstrated a twelve-channel 10 Gb/s optically-enabled printed circuit boards. The waveguide was fabricated using laser direct writing.		33
Interconnects by Optics (IO) Project	It is an IST EU funded project (2001 - 2004). During the project a 2-D optical OI was developed and demonstrated.	INTEC,ELIS and TFCG of Ghent University, Alcatel CIT, Avalon Photonics Ltd, Albis Optoelectronics, Helix, FCI, Nexans Research Centre, Nexans Cabling System, PPC Electronics, and CEA-LETI.	34, 35
Dow Corning, USA	It is a company that focuses on silicon-based technology and innovation. In 2003, the company involved in optical waveguide fabrication using photolithography based on its photopolymer. Dow Corning is an industrial partner to OPCB IeMRC providing optical polymer and waveguides based on photolithography. Polysiloxane, sometimes called		13, 36

	siloxane or silicone, is a product of Dow Corning and is described further in chapter 3.	
Exxelis, UK	A spinout of Heriot-Watt University, Edinburgh, UK. It was formerly called Terahertz Photonics. Since its establishment, it has been engaging in optoelectronic and optical interconnection. It is acrylate-based polymer, Truemode™ suitable for optical polymer waveguide fabrication. The company has demonstrated the use of the polymer to make waveguides employing photolithography and it is the material of choice in this project though by applying laser ablation technique. Exxelis participated in StorLite project with Xyratex and University College London (UCL) and it is also a partner to OPCB I*e*MRC consortium.	2, 37

1.2.2 Research collaboration

The *IeMRC* Optical-PCB flagship project was an academic-industry collaborative research project (figure 1.2) aimed at developing design rules and different waveguide manufacturing techniques, namely photolithography, inkjet printing, laser direct writing and laser ablation. The latter technique forms the basis of this thesis as the infrastructure is currently being utilised in the PCB industry for microvia drilling; thus, it would facilitate the deployment of the technology at little or no additional cost to the PCB manufacturers.

Academic partners: Loughborough University, Heriot-Watt University and University College London

Industrial partners: Xyratex, Stevenage Circuits, Renishaw, BAE Systems, Exxelis, Dow Corning, Cadence and NPL
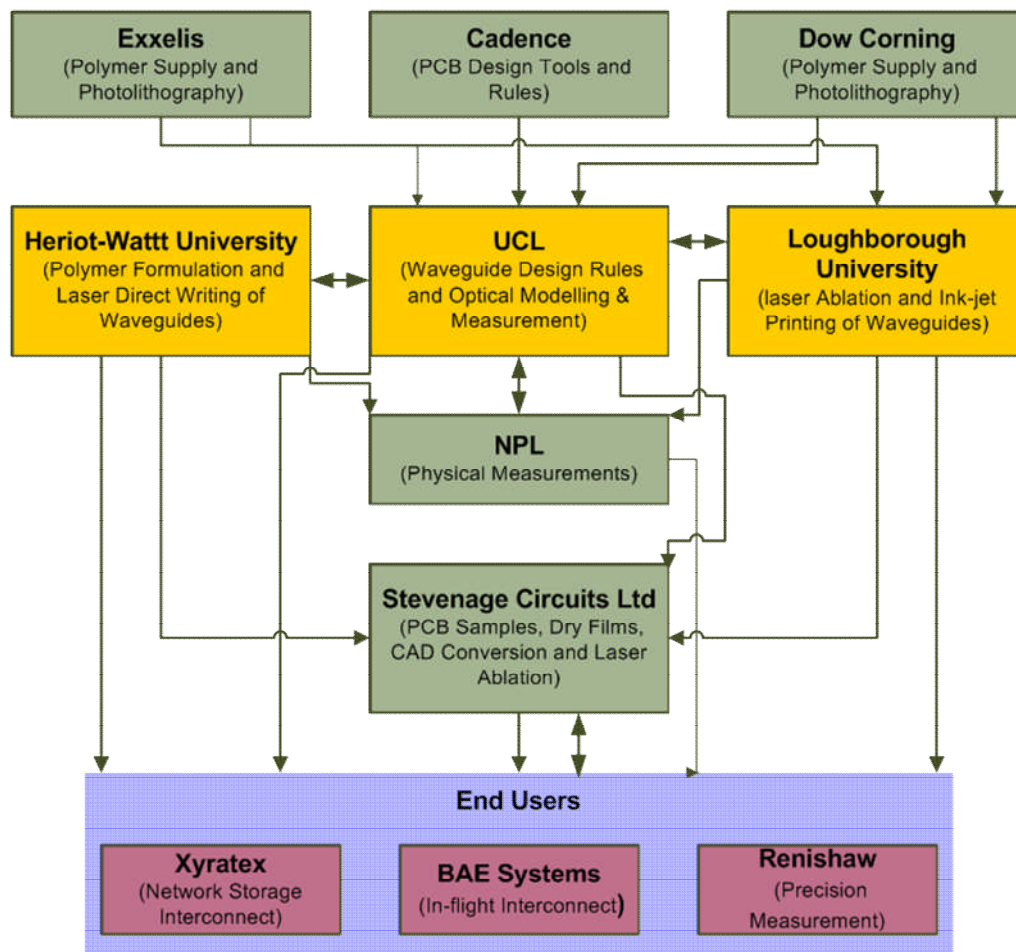
Figure 1-2: *IeMRC* OPCB flagship showing both academic and industrial partners in the consortium and network of activities.

The author's contribution in the flagship project was primarily on laser ablation of optical polymer waveguides using Truemode™ photopolymer, provided by Exxelis. Furthermore, since research has been focused on the out-of-plane coupling of optical waveguide signals, for example, from board to board, the author considered in-plane mirror fabrication for routing signals on board, on backplane and on chip, albeit the later is still a long term consideration.

1.3 Research Concept

1.3.1 Research goal

This PhD research programme was geared towards the fabrication of low-cost waveguides for optical interconnection on PCB using 248 nm KrF Excimer laser, 355 nm tripled-frequency UV Nd:YAG and 10.6 µm CO_2 lasers with the following objectives:

- **Material deposition to form optical waveguide layers**: A suitable technique to deposit wet formulation of Truemode™ polymer to form an optical layer consisting of lower cladding, core and upper cladding, in a manner that the thickness of the layers can be controlled to provide the right thickness for a typical multimode waveguide of a value ≥ 9 µm. The optical layer is to be patterned on an FR4 substrate; this also requires that the adhesion between the substrate and the deposited polymer should be controlled.

- **Laser system characterisation using Truemode™**: The aim here is in two folds: (i) to investigate the potential of the chosen class of lasers, especially UV Nd:YAG and CO_2, for the proposed application, and (ii) to understand the effects of various laser system parameters, which include fluence, power, pulse repetition frequency, speed, number of pulses and number of passes, on the depth of ablation. The choice of parameters to be investigated was largely dependent on the laser setup and capabilities; for example, the effect of pulse repetition frequency was only possible on pulsed lasers, i.e. UV Nd:YAG and Excimer lasers.

- **Polymer waveguide fabrication**: A single-layer straight waveguides were projected for each of the lasers identified. The speed and running cost of Excimer laser – its comparatively low 'approval' in high volume production in the PCB manufacturing industry – were some of the key factors in exploring potential candidates and, indeed competitors in order to meet the low cost objective/criteria of any successful commercialization.

- **Formation of 2D mirrors for in-plane coupling**: A suitable coupling mechanism was

desired such that signals can be routed horizontally with a layer required for communication between components of the layers, e.g. chip-to-chip communication.

- **Waveguide assessment and improvement**: The third key criterion for successful deployment of optical interconnects – the first two being the cost and compatibility of the technique – is the optical power loss. It is therefore an integral part of this PhD research programme to assess the quality of the waveguides in terms of the losses and roughness and providing/suggesting ways of improving this.

1.3.2   Contribution to the body of knowledge

This thesis and the research reported therein has played a role in advancing the current state of research in the field under investigation not only in exploring new designs but also in facilitating the deployment of the technology to its targeted industry, i.e. PCB. The key contributions of this research to the existing body of knowledge are in the following:

- **Excimer Laser system characterisation**: Although, reports are available on the effects of fluence, pulse repetition frequency and number pulses on the etch rate for polymers such as polymethyl methacrylate (PMMA), polycarbonate (PC), polyimide (PI), poly ethylene terephthalate (PET) and polystyrene (PS) among others but such a report is lacking for Truemode™ photopolymer, which adequately satisfies the key requirements of polymer waveguide on PCB such as compatibility and absorption loss, measuring less than 0.04 dB/cm at 850 nm. The author has thus made available such important information advancing the deployment a step forward. Ablation threshold of ~ 0.02 J/cm^2 was obtained for Excimer laser ablation of Truemode™ polymer at 248 nm wavelength which agrees with the thresholds reported for polymers. The tapering effect – a major issue in Excimer laser ablation – was overcome by process optimisation with a near-vertical profile obtained at an operating fluence of 200 mJ/cm^2. The etch rates was found to vary with fluence; a value of 0.252 µm/pulse and 2.5 µm/pulse were achieved at 30 mJ/cm^2 and 280 mJ/cm^2 respectively. Although the straight waveguide achieved using this laser was relatively lossy (estimated to 3.9 dB/cm), the Ra surface/bottom and wall roughness were measured to be 30 nm and 260 nm respectively, suggesting that factors other than fabrication/waveguide were responsible for this.

- **CO_2 laser ablation of optical polymer waveguide**: The suitability of Continuous Wave (CW) and Infra-Red (IR) laser in machining photopolymer was successfully

demonstrated; the machining was carried out on three polymers, namely PMMA, polysiloxane and Truemode™ at varying power and scanning speed – the only two changeable parameters of interest. The CW CO_2 laser micromachining of the optical polymers was understood to be governed by what the author regarded as the 'Scanning Power Density' (SPD) calculated using the input power and scanning speed. While polysiloxane-based polymer ablation gave clean structures at SPD values between 12 mJ/mm and 20 mJ/mm, the laser ablation of Truemode™ polymer produced a better result at the range between 15 mJ/mm and 50 mJ/mm. Multimode waveguides in Truemode™ was successfully fabricated, for the first time at the point of writing, with propagation loss estimated to be 1.3 dB/cm at 850 nm wavelength.

- **UV Nd:YAG laser ablation of optical polymer waveguides**: In this work 355 nm 60 ns pulse length UV Nd:YAG laser ablation of Truemode™ was investigated at various processing speed, power and pulse repetition rate to determinate optimum setting which was followed with successful demonstration of multimode optical waveguide with a propagation loss estimated to be 1.4 dB/cm at 850 nm datacom wavelength . This proved its potential as a possible alternative to Excimer laser micromaching in order to overcome the drawbacks associated with Excimer and to facilitate rapid deployment of the technology into the targeted industry. Laser ablation of Truemode™ polymer at 355 nm using Nd:YAG laser was considered to be a photochemical-photothermal process thus favouring Srinivasan-Smrtic-Babu (SSB) explanation; it was found that input power below 0.15 Watt at 5 mm/s – 10 mm/s speed and a frequency of 5 kHz – 10 kHz is an effective operating condition. The depth of ablation was also found to increase linearly proportional to an increase in the number of laser scans; however, a single scan was considered optimum and sufficient to obtain the required depth of ablation during optical waveguide. Therefore, it can be understood that at the point of writing this thesis, there are no available quoted values (of propagation loss) for laser ablation of multimode waveguide in Truemode™ polymer using either 355 nm UV:YAG or 10.6 μm CO_2 laser.

- **Integrated 2D in-plane mirror fabrication using Excimer laser**: A novel 45-degree signal coupler, which would allow the redirection of optical signals within the plane of the board, was achieved. Laser ablation approach was chosen to fabricate the 2D mirror as the technique has also been used for 3D out-of-plane coupling. In addition, since 2D in-plane coupling would mostly be useful at the board level where OI deployment is expected to reach in the next decade for chip-to-chip communication, the introduction

of any additional micro-optical component at this level of integration could face serious challenges such as alignment. Among the three laser candidates, Excimer laser was preferred due to its capabilities and potentials in patterning complex shapes as opposed to the others, however, it is expected that such current limitations (on the two other lasers) can be overcome once the deployment is accomplished by, for example, by customising the system functionalities once the deployment is accomplished.

1.4　Thesis Organisation

The nine-chapter research thesis (figure 1.3) has chapter 1 and 9 forming the introduction and conclusion of the work respectively. Chapter 2 provides literature coverage of reports relevant to the research in question by giving background insight into optics and optical communication, laser material processing, optical polymer waveguide fabrication techniques and concluding with laser hazards.

Experimental design, procedure, measurement and analysis are the backbone of Chapter 3. It presents methodological designs of various aspects of the research and procedures for depositing the polymer waveguide using a spin coating technique. Furthermore, the chapter accounts for spin coating characterisation of Truemode™, necessary to achieve a desired layer thickness. This chapter concludes with measurement techniques and various equipment used to achieve this.

 In chapter 4, the author presents the experimental investigation of CO_2 laser machining which is followed with the successful waveguide fabrication. Chapter 5 presents experimental results of 355 nm UV Nd:YAG laser system characterisation hosted by Stevenage Circuits Limited, Stevenage, UK – an industrial partner to the *IeMRC* OPCB flagship.

Chapter 6 is a characterisation of 248 nm Excimer laser at Loughborough University with Chapter 7 presenting the results of waveguide fabrication carried out using UV laser systems, namely Excimer, UV Nd:YAG and IR laser, CO_2.

Integrated mirrors for in-plane signal couplings are presented in Chapter 8. This chapter further provides information on metallization processes for 45-degree design. Finally, Chapter 9 is devoted to the summary of the research and proposed future work.
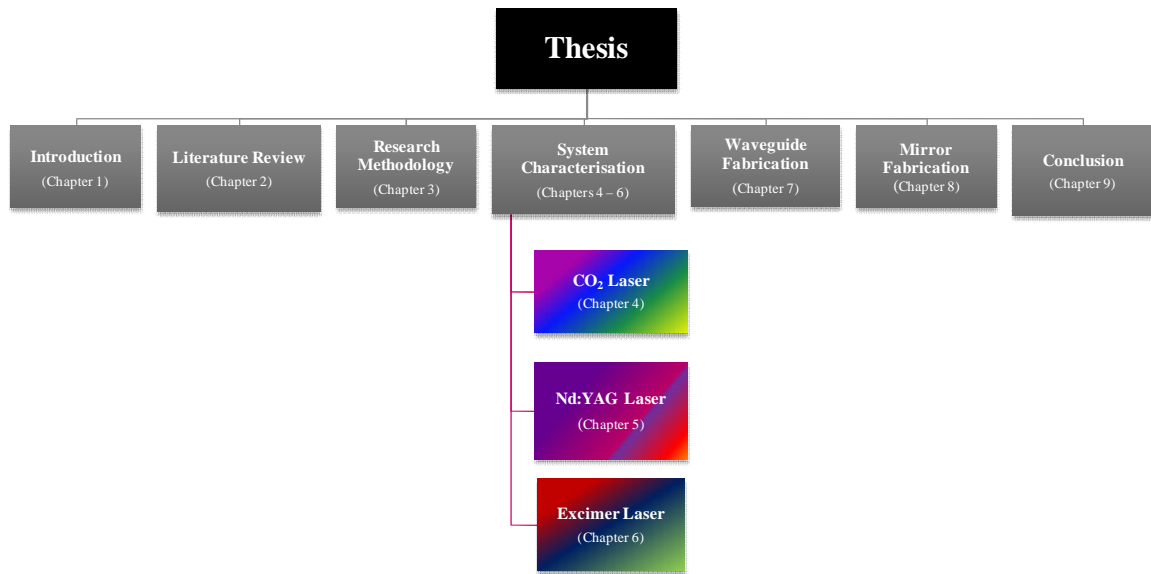
Figure 1-3: Thesis structure (schematic representation).

1.5   Summary

This chapter has provided an account of the current problems, in terms of BW, facing the traditional copper interconnection used in most electronics devices. It has presented OI deployment on PCB as a way of overcoming this inherent bandwidth-limited electrical connection supported by the literature survey of the past and ongoing research in this direction. This proposed solution is also the author's consideration in the research presented in this thesis. The chapter then provided the research goals, collaboration and its contribution to the body of knowledge. The chapter was concluded by presenting the organisation of this thesis chapter by chapter.

Reference

1. Savage, N. Linking with light. *IEEE Spectrum* 39, 32-36 (2002).

2. Holden, H. T. The developing technologies of integrated optical waveguides in printed circuits. *Circuit World* 29, 42-50 (2003).

3. Bockstaele, R., et al. A scalable parallel optical interconnect family. IO overview paper, April 2004.

4. Lau, J. H. An overview of microvia technology. *Circuit World* 26, 22 (2000).

5. Huang, D., Sze, T., Landin, A., Lytel, R. and Davidson, H. L. Optical interconnects: out of the box forever? *IEEE Journal of Selected Topics in Quantum Electronics* 9, 614-April (2003).

6. Pitwon, R., Hopkins, K. and Milward, D. An optical backplane connection system with pluggable active board interfaces. *Proceedings of the Sixth IASTED International Multi-Conference on Wireless and Optical Communications*, 302, (2006).

7. Uhlig, S. and Robertson, M. Limitations to and solutions for optical loss in optical backplanes. *J. Lightwave Technol.* 24, 1710-24 (2006).

8. Dangel, R. *et al*. Development of a low-cost low-loss polymer waveguide technology for parallel optical interconnect applications. *Biophotonics/Optical Interconnects and VLSI Photonics/WBM Microcavities, 2004 Digest of the LEOS Summer Topical Meetings*, 2 pp. (2004).

9. Yoon, K. B. *et al*. Optical backplane system using waveguide-embedded PCBs and optical slots. *J. Lightwave Technol.* 22, 2119-2127 (2004).

10. Van Steenberge, G. *et al*. Laser ablation of parallel optical interconnects waveguides. *IEEE Photonics Technology Letters* 18, 1106-1108 (2006).

11. Fritze, A. Integration of Optoelectronic Devices, Electronic Circuitry and Optical Waveguides. *Department of Physics, Heriot-Watt University*, PhD Thesis (2002).

12. Glebov, A. L., Yokouchi, K., Roman, J. and Lee, M. G. Optical interconnect modules with fully integrated reflector mirrors. *IEEE Photonics Technology Letters* 17, 1540-1542 (2005).

13. Usui, M. *et al*. Low-Loss Passive Polymer Optical Waveguides with High Environmental Stability. *Journal of lightwave technology: a joint IEEE/OSA publication.* 14, 2338 (1996).

14. Maeda, Y. *et al*. Polysiloxane based optical waveguide equipped with fibre guides by using direct photolithography technique. 1 (2005).

15. Bityurin, N. Studies on laser ablation of polymers, Annu. Rep. Prog. Chem., Sect. C: Phys. Chem., 2005, 101, 216 – 247

16. Gower, M. C. Industrial applications of laser micromachining. *Optics Express* 7, 56-67 (2000).

17. Van Steenberge, G. *et al*. MT-compatible laser-ablated interconnections for optical printed circuit boards. *J. Lightwave Technol.* 22, 2083-90 (2004).

18. Griese, E. A high-performance hybrid electrical-optical interconnection technology for high-speed electronic systems. *Advanced Packaging, IEEE Transactions on* 24, 375-383 (2001).

19. Burns, F. C. and Cain, S. R. The effect of pulse repetition rate on laser ablation of polyimide and polymethylmethacrylate-based polymers. *Journal of Physics D (Applied Physics)* 29, 1349-55 (1996).

20. Harvey, E. C., Remnant, J. L., Rumsby, P. T. and Gower, M. C. Microstructuring by Excimer laser. *Proc SPIE Int Soc Opt Eng* 2639, 266-277 (1995).

21. Li, J. and Ananthasuresh, G. K. A quality study on the Excimer laser micromachining of electro-thermal-compliant micro devices. *Journal of micromechanics and micro engineering: structures, devices, and systems.* 11, 38-47 (2001).

22. Immonen, M. P., Karppinen, M., Kivilahti, J. K. and Wroclaw University of Technology. Investigation of environmental reliability of optical polymer waveguides embedded on printed circuit boards. *Microelectronics Reliability* 47, 363-371 (2007).

23. Karppinen, M. Embedded optical interconnect on printed wiring board. *Proc SPIE Int Soc Opt Eng* 5453, 150-164 (2004).

24. PPC- Optoboard® http://www.ppc-electronic.com/english/products/optoboard.html [Accessed February 2010]

25. www.varioprint.ch

26. www.vario-optics.ch

27. Zakariyah, S.S., et al. Polymer Optical Waveguide Fabrication Using Laser Ablation. EPTC 11th Electronics Packaging Technology Conference, Singapore, 9th-11th December 2009, pp. 936-941.

28. Selviah, D.R., Fernández, F.A., Papakonstantinou,I., Wang, K., Baghsiahi,H., Walker, A.C., McCarthy,A., Suyal,H., Hutt,D.A., Conway,P., Chappell,J., Zakariyah,S.S., Milward, D. Integrated Optical and Electronic Interconnect Printed Circuit Board Manufacturing. Circuit World 34(2), 21-26. ISSN: 0305-6120 [Online]

29. Papakonstantinou,I., Selviah,D.R., Pitwon,R.C.A., Milward,D. Low-Cost, Precision,

Self-Alignment Technique for Coupling Laser and Photodiode Arrays to Polymer Waveguide Arrays on Multilayer PCBs. IEEE Transactions on Advanced Packaging 31(3), 502-511. ISSN: 1521-3323

30. Krabe, D., Ebling, F., Arndt-Staufenbiel, N., Lang, G. and Scheel, W. New technology for electrical/optical systems on module and board level: the EOCB approach. *Electronic Components and Technology Conference, 2000. 2000 Proceedings. 50th*, 970-974 (2000).

31. http://cmst.elis.ugent.be/projects/projects.html [Accessed February 2010]

32. http://cordis.europa.eu/ist/about/about.htm [Accessed February 2010]

33. Lamprecht, T. et al. Technology Demonstrator of an Optical Board-to-Board Data-Link, in *Proceedings Symposium IEEE/LEOS* Benelux Chapter, 2006, Eindhoven

34. Bockstaele , R. "Chip-to-chip parallel optical interconnects over optical backplanes based on arrays of multimode waveguides", in Proceedings Symposium IEEE/LEOS Benelux Chapter, 2004, Ghent

35. http://io.intec.ugent.be/index.html [Accessed February 2010].

36. Kopetz, S., Rabe, E., Kang, W. and Neyer, A. Polysiloxane optical waveguide layer integrated in printed circuit board. *Electron. Lett.* 40, 668-669 (2004).

37. www.exxelis.com [Accessed February 2010].

2   LITERATURE REVIEW

2.1   Introduction

Having set out the goals, relevance and importance of this research in proffering solutions to the challenges faced in meeting technology roadmaps for consumer electronics vis-à-vis data rate and size, in the preceding chapter, this chapter reviews some of the fundamental principles, concepts, literature and limitations surrounding this emerging technology. This is addressed by first considering optical communication in general and why its deployment at short distance would be beneficial, and of course a potential solution, to the bandwidth-limited copper transmission. Thereafter, some of the available techniques employed in patterning waveguides for OI are briefly examined. Since laser ablation is a technique of choice in this research, and for the fact that lasers are the key tools in this concept, laser operation, principle and types are reviewed; this is succeeded by discussion on laser-matter interaction, optical polymer waveguide fabrication and limitations. This chapter is concluded by highlighting some of the potential hazards involved in the use of lasers.

2.2   Optical Interconnections

Interconnection using optical principles for long-haul communication is now an established technology with optical fibre (or waveguide) used as light pipes to convey signals. In recent years, there has been ongoing research geared towards adapting the same principles at board level, driven by the requirement for higher data transfer rate, higher density interconnection, smaller packages, and low power consumption/dissipation among others, which is impracticable due to the limitations of conventional electrical connections [1-7]. Light can carry a huge amount of information due to its optical frequencies, typically in the infrared region, namely 850 nm and 1300 nm / 1550 nm for datacom and telecom respectively, and this is where low losses are achieved in light propagation. The high frequencies of optical communication medium (i.e. light) mean a very broad BW which is a requirement for carrying large amounts of data. For example, a carrier source such as VCSEL with a wavelength of 850nm (carrier frequency is 3.5×10^5 GHz) has a BW of $\approx$ 2.08×10^6 MHz (Equation 2.1) if a 5 nm [8] linewidth is chosen for a multimode operation. What this means is that for a TV transmission using a typical BW of 6 MHz (based on Shannon sampling theory) the number of channels that can be transmitted along the fibre is

$2.08 \ x \ 10^6$ MHz/6 MHz i.e. 346,667 channels as compared to 50 channels (i.e. 300 MHz / 6 MHz) that can be obtained from radio-frequency (RF) transmission systems, even though the latter still offers huge advantages over cable links (i.e. coaxial cable). This has made it possible for optical fibre to replace RF in most applications where information capacity is the priority.

$$\Delta v = \frac{c}{\lambda^2} \Delta \lambda \qquad (2.1)$$

There are three basic building blocks of any optical communication system (Figure 2.1), namely: (i) transmitter, (ii) channel, and (iii) receiver, each of which consists of sub-elements depending on the type of information, means of transmission, distance of transmission and type of carrier source. For instance, a typical fibre optical communication system used for long distance transmission would contain a modulator, carrier source and channel coupler as elements of the transmitter, while with free-space radio-frequency wireless communication an antenna is required as a carrier source (or RF generator). A hierarchical classification of a communication system based on distance is shown in figure 2.2. The silica-based fibre – a form of waveguide – dominates the long distance transmission while polymer-based waveguides have been suggested for short-distance (e.g. board-level) interconnections, primarily based on their relative achievable low-loss (at 850 nm) and low-cost benefits respectively [9]. On the other hand, unprotected (i.e. unguided) transmission has also been used for both long- and short-distances. In fact, the former is achievable and thus used at both optical and RF wavelengths (Section 2.2.2).

Transmitter → Information Channel → Receiver

Figure 2-1: Basic building block of a typical optical communication system.
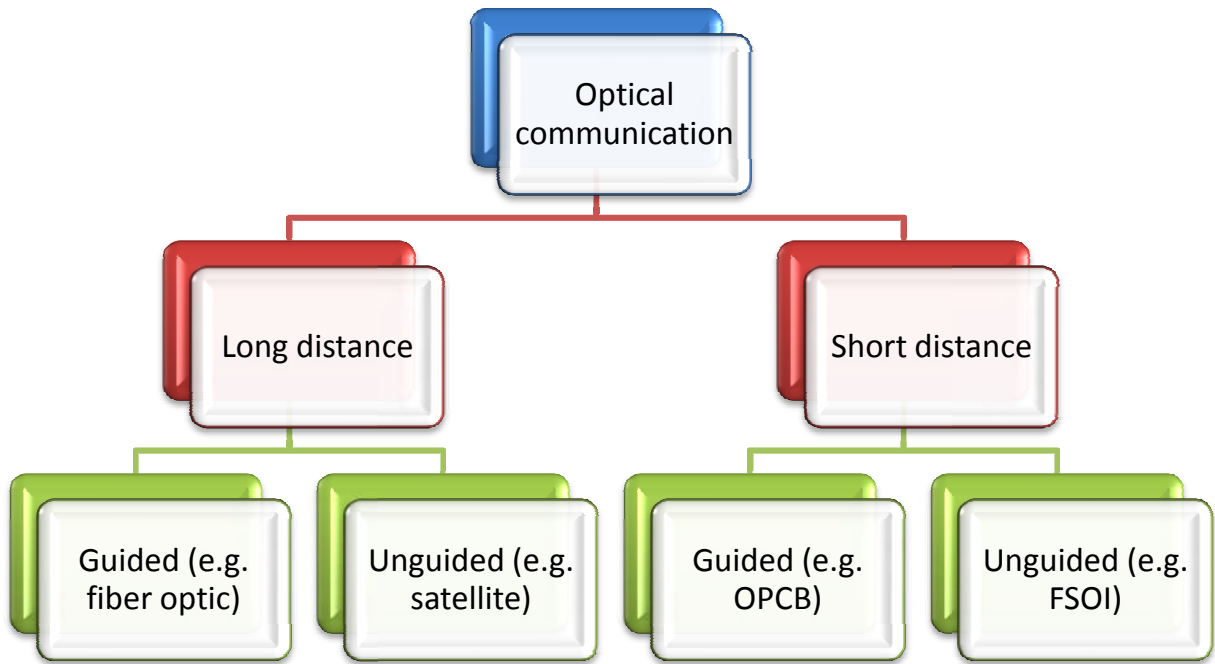
Figure 2-2: Hierarchical classification of optical communication system based on distance and guided mechanism.

2.2.1 *Free space communication*

The free space communication is a form of unguided wave using carriers at either optical wavelength or RF wavelength.

2.2.2 *Radio-frequency (RF) communication*

In RF communication systems, frequencies typically in the range 3 kHz – 300 GHz are generated at the antenna and used as the carrier source. The fact that RF is part of the electromagnetic spectrum in which light is a portion, means that its principle of transmission is fundamentally similar to that of optical transmission, because its wave constituents are made of electric and magnetic fields which are orthogonal to the direction of propagation of the signal travelling at the speed of light (in a vacuum or air). Radio wave transmission utilizes antennas (or aerials) at the transmitting and receiving ends, as against VCSEL and Photo-Diodes (PDs) used respectively in optical communication. The fact that RF is unguided means its use is affected by possible obstruction along the path of propagation, such as absorption of the signal by walls or reflections from surfaces.

Furthermore, the signal is easily affected by the presence of moisture in the air and any other signal in the transmission medium which might constitute a noise.

Another problem with this wireless (unguided) communication system is that the signal is not naturally polarized, which requires that only a particular polarisation can be transmitted by the aerial while the receiving aerial can only receive the maximum signal when its direction is in line with the receiving signal. Even though the polarisation in free space is thought to remain the same once a signal is launched, reflections along the transmission line can cause slight changes to the polarisation of the signal. This poses challenges in alignment (of antennas) and consequently causes signal loss along the transmission line. Furthermore, the aerials, and thus the system, is characterised by impedance matching that is dominated by capacitance and inductance of the transmission line circuit. These are some of the drawbacks in this system of communication. However, one of the advantages of this system over fibre- or waveguide-based communication is the elimination, or at least minimisation, of losses due to its absorption and bending (required for signal routing/coupling), which are found limiting in fibre applications. Furthermore, the system offers huge advantages over twisted pair cable used for telephony and coaxial cable for TV and internet broadband [8, 10].

2.2.3   Free space optical communication

Free space optical communication is fundamentally similar in principle to the fibre optical communication described later in section 2.2.4, except that the atmosphere is used in lieu of fibre (or any other suitable candidate) as the transmitting channel. For this reason, the establishment of an unobstructed path, i.e. line-of-sight, between the transmitter and receiver is a requirement in this technology. There are some challenges facing this type of communication, especially inland, such as divergence, directionality of the beam, presence of moisture, and cloud in the medium among others, all of which can affect the signal and thus decrease the quality of information in terms of the signal-to-noise (S/N) ratio. Nevertheless, this type of communication is still required and mostly used in satellite communication and possibly for chip-to-chip interconnection [8, 11].

2.2.4   Fibre optical interconnections

Fibre, typically a dielectric material (polymer, silica or glass), is an optical waveguide for

long-distance communication. Fibre optical communication has overcome the challenges facing both free space optical communication and that of coaxial-cable communication, especially for long-haul transmission of information and has been successfully used for internet broadband. This technology has seen acceptance among electronic consumers from telephony to cable TV and down to internet traffic for Local Area Network (LAN), Metropolitan Area Network (MAN) and Wide Area Network (WAN). The most important advantages of this system include its high information capacity, relatively low cost, space reduction, reduced losses, low level of distortion, reduced power consumption and immunity to EMI, all (or some) of which have been limiting the performance of electrical interconnection based on copper. The first generation of fibre optical communication was provided about three decades ago using GRaded INdex (GRIN) fibre operated at 850 nm (wavelength) followed by the use of 1300 nm wavelength for single mode propagation.

A fibre optical communication system is based on the principle of total internal reflection (TIR) at core-clad (or core-air) interface. TIR is an optical phenomenon where a light travelling from a denser to less dense medium, on striking a medium boundary at an angle larger than the critical angle, will totally reflect back into the medium with no fraction (theoretically) transmitted. The core, which can be either glass or plastic, is sandwiched between materials of low refractive index (RI), commonly called the clad layers. This cladding ensures that light propagating inside the core is totally contained along the fibre by TIR. Furthermore, the cladding serves as a mechanical support for the core and also as a shield against any contamination which can contribute to Rayleigh loss arising from microscopic impurities [8, 10, and 12].

When light is launched at one end of the fibre it undergoes a series of internal reflections, known as Fresnel reflection, along the fibre before emerging at the receiving end (figure 2.3). Even though the numerical aperture restricts the amount of coupling signal, not all light that enters within an acceptance cone emerges from the waveguides, but only those that strike at an angle ≤ critical angle of the medium (Equation 2.2). Therefore, the size of the core and the difference between the refractive indices of the core-cladding material (Table 2.1) play important roles in determining the numbers of allowed paths or modes that can be propagated. This leads dimensionally to two types of optical fibre or waveguides, known as single-mode and multimode. The main differences between the two types are the size of core and the number of modes operating in the core.

$$\theta_c = \arcsin\left(n_{cladding}/n_{core}\right) \quad \text{for } n_{core} > n_{cladding} \qquad (2.2)$$

The core/cladding dimensions for a single mode fibre and step index multimode fibre are typically 9 µm / 125 µm and 50 µm / 125 µm respectively [13]. Single mode fibre is favoured for long-distance communication as it gives lower attenuation and dispersion. However, even though it reduces the dispersion, it poses a problem of alignment and coupling of signals for the transmitter-fibre and fibre-receiver. The solution to this is achieved by the use of multimode fibre in which the RI of the core decreases continuously with distance from the fibre central axis so that various incident signals can reach the end of the fibre at roughly the same time, thus avoiding signal distortion. This method of propagation is known as Graded Index, GRIN [8]. Transmission in a GRIN fibre is technically due to refraction rather than TIR as the light is refracted as the RI reduces gradually from the core centre and no abrupt change occurs at the core-clad interface.

Table 2-1: Various core-cladding materials used for fibre optical communication with their associated optical properties [8].

Boundary (Core/Cladding)	RI of the core	RI of the cladding	Critical angle θ_c	N.A
Glass-air	1.5	1.0	41.80^o	1
Plastic-plastic	1.49	1.39	68.9^o	0.54
Glass-plastic	1.46	1.4	73.5^o	0.41
Glass-glass	1.48	1.46	80.6^o	0.24
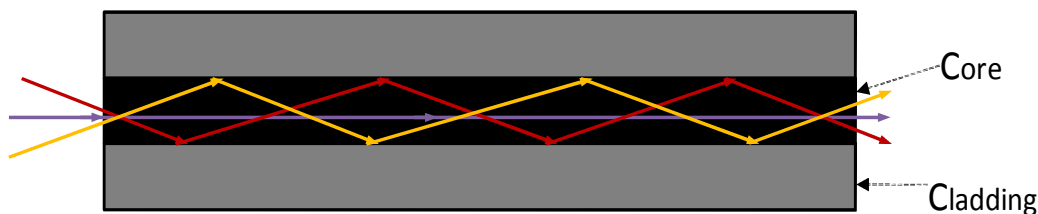
Figure 2-3: The principle of waveguiding in core/cladding structure of different RI for a multimode fibre or waveguide.

2.3   Optical Interconnection on PCB

The PCB is the backbone of connections in almost all electronics products. They are used to mechanically support and electrically connect circuit components such as ICs, logic gates, transistors, diodes, capacitors, inductors and resistors, for board, rack, chip and backplane applications. Conventional electrical interconnection is limited with frequency-dependent (L-C) attenuation, cross-talk due to interconnection density, impedance matching, power dissipation due to impendence of the line, voltage isolation, EMI and interconnection density limitations. These limitations pose serious drawbacks in their use for micro- and nano-technology such as in Micro-Optical-Electrical Mechanical System (MOEMS), Micro-Electro Mechanical System (MEMS) and opto-electronics [1-7].

The introduction of microvia technology, i.e. HDI, into the PCB manufacturing process (used for 'buried' and 'blind' vias to connect multi-layer boards) which is assisted by laser ablation has dramatically improved interconnection density and package size. However, as the speed of signal on-board approaches and tends to exceed 10 gigabits per second (Gb/s) there occurs even greater loss – a real bottleneck in electrical interconnection. The aforementioned limit in electrical transmission on board is becoming unbearable despite using a number of correcting measures:

- minimizing conductor length
- shielding each signal with grounded pins
- filtering and noise elimination
- development of new dielectric substrate, and
- multi-level data coding [14-15].

To resolve the problem due to losses, optical interconnection on the PCB has been suggested as a viable solution. The first application of OI technology is required at the backplane, the most widely used interconnection between boards, but it is expected to extend to lower hierarchical levels of interconnection up to chip level according to some reports even though this, i.e. chip level, is not anticipated soon. For optical interconnection at inter- and intra-board level communication there are currently four different identified concepts using either polymer or glass as the guiding material; they are: (i) overlay technology with polymer optical waveguides, (ii) embedded technology with polymer optical waveguides, (iii) embedded technology with glass waveguides, and (iv) embedded

technology with optical multiwire technology [16]. Polymer-based connection has been a preferred choice for its cost-effectiveness and compatibility with manufacturing in the PCB industry [9, 14, 17 - 19].

2.3.1.1 Light coupling methods for OPCB application

Signals are coupled in and out of optical waveguides using the transmitter and receiver respectively as previously mentioned. The optical transmitter is used to convert an electrical signal to light pulses which is then coupled into the waveguide using a carrier source in the optical-PCB. The reverse process, i.e. conversion of light pulses into electrical signals, is achieved at the receiving end. The commonly-used components for impressing and detecting signals are considered below.

2.3.1.2 Laser Diode (LD)

Laser diodes combine the characteristics of both a simple diode, such as Light Emitting Diode (LED), and a laser. Unlike a LED, it emits coherent narrow-spectrum light when forward-biased (figure 2.4) but no light when reverse-biased. Biasing a diode refers to the act of connecting a dc voltage to its respective terminals. In forward biasing, the positive and negative terminals of a voltage supply are connected to the p- and n-junction respectively of the pn junction diode; the opposite is the case during reverse biasing.

It should be mentioned here that the emitted photon in a laser diode is a product of stimulated emission as opposed to spontaneous emission in an LED. This emission occurs when an electron moves from a conduction band to a valence band. The wavelength emitted depends on the composition and condition of the semi conducting material used, and lies between infrared to near-ultraviolet. For example, for a binary semiconductor – those with two elements – such as gallium arsenide (GaAs), the wavelength of the emitted photon corresponds to the band gap energy, however for ternary semiconductors such as gallium aluminium arsenide (GaAlAs), the wavelength depends on the concentrations of the three elements in the crystal, in other words, the wavelengths of ternary semiconductors are tuneable. There is a threshold level of current above which the laser action occurs (monochromatic coherent light) but below which the laser diode behaves like a LED (emitting incoherent light) [20 – 22].
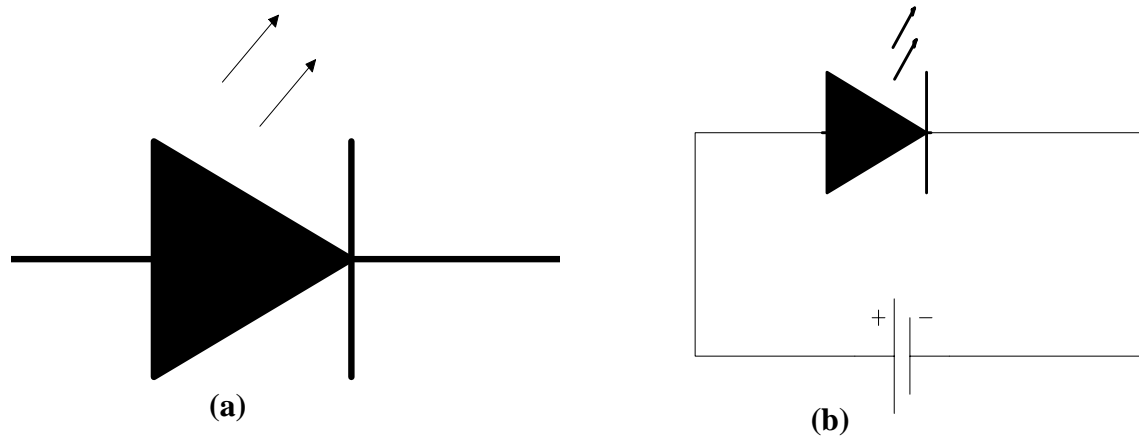
Figure 2-4: Circuit representation of Forward-biasing of LD: (a) Conventional Symbol, and (b) Circuit representation.

2.3.1.3 *Vertical Cavity Surface Emitting Laser (VCSEL)*

Unlike a conventional laser diode, a VCSEL (pronounced as '*vixel*') has its optical cavity axis shorter and along the direction of current flow rather than perpendicular to the current flow. This results in laser beam emission perpendicular to the top surface of the wafer with a small degree of divergence. In other words, the VCSEL is a surface emitter. The short size of resonator in a VCSEL limits the viable longitudinal mode that can oscillate to one [23].

The VCSEL proves to be an ideal component for on-board optical interconnect because it is small, compact with a favourable Gaussian beam profile, highly efficient and with relatively low manufacturing cost because the beam quality can be assessed before the final stage of the process. In addition, the VCSEL is also characterised with a small angular divergence making coupling and alignment comparatively easy [24].

2.3.1.4 *Photodiode (PD)*

A PD is a P-N junction semiconductor diode that functions as a photodetector. Figures 2.5 a and 2.5 b are symbol and circuit representation for a typical PD; the direction of the arrows in the figure depict the path of the incoming light which is in an opposite direction to that of a laser diode shown previously. When a photon of light of sufficient energy strikes the diode surface it excites an electron thus creating a mobile electron-hole pair. A typical PD is packaged with either a window or optical fibre connection in order to let light into the sensitive part of the device. PDs are designed to have wide detecting range for easy and

efficient coupling of the signals [1, 24, 25].
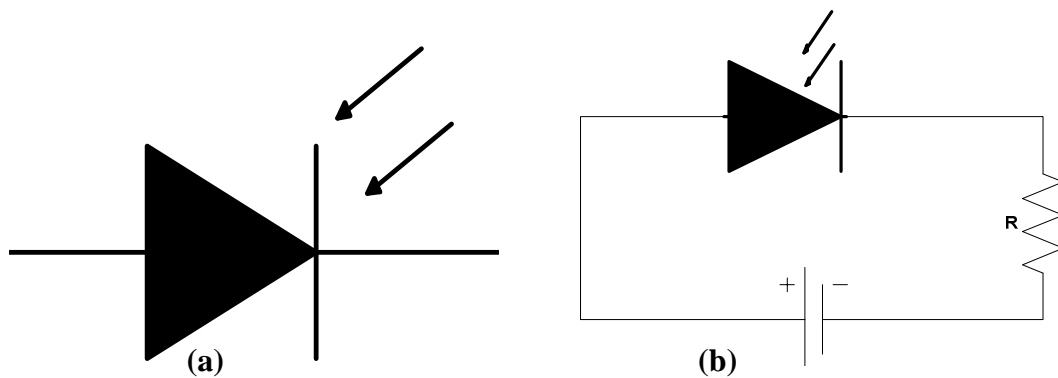
Figure 2-5:   Photodiode (a) Circuit diagram showing
biasing condition, and (b) Symbol representation with arrow
showing direction of light.

In summary, the above optoelectronic devices should, in essence, possess certain features in order to be used as either a light transmitter or a receiver, including but not limited to the following:

➢ The ability to launch light directly into (or couple light out of) an optical waveguide (or fibre) and be small enough for mounting on equipment.

➢ The ability to generate enough power so that sufficient light power can be coupled into / out of the waveguide.

➢ A narrow spectral line width is essential to minimise signal broadening caused by dispersions as previously mentioned.

➢ It should emit light at a wavelength where the waveguide has low loss and dispersion.

➢ It should meet the failure rate and life requirements for the system application.

2.3.2   Challenges in current optical interconnects

Signals launched at one end of an optical waveguide, either for short or long distance applications, are not in many cases, identical to those arriving at the receiving end, either due to attenuation (change in amplitude) and/or distortion (change in waveform). These losses (propagation, insertion, coupling, angular misalignment, etc.) in optical communication are quantified using a logarithmic unit called decibels (dB) using Equation 2.3, where P_1 and P_2 represent the input and output power respectively. For a loss, it is a

negative dB while a positive value indicates a gain of power, usually obtained in amplifiers or amplification circuits. Sometimes the negative sign is omitted but replaced with 'loss' to mean attenuation in signal.

$$\text{Loss (dB)} = 10\text{Log}_{10}^{p_2/p_1} \qquad (2.3)$$

Attenuations are caused by a number of factors including inhomogeneities and geometric (sharp bend and core-clad boundary irregularities) effects of the core, coupling losses resulting from misalignment, absorption by the core (due to electronic, molecular and vibrational bands), and scattering (i.e. Rayleigh) from microscopic impurities dimensionally smaller than the light wavelength. Distortion, on the other hand, is largely due to waves travelling different distances along the optical channel due to a difference in launching angles causing phase delay of the light signal. The light along the waveguide axis or any path parallel to it travels the least distance and thus reaches the receiver first. Distortion is caused by different mechanisms among which are modal distortion, material dispersion and chromatic dispersion. Dispersion cannot be totally eliminated but can be reduced; this is because there is no absolute monochromatic light and RI is a function of wavelength. Thus the more monochromatic a light is the less the problem encountered with dispersion. One of the ways of reducing problems associated with dispersion is by using a single-mode or GRIN waveguide [8, 10, 12].

Apart from propagation and dispersion of waveform there are other issues that have to be considered in any optical communication system for either short- or long-distance transmission. These are addressed in the following sections.

2.3.2.1 Numerical aperture

Numerical aperture (NA) – the sine of the maximum angle of incident light normal to the fibre axis for which transmitted light is guided in the core by TIR – is an important factor in optical waveguide communication because it is directly related to the acceptance cone. For example, a Truemode™ polymer with clad and core having refractive indices of 1.5264 and 1.556 [17, 26] respectively, the NA and the acceptance angle are 0.302 and 17.8$^{\text{o}}$ respectively using equations 2.4 and 2.5 where NA is the numeric aperture and n_{core} and n_{clad} are the refractive indices of core and clad respectively. This is a typical value for a multimode waveguide. This value of acceptance angle can be increased by widening the RI

difference between the clad and core but this, in most cases, is at the expense of propagation loss. However, current polymer waveguides (e.g. polysiloxane and Truemode™) are made in such a way that the RI of both layers can be tuned to suit various applications. Truemode™ for instance, has RI tunable between 1.45 and 1.58. With this, an acceptance angle 38.87^o (and NA of 0.628) could be achieved, which is more than doubling the acceptance angle; this high acceptance angle might be very useful in photonic applications. Another way of overcoming this problem is by the use of 'uncladded' (i.e. using air as the clad with a RI of 1), though this increase in NA would be at the compromise of low loss.

$$NA = Sin\theta = \sqrt{n_{core}^2 - n_{cladding}^2} \qquad (2.4)$$

$$\theta = arsin\sqrt{n_{core}^2 - n_{cladding}^2} \qquad (2.5)$$

2.3.2.2 Coupling loss

Light is required to be transferred in and out of the waveguide via LD/VCSEL and PD to complete the transmission system. During this transfer, designers are faced with alignment of these components mainly due to the dimensional characteristic of the waveguide and also the NA constraint of any guided system. This results in loss, termed as the coupling loss.

2.3.2.3 Bit-error

The fact that information are coded in a defined series of zeros and ones, known as bits, does not eliminate error in digital communication systems, but the ability to design a mechanism with which to detect and subsequently correct the error is a key issue in optical communication. The Bit Error Rate (BER), the fraction of incorrectly transmitted data or signal, determined using what is called a Bit Error Rate Tester (BERT), must be as low as possible to guarantee the reliability of the information received. This problem is one of the current challenges in any form of optical communication system be it for short distance or long distance, guided or unguided, glass-based or polymer-based communication systems [27].

2.3.2.4   Crosstalk

Cross-talk is a situation whereby signal from a channel interferes with another adjacent channel, causing an undesirable effect such as noise. This effect in optical interconnection can be reduced using an appropriate thickness of cladding material to prevent any possible leakage of signals between closely packed waveguide channels or by digitalising the signal, which is less susceptible to interference [28].

2.4   Waveguide Fabrication Techniques for OI

Many fabrication techniques have been identified and reported in the literature; from these lists, four techniques, including laser ablation, were investigated as part of the OPCB flagship. Photolithography and Laser Direct Writing (LDW) are now established techniques for fabricating optical waveguides while laser ablation is an emerging alternative. Inkjet printing, though a form of direct writing – an established deposition technique – is not well known for optical waveguide fabrication.

2.4.1   Photolithography

This is an established technique of microfabrication used in the electronic industry, for example, in silicon wafer patterning. During the photolithographic process of fabricating waveguides, a photosensitive polymer is illuminated in such a way that a mask is used to create the pattern, i.e. waveguide, on a photopolymer. This is achieved while the polymer acts as either a positive or negative resist. With the positive resist, the unexposed areas form the waveguide structures while with the negative type, the exposed part forms the waveguides. In either case, the unwanted areas are developed or washed away. Figure 2.6 shows the major steps involved in photolithographic fabrication of waveguides.
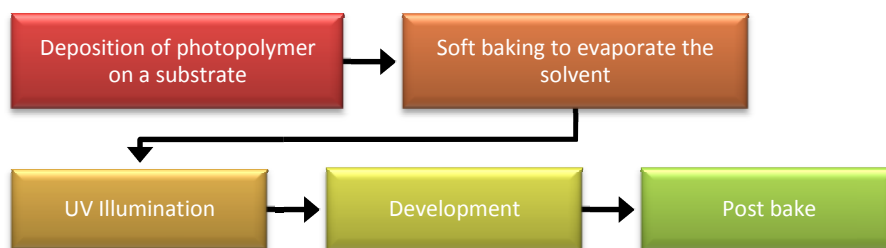
Figure 2-6:   Steps involved in the optical fabrication of waveguides by photolithography.

2.4.2 Laser Direct Writing (LDW)

The LDW process involves using UV laser sources such as Helium Cadmium (HeCd) at 325/442 nm wavelength. In this process, a substrate with a liquid photopolymer deposited using any suitable deposition technique such as spin coating, is placed on a translation stage. While the laser is stationary, in most cases, the stage is moved in such a way that the laser light passes over the sample in order to create the waveguide structures. The interaction of the UV laser beam with the (negative working) photopolymer results in cross-linking of the polymer molecules; thereafter, the unwanted or unexposed areas are then washed in a solvent. The manufacturing speed depends largely on the capability of the stage; furthermore, the waveguide dimensions are functions of the power of the UV source and speed of the translation stage. This technique is similar to the photolithography described above except that: (i) the UV light source is a laser, and (ii) no mask is employed.

2.4.3 Inkjet printing

Inkjet printing is a type of Direct Writing (DR) technology as shown in the classification of figure 2.7. Inkjet printing is well known for marking and printing of text and graphics, however, its use for deposition of structures on substrates has only begun in the last decade [29]. For the fabrication of polymer waveguides, the lower cladding layer is first deposited on an FR4 substrate using spin coating and then cured. In the second stage, the core is deposited using an appropriate dimension of nozzles to sequentially deposit a liquid polymer on the lower cladding placed on a translation stage. Finally, in the third stage, an upper cladding is formed. Although, the inkjet printing technique is very cost effective – an essential requirement for OI deployment – its use for optical waveguides poses certain challenges such as the viscosity, surface tension and wettability of the polymer in relation to the substrate which has to be thoroughly studied and optimised. Other barriers include the ability to control the waveguide dimension; this is because since the process is maskless, the dimension relies, among other factors, on the rate at which the polymer can be cross linked.
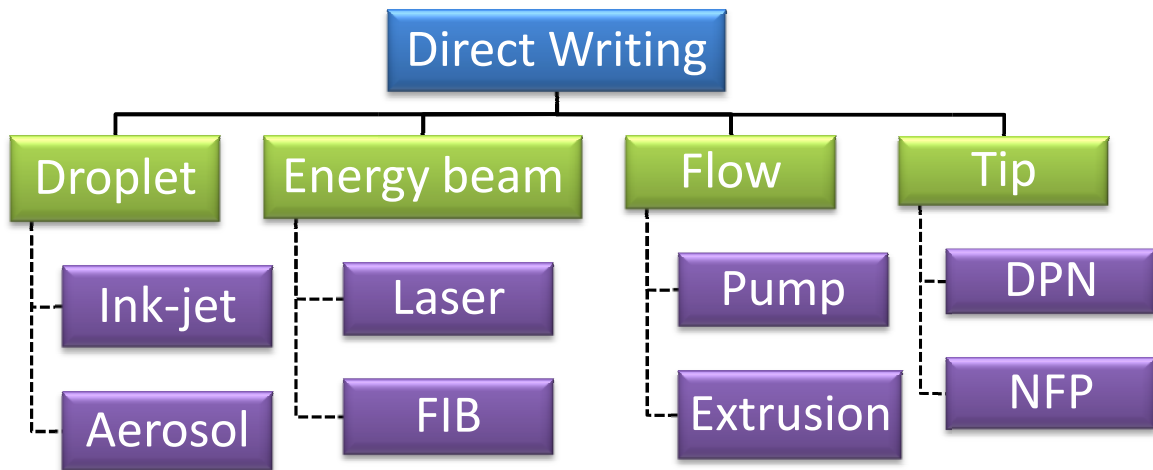
Figure 2-7: Classification of DR techniques [29].

2.4.4   *Laser ablation*

Laser ablation of optical waveguides, as a technique, has been demonstrated by many [30 - 36] as a viable technique and is also considered in this thesis. When it comes to defining integrated mirrors required for coupling light in and out of optical waveguides, laser ablation is a more suitable choice compared to those previously mentioned. The following sections will discuss in detail the relevant features of laser ablation for optical waveguide fabrication.

Apart from these four waveguide fabrication techniques, other methods have also been investigated and/or reported; some are very similar, in concept and step, to those already described or to microfabrication techniques in general. The methods are:

    i.   Casting + Doctor blade [37].

    ii.   DPP (Direct Photo Patterning) [38].

    iii.   Hot embossing [39].

    iv.   LIGA-like process [40].

    v.   Milling [41].

    vi.   Reactive Ion Beam Etching (RIBE) [42].

    vii.   Reactive Ion Etching (RIE) [43].

    viii.   Photobleaching [44].

ix. Photocrosslinking [45].

x. Photolithography + Reactive Ion Etching (RIE) [46].

xi. Photolocking and selective polymerisation [47].

xii. UV-embossing [48].

2.5 Laser Fundamentals

Since the laser was chosen as a tool for the fabrication of optical waveguides in this project, it is pertinent that the fundamental of laser operation is examined; this is the focus of this section.

2.5.1 Introduction to laser

The word 'laser' has been part of ordinary English language since its invention in early 1960, and subsequent commercialisation in 1964. The word is an acronym that stands for Light Amplification by Stimulated Emission of Radiation. Furthermore, laser is considered as a modified version of its predecessor, 'maser', meaning Microwave Amplification by Stimulated Emission of Radiation by Townes (or Gordon Gould as asserted in [49]). In other words, laser is an optical maser. The first laser, ruby, emitted red-colour light at a wavelength of 694.3 nm.

Just approximately five decades later, laser (and laser technology) controls a remarkable market share in various applications ranging from research to medicine, manufacturing to domestic applications. One of the sectors that have seen dramatic advancement with the advent of lasers is medical surgery (ophthalmology, cosmetic surgery and dentistry). For instance, in ophthalmology – the sector that benefited the most – Excimer is used for the treatment of myopia and hypermetropia by a process commonly known as LASIK (Laser in-situ Keratomileusis) where it is used to machine the cornea [50]. This makes laser a very powerful and indispensable machine with the potential of multi-tasking operations. Other industrial applications of lasers are on metals and non-metals (polymers, ceramics, glass, etc.) including surface hardening, surface cleaning, cladding, welding, soldering, brazing, cutting, marking and drilling [50].

2.5.2 Principle of laser generation

There are some fundamental phenomena that need to be understood when considering laser

beam design and generation; they are addressed in the following sub-sections.

2.5.2.1 *Spontaneous versus stimulated emission*

Most light sources such as a bulb, work on a principle of spontaneous emission in which an excited atom or molecule releases photons by falling from a higher energy level to a lower one. Conversely, at the ground state – the stable state in which most species could be found as compared to the excited state under normal conditions – an atom or molecule, can only absorb a discrete packet of light known as a photon, in order to move to a higher energy level which is released again as light on falling back down. According to equation 2.6, this process is reversible. The photons released in this case are non-coherent with different frequencies, and of course wavelengths, since they are constantly and indiscriminating falling to different energy levels.

$$Absorption \ + h\upsilon \ \leftrightarrow Spontaneous \ emission - h\upsilon \qquad (2.6)$$

However, when the aforementioned process is triggered by an external source (i.e. another incident photon) an interesting result is obtained. In this case, photons are not only released prematurely but the emitted photons have the same characteristics – wavelength/frequency, direction of propagation, phase relationship, and plane of polarisation – with the triggering photon, thus resulting in a pool or family of photons. This is known as stimulated emission – the principle of generation of a laser beam. Depending on the laser the beam of light generated in this way can comprise of UV, visible or IR light with wavelengths in the range of $10^2 - 10^4$ nm (figure 2.8) [50]. In fact, nowadays, lasers in the soft X–ray region can also be produced using a Free Electron Laser (FEL).

| IR - C | IR - B | IR - A | Visible light | UV - A | UV - B | UV - C |

700 mm – 1 mm 400 nm – 700 nm 400 nm – 100 nm
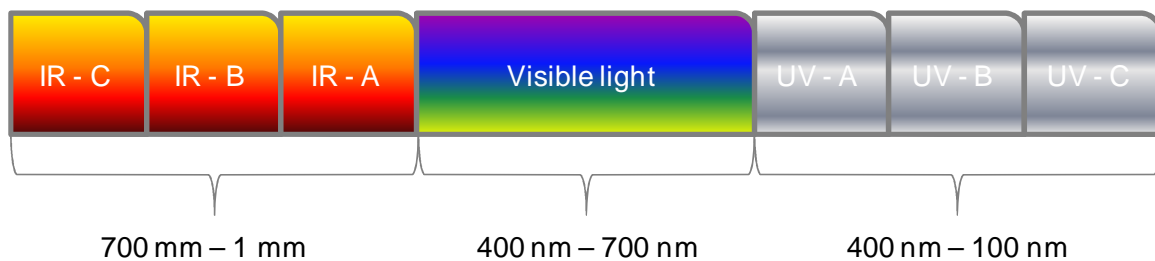
Figure 2-8: Portion of electromagnetic spectrum at which lasers operate based on ANSI Z136 definition.

2.5.2.2   Population inversion

The thermodynamic equilibrium condition of matter represented by the Maxwell-Boltzmann distribution (Equation 2.7) explains the way in which energy is distributed in matter under normal conditions where N_2 and N_1 are the population of species at energy levels E_2 and E_1 respectively, T is the absolute temperature and k is a constant, known as Boltzmann constant with a value of ~ 1.38 x 10^{-23} J/K

$$N_2/N_1 = e^{-(E_2-E_1)/kT} \qquad\qquad (2.7)$$

In practice, what the Boltzmann distribution represents is that even though there is an increase in the number of species at energy E_2, for example, at higher temperature, the distribution however remains constant such that the ratio of N_2/N_1 at any given temperature is less than one as shown in figure 2.9. To put it in a different way, for any given temperature of the system, no energy level is practically expected to have more species than any immediate lower energy though the number of species in that higher state can increase proportionally with temperature. It further follows from equation 2.7 that since $(E_2 - E_1)$ will always be positive and that temperature cannot be negative then population of the lower state would always be greater than that at a higher level or that N_2/N_1 would always be less than one. Unfortunately, this 'normal' distribution needs to be reversed for laser action to occur in order to ensure that stimulated emission is sustained rather than mere absorption and spontaneous emission. This process by which the thermodynamic equilibrium state is reversed is known as population inversion.
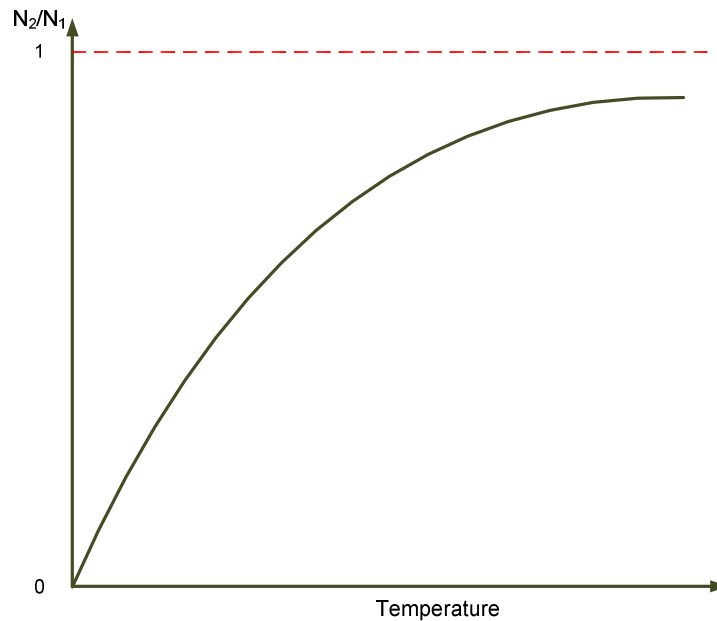
Figure 2-9: Maxwell-Boltzmann thermal population distribution.

Population inversion is achieved through externally supplied energy in the form of excitation, commonly known as 'pumping'. The source of this excitation depends mainly on the type of laser and/or the active medium which could be gas, liquid or solid. The common forms of excitation are electrical (DC, AC or RF), optical (flash lamps, arc lamps, semiconductor lasers, etc.) and chemical pumping. Sustaining this population inversion is essential for continuous laser production, which can be accomplished by:

- creating a situation whereby the rate of populating, via excitation, the upper state is greater than that of the lower state; and
- making the lifetime of the lower state shorter than the upper state. In other words, the upper lasing state is metastable with lifetime greater than spontaneous lifetime.

Thus, for laser generation to take place, essentially, there are three factors, principles and/or phenomena that must be preceded. The first two are: (i) stimulated emission to defeat spontaneous emission and absorption, and (ii) population inversion to temporarily disturb normal distribution. These two processes require that species move from a lower energy level to a higher one, and this is known as laser transition which is considered next.

2.5.2.3   Laser transition stages

In the simplest form, laser light is obtained by transition between the ground and excited states, i.e. only two energies involved, say E_1 and E_2. This system is not efficient for the amplification of light required in an industrial laser application, however Excimer laser is, naturally, generated using a two-state design like the one schematically depicted in figure 2.10 a. In a 3-level laser (Figure 2.10 b) typically used for a ruby laser, species are excited to a pump level – E_3 in this case – which is then quickly and spontaneously decayed to a metastable state at energy level E_2 where the lasing takes place. A state is called metastable because species at this state have life times longer than the spontaneous life such that the state can 'inversely' be populated with species and laser action can be invoked between the state in question and the state immediately below it.

 The three-level design reduces the problem encountered with a 2-level system where the sustenance of population inversion is an issue. However, the problem is not totally solved in this system, which necessitates using a 4-level system (figure 2.10 c) where lasing transition occurs between two intermediate energy states, thus sustaining the population inversion [51]. Today most industrial lasers are operated on a 4-level transition with the exception of few such as Excimer laser.
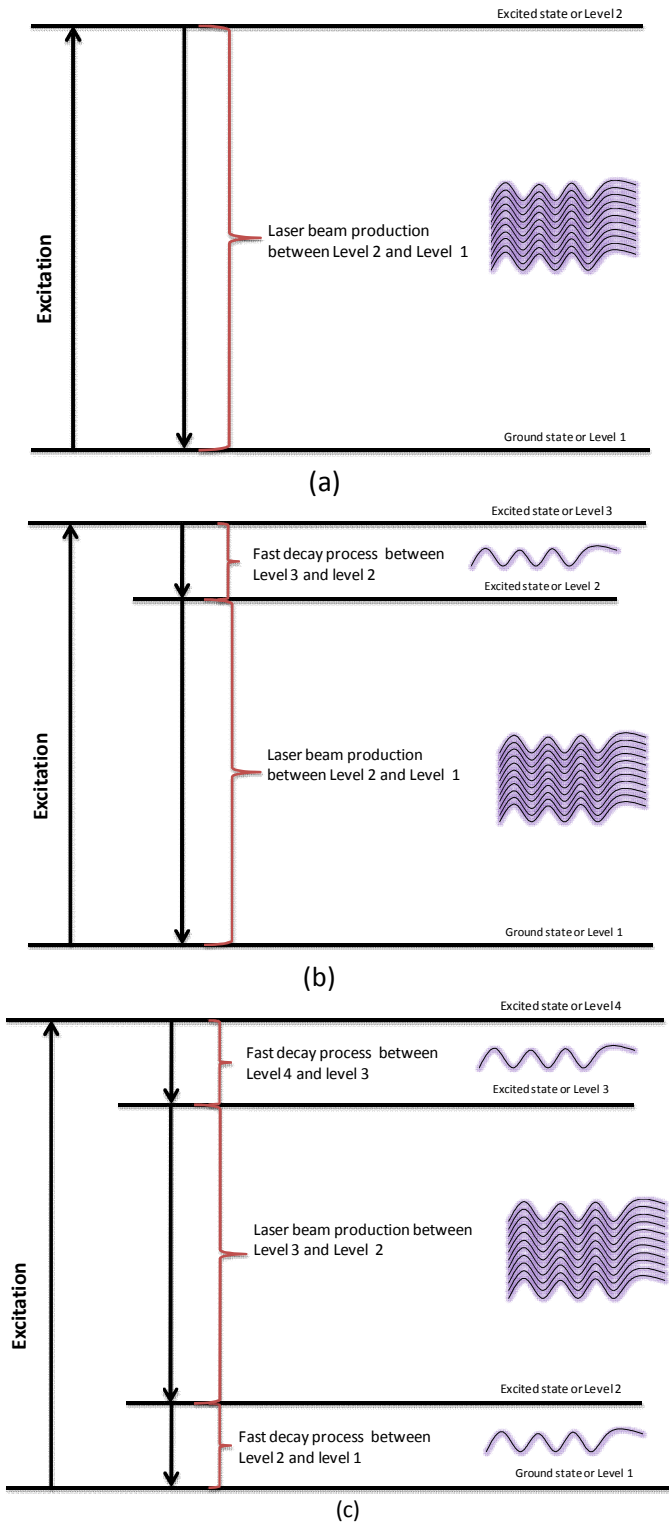
Figure 2-10: Laser transitions process (a) two-level (b) three levels, and (c) four-level.

2.5.2.4   Feedback system – active medium and laser cavity

The third factor for laser generation is the laser amplification achieved through a feedback system. Laser feedback is quite similar to feedback in audio amplifiers except that it is a two-way operation. This process is required in order to create a 'pool' of photons to form the laser beam which takes place in a laser medium.

This medium (gas, liquid, or solid) – through which light is amplified by stimulated emission – is usually contained in an optical cavity consisting of two parallel mirrors, totally- and partially-reflecting mirrors, in which light travels in both directions. The partially-reflecting mirror is coupled to an output window or exit, which delivers the output beam to, for example, the workpiece. The totally-reflecting mirror is made such that its reflectivity is as close as possible to 100%, while the reflectivity of the partially-reflecting mirror varies from laser to laser depending on the power output desired. For example, 35 % reflectivity is employed in CO_2 lasers while 8% of the beam is fed back into the cavity for the purpose of amplification in Excimer lasers [52].

For cavity design, curved mirrors are used to minimise alignment issues usually encountered with flat mirrors and losses due to the diffraction of the oscillating beam [10, 50]. This phenomenon, i.e. loss in coupling light via a flat surface, is also a consideration in the implementation of integrated mirrors for coupling light in and out of waveguides. Figure 2.11 shows various processes involved in the laser generation with the cavity designed is such a way that the oscillating beam tends to converge towards the centre and it is called a stable cavity; it is suitably used for low power lasers up to 1 kWatt for YAG and 5 kWatt for CO_2 [53] where it is safe to transmit the beam through the mirror without the potential of a damage or breakage [52]. On the other hand, a cavity can be designed in such a way that the beam diverges from the central axis; this is called an unstable cavity often used for high-power lasers. In this design, the output power is taken at the edges of the mirror and the two mirrors are totally reflecting.
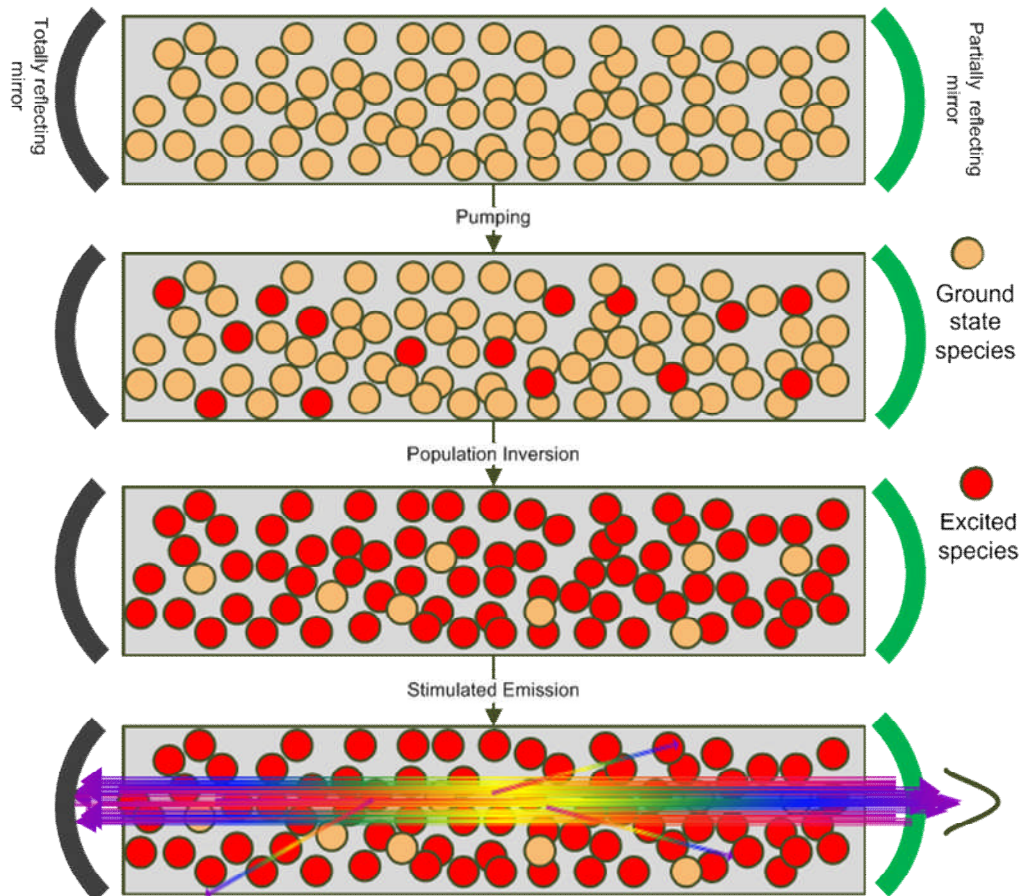
Figure 2-11: Schematic diagram of laser beam design and
generation.

2.5.3   Characteristics of laser beam

It must be surprising to know that lasers are not as efficient as common light sources such
as bulbs with operating efficiency as low as 2 % for flash-pumped YAG laser. However,
what distinguishes a laser beam from other light and makes it a powerful tool despite these
'huge' energy losses, i.e. low efficiency, are its unique properties. These characteristics
include the following:

i.   Polarization

A light wave (e.g. laser beam) possesses both electric and magnetic field that are
orthogonal. The orientation of the E-field is mostly considered to define the direction of
polarization. If the direction of the E-field is always pointing in a particular direction,
which is perpendicular to the direction of travel of light, then it is said to be linearly-
polarized. Consequently, two incoherent waves can be propagating in the same direction

but with different plane of polarization. This is not the case with a laser beam as all photons in a beam are polarized in the same direction [54].

ii. Chromaticity

Chromaticity is an attribute in which the beam produced is of a particular colour and thus frequency. The monochromatic nature of a laser beam makes it possible for it to retain its energy (with much less attenuation or distortion) on passing through optical components (e.g. lens) used in a beam delivery system. It merits mentioning here that although a laser is said to be monochromatic, i.e. having a single wavelength or frequency, there is no such ideal monochromatic light. In other words, in practice, the laser light has a narrow band of wavelength rather than a pure single wavelength [22, 54]. For example, the linewidths ($\delta\lambda$) of Nd:YAG (1064 nm), Excimer (248 nm KrF), and CO_2 (10.6 µm) lasers are 0.5 nm, ~ 2 nm and 1.6 µm respectively [23].

iii. Directionality or Divergence

Divergence is the tendency of a beam to spread out as it travels; it is measured in radians (rad). A typical value of divergence is between 2 – 3 mrad for most industrial laser applications [50].

iv. Coherence

Coherence is another important property of a laser beam which can be described as correlation between phases of monochromatic radiation. In other word it is a measure of degree of phase correlation that exists in the radiation field of a light source at different locations and different times. In fact, polarization, chromaticity and directionality of laser beam are related to each other and to the coherent property; thus, it is often found that the characteristic of the latter is of utmost concern when dealing with the property of a laser beam.

Coherence is of two types, temporal and spatial; spatial coherence can be either longitudinal or transverse. The transverse electromagnetic mode (TEM) indicates the variation of the laser beam intensity in a plane normal to the direction of beam propagation. The most useful of these modes is the fundamental mode, TEM_{00}, with a profile described as Gaussian. Although other higher modes are produced alongside,

which could be found useful for other applications, but for most material processing applications, it is useful to keep the cavity operating at the fundamental mode. Figure 2.12 shows some of the examples of low-orders of TEM modes including the fundamental mode TEM_{00}; the TEM is generally written with two subscripts as TEM_{xy} [23].

TEM_{00}   **TEM_{10}**

TEM_{01}   **TEM_{11}**
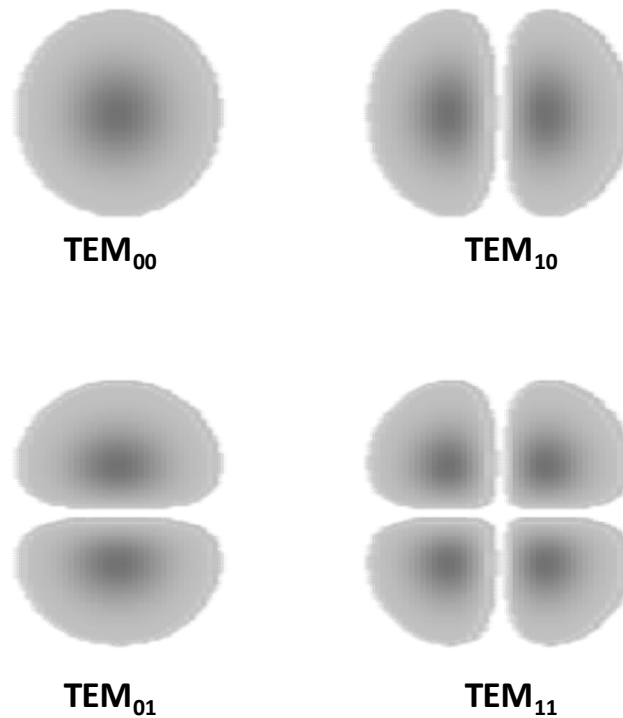
Figure 2-12: Transverse electromagnetic modes (TEM).

2.5.4   Gaussian versus 'tophat' beam profile

The intensity distribution in a Gaussian beam is shown in figure 2.13a. The beam intensity variation can be described according to equation 2.8, where $I_o = I_{max}$ = intensity at the centre of the profile, I, is the intensity at any other point, and r is the radius of the beam taken at a point where the beam axis intensity has fallen to $1/e^2$ of its maximum. Although this Gaussian profile is better than and preferred to higher order modes, its intensity variation is still something of a concern in laser material processing and particularly in laser ablation. For this reason, a modified version of the beam profile is generated with uniform intensity across the entire profile similar, in principle, to that shown in figure 2.13 b. This profile is called a 'top-hat' (or 'flat-top') profile perhaps due to the 'flatness' of the top of the profile. This profile is thought to improve the tapering nature of ablated profiles using the Gaussian.

As shown in figure 2.13 c, a tophat profile is obtained from its Gaussian counterpart by taking the energy from the weak intensity region, where beam intensity distribution is lower than $1/e^2$ (i.e. 13.5 %) of the centre, and folding it back into the region within the beam waist; this is the concept used in the HY120 beam shaper from OPTEC [55]. A point should be made here that, to say that a laser operates in a single mode, i.e. TEM_{00}, simply means that this is the dominant mode of operation just like a given wavelength implies the fundamental wavelength of operation.

$$I = I_0 \, e^{-\,(r/r_0)^2} \tag{2.8}$$
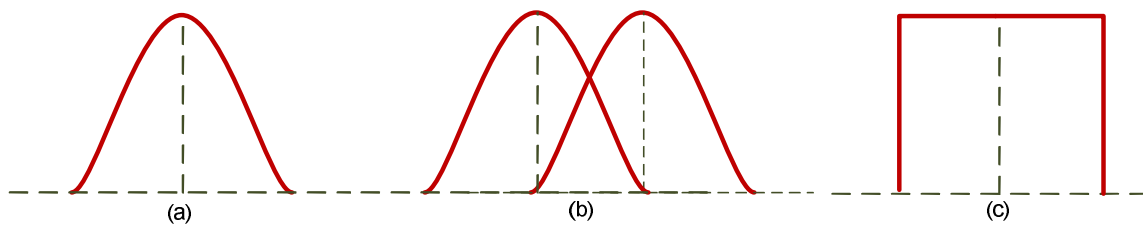
Figure 2-13: Typical laser bean profile (a) Gaussian beam profile, (b) overlapping of Gaussian profile to generate 'top-hat', and (c) 'Top-hat' beam profile.

2.5.5   Types of industrial lasers

Lasers can be classified on a number of factors e.g. active medium (solid, liquid and gas), output power (low, medium and high power lasers), excitation method (electrical, optical and chemical), efficiency, applications and operating mode (continuous wave, pulsed mode and Q-switched output mode). Table 2.2 is a list, though not exhaustive, of some of the commonly available lasers. CO_2, Nd:YAG and Excimer lasers are the key lasers in material processing due to their relatively high power. These three form a complete laser assembly in PCB manufacturing processes, and are thus described under this section.

Table 2-2: Properties of some common lasers used both in research and industrial applications [12, 23, 52].

Property	Solid State (Ruby, YAG)	Molecular Gas (CO$_2$, HeCd)	Dye Laser	Excimer Laser	Laser Diode
Lasing medium	Al$_2$O$_3$:Cr^{+3} Y$_3$Al$_5$O$_{12}$	CO$_2$, Cd	Dye in solvent	Ar, Kr, Xe	Semiconductor
Pumping technique	Flash lamp, diodes	HV discharge	Flash lamp laser	HV discharge	Current
Operating mode	Ruby : Pulsed YAG : Pulsed, CW, Q-switched	CW, Pulsed	Pulsed	Pulsed	CW, Pulsed
Wavelength (nm)	Ruby : 694 YAG: 266 – 1320	CO$_2$: 9.6 - 11 x 10^3 HeCd : 325 - 442	300 – 1000	190 – 350	670 -1550
Beam divergence (rad)	Ruby : 0.2 - 10 YAG : 0.3 - 20	CO$_2$: 0.5 – 10	0.5 -5	2 – 6	0.2 – 0.5
Output power (CW) or average (pulsed) (Watt)	Ruby : YAG : 10-3 -500	CO$_2$: 0.1 – 15,000 HeCd : 0.001 – 0.1	0.1 – 50	1- 100	0.01 - 5
Cooling method	Water	Water, Air	Water, Air	Water, Air	Air
Wall plug efficiency (%)	4 – 12	12		0.5 – 2	50

2.5.6   Solid-state laser: Nd:YAG

Solid-state lasers (it excludes semiconductor lasers in the general usage of the term) such as ruby or Nd:YAG/Glass are generally made of a central material – crystalline or amorphous – doped with a small amount ($\approx$ 1% by concentration) of other material that is transparent at the emission/absorption of the laser wavelength; for example, Chromium (Cr) and Neodymium(Nd) are used as dopants (or active ions) in ruby and Nd:YAG/Glass respectively.

Generally, Nd:YAGs are optically pumped using a flash lamp, but the efficiency of the lasers pumped using this method is low due to the broad range of the illumination coupled with the fact that the YAG rod is unnecessarily heated as a result of this; however, nowadays diode lasers are used instead which increases the operating efficiency by a factor of five from 2% to ~10%. Another advantage of diode-pumped lasers is that the life span of diodes is much longer than that of a flash lamp [52]. Nd:YAG lasers are usually operated as a 4-level system with a fundamental (i.e. dominant) wavelength of 1.06 µm.

Due to the relatively high roughness achieved with Nd:YAG, they are not generally considered for optical polymer waveguide fabrication. However, they are quite useful for other material processing applications such as in cutting and welding of materials. In fact, owing to their ability to be operated in pulsed mode and UV region of wavelengths they are now competing with Excimer in some applications, such as laser ablation in general and in particular, for polymer waveguide fabrication. The latter is considered by the author as will be shown later in this thesis. Also, UV Nd:YAG lasers at wavelengths of 266 nm and 213 nm for example, compete with Excimer lasers in biomedical processes [10, 12].

2.5.7   Gas lasers
2.5.7.1   Carbon dioxide (CO_2) laser

The most common gas laser – the carbon dioxide laser (CO_2) – operates mostly in CW mode at 10.6 µm wavelength (i.e. the strongest or fundamental wavelength, albeit other emission are possible between 9 to 11 µm). The active medium is a mixture of CO_2, N_2 and He in varying proportions, typically 0.8:1:7:: CO_2:N_2: He [52]. CO_2 is widely used for surface treatment, cutting, welding, drilling and marking, all of which are photothermal reactions. The thermal effect of CO_2 laser beam interaction is found useful in surgical

operations where the heat produced is used to vaporize water brought about during the surgical process and also limits any bleeding at the region.

One of the problems with the CO_2 laser is the possibility of producing poisonous carbon monoxide (CO) during the course of generation of the former, but this situation is overcome by introducing water vapour into the chamber to react with any CO gas generated thus forming CO_2 gas according to equation 2.9 which, advantageously, increases the population inversion and thus the efficiency of the system [10, 12].

$$CO \ + \ H_2O \ \ \rightarrow CO_2 + \ H_2 \tag{2.9}$$
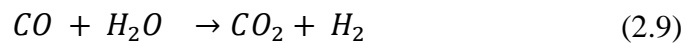
2.5.7.2   Excimer laser

Another commonly used gas laser is the halides of noble gases i.e. Excimer, which is a contraction of the term 'excited dimer'; more technically referred to as 'exciplex' meaning excited complexes. This is because a dimer, in chemistry, strictly refers to a molecule composed of two similar subunits (ions, monomers, etc.). The wavelengths of Excimer lasers vary from about 160 nm to 350 nm (figure 2.14) but ArF, KrF and XeCl are the most commonly used.
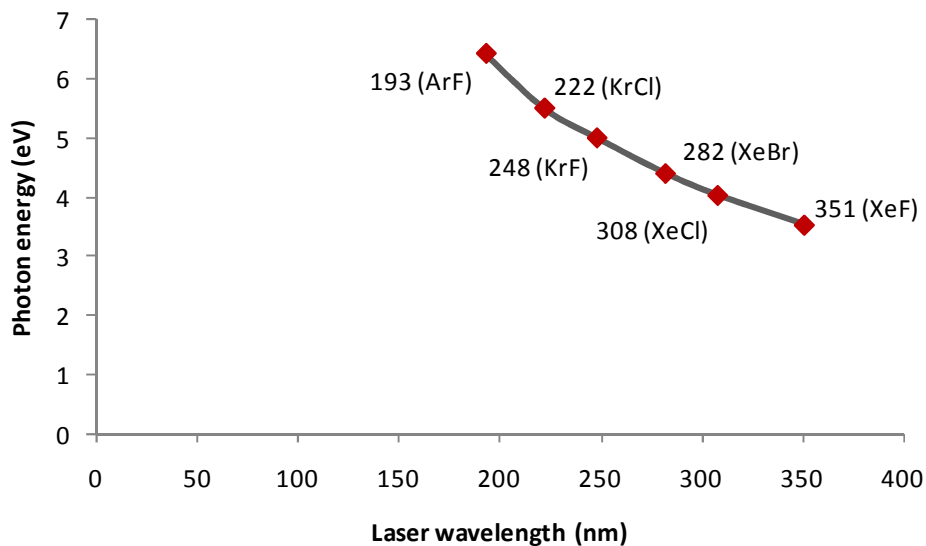
Figure 2-14: A graph of photon energy (eV) against various Excimer laser wavelengths.

In Excimer, the laser beam is produced by chemical reaction between the inert gas and halogen ion through electrical discharge [Equations 2.10 - 2.12 and figure 2.15 for KrF

beam]. Microwave discharge, electron beam pumping and pumping by electrical discharge are three commonly used methods of pumping energy into the laser chamber in Excimer [50, 51].

$$Kr_2 + F_2 \rightarrow 2Kr^+ + 2F^- \qquad (2.10)$$

$$F^- + Kr^+ + He \rightarrow KrF^* + He \qquad (2.11)$$

$$krF^* \rightarrow Kr + F + Energy(h\upsilon) \qquad (2.12)$$
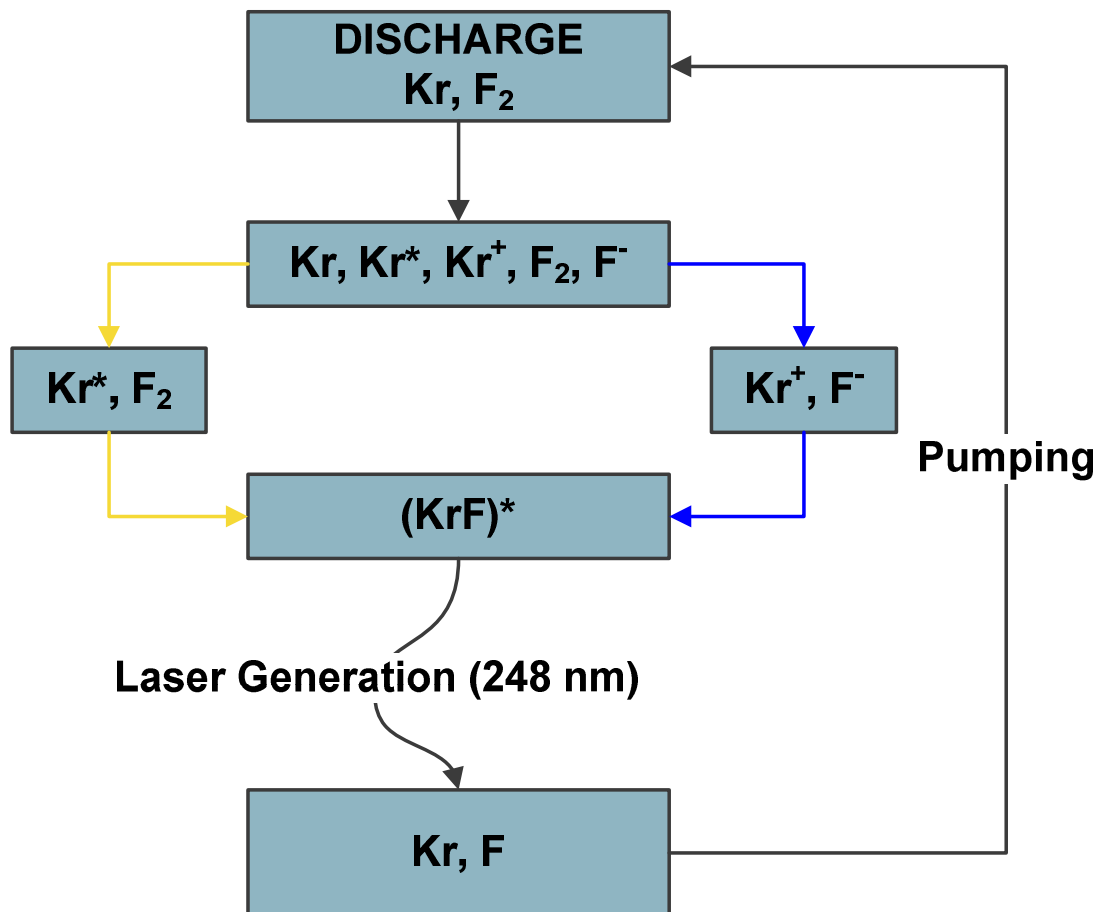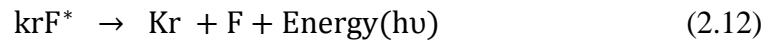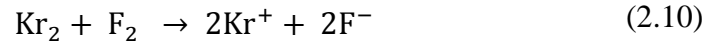
Figure 2-15: Block diagram showing chemical reactions in the production of KrF laser beam.

Helium gas is used, as shown in equation 2.11, to act as a buffer which, for KrF, constitutes by volume about 90 - 99% of the mixture with Kr and F representing 1 - 9% and 0.05 – 0.3% respectively at an atmospheric pressure of 2.5 – 3.0 bars. The KrF* produced in the

process is unstable with a lifetime of about 2.5 ns, falling to a lower energy level with emission of the laser beam; the dissociation of the compound, i.e. bond-breaking, results in energy gain which comes as photons [51].

Due to its wavelengths in the Medium Ultraviolet (MUV) and Far Ultraviolet (FUV), high pulse energy and photochemical-nature of its interaction with matter, especially polymers or polymer-like materials, Excimer laser has been very useful in medicine, micromachining (laser marking, drilling, etc.), scientific research (for example, in laser ablation of optical waveguides, and pulsed laser deposition (PLD)), and also in metrology and semiconductor industry. It is also used for surface modification and the treatment of metals and semiconductors which can be used to improve adhesion between two components, changing the hydrophilicity of materials, and improving friction [56]. Having said this however, one of the concerns and, indeed, limitations with regards to the use of Excimer laser is its cost and also the corrosive-nature and potential danger associated with the halogen gases resulting in a relative shift to close competitors, i.e. UV Nd:YAG and Ti-sapphire lasers.

2.6   Laser Micromachining

2.6.1   Laser material processing overview

Laser material processing is generally, though not technically, referred to as laser processing of engineering materials such as metals, polymer, glass and ceramics. This definition thus excludes applications of lasers to human tissues even though the mechanism is, to some extent, similar. The possible reason for this exclusive usage might be as a result of the fact that early laser candidates, e.g. YAG and CO_2, found application in engineering sectors such as in drilling and cutting of materials where high energies, irrespective of wavelengths, are needed. For laser material processing, there are four key stages/processes (or sub-processes) of importance as schematically shown in figure 2.16, the complexity of which depends on a number of factors among which is the desired application. The processes or mechanisms are explained below.
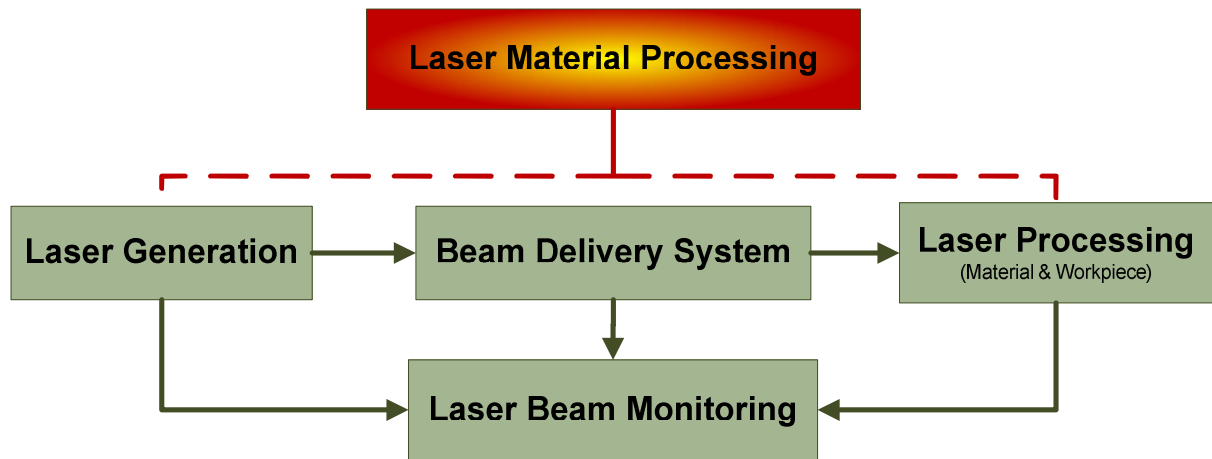
Figure 2-16: Schematic diagram showing key stages of a typical laser material processing.

i.   Beam generation

This is the first stage and the backbone of any material processing; the principle of this has been covered under section 2.4 and its output determines the components of the remaining stages. For example, if a ceramic material is to be processed then the output at this stage should be high-power laser; furthermore, if the ceramic is to be processed with minimum thermal damage then the output beam should be either q-switched or pulsed with short pulse duration to provide a minimum time interaction between the beam and the material. It is thus obvious that a laser material engineer or production engineer would have to carry out a rigorous exercise in matching the output from this stage with, most importantly, the last stage while also considering the cost implication.

ii.   Beam delivery or propagation

This involves transporting the output beam in the first stage to the site of processing, i.e. workpiece. What constitutes the beam delivery system depends on the application under consideration but in general, the elements of the stage include various optical devices such as mirrors, lenses and attenuator. The number and the arrangement of the components of this stage vary so much that it would be difficult to classify or standardise such design. However, it is imperative that careful combination is made to achieve optimum result without losing much power as a small fraction of beam energy/power is lost per each element. It should be noted that, even though the fraction lost per element might be small, when many elements are used, for example for beam homogenisation in Excimer, coupled

with long path length this will eventually be a significant loss.

Also to be considered is the length of the path between the laser chamber output window and the workpiece, which needs to be kept to the minimum length possible in order to avoid beam profile distortion and divergence among other issues. Sometime, the use of a fibre is employed, currently considered in YAG lasers [53], to convey laser to the workpiece with minimum optical devices incorporated. Among prominent lasers used in material processing, Excimer laser usually has the longest beam path with the highest number of optical components while CO_2 employs the least.

Beam profile distortion and losses due to reflection from the optical surface are also problematic; although the former can be minimised by using a spherical mirrors while the latter is mitigated using anti-reflection coatings, nevertheless this is still worth considering [53].

iii.   Laser beam monitoring

There are many properties of the laser beam that are essential for an optimum process; however, three of these properties are highly important in material processing. They are: power/energy, beam diameter and beam profile or intensity distribution. Beam power is very important for laser processing so its quantity is specifically monitored, and there are two methods of obtaining the beam energy. In the first approach, the beam is sampled during the processing, this provides an accurate account of beam energy/power utilised during a particular process, and however, the task is somehow difficult and risky. Three methods of beam sampling, namely static beam splitter, rotating chopper mirror and leaky resonator mirror, are discussed in [53].

The second approach is by total beam measurement; although the method might not be a real account of what happens during a process, but it is easier than the sampling method generally employed. This approach involves measuring the energy or power at the workpiece using a power meter. Apart from it not being an accurate representation of the amount of energy used during a process, another 'clause' with this method is the fact that safe access to the workpiece is required and during a scanning process (where the laser is moved with the stage static) measuring the beam might prove difficult or/and impractical depending on the system setup.

A common way of examining both the beam diameter and profile is by using low energy to irradiate a suitable material, the etched sample is then analysed to measure the diameter and observe the profile. This is an indicative method only especially when the process is thermal; and it also depends on power usage and irradiation time [53]. Alternatively, beam profile is monitored using a beam profiler which shows, in real-time, the shape of the beam during a process.

iv.   Laser processing

When the laser beam strikes the material, the photon energy is transferred to the material wherein it is then converted to other forms of energy depending on the material. With metals, this is transferred to the mobile electrons which results in the heat energy that can cause vaporisation and disintegration of the metal. However, with non-metals, the energy can either be converted to chemical energy required for bond-breaking or heat energy for vaporization; these two possibilities depend on the type of material, its bond energy and the wavelength of the laser or more precisely the photon energy. Essentially, there are two common mechanisms for laser material interactions; they are:

   i.   Thermal (photothermal or pyrolytic): This is an electronic absorption in which the photon energy is used to heat up the material to be processed and thus removed as a result of molecule vaporization, e.g. CO_2 laser cutting. This type of process is commonly and broadly referred to as laser micromachining.

   ii.   Athermal (photochemical or photolytic): This is a photochemical process whereby the material is ablated by direct breaking of molecular bonds when hit by photons (energy) of the incident beam. This is only possible, in principle, if the photon energy is equal or greater than the bond energy of the molecules of the material to be processed. During this process, a particular area of the surface of the material is removed without any damage (by heating) done to the surroundings or the bottom of the material. This process is generally called ablation, though photothermal processes are in some cases also referred to as ablation; in an ideal situation, the process is called 'cold ablation' [57]; it is generally used in reference to polymer materials, but laser ablation is also possible with other materials such as ceramic and glass, but higher fluencies are required in their case.

2.6.2 Laser ablation of polymer

2.6.2.1 Laser-matter interaction

The wave-particle duality concept is quite useful in treating laser matter-interaction; for example, laser generation is better described using the quantum (or particle) approach while propagation and delivery is suitably described using the wave concept. For laser matter-interaction, it is appropriate to use the quantum mechanics thus viewing the beam as a packet of photons hitting the matter with which it is interacting. This makes photon energy a useful tool in this situation.

When photons come in contact with a polymer material, the photons are absorbed which then results in the bond breaking. The net energy, i.e. photon energy minus bond energy, is then transferred to the ablated fragments in the form of mechanical energy, precisely kinetic energy, in order to eject the fragments from the ablated zone. Sometimes, the ejected materials interact with incoming photons and thus get excited by this which then produces flame-like effects during laser processing [53]. This explanation holds only when the process, i.e. laser ablation of polymers, is considered to be photochemical.

However, it is still a subject of debate as to what exactly are the mechanisms of material removal during ablation, whether it is photochemical, or a combination of photochemical and photothermal [58 - 63] or even simply photothermal as argued by some authors [64] in their model in favour of this approach. In fact, optimization of experimental parameters was justified [64] as the best practice in achieving an experimental goal rather than relying on models such as Beer's law (Equation 2.13) or the Srinivasan-Smrtic-Babu (SSB) model (Equation 2.14) [60],which are based on pure photochemical and combination of photochemical and photothermal mechanisms respectively. The two models, widely cited and referred to, are similar except that SSB's model adds a photothermal part to Beer's modes as shown below where L, β, f and f_{th} are the etching depth per laser pulse, coefficient of absorption (cm^{-1}), laser fluence per pulse (J/cm^2) and threshold fluence (J/cm^2) respectively.

$$L = \frac{1}{\beta} \ln\left[\frac{f}{f_{th}}\right] \ , \quad \text{for } f > f_{th} \qquad (2.13)$$

$$L = \frac{1}{\beta} \ln\left[\frac{f}{f_{th}}\right] + L_{photothermal} \ , \quad \text{for } f > f_{th} \qquad (2.14)$$

It is difficult to accept the concept of a pure photothermal process as argued by some authors [64] based on the investigation of two materials, namely, polyimide and Vacrel[TM]8230 at varying repetition rates, just as it is hard to apply Beer's model to many cases of ablation, for example, at high pulse repetition rates for poorly absorbing polymers. Thus, the two mechanisms occur in varying degrees depending on the experimental settings, the ratio of which still puzzles researchers [62].

In summary, since more explanations and observations accounting for the physics and chemistry of the laser-matter interaction are still being researched, it is therefore believed that, until a clear and fundamental account(s) of the mechanism is documented, the process can only be explained by relying on energy conversion via thermal, athermal or thermal-athermal mechanisms. This would then mean that for each experimental case, the phenomenon would be a subject of the polymer and the laser wavelength involved.

2.6.2.2 *Optical polymer*

Polymer is an essential material for engineering processes; it is composed of large molecules with repeating units. The classification of polymer based on origin can be broadly made into organic and inorganic with carbon as the backbone of the unit of the former, while elements such as silicon act as the backbone to the latter [65]. Examples of polymers that are currently considered for laser ablation include acrylate, halogenated acrylate, PC, PET, PI, and polysiloxane among others [14, 19, 66].

Table 2.3 shows a list of common bonds in polymers with their respective bond energies; these energies need to be overcome during any laser ablation irrespective of the nature of the mechanism, i.e. thermal or athermal. For photochemical ablation, the laser wavelength has to be carefully chosen such that the photon energy emitted or obtained from the laser is equal or greater than the bond energy of the polymer to be processed.

Table 2-3: Table showing different type of bonds in polymers and their respective bond energies [51, 53, 67].

Group	Bond Energy (eV)
C = C	6.9 – 7.75
C = O	6.7, 4.2
-NO2	4.4, 5.9
-N = N	3.5, >4.8
Benzene Ring	4.9, 6.2, 7.75
Si-Si, Cl-Cl	1.8 – 3
C-H, C-N, C-C	3 – 3.5
C-H, O-H, N-H	3.0 – 4.9
C-O, O-O	5.1 - 11.2
N-N, N-O	6.0 - 9.8

2.6.3 *Laser ablation of optical waveguides*

Laser ablation of optical polymer waveguides is considered to be a photochemical process as previously mentioned and it is a non-contact micromachining technology. Excimer laser ablation of polymers has been successfully demonstrated [68 - 70]. The key feature of this class of laser is their wavelength and pulse duration; the latter hel.ps in thermal diffusivity while the former is a key to absorptivity of the laser beam in the polymer. The pulse duration of Excimer laser is of significance when it comes to quality because shorter pulse width lasers give better machined quality though a costly task as Chen, X. and Liu, X. asserted in [71]; furthermore, it helps in reducing the ablation threshold [72]. In fact, most of the close competing lasers, for example, YAGs and Ti-Sapphire, are found to operate either in the UV regions or with very short pulse duration, and also possibly with a combination of both features thus intensifying competition. Another area where Excimer excels is in its ability to 'mask-project' patterns on to a sample placed at the workpiece; this feature is mostly found useful and unique with Excimer laser micromachining.

The suitability of a UV laser (e.g. Excimer) for the application under discussion, i.e. photochemical ablation mechanism, over any other laser operating either in the IR (or visible) region of wavelength, such as CO_2, could be demonstrated as follows. For example, using the Planck equation, the energy ($E = hv$) of a photon is inversely proportional to its

wavelength , thus a CO_2 laser operating at 10.6 µm will produce an energy more than 40 times less than that produced by a KrF laser [Equations 2.16 – 2.20]. This, obviously, is not in the order of magnitude of the energies for chemical bond scission of typical polymers, usually between 3 – 10 eV. Increasing the number of pulses to match the required bond energy will merely result in a cumulative heat effect on the polymer surface. This is why a laser such as CO_2 is mainly used in applications where a thermal mechanism is required.

$$E = h\upsilon \;\rightarrow h = \frac{E}{\upsilon} \tag{2.16}$$

$$h_{CO_2} = \frac{E_{CO_2}}{\upsilon_{CO_2}} \tag{2.17}$$

$$h_{KrF} = \frac{E_{KrF}}{\upsilon_{KrF}} \tag{2.18}$$

$$h_{KrF \;=\; h_{CO_2} = Planck's\; constant}$$

$$\frac{E_{KrF}}{\upsilon_{KrF}} = \frac{E_{CO_2}}{\upsilon_{CO_2}} \tag{2.19}$$

$$\frac{E_{KrF}}{E_{CO_2}} = \frac{\upsilon_{KrF}}{\upsilon_{CO_2}} = \frac{\lambda_{CO_2}}{\lambda_{KrF}} = \frac{10.6\; x\; 10^3 nm}{248nm} = \approx 43 \tag{2.20}$$

It is thus clear from table 2.3 that Excimer lasers have the right order of photon energy to ablate polymers chemically, in fact, other UV lasers such UV Nd:YAG and HeCd also possess enough energy for photochemical processes to be undertaken. On the other hand, IR laser sources have photon energy much lower than 3 eV and thus mean that with such lasers the process would be dominated by thermal mechanism. A cross-over from between thermal and athermal processes can be found for a 3 eV polymer bond as follows:

$$E = h\, c / \lambda \tag{2.21}$$

Let E = Bond energy of the polymer to be processed = 3 eV

H = Planck's constant = 4.14 x 10 $^{-15}$ eV

c = velocity of light in vacuum = 3 x 10^8, and

λ = wavelength of the laser

Rearranging equation 2.21

$$\lambda = h\,c/E \qquad\qquad (2.22)$$

$$\lambda = \frac{4.14\ x\ 10^{-15}\ x\ 3\ x\ 10^{8}}{3} = 414\ \text{nm}$$

Therefore, in principle, laser of a maximum wavelength of 414 nm (visible region of electromagnetic spectrum) is required in order to photochemically ablate a polymer material with bond energy of 3 eV. There would be a shift in the dominance of the mechanism by changing the wavelength of the laser source. For example, a shorter wavelength, e.g. 355 nm would guarantee or increase the dominance of a photochemical process, on the other hand, a longer wavelength, e.g. 1064 nm in the IR, would both reduce the dominance of photochemical and introduce the presence of thermal process for the same polymer.

Table 2-4:   Different Excimer Lasers in operation today
with their respective wavelengths and photon energies.

Laser	Wavelength (nm)	Region	Process mechanism *	Photon energy (eV)
XeF	351	UV	Photochemical	3.53
XeCl	308	UV	Photochemical	4.03
KrF	248	UV	Photochemical	5.00
KrCl	222	UV	Photochemical	5.50
ArF	193	UV	Photochemical	6.42
Nd :YAG	1064	IR	Photothermal	1.18
UV Nd:YAG	355	UV	Photochemical	3.50
CO_2	10600	IR	Photothermal	0.12
CO	5400	IR	Photothermal	0.23
HeCd	325	UV	Photochemical	3.82

* Assumed mechanism based on the calculated photon energy and the bond energies shown in table 2.3.

It is worth noting here that even though Excimer laser has been proven as a suitable candidate for this process, the emergence of UV Nd:YAG which operates in the UV region means the possibility of laser ablation with this type of laser which has already been applied

in PCB manufacturing for microvia drilling. In addition, as shown in table 2.4, the UV Nd:YAG laser can also produce photon energy needed to cause non-thermal processes on some polymers.

2.6.4 *Glass- versus polymer-based waveguides*

Glass-based optical layers are integrated into PCBs by embedding thin glass sheets into a standard FR4 stack. They have low CTE and high thermal resistance with very low absorption loss. Although glass optical fibre (GOP) has the potential of carrying large amounts of information (at low loss) required in OPCB, they are not widely considered for this application for a number of reasons. This is because: (i) glass is not as cheap as a polymer alternative, (ii) it is difficult to fabricate due to its fragility, and (iii) it is heavy when compared to polymer. These factors, and others, make polymer-based waveguides a suitable choice for optical-PCB interconnections [6, 14, 17 - 19]. Furthermore, if an ablation technique is to be used for fabrication, the ablation threshold for a glass is higher compared to a polymer, which in turn, can lead to possible cracks and rougher surfaces for glass-based waveguides. This simply means a lossy waveguide. However, this is not to say that the process cannot be optimised to mitigate the aforementioned problems, but this choice would certainly delay the deployment of the technology which of course is an undesired option.

Polymer waveguides are favoured for optical-PCB not only because of the ease in their fabrication and integration with other optoelectronic devices but more importantly their compatibility with PCB manufacturing process vis-à-vis pressure and lamination. Although Polymer Optical Waveguide (POW) is compatible with current PCB manufacturing process, there are some drawbacks:

i. Although a lot of polymer materials have been investigated, still new materials require new processes, equipment and experimentation, both during the deposition of optical layer and the fabrication of the waveguides.

ii. Polymers show high losses in the IR region due to the C-H bond absorption that is why higher loss is recorded at telecom wavelengths than datacom; and the same reason makes polymer waveguides unsuitable for long distance communications.

iii. The optical loss or attenuation is not constant, but dependent on variable parameters such as temperature and humidity which might be difficult to keep constant [16].

2.6.5 Ablation threshold

The ablation threshold is the point at which the applied power or energy density is enough to cause ablation either thermally (or pyrolitic) and athermally (or photolytic). The value of this varies from polymer to polymer depending on the nature and strength of the bonds in the polymer (table 2.3). The ablation threshold of a particular polymer can be easily obtained by extrapolating a graph of ablation depth against fluence, the value of which also depends on other factors such as the pulse repetition frequency (PRF). When working below this threshold, no ablation is expected to occur, however, the chemical properties of the materials are subject to certain changes. Furthermore, operating at well above the threshold can cause or increase the HAZ effect and debris deposition; the former is due to high energy while the latter is as a result of bombarding the ejected materials. In fact, it should be noted that intense bombardment of ejected particles above the ablation zone can retard the ablation rate; the reason for this is that, the ejected materials might absorb fractions of the incoming beam thus reducing the effective fluence at the ablation zone, i.e. the material. Wavelength is one of the factors that determine the thresholds of ablation, for example, the ablation threshold for PMMA is ~150 mJ/cm^2 at 193 nm and ~500 mJ/cm^2 at 248 nm – this is a 3-time increase in value between the two wavelengths. The rule-of-thumb for laser ablation of polymers is to have lower threshold fluences for ablation at shorter wavelengths. In other words, the shorter the wavelength of the laser beam the lower the fluence required for ablation [73, 74].

Table 2-5: Ablation threshold fluence for some selected material [57, 59, 74, 75].

Material	Fluence (mJ/cm^2)	Wavelength (nm)
Photo resist	30	-
Polycarbonate	40	-
Polyimide	~ 40	248
Polyimide	50	308
Polyimide	100	355
PMMA	150	193
Silicon nitride	195	-
SiO$_2$	350	-
PMMA	500	248
Glass, metal oxide	700-1200	-

2.6.6 Challenges in laser ablation of optical waveguides

The three main challenges that frequently occur during laser ablation are discussed here. They are:

2.6.6.1 Debris

The micro particles ablated (or removed) from polymer materials during the ablation process are of different materials (gas, plasma and carbon clusters) depending on a number of factors but, in most cases, it mainly contains carbon residues from the long C-H bonds. The mixture of these microparticles is collectively referred to as 'debris', the quantity of which depends on the laser material interaction, laser beam settings, type of material being ablated and constituents of the surrounding atmosphere. The redeposition of debris on to the surface of the material, especially around the region of waveguide structures, is highly undesirable as this contributes to propagation losses resulting from micro impurities or diffused reflection on hitting the particles [76, 77] and need to be minimised, if it cannot be eliminated.

Controlling the amount of debris is crucial in optical polymer waveguide fabrication in order to ensure that optical power budget for OI is satisfied. Any suitable techniques can be used to control this effect but here are some of the currently employed methods:

1. **Process optimisation:** Laser process should be controlled in such a way that the velocity of the ejected particle is low enough such that the momentum exchange between the ejected molecules and the constituents of the surrounding atmosphere is at its minimum. This can be achieved by a careful selection of experimental parameters so that optimal photon energy corresponding to the bond energy of the polymer is used, by applying lower J/cm² fluences and/or shorter duration pulses in the range of *fs* to *ns*. This is because working well above the ablation threshold, especially for photochemical ablation, would result in the ejected particles moving at high velocity, due to increases in kinetic energy acquired, making it liable to strong collision with molecules and particles in the surrounding air, thus causing debris deposition [77].

2. **Control of the ablation zone**: This is to reduce (or eliminate) any unwanted particles that might be deposited on the machined waveguides through collisions or bombardment. One way of achieving this is by working in what is generally described as a 'clean room'. Another method is to eliminate the atmosphere either by 'vacuum ablation', i.e. ablating in a vacuum chamber or atmosphere which is difficult or impracticable or by introducing a lighter gas, such as Helium (He) which resulted in improving the surface of ablated samples in [72, 78]; in fact, ablation of materials in Helium atmosphere was said to be capable of reducing the roughness to Ra < 200 nm for PEEK and PSU, lower Ra values, below 100 nm, were obtained for PI [74]. Ablating in water environment has also been shown as a means of reducing debris for both polymeric and metallic materials [63, 74].

3. **Others**: Post-ablation of debris removal is also employed, for example, cleaning using methanol, sonic agitation and plasma etching [79]. Shorter pulse-width lasers, such as femto second lasers, are also possible ways of reducing debris.

2.6.6.2 Tapering

One of the common problems with ablation is the tapering of the ablated profile, this, in most reported cases, is unavoidable; however, the effect can be reduced by working at a relatively high fluence above the threshold. For example, Meijer [8] observed that tapering can be reduced from 20 degree at 150 mJ/cm^2 to 2 degree at 500 mJ/cm^2. Gower [53] also observed similar trends on holes drilled in polyimide using ArF laser where tapering was reduced from ~50 degree to ~15 degree for fluence increase from ~ 350 mJ/cm^2 to 1050 mJ/cm^2. This approach, i.e. increasing the fluence, cannot be taken as a general trend and/or

a way of reducing the tapering effect, as high fluence well above the threshold can also result in other negative effects such as increase in HAZ as previously mentioned. Harvey, et al [10] also observed that the tapering of the wall depends largely on the fluence and the numerical aperture of the objective or projection lens.

What actually is responsible for tapering is still relatively unclear but Harvey, et al [10], in their study of the effect of fluence on tapering for PET and Polyimide found the phenomenon was attributed to the incident light diffraction. Gower [53] also supported this explanation; he however argued that such tapering can find applications in fluid dynamics such as laminar flow where a tapered nozzle is preferred. Generally, to overcome this effect, an optical device or component, namely a homogeniser, is used to obtain what is termed a 'top-hat' profile. The top-hat beam profile, to a large extent, is considered to minimise the tapering effect, however, it is possible to obtain a near-vertical profile without using an homogeniser or beam shaper as obtained in [10]; this was also the case during this research especially when proper combination of laser parameters were used.

2.6.6.3   HAZ

Heat affected zone is the area adjacent to the ablated zone where the chemical structure has been altered without causing or resulting in ablation. This could be due to, among other factors, the excess energy applied which is not completely required during the process of ablation. HAZ is believed to be pronounced in a thermal process – a notion that cannot be substantiated. This minimal HAZ is attributed to the short interaction between the laser beam and the material. Today, picoseconds and femtosecond lasers are now available, designed to further reduce the HAZ effect and these class of lasers are also characterised with higher etch rate and lower ablation thresholds.

2.7   Laser Hazards

The laser has turned out to be an indispensable tool in current technological advancements, however any improper abuse in its usage, for example if the accessible emission limit (AEL) (the maximum accessible level of laser radiation permitted within a particular laser class) is exceeded, this could pose serious potential danger to its users. The two main organs that are mostly affected by laser beam radiation are the eye, causing for example cataracts, and the skin, which could result in skin burns or cancer. The former is more

affected due to the optical power of the human lens (in the eye) which can magnify beam intensity by a factor of 100000, i.e. the optical density of the lens in human eye is $\approx$ 100, 1000. For example, a beam of radiant exposure of 1 mJ/cm^2 entering the eye would produce radiant exposure (H) of 100 J/cm^2 at the retina (figure 2.17).

Lasers are, therefore, classified as Class 1, Class 1M, Class 2, Class 2M, Class 3R, 3B and Class 4 with increasing order of their potential danger based on American National Standard for Safe Use of Lasers, ANSI Z136.1, and British Standards BS EN 60825-1:1994 and BS EN 60825-2:1995. Most lasers used for material processing (e.g. Excimer, UV Nd:YAG) are under the most hazardous, i.e. Class 4, except if the equipment is properly and completely shielded against human exposure so that Maximum Permissible Exposure (MPE) – the level of laser radiation to which a person may be exposed without hazardous effects or adverse biological changes in the eye or skin – is not exceeded. For this reason appropriate engineering, administrative and procedural controls, along with the use of Personnel Protective Equipment (PPE) are highly recommended. Laser hazards, laser standards and safety procedure are detailed in [80 - 83].
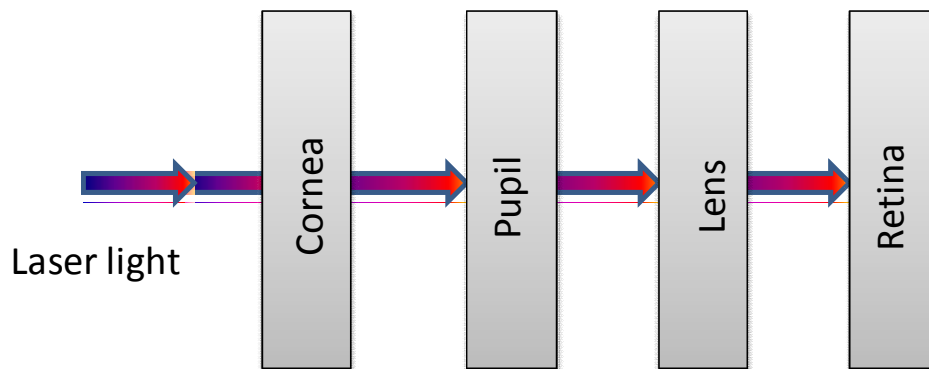
Figure 2-17: Schematic diagram of propagation of laser light through human eye.

2.8   Summary and Conclusion

Optical fibre (or waveguide) technology, at 850 nm and 1300 nm / 1550 nm for datacom and telecom respectively, has indeed complemented the data rate barriers of traditional copper transmission for LAN, WAN and MAN; its adaption to Very Short Reach (VSR) is thought to be needed for the bottlenecks facing the copper transmission at board-level. In this chapter, the author presented the need for OI for both intra- and inter-board

applications, such as for the backplane where this deployment is expected to take place due to prevailing limitations with electrical interconnection on the PCB despite the various rectifying measures being considered – e.g. minimizing conductor length, filtering and noise elimination, development of new dielectric substrate, etc. – used to overcome these problems Even though optical interconnection is necessary and essential to meet the current clock rates which is about to cross the limit of 10Gb/s, electrical connection is still expected to be used for a larger part of connections on a PCB where an optical link is only used when high data transfer rates are required. For successful implementation of OI at the board-level, three goals must be met viz:

- Material that would be compatible with PCB manufacturing procedure,
- Fabrication technique that would be easy, cost effective and efficient from the production point of view, and
- Material/waveguide that would satisfy the optical power budget requirement

A polymer-based waveguide is being favoured for this application for many reasons, among which is its compatibility with current PCB manufacturing conditions in terms of pressure, temperature and soldering process. In addition, polymer are considered to be readily available, tunable to meet certain features and cheap thus satisfying the need for a cost effective technique. Finally, the current available photopolymers have low absorption loss thus relaxing the power budget demand of OI. Multimode polymer waveguide, with core dimension > 9 µm, is the choice for optically-enabled PCB because, contrary to single mode, it would not pose any alignment issues and coupling loss. Additionally, losses due to attenuation and dispersion would be tolerable within the short distance of communication.

Current polymer waveguide fabrication techniques include photolithography, laser ablation, laser direct writing, hot embossing, milling and RIE. Although, the aforementioned techniques are well-established microfabrication techniques and are used in one way or the other during PCB manufacturing, however, the fact that laser ablation is currently being used for the drilling of µvias (for HDI) makes it much compatible and a cost effective alternative. Furthermore, for the fabrication of integrated mirrors, either in-plane or out-of-plane, laser ablation using an Excimer laser, for example, is a much suitable option for this due to its excellent laser matter interaction, resulting in clean removal at micro-level scales. In addition, the mask projection available with Excimer

laser material processing makes it possible for complex features to be easily defined. Excimer specifically KrF operating at 248 nm, has been widely adopted for this purpose. Although the cost and speed of Excimer laser could be an issue from the production point of view at this stage of the deployment, the author has proposed two alternative laser systems, namely UV Nd:YAG and CO2, that will supplement and complement the perceived 'deficiency/drawbacks' of an Excimer laser thus making laser ablation an all-encompassing technique meeting the production speed, cost, efficiency and quantity.

Finally, the author presented the laser-matter interaction with reference made to the bond-energies of common polymers – typically between 3 eV and 10 eV – and the photon energies available at different wavelengths in order to determine, for a particular polymer of a given bond energy, the laser wavelength at which either photochemical or photothermal ablation can be the mechanism of interaction. Having reviewed the various submissions on this, the author concludes that although polymers can be broken photochemically during laser ablation provided that the photon energy, a function of wavelength, of the laser beam is equal or greater than the bond energy of the polymer, this does not guarantee that such interaction at that given wavelength is purely photolytic. For example, if the photons available at the ablation zone are not totally used in bond breaking, the remaining would be left at the site of ablation and contribute to thermal effect; furthermore, the absorption characteristic and thermal-optical properties of the materials would play a part in determining the degree of each mechanism, and although waveguide fabrication using a photothermally-dominated mechanism can be relatively rougher than that of photochemically-processed materials, this does not mean that such waveguides would be lossy and/or that the technique is unsuitable; in fact, its contrary is proven in this work.

Reference

1. Levi, A. F. J. Optical interconnects in systems. *Proceedings of the IEEE* 88, 750-757 (2000).

2. Ahn, S., Cho, I., Han, S., Byoung Yoon, K. and Lee, M. Demonstration of high-speed transmission through waveguide-embedded optical backplane. *Optical engineering: the journal of the Society of Photo-optical Instrumentation Engineers.* 45, 85401 (2006).

3. Agarwal, D. Optical Interconnects to Silicon Chips using Short Pulses. Department of Electrical Engineering, Stanford University, PhD Thesis (2002).

4. Liu, Y. Investigation of Polymer Waveguides for Fully Embedded Board-level Optoelectronics Interconnects. University of Texas at Austin, PhD Thesis (2004).

5. Kivilahti, et al. WP1: Background – State-of-the-art. Helsinki University of Technology. [OHIDA – Technology Evaluation Report for Optical Interconnections and Enabling Technologies].

6. Glebov, A. L., Lee, M. G. and Yokouchi, K. Integration technologies for pluggable backplane optical interconnect systems. Optical engineering: the journal of the Society of Photo-optical Instrumentation Engineers. 46, 15403 (2007).

7. Windover, L. A. B. *et al.* Parallel-optical interconnects >100 gb/s. *J. Lightwave Technol.* 22, 2055-63 (2004).

8. Palais, J. C. in *Fiber optic communications* 441 (Prentice Hall, Upper Saddle River, N.J. ; London, 2005).

9. Van Steenberge, G., Geerinck, P., Van Put, S. and Van Daele, P. Integration of multimode waveguides and micromirror couplers in printed circuit boards using laser ablation. Proceedings of the SPIE - The International Society for Optical Engineering 5454, 75-84 (2004).

10. Meschede, D. in *Optics, light and lasers: the practical approach to modern aspects of photonics and laser physics* 430 (Wiley-VCH, Weinheim; Cambridge, 2003).

11. Savage, N. Linking with light. *IEEE Spectrum* 39, 32-36 (2002).

12. Uiga, E. in *Optoelectronics* (Prentice Hall, Englewood Cliffs, N.J., 1995).

13. Misselbrook, P. Novel manufacture of Out-of-Plane Optical Interconnects to Enable Low-Cost OECB substrates. Wolfson School of Mechanical and Manufacturing Engineering, Loughborough University, PhD Thesis (2006).

14. Holden, H. T. The developing technologies of integrated optical waveguides in printed circuits. Circuit World 29, 42-50 (2003).

15. Bockstaele, R., et al. A scalable parallel optical interconnect family. IO overview paper, April 2004.

16. Immonen, K.WP1 *Helsinki University of Technology* [OHIDA – Technology Evaluation Report for Optical Interconnections and Enabling Technologies].

17. Van Steenberge, G. et al. MT-compatible laser-ablated interconnections for optical printed circuit boards. *J. Lightwave Technol*. 22, 2083-90 (2004).

18. Dangel, R. *et al*. Development of a low-cost low-loss polymer waveguide technology for parallel optical interconnect applications. *Biophotonics/Optical Interconnects and VLSI Photonics/WBM Microcavities, 2004 Digest of the LEOS Summer Topical Meetings*, 2 pp. (2004).

19. Eldada, L. Polymer integrated optics: Promise vs. practicality. Proc SPIE Int Soc Opt Eng 4642, 11-22 (2002).

20. Halliday, D. and Resnick, R. in Fundamentals of physics (Wiley, 1970).

21. Theraja, B. L. in A text book of Electrical Technology; (Tech India Publications, New Delhi, 1962).

22. Al-Azzawi, A. in Light and optics: principles and practices 378 (Crc, Boca Raton, Fla.: London, 2007).

23. Hitz, C. B., Ewing, J. J., Hecht, J. and Hitz, C. B. in *Introduction to laser technology* (IEEE Press, New York, 2000).

24. King, R. et al. 2D VCSEL arrays for chip-level optical interconnects. *Proceedings of the SPIE - The International Society for Optical Engineering* 3632, 363-72 (1999).

25. Eitel, S. et al. Highly uniform vertical-cavity surface-emitting lasers integrated with microlens arrays. IEEE *Photonics Technology Letters* 12, 459-461 (2000).

26. Material Data Sheet [Accessed October 2008] : Available from : http://www.exxelis.com/products/Truemode-datasheet-f.pdf

27. Optical data transmission [Accessed November 2008]. Available from : http://www.rp-photonics.com/optical_data_transmission.html

28. Rho, B. S. et al. Low-crosstalk and high-efficiency optical interconnection using 45 deg -ended connection rods. Electron. Lett. 40, 730-2 (2004).

29. Hon, K.K.B, Li, L. and Hutchings, I.M. Direct writing technology – Advances and developments.

30. Naessens, K., Ottevaere, H., Van Daele, P. and Baets, R. Flexible fabrication of microlenses in polymer layers with Excimer laser ablation. Appl. Surf. Sci. 208, 159-164 (2003).

31. A.L. Glebov, J. Roman, M.G. Lee and K. Yokouchi. Optical interconnect modules with fully integrated reflector mirrors. *Photonics Technology Letters*, IEEE 17, 1540-1542 (2005).

32. Griese, E. A high-performance hybrid electrical-optical interconnection technology for high-speed electronic systems. *Advanced Packaging, IEEE Transactions on* 24, 375-383 (2001).

33. Immonen, M., Karppinen, M. and Kivilahti, J. K. Fabrication and characterization of polymer optical waveguides with integrated micromirrors for three-dimensional board-level optical interconnects. *Electronics Packaging Manufacturing, IEEE Transactions on* 28, 304-311 (2005).

34. Krabe, D., Ebling, F., Arndt-Staufenbiel, N., Lang, G. and Scheel, W. New technology for electrical/optical systems on module and board level: the EOCB approach. *Electronic Components and Technology Conference, 2000. 2000 Proceedings. 50th*, 970-974 (2000).

35. Lunitz, B., Guttmann, J., Huber, H. -. Moisel, J. and Rode, M. Experimental demonstration of 2.5 Gbit/s transmissions with 1 m polymer optical backplane. Electronics Letters 37, 1079 (2001).

36. Mederer, F. *et al*. 3-Gb/s data transmission with GaAs VCSELs over PCB integrated polymer waveguides. *Photonics Technology Letters, IEEE* 13, 1032-1034 (2001).

37. Kopetz, S., Rabe, E., Kang, W. and Neyer, A. Polysiloxane optical waveguide layer integrated in printed circuit board. *Electron. Lett.* 40, 668-669 (2004).

38. Enbutsu, K. *et al*. Multimode Optical Waveguide Fabricated by UV Cured Epoxy Resin for Optical Interconnection. *APCC OECC -Proceedings-*, 1648-1651 (1999).

39. Yoon, K. B. *et al*. Optical backplane system using waveguide-embedded PCBs and optical slots. *J. Lightwave Technol.* 22, 2119-2127 (2004).

40. Chuang, W.-C, Ho, C.-T and Shyu, R.-F A New Method to Fabricate Polymer Waveguides, in Progress In Electromagnetic Research Symposium 2005, Hangzhou, China, August 22-26.

41. Snakenborg, D., Perozziello, G., Klank, H., Geschke, O. and Kutter, J. Direct milling and casting of polymer-based optical waveguides for improved transparency in the visible range. *J Micromech Microengineering* 16, 375-381 (2006).

42. C. Cornic, B. Lucas, A. Moliton, B. Colombeau, and R. Mercier. Elaboration and characterization of a 6FDA/MPDA polyimide-based optical waveguide. Synthetic Metals, 127(1–3):299–302, March 2002.

43. S. Ponoth, Peter D. Persans, Ram Ghoshal, N. Agarwal, Joel L. Plawsky, A. Filin, and Q. Z. Fang. Siloxane-based polymer epoxies for optical waveguides. In *Proceedings of SPIE Applications of Photonic Technology* 6, volume 5260, pages 331–335, 2003.

44. Diemeer, M. B. J., F. M. M. Suyten, E. S. Tromml, A. McDonach, J. M. Copeland, L. W. Jenneskens and W. H. G. Horsthuis, Electron. Lett. Vol. 26, 379, 1990.

45. Kang, Jae-Wook, Jang-Joo Kim, Jinkyu Kim, Xiangdan Li, Myong-Hoon Lee, ―Low-loss and Thermally Stable TE-mode Selective Polymer Waveguide Using Photosensitive Fluorinated Polyimide, Photonics Technology Letter," IEEE, Volume: 14, Issue: 9, 1297-1299, Sep. 2002.

46. Usui, M. *et al*. Low-Loss Passive Polymer Optical Waveguides with High Environmental Stability. *Journal of lightwave technology: a joint IEEE/OSA publication.* 14, 2338 (1996).

47. Booth, B. L., Low Loss Channel Waveguides in Polymers, J. Lightware Technol., Vol. 7, 1445-1453, 1989.

48. Ferm, Paul M. and Lawrence W. Shackjette, High Volume Manufacturing of Polymer Waveguides via UV-Embossing, SPIE, Vol. 4106, 1-10, 2000.

49. Andrews, D. L. in *Lasers in chemistry* (Springer-Verlag, New York; London, 1997).

50. Ion, J. C. in *Laser processing of engineering materials: principles, procedure and industrial application* 556 (Elsevier Butterworth-Heinemann, Oxford, 2005).

51. Basting, D. Excimer Laser Technology. , 451 (2005).

52. Steen, W. M. in Laser material processing (Springer, London, 2003).

53. R. Crafer and P.J. Oakley, ―Laser Processing in Manufacturing. London : Chapman and Hall, 1993, pp.292

54. Pedrotti, F. L., Pedrotti, L. M. and Pedrotti, L. S. in *Introduction to optics* 622 (Pearson Prentice Hall, Upper Saddle River, N.J., 2007).

55. "HY120 beam shaper foe Excimer Lasers" [Accessed October 2008]. Available from: http://www.optec.be/pdf/technote_ra06.pdf.

56. Thomas, D. W. Surface modification of polymers and ceramics induced by Excimer laser radiation. *Laser Ablation of Electronic Materials* 4, 221-228 (1992).

57. Meijer, J. Laser beam machining (LBM), state of the art and new opportunities. Journal of Materials Processing Technology 149 (2004) 2-17

58. Rumsby, P. T. and Gower, M. C. Excimer laser projector for microelectronics applications. Proc SPIE Int Soc Opt Eng 1598, 36-45 (1991).

59. Yung, W. K. C., Liu, J. S., Man, H. C. and Yue, T. M. 355 nm Nd:YAG laser ablation

of polyimide and its thermal effect. J. *Mater. Process. Technol.* 101, 306-311 (2000).

60. Shin, B. S., Oh, J. Y. and Sohn, H. Theoretical and experimental investigations into laser ablation of polyimide and copper films with 355-nm Nd:YVO4 laser. J. *Mater. Process. Technol.* 187-188, 260-263 (2007).

61. Illy, E. K., Piper, J. A., Brown, D. J. W. and Withford, M. J. Enhanced polymer ablation rates using high-repetition-rate ultraviolet lasers. *IEEE Journal on Selected Topics in Quantum Electronics* 5, 1543-1548 (1999).

62. Balint Balogh, Peter Gordon and Balint Sinkovics. Description of 355 nm Laser Ablation of Polyimide as a Thermal Process. *Electronics System integration Technology Conference*, 2006. 1st 1, 360-364 (2006).

63. Li, J. and Ananthasuresh, G. K. A quality study on the Excimer laser micromachining of electro-thermal-compliant micro devices. *Journal of micromechanics and microengineering: structures, devices, and systems.* 11, 38-47 (2001).

64. Burns, F. C.; Cain, Stephen R. 15. The effect of pulse repetition rate on laser ablation of polyimide and polymethylmethacrylate-based polymers. *Journal of Physics D: Applied Physics*, Volume 29, Issue 5, pp. 1349-1355 (1996).

65. Mark, J. E., Allcock, H. R. and West, R. Inorganic Polymers. , 353 (2005).

66. DeGroot, J., Norris, A., Glover, S. and Clapp, T. Highly transparent silicone materials. *Linear and Nonlinear Optics of Organic Materials IV* 5517, 116-123 (2004).

67. Meijer, J. Laser Micromachining, pp. 203-237 in Micromachining of Engineering Materials, Ed. Joseph McGeough, 0-8247-0644-7, Marcel Dekker, Inc., January, 2002.

68. Chen, Y., Ma, K., Zhou, J. G. and Tseng, A. A. Excimer laser ablation of glass-based arrayed microstructures for biomedical, mechanical, and optical applications. *J. Laser Appl.* 17, 38-46 (2005).

69. Zhao, Q. *et al*. Development of Wide Bandgap Semiconductor Photonic Device Structures by Excimer Laser Micromachining. *Mater. Res. Soc. Symp. Proc.* 595, W11.69.1-W11.70.0 (2000).

70. Chen, Y., Naessens, K., Baets, R., Liao, Y. and Tseng, A. Ablation of transparent materials using Excimer lasers for photonic applications. *Optical Review* 12, 427-441 (2005).

71. X.Chen, X. Liu, Short pulsed laser machining: how short is short enough? *J. Laser Appl.* 11 (6) (1999) 268-272.

72. Ihlemann, J., Excimer laser micro machining of inorganic dielectric. *Applied Surface Science* 106 (1996) 282-286.

73. Chan, K. F. et al. Free electron laser ablation of urinary calculi: An experimental study. *IEEE Journal on Selected Topics in Quantum Electronics* 7, 1022-1033 (2001).

74. Pfleging, W. Excimer laser material processing – state of the art and new approaches in microsystem technology *Proc of SPIE* Vol 6107 (2006).

75. Zeng, D. W., Yung, K. C. and Xie, C. S. UV Nd:YAG laser ablation of copper: chemical states in both crater and halo studied by XPS. *Appl. Surf. Sci.* 217, 170-180 (2003).

76. O'Connor, G. M., Glynn, T. J., Howard, H. and Conneely, A. J. Analysis of debris generated during UV laser micro-machining of silicon. *Proc SPIE Int Soc Opt Eng* 5339, 241-249 (2004).

77. Shin, D. S., Lee, J. H., Suh, J. and Kim, T. H. Determination of the debris produced from poly (ethylene terephthalate) during KrF Excimer laser ablation. *Applied surface science.* 252, 2319 (2006).

78. Henderson, A. R. in *A guide to laser safety* (Chapman and Hall, London, 1997).

79. B. Bodil, Materials patterning with Excimer laser ablation, in special issue laser Processing of Materials, *Optics and Photonic News,* Optical Society of America, June 1992, pp. 20-23

80. Liu, Y. S., Cole, H. S. and Guida, R. Laser ablation of polymers for high-density interconnect. *Microelectronic Engineering. Vol. 20* 20, 15-29 (1993).

81. Laser Institute America. in *American National Standard for Safe Use of Lasers in Educational Institutions* 44 (Laser Institute of America, Olando, USA, 2000).

82. Barat, K. in *Laser safety management* 267 (CRC/Taylor and Francis, Boca Raton, Fla., 2006).

83. Laser Institute of America. in *LIA handbook of laser materials processing* (eds Ready, J. F. and Farson, D. F.) 715 (Laser Institute of America, Orlando, Fla., 2001).

3   METHODOLOGY, EXPERIMENTAL DESIGN, PROCEDURE AND MEASUREMENT

3.1   Methodology

In the two preceding chapters, efforts were made to present the research problems and possible solution to the bandwidth-limited copper transmission. The current chapter is devoted to the methods and procedures devised to address the research goals which include laser system choice, optical polymer preparation, waveguide fabrication and measurement.

It is evident that the laser and optical polymer choice is of great importance for polymer waveguide fabrication using laser ablation. It followed from this literature survey that the Excimer laser has largely been favoured as the sole candidate for this technology, i.e. laser ablation of optical waveguide, while the suitable polymer materials were selected based on their optical properties, e.g. absorption loss and compatibility with the PCB manufacturing. Considering these facts, the author's initial stage of research was, mainly, concentrated on the use of Excimer laser for both waveguide and integrated mirror fabrication. However, since the technology under investigation was a product-oriented research that would require mass production in a typical PCB industry, there is therefore a necessity to provide a means through which this high volume production can be accomplished with a minimum possible cost. It was for this reason that the attention was shifted, or better still extended to the use of both UV Nd:YAG and CO_2 lasers; both of which are key tools in laser processing of PCB materials.

The main optical material, Truemode™, used in the project was supplied by a partner to this consortium. This was demonstrated to satisfy the properties required of any optical polymer, in fact its supplier showed its successful use for photolithographically-fabricated waveguides. Furthermore, it is gathered from the literature that Truemode™ has also been used for laser ablation of optical polymer waveguides. The supply of this material was not underway until the second quarter in the first year of the collaboration. For this period, the author relied on the use of PMMA which is cheap and readily available at the site where the major work of the research reported here was carried out, i.e. at Loughborough University. The use of PMMA subsequently became the means by which preliminary test or feasibility study was conducted during the course of the project which proved to be economical; in

other words, PMMA was largely utilised not during the initial investigation on Excimer laser but also, and more importantly, during the trials carried out with both UV Nd:YAG and CO_2 lasers as both were new for this technology. It is worth while mentioning here that, at a later part of the collaboration, another optical polymer – polysiloxane-based polymer – was also made available, however, due to the time constraints, this could not be significantly investigated.

3.2   Laser System

To achieve the research goals (section 1.3), careful appraisal of different laser systems and their capabilities was essential and challenging. Following thorough research evaluation, three laser candidates were identified with various achievable tasks projected for each of them (Figure 3.1). The choice of investigation was primarily based on laser system capability in-line with the existing reports and the trends in research. For instance, 2D embedded mirror fabrication was limited to the Excimer laser system mainly because: (i) the current design of Excimer laser could easily accommodate system modification required by this design, and (ii) the ablation with this laser is a photochemically-dominated process and thought to be smoother compared to other choices. However, the same goal could be achieved by employing any of the two systems used in this thesis and perhaps others not investigated here, provided that the flexibility of laser scanning/machining could be achieved and the process can be optimised or the system customised in order to achieve a smooth finish on the mirror.

With the constraints in the current designs of other systems in mind, the author investigated the use of UV-source Excimer laser machining which offered highly flexible processing capabilities especially for integrated mirror fabrication though at the expense of speed and cost. Furthermore, 355 nm UV Nd:YAG was also tried as this has the capability of the pulse energy and pulse duration that characterise the minimum HAZ associated with Excimer in order to broaden the potential application of the technology contained in this research. To complete this investigation, an infrared laser source, namely 10.6 µm CO_2 was used which, to an unprecedented expectation, was found to be capable of producing optical waveguides as will be shown later in the thesis. The CO_2 laser used, unlike the two other lasers, not only operates in the IR but is also a CW mode.
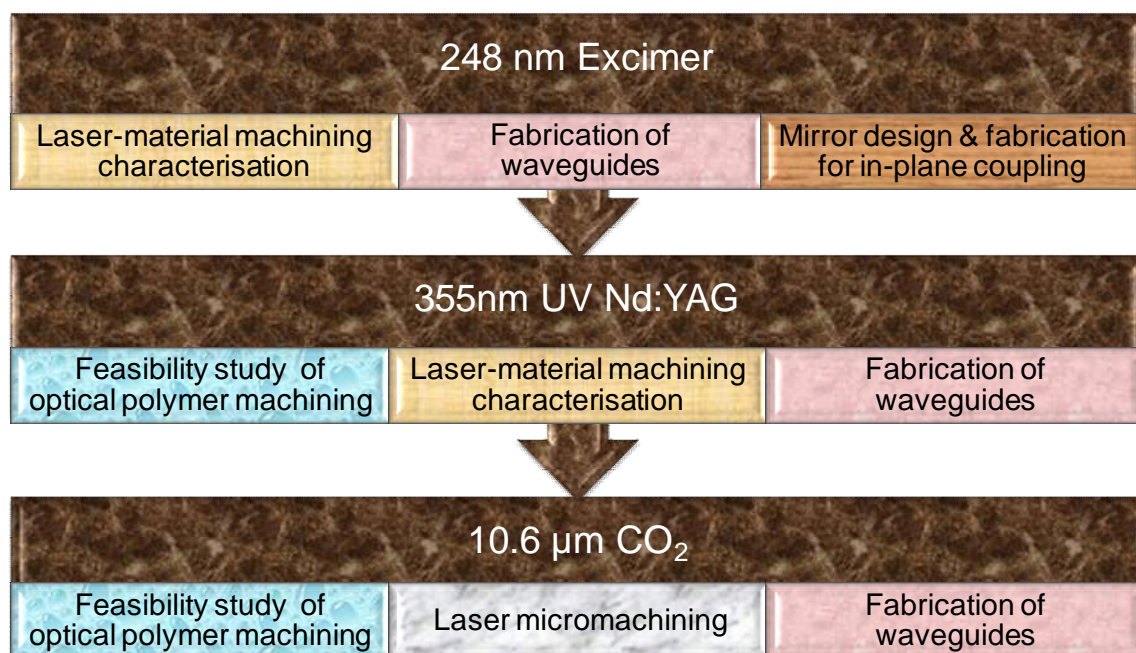
Figure 3-1: Overview of laser system and experimental activities for low cost optical polymer waveguide fabrication.

3.3 System Characterisation

System characterisation was highly essential in understanding the laser-material interactions that characterise each laser system; this was primarily required in order to be able to control the depth to which ablation into the optical polymer layer was to terminate and ensuring that the etching was not into the FR4 substrate layer. This latter point was important because ablation at the optical polymer-FR4 substrate interface accompanies a huge 'jump' in ablation threshold causing not only thermal damage and debris but also involves unnecessary energy/power input as much more energy or fluence is required to ablate an FR4 substrate.

The main factors investigated depended on the individual laser system and included: PRF, laser power/energy, fluence, number of pulses, beam width, number of passes, translation stage speed and laser scanning speed, all in relation to both depth and quality of fabrication. System characterisation (looking at the effect of fluence, power, etc. on the etch rate) was achieved on both Excimer and UV Nd:YAG lasers with a feasibility study preceding the latter as shown in figure 3.1, to establish its suitability, as little literature was available regarding UV Nd:YAG optical waveguide fabrication. Although CO_2 laser is currently used

for drilling of vias, a feasibility study was also necessary and thus carried out to ascertain its suitability for optical waveguide fabrication which was followed with a successful fabrication of polymer waveguides, making it a novel achievement. As a result of the study conducted, extensive information emerged providing trade-offs among the three main lasers used in PCB assembly, a prerequisite for the deployment of the technology in the targeted industry without incurring additional cost in the process.

3.4   Waveguide Fabrication

The stages or processes involved in laser ablation of a polymer waveguide as employed in this research are shown in (Figures 3.2 and 3.3). A single layer of waveguide fabrication was the focus of research as this is currently enough to provide the data rate requirements for OI; future work could extend these processes to multiple layers of waveguides.
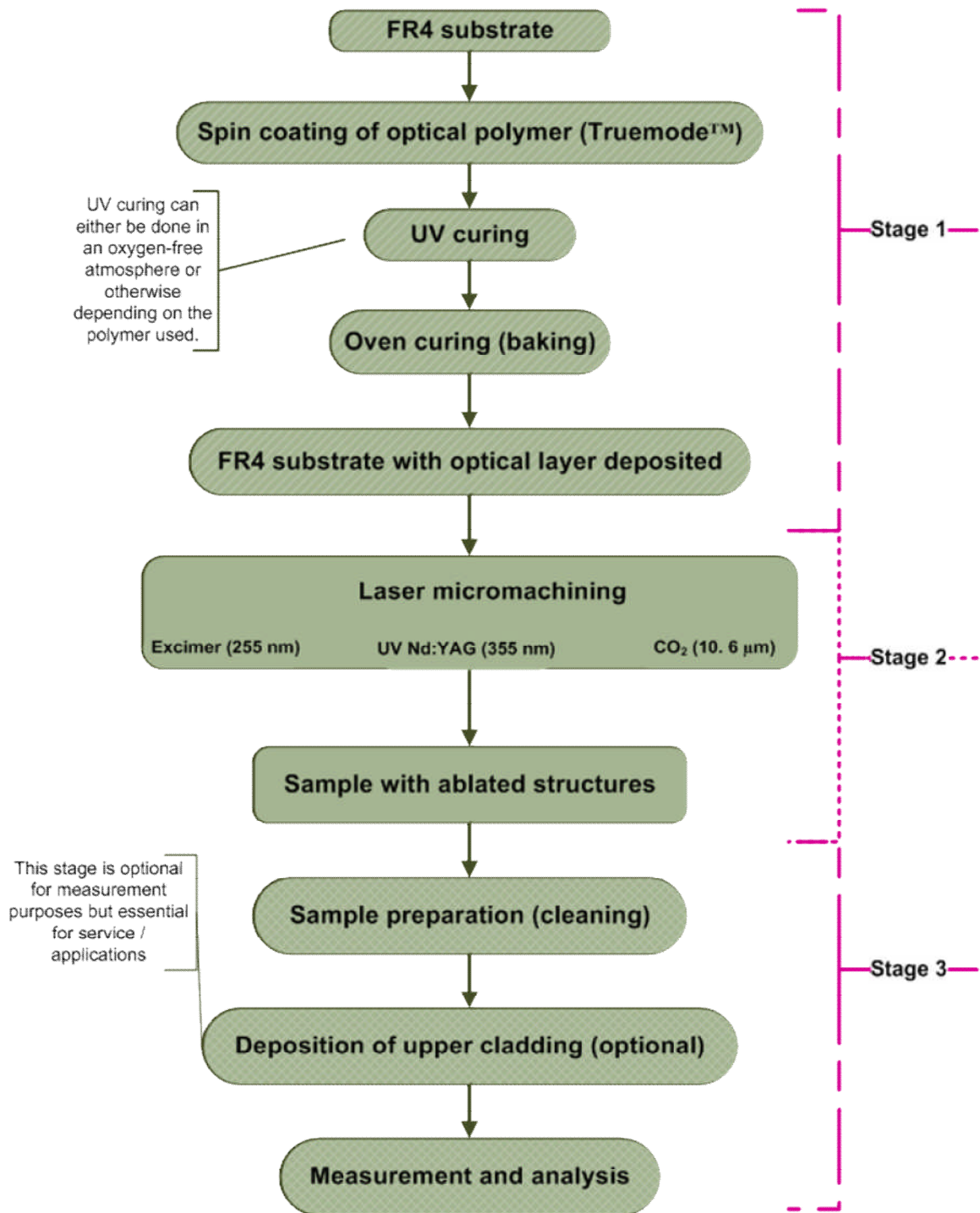
Figure 3-2: Flow diagram of the processes involved in patterning optical polymer waveguides using laser ablation.

3.4.1 Single-layer fabrication process

The process involved in the fabrication of a single-layer optical waveguide can be divided, for simplicity, into three main stages as represented in figures 3.2 and 3.3. They are:

1. Deposition of optical polymer on FR4 laminates to form both the lower cladding and core layers, achieved by spin coating. The core layer thickness should be the same as the final height of the waveguide; while the cladding layer should be made thick enough for support and to ensure that signals are completely contained by total internal reflection. For instance, 20 µm lower cladding has been used for a multimode waveguide of 50 µm by 50 µm primarily to keep the optical layer thickness minimal, but that was at the expense of a propagation loss as asserted by the author of [1].

2. Laser ablation of grooves in the core layer to purposely leave a ridge of polymer in-between which represents the waveguide channel. Typical dimensions are 50 µm x 50 µm, 50 µm x 70 µm and 70 µm x 70 µm for multimode waveguides, but other dimensions such as 40 µm x 45 µm [2] and 35 µm x 35 µm [3] have been reported. The material removal process (ablation) is continued to penetrate beyond the core layer in to the lower cladding to ensure that the light signal is completely contained in the core by TIR.

3. The last stage is to deposit another layer of clad known as the upper cladding. This is to ensure that TIR is achieved. For measuring purposes, this stage is not vital because the surrounding air is of lower RI, typically 1, and can thus serve as an upper cladding layer, however without protection the core/air interface could become contaminated or damaged in service leading to optical losses.
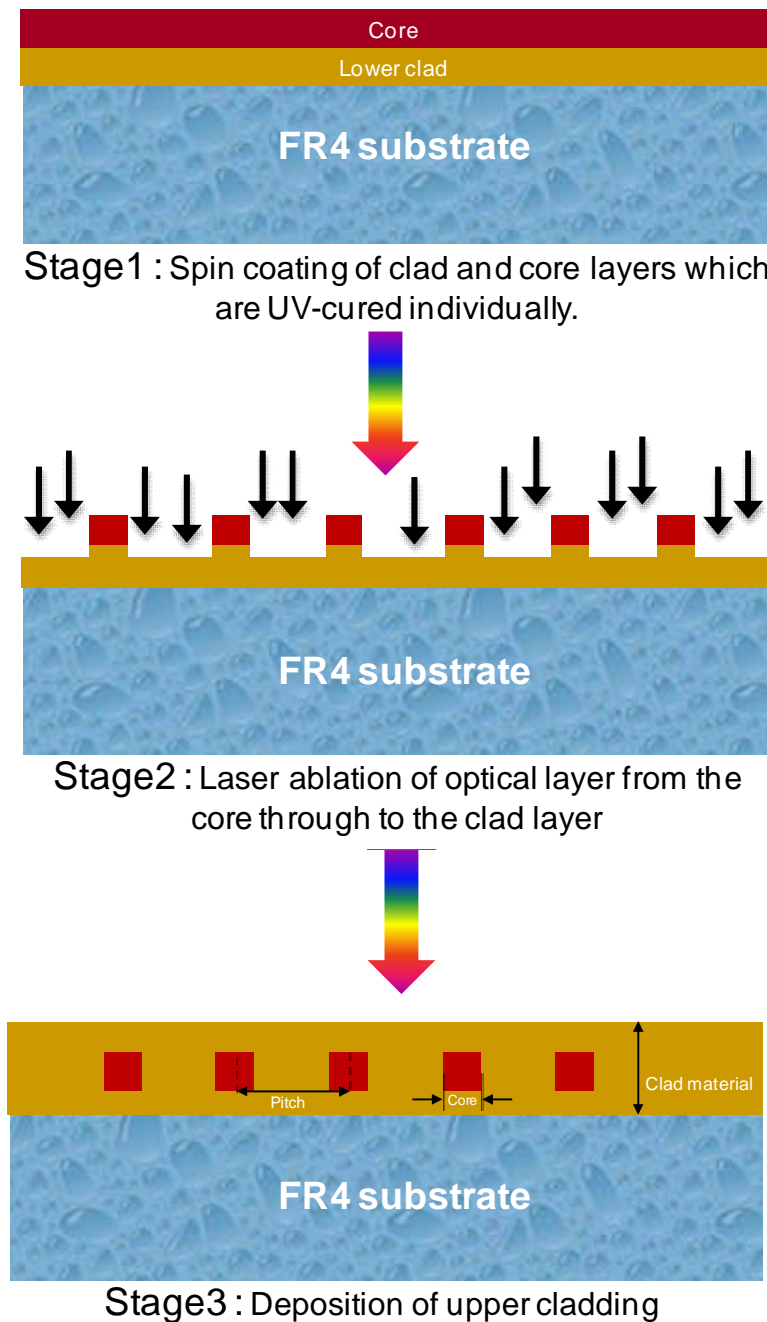
Figure 3-3: Schematic diagram (side view) of the three major stages in the fabrication of optical waveguides by laser ablation.

3.4.2   *Optical density (OD)*

OD, as used in this thesis, refers to the concentration of optical channels within an area of the substrate, while waveguide pitch is the distance between two adjacent waveguides measured from the centre of one waveguide to the centre of the next adjacent waveguide. In the future, more optical channels would be required if the technology should be efficiently

used especially in HDI provided that it is not at the expense of loss due to crosstalk. The value of the waveguide 'pitch' has direct or indirect effects on the losses due to crosstalk as does OD. Therefore, OD was considered in the design of experiments, and to achieve this, one, two, three, and up to ten adjacent optical waveguide were fabricated; figure 3.4 is an example of three waveguides formed by machining four channels adjacent to one another.
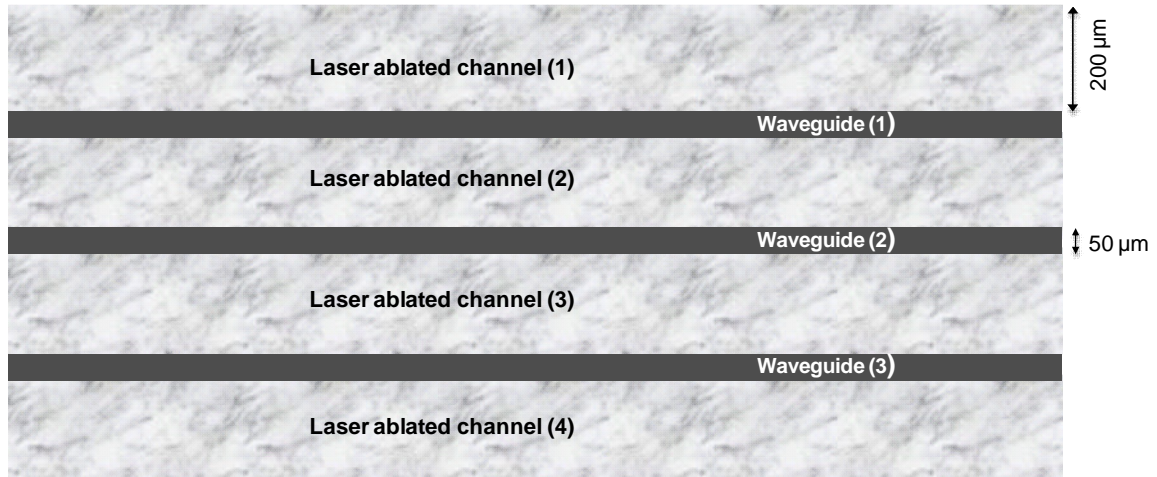
Figure 3-4: Schematic diagram showing experiment design
for a three-channel waveguide.

3.5   Optical Polymer Materials

The two main polymers of choice in this research were Truemode^{TM} and polysiloxane-based photopolymer (OE4140 and OE 4141) manufactured by Exxelis, UK and Dow Corning, USA, respectively. Both of these companies were partners to the OPCB project. While Truemode™ was the main focus of this research; polysiloxane-based polymer was also partially investigated as the latter became available at a later stage in the project when its manufacturer joined the consortium. The author also investigated the use of PMMA at the initial stage of the research for Excimer laser characterisation, the result of which is reported in chapter 6. A brief description of Truemode™ and polysiloxane-based optical polymers is given below.

3.5.1   Truemode™ optical polymer

Truemode™ is the product of Exxelis previously owned by Terahertz Photonics Edinburgh, UK – a spinout of Heriot-Watt University. It is a UV-curable mixture of acrylate and methacrylate monomers that is liquid at room temperature and pressure. It is a light yellow

(or orange) colour material which is insoluble in water. Table 3.1 shows some of the optical, thermal and electrical properties of this organic polymer. The fact that its absorption loss is very low with a typical value of < 0.04 dB/cm @ 850 nm datacom wavelength, a controllable RI for clad-core, and its compatibility with current PCB fabrication processes makes it an excellent choice for VSR interconnections. In this project, three different formulations of Truemode™ were investigated. They were:

1. Formulation 1 : LB-clad 520 and LB-core 561
2. Formulation 2 : EXX-clad 277 and EXX-core 37E
3. Formulation 3 : EXX-TM clad and EXX-TM core

These formulations were based on different monomer compositions and photoinitiator; however, the fundamental difference in these formulations lies in their viscosity. Moreover, it was observed that these three formulations have different UV curing time with formulation 1 and formulation 3 having the least and highest curing durations respectively. The author also noticed that their behaviour to laser radiation was not the same. Following careful assessment and to be consistent during the process of experimentation, Truemode™ formulation 2 was chosen as the sole candidate to be employed for the research, thus, any subsequent experimental results of Truemode™ are based on formulation 2 except if otherwise mentioned.

Table 3-1: Some key properties of Truemode™ optical polymer [4].

Properties		
Waveguide loss (dB/cm)	<0.04 @ 850 nm	<0.4 @1300 nm
RI		1.45 – 1.58
Thermo-optic coefficient		$-2.2 \times 10^{-4}\ ^{0}C^{-1}$
Coefficient of thermal expansion		60 ppm $^{0}C^{-1}$
Thermal conductivity		0.21 W/mK
Glass transition temperature		150 ^{0}C
Decomposition temperature		350 ^{0}C

3.5.2 Polysiloxane photopolymer

The polysiloxane used in this work, sometimes called siloxane or silicone, is a product of

Dow Corning, USA. Siloxane is an established organic-inorganic polymer suitable for telecommunication and photonic applications due to its excellent optical properties, and thermo-mechanical stability which can be tuned by changing the constituents of the molecule. For example, the ratio of methyl to phenyl group in a given silicone is a key to RI control typically in the range of 1.4 to 1.6. Furthermore, the polymer is very hydrophobic with low moisture absorption – an essential property for optical-PCB applications. The structural formula of polysiloxane is based on Si-O-Si bonds, for example polydialkylsiloxane, the most common silicone family, has a structural representation of $(R_2SiO)_n$. [5 - 8]. The photopolymer material used in this project was coded as OE4140 and OE 4141 for clad and core respectively. Samples of this polymer were obtained from Dow Corning after being processed. In other words, the samples were received as optical polymer layers of core on clad on FR4 substrate without needing to undergo stage 1 of figure 3.3. Unlike Truemode™, the OE4140 and OE 4141 polymer does not require an oxygen-free atmosphere for the curing process; additionally, pre-baking is essential for this photopolymer in order to remove the solvent, Toluene in this case.

3.6 Deposition of Optical Polymer

To form the optical layers of the samples utilised in this project, i.e. clad and core, there are essentially two main processes involved: spin coating and curing of the material. Figure 3.5 is an overview of the stages involved in patterning an appropriate thickness of clad and core of Truemode™ polymer on an FR4 substrate in order to form a single-layer optical channel, though the flow diagram could be extended to accommodate any number of multilayer optical channels if needed.
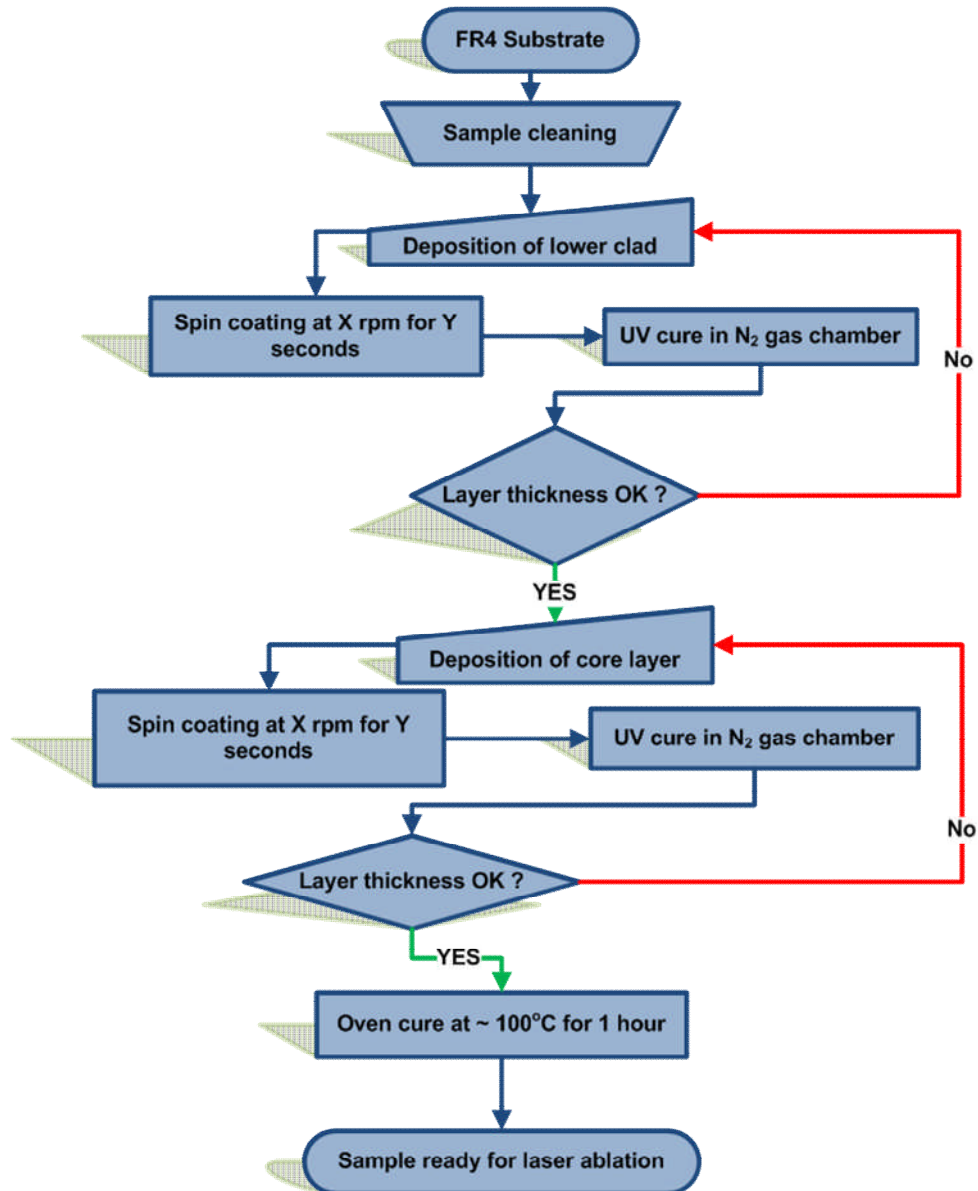
Figure 3-5: Schematic flow diagram showing experimental procedure for depositing Truemode™ (core and clad) on FR4 substrate.

3.6.1   Spin coating

The spin coating process relies on the centrifugal force to spread the material evenly over the surface. It is thought to be governed by both fluid flow and evaporation; although the latter factor is only important where the polymer contains some solvent component such as toluene in polysiloxane as previously mentioned. During the spin-coating process, the fluid flow dominates the early stage, while evaporation dominates the later stage. The final thickness of the resulting layer depends on a number of factors such as the speed of rotation,

duration of spinning, viscosity of the material, solvent evaporation and density among others. There are many models relating to the final thickness on some of the above factors [9 - 12]. By and large, the final thickness and uniformity has more to do with experimentation and optimisation of the process rather than relying on a mathematical model, thus, for this reason, a study into this relationship was carried out for Truemode™.

Prior to polymer deposition, FR4 samples were normally cleaned in methanol, either by immersing the sample into a beaker of methanol and then washing it with water or by spraying methanol onto the sample and then rinsing with water, to remove mirco-particles from the substrate surface which if not considered could mar the uniformity of the layers deposited forming bubbles or bubble-like spots on the surface. Once cleaned, samples were dried in an oven at $80\,^{o}C$ – $100\,^{o}C$ for about 1 min. to ensure they were moisture-free.

During spin coating, a square or rectangular sample – 6 cm square, 8 cm square and 6 cm x 8 cm were normally used – of FR4 substrate was placed on a motor-driven vacuum chuck to secure it in position. The liquid optical polymer (core or clad) was centrally dispensed onto the FR4 substrate using either a pipette or syringe. Usually, to ensure total coverage of the substrate, an excess solution of the material was employed. For example, a 6 cm square FR4 sample would require 2 ml (approx.) of polymer, however, visual examination was highly essential in every case to ensure the final coverage. Having dispensed the polymer, the whole specimen was then accelerated to the desired spin speed.

The two main factors that could be easily controlled during spin coating of the samples used in this project were the speed of spinning, measured in revolution per minute (rpm), and the duration of spinning, measured in seconds. Therefore, to establish how these two factors related to the final thickness of the optical layer, optical polymer deposition of Truemode™ was carried out at speeds between 200 rpm – 1000 rpm for both clad and core for a duration of 30 seconds which they were cured. Figures 3.6 and 3.7 are graphical relationships between the spin speed and layer thickness for core and clad respectively; in both cases, the slope of the curves becomes smaller from left to right. This means that thick layers were achievable at low spin speed; however, observations revealed that this was at the expense of uniformity of the layer which varied in thickness from the centre to the edge of the sample. It therefore became important to spin at higher speeds to avoid such non-uniform coatings. At this stage, it is worth noting the following:

1. The measurement of the samples was carried out by employing the dicing-potting-polishing process as would be explained later in the chapter. This was to make sure that measurement was taken to reflect the actual thickness of each layer determined visually by the optical (or colour) change in the layers as evident in figure 3.8.

2. Although the thickness was not expected to be uniform across the entire area of a sample, a significant uniform area was achievable at the middle of any coating. Therefore, measured samples were those obtained by dicing through (or close to) the middle part on any spun substrate.

3. Since Truemode™ optical polymer was received in batches from Exxelis, the author noticed that there were some discrepancies in the results. In other words, results from the characterisation might and might not agree with a new batch of polymer. In such case(s), the following approaches/considerations were made: (a) with new batches a few trials were conducted and compared with the results of the characterisation and then an offset applied as per the new data values, and (b) more importantly, a special request was made to Exxelis that a sufficient volume of the polymer be made available in a single batch in order to allow for consistency in the results not only during deposition but also in the course of ablation.

4. This investigation was also tried at other spin times namely 45 seconds and 60 seconds but the effect of time was not found to be significant over this range.
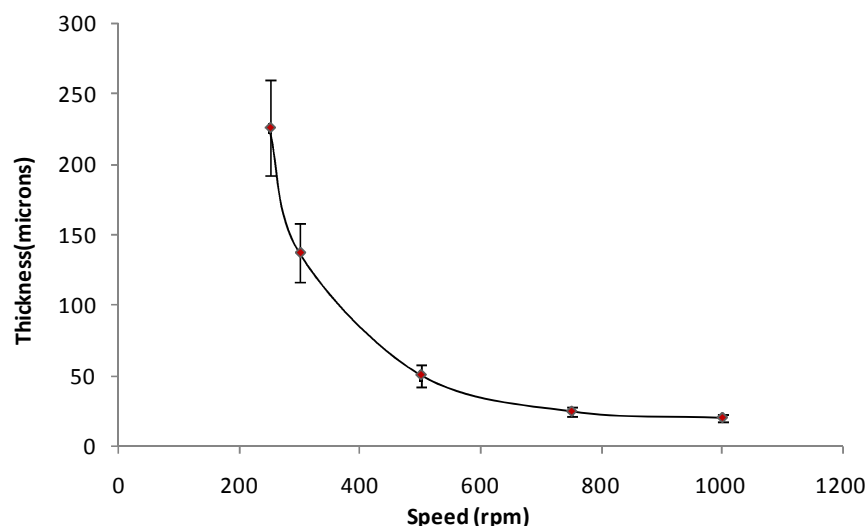
Figure 3-6: Graphical representation of the relationship between speed of spinning and thickness of coating for Truemode™ core polymer material.
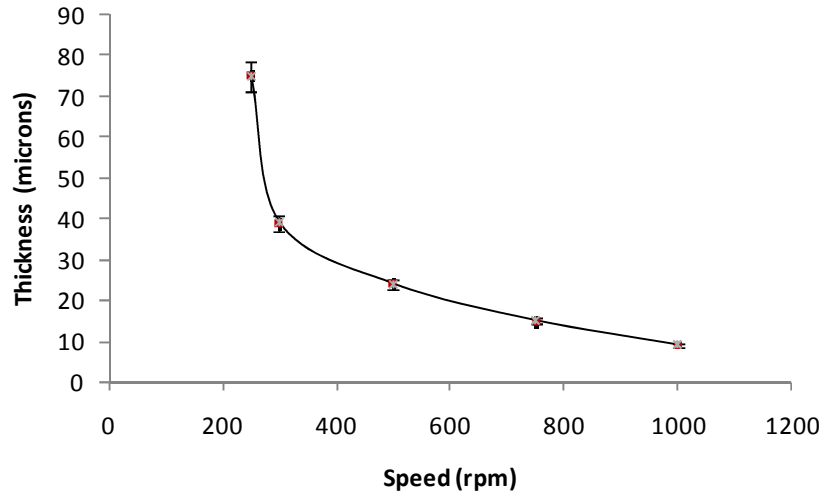
Figure 3-7: Graphical representation of the relationship between the speed of spinning and the thickness for Truemode™ clad polymer material.
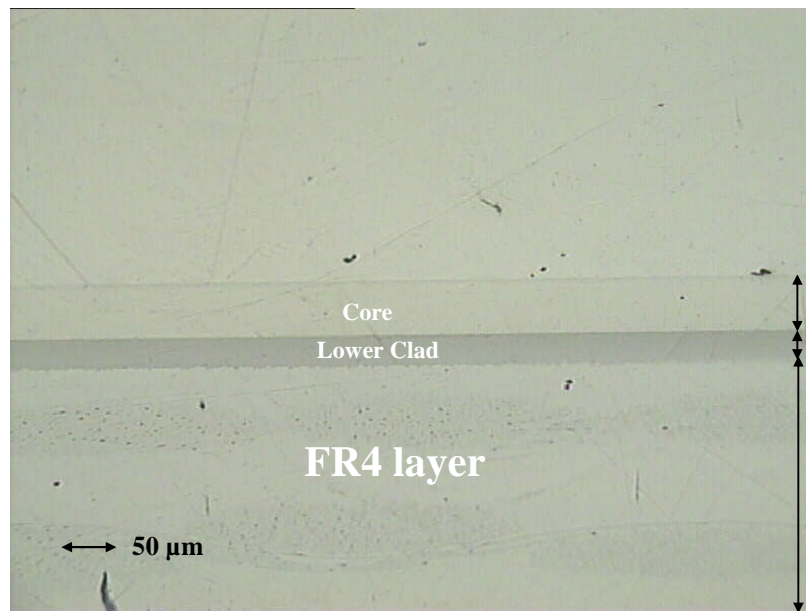
Figure 3-8: Diagram showing layers of Truemode™ spin-coated at 500 rpm for 30 seconds.

3.6.2 UV curing

UV curing is a widely-used mechanism for processing polymers. Unlike IR radiation, Microwave and RF wave curing systems, UV curing is a non-thermal process based on crosslinking the molecules of the polymer brought about by the presence of a photoinitiator, also known as a photosensitizer or photosynergist. This photoinitiator is usually mixed

during the preparation stage of the polymer and constitutes 2 – 15 % by volume of the formulation [13, 14].

UV curing of Truemode™ requires an oxygen-free nitrogen atmosphere. For this reason, an oxygen analyzer was employed to monitor and indicate the composition by volume of oxygen in the exposure chamber in parts per million (ppm). As shown in figure 3.9, the setup consisted, essentially, of three components: (i) a nitrogen gas bottle, (ii) UV curing chamber with sample placed inside, and (iii) an oxygen analyser. Both the gas bottle and the oxygen analyser were 'linked' to the UV chamber by separate tubes with nitrogen fed into the chamber from the gas bottle and a sample of the atmosphere taken from the chamber into the analyser. The UV curing process was only initiated when the oxygen indicator showed 80 parts per million (ppm) of oxygen and run for 200 - 250 seconds for both clad and core.

After UV curing, the sample was placed in an oven to bake the optical layer in order to complete the curing process. This was performed at ~100°C for one hour. It should be noted that for samples where oxygen-free nitrogen atmosphere is not a condition, e.g. polysiloxane-based polymer, only the UV chamber is required as a component of the setup.
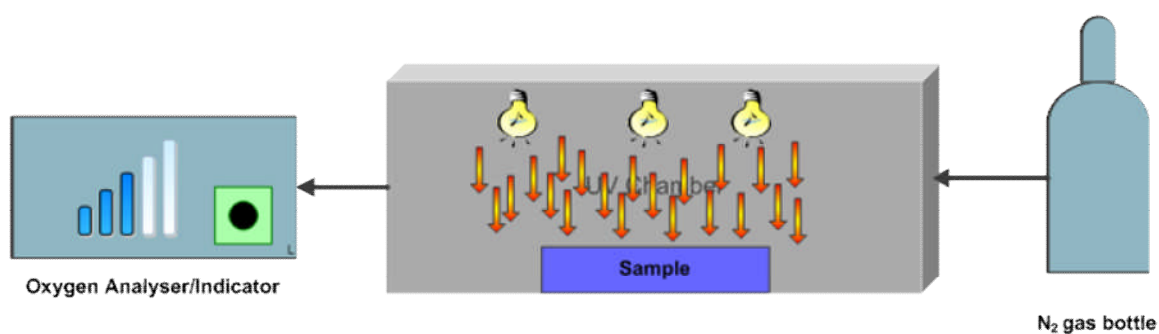
Figure 3-9: Schematic diagram showing UV curing setup.

3.6.3   Challenges with optical polymer deposition

There were some challenges faced with the deposition of photopolymer on FR4; the main problem had to do with its adhesion and could be grouped into two areas:

1. **Adhesion between the optical layers**

This is a situation when there was a delamination between the clad and core layers or sometimes between two core layers. The latter (i.e. delamination between two core layers) occurred because for example, to obtain a uniform thickness of 70 µm of the core layer polymer would be deposited as two layers by spinning at a higher revolution ~700 rpm twice in succession with UV curing in between. Figures 3.10 a and 3.10 b show such cases where delamination occurred between two different optical layers of Truemode™ polymer.

Following consultation with Exxelis (and also partly with Dow Corning), this problem was addressed and overcome by ensuring that: (i) The FR4 substrate was prebaked for a minute to remove any moisture that might have been introduced during sample cleaning with methanol, (ii) that samples were prevented from dust contamination; for instance, when the clad was spun and UV-cured, it was ensured that no contamination was introduced which could form point(s) of detachment. This is easily avoidable if the process were to be undertaken in a clean room; and (iii) in the case of delamination between two different core layers, the first deposited layer was partially cured for a shorter duration, say 100 seconds as against 200 – 250 seconds. This was done to ensure that crosslinking occurred between the two layers of the core thus 'locking' them together.

2. **Adhesion between FR4 substrate and optical layer**

The delamination between the FR4 substrate and an optical layer was a major issue as, sometimes, this would only be noticed after waveguides were fabricated (Figures 3.10 c and 3.10 d). Initial investigation was to check the dicing process to see if it was too damaging for the samples, but this seemed not to be the case. Thereafter, the dicing was always done at a reasonably low speed, typically 5 – 6 rpm, and with relatively light loads. The second and/or next action taken was to ensure that FR4 substrates were thoroughly cleaned and dried i.e. prebaked, before any deposition took place. These two actions seemed to temporarily solve the problem but occasionally this problem reoccurred, an indication that the approaches were either not enough or the main cause had not been identified.

Finally, a close examination of the available FR4 substrates was carried out; it was noticed that the FR4 substrates were not the same in terms of roughness. In addition, the two sides

of an FR4 substrate are of different roughness. For this reason, samples were taken from the available sets of FR4 substrate materials with surface roughness of both sides of a sample measured using a CLI Talysurf before deposition was carried out. Table 3.2 and figure 3.11 show the result of the test carried out on four samples with optical polymer deposited on either of the two sides of the substrates. After deposition, the samples were diced and were thereafter observed for possible detachment; it was noticed that smooth samples, with Ra < ~ 800 nm delaminated with varying degree while above that, no delamination was observed. It did become obvious that the rougher the substrate the better it adhered to the optical polymer layer. Following this investigation, not only did the author choose the rougher side of an FR4 material for deposition but also a similar set of material was constantly used.

Table 3-2: Table showing the effect of roughness of FR4 substrates on the potential of delamination between FR4 and optical layers.

No	Ra (nm)	Observation
1	458	Delamination occurred
2	619	Delamination occurred
3	958	No Delamination occurred
4	1020	No Delamination occurred
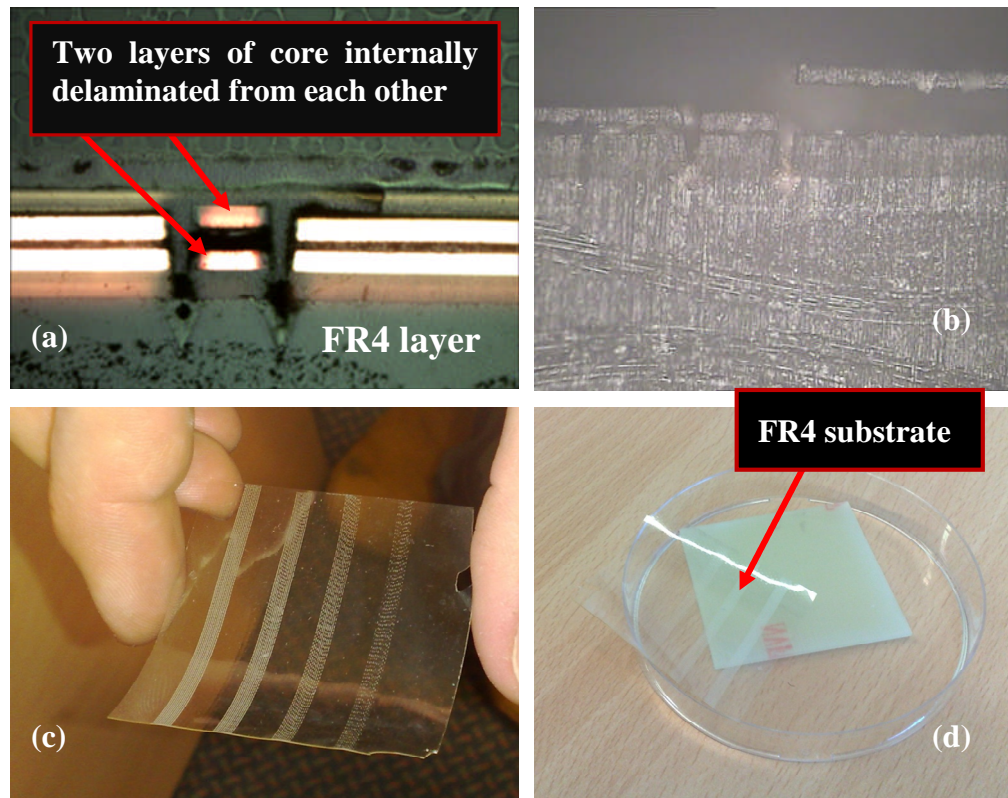
Figure 3-10: Various images taken showing the delamination between two layers of core and between FR4 substrate and optical layers : (a) Truemode™ -based optical layer polymer showing partial delamination between two core layers; the waveguides were patterned using UV Nd:YAG, (b) same as (a) but a worse case of delamination (c) polysiloxane-based optical layer polymer which was completely delaminated from an FR4 substrate; the waveguides were patterned using CO_2 laser, and (b) same as (c) showing the FR4 substrate from which it was delaminated.
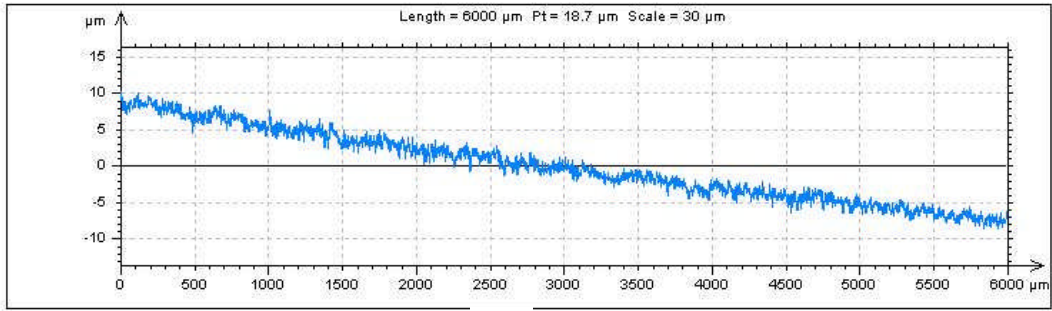
(a)
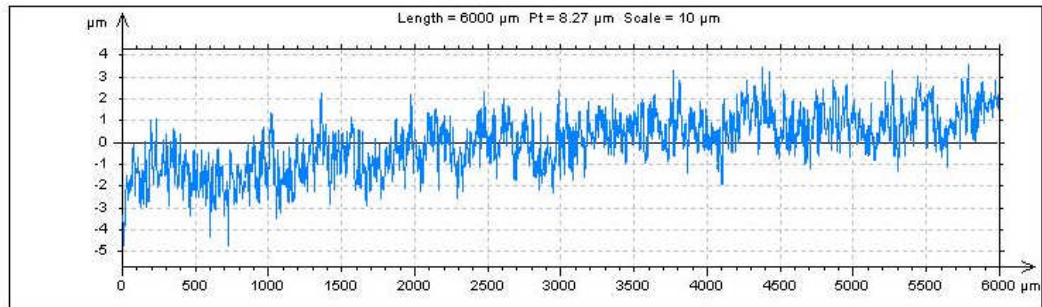
(b)
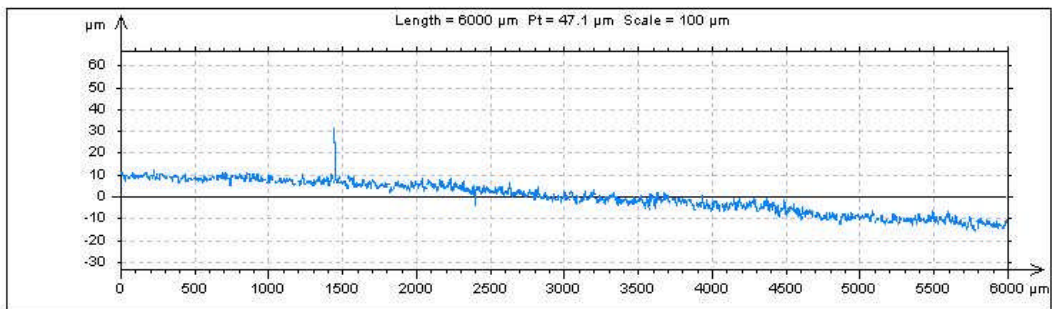
(c)
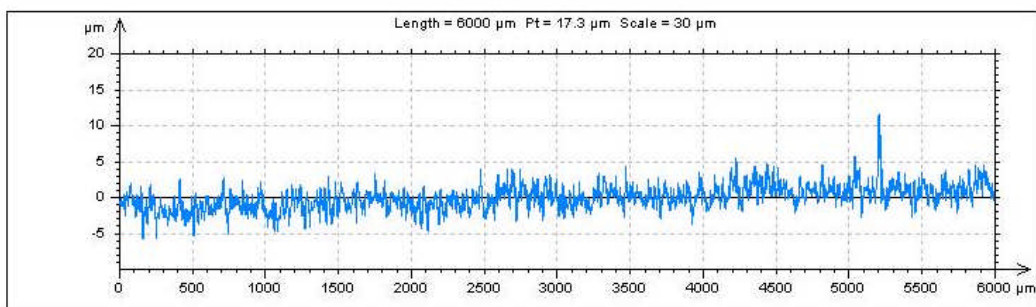
(d)

Figure 3-11: Some images from the experimental analysis carried out using Talysurf CLI to determine the roughness of an FR4 substrate: (a) Ra = 458 nm (b) Ra = 619 nm (c) Ra = 958 nm, and (d) Ra =1020 nm.

3.7   Sample Preparation

The following are some of the processes that were usually applied after laser ablation.

1. **Cleaning**: Due to possible debris deposition on the ablated structures and other forms of contamination, samples required cleaning before depositing the upper cladding. It was also required during sampling and polishing of mounted sample(s) (figure 3.12). Water and alcohol, either methanol or iso-propanol, were employed for cleaning. In the case of serious contamination which could be seen visually, and sometimes, with the aid of an optical microscope, ultrasonic agitation (sonication) was additionally required. This was achieved by putting the sample(s) in a beaker containing methanol or propanol which was then immersed in an ultrasonic bath. The sonication period varied from a minute to three minutes, depending on the nature or amount of debris to be removed.

2. **Sampling**: For measurement and analysis purpose(s), especially if mounting was required, a small piece of the ablated structures was usually obtained by dicing the sample using a Buehler ISOMET low speed saw. During this process, the sample would be positioned in such a way that the optical layer was in contact with the blade of the saw to avoid possible detachment of the layer during dicing. The speed at which samples were sliced depended on the combined thickness of the layers (i.e. FR4, core and cladding) but generally, samples were diced at a speed between 5 rpm and 7 rpm.

3. **Mounting**: Cold-mounting a sample involved mixing seven to one by ratio of resin to hardener which would be thoroughly stirred, for approximately 3 minutes, to ensure an efficient mixture necessary for good curing. The diced sample would then be placed in a container with the mixture of resin-hardener poured over it and thereafter left for 12 - 18 hours at room temperature. The above description was used for a Buehler acrylic-based resin. Sometimes, Buehler epoxy resin, known as EpoColor was employed; this allowed for direct visual examination of the optical polymer layer in the mounted specimen, and the subsequent detection of any waveguide when investigated using an optical microscope, such as Flash™200.

4. **Polishing**: This was required to obtain a good and fine surface finish for better examination on either Scanning Electron Microscope (SEM) or optical microscope. Mounted samples were polished using a series of abrasives (or polisher) capable of

removing different amounts of material from the samples, down to 1 μm diamond paste. During polishing, the sample was either held stationary or moved counter clockwise to the direction of rotation of the wheel. Usually, polishing was sequentially carried out on four different wheels of 240, 400, 600 and 800 grit SiC paper then washed with water before transferring to wheels with 6 μm and 1 μm diamond paste. Sometimes mounting was not required for sample examination; in this case the unpotted specimen was manually ground on silicon carbide paper in sequence over four different papers of 220, 400, 600 and 800 grit in increasing order of smoothness.

Dicing (1)
Samples were cut using Buehler ISOMET low speed saw at appropriate speed, typically 5 – 7 rpm

Mounting (2)
Potting was achieved by pouring resin over the sample which was supported in a mould

Sample cleaning (4)
Debris and other particles were removed using either methanol or isopropanol (and sonication)

Polishing (3)
Samples were polished using a series of abrasives with grit sizes down to 1 μm

Figure 3-12: Typical flow process for preparing a mounted sample of optical polymer waveguide structure for measurement and analysis.

3.8   Sample Measurement and Analysis

This section addresses specific quantities that were essential for waveguide analysis and the systems used in determining them, namely measurands and measuring system respectively.

3.8.1   Measurands

Measurands are specific physical quantities determined during any measuring process; for

full characterisation of the results of the research here, the measurands determined could be grouped into the following:

1. **Quantitative measurement**: In this case, measurands such as the length, width and pitch of waveguides fabricated were determined using a Flash™200 measuring device. Optical layer thickness and depth of waveguides were also determined using Talysurf, Flash™200 or both. For depth measurement on Flash™200, the samples had to be sectioned and mounted such that a vertical profile could be directly examined.

2. **Qualitative measurement**: The quality of ablated waveguides is very essential to ensure minimum propagation loss. Two measurands were of interest in this case; one was the surface roughness and the second the wall roughness of the waveguides. The former was successfully examined using Talysurf and Atomic Force Microscope (AFM); however, the latter was investigated using a number of equipment such as Talysurf CLI and/or Zygo but this proved unsatisfactory for which the challenges observed for wall roughness measurement are further detailed in chapter 7.

3. **Waveguide measurement (detection and loss)**: - To establish continuous waveguide paths before any propagation loss measurement was to be carried out, the Flash™200 was employed. In this case, the backlight feature of the system was used to shine white light into one end of the waveguide which should produce a spot-light feature/pattern, dimensionally replicating the waveguides. Once this was established, then the waveguide was ready for propagation loss assessment using an 850 nm VCSEL connected via a 50 micron core multi mode step index fibre which was carried out separately using the facilities at University College London (UCL), an academic partner to the *IeMRC* OPCB flagship project.

3.8.2 *Measuring systems*

The following measuring systems were extensively employed during the research under discussion; they are:

- **Talysurf CLI:** Talysurf CLI is a scanning topography-measuring instrument. This system allows for both contact and non-contact measuring techniques. It is equipped with four different types of gauges: a diamond-stylus inductive gauge (2.5 mm

range), a laser triangulation gauge (10 mm range) and one or two CLA confocal single point sensor gauges (3 mm / 300 μm ranges). It provides automated movement of the X, Y and Z slides up to a maximum speed of 20 mm/sec.

- **Zygo:** Zygo is a three dimensional surface structure analyzer. It uses scanning white light interferometry to image and measure surfaces; it employs MetroPro™ software to provide surface structure analysis in a non-contact manner. Depths up to 100 micrometers, with 0.1 nm resolution and 0.4 nm RMS repeatability are possible independent of objective magnification.

- **SmartScope® Flash™ 200:** SmartScope® Flash™ 200 is an optical measuring device; its XYZ travel is 200 x 200 x 150 mm with a resolution of 0.5 μm in all directions. It has highly inclusive (and modifiable) measurement capabilities and provides, among other things, feature dimensions such as width, length and height.

3.9   Summary and Conclusion

This chapter laid down the methodology, procedures and principles upon which the goals of this research were undertaken. It started by identifying the main tools, i.e. 248 nm Excimer, 355 nm UV Nd:YAG and 10.6 μm CO_2 lasers, which are to be employed in the research and different investigations needed on each laser. The lasers were chosen since they have been used for the drilling of vias during production of PCBs – an evident of the compatibility of the chosen technique with the current practice in the PCB manufacturing.

Optical polymer deposition on an FR4 substrate to form lower and upper cladding and core layers were investigated; the wet formulation of Truemode™ was deposited using spin coating at spinning speeds between 200 rpm – 1000 rpm for 30 – 60 seconds, which was then subsequently cured for 3 – 4 minutes in a nitrogen oxygen-free chamber to cross-link the polymer and finally oven-baked. Although polymer deposition characterisation was highly needed and essential, it was observed that there would be a tendency for a small range of deviation influenced by other factors that would be impractical to account for during the course of the experiment. Because a multimode waveguide was intended, spinning at 350 – 450 rpm was constantly utilised to obtain 30 – 50 microns thickness; the lower cladding was made such that its thickness is equal (at minimum) or greater than that of the core, for reasons already mentioned such as containment of signal by TIR and structural integrity. The adhesion between the optical polymer and FR4 substrate was maintained by depositing a relatively rough side with Ra

~ 950 nm or above.

Sample preparation – cleaning, sampling, mounting and polishing – and measurement using a number of systems including Talysurf CLI, Zygo, SmartScope® Flash™200 were described with both intrinsic and extrinsic problems and challenges identified and solved at an early stage of the research. Furthermore, pre- and post-treatment of samples were found to be of paramount priority if consistency of the results was to be guaranteed. Having covered the experimental design and methodology in this chapter, the next five chapters focus on experimental results.

References

1. Misselbrook, P. Novel manufacture of Out-of-Plane Optical Interconnects to Enable Low-Cost OECB substrates. Wolfson School of Mechanical and Manufacturing Engineering, Loughborough University, PhD Thesis (2006).

2. Enbutsu, K. *et al*. Multimode Optical Waveguide Fabricated by UV Cured Epoxy Resin for Optical Interconnection. *APCC OECC -Proceedings-*, 1648-1651 (1999).

3. Dangel, R. *et al*. Development of a low-cost low-loss polymer waveguide technology for parallel optical interconnect applications. *Biophotonics/Optical Interconnects and VLSI Photonics/WBM Microcavities, 2004 Digest of the LEOS Summer Topical Meetings*, 2 pp. (2004).

4. Material Data Sheet [Accessed October 2008] : Available from : http://www.exxelis.com/products/Truemode-datasheet-f.pdf

5. DeGroot, J., Norris, A., Glover, S. and Clapp, T. Highly transparent silicone materials. *Linear and Nonlinear Optics of Organic Materials IV* 5517, 116-123 (2004).

6. Su, K. Sioxane materials for optical applications. *Proc SPIE Int Soc Opt Eng* 6029 (2006).

7. Norris, A. High Reliability of Silicone Materials for Use as Polymer Waveguides. *Proc SPIE Int Soc Opt Eng* 5212, 76-82 (2003).

8. Colas, A., "silicones: preparation, properties and performance", Dow Corning, Life Sciences. Source: http://www.dowcorning.com/content/webabstract/ABS_01-3077.asp. [Accessed : August 2007]

9. Honda, H. Stochastic control in the spin coating systems. *2006 SICE-ICASE International Joint Conference, Vols 1-13*, 3309-3312 (2006).

10. Haas, D. and Quijada, J. Effect of solvent evaporation rate on "Skin" formation during spin coating of complex solutions. *Sol-Gel Optics V* 3943, 280-284 (2000).

11. Peurrung, L. M. and Graves, D. B. Spin Coating Over Topography. *IEEE transactions on semiconductor manufacturing : a publication of the IEEE Components, Hybrids, and Manufacturing Technology Society, the IEEE Electron Devices Society, the IEEE Reliability Society, the IEEE Solid-State Circuits Council.* 6, 72-76 (1993).

12. Flack, W. W. *et al*. A mathematical model for spin coating of polymer resists. *J. Appl. Phys.* 56, 1199-206 (1984).

13. Allan, N. S. and Oldring, P. K. T. in Chemistry and technology of UV and EB formulation for coatings, inks and paints (SITA Technology, London, 1991).

14. Tracton, A. A. in Coatings materials and surface coatings (CRC Press, Boca Raton, Fla.; London, 2007).

4 LASER ABLATION USING A CO2 (10.6 μM) INFRARED LASER

4.1 Introduction

The current chapter presents the feasibility study and the laser micromachining carried out using a CW CO_2 laser aimed at optical polymer waveguide fabrication. The chapter begins with a review of CO_2 laser machining, describes the experimental setup and then goes on to present the results of the laser micromachining accomplished.

4.2 CO$_2$ Laser Micromachining

The CO_2 laser is one of the most widely used gas lasers operating mostly in the CW mode, albeit pulsed mode operations are now being used. They are highly efficient with relatively low maintenance cost and high processing speed. The power output from CO_2 lasers varies from as low as 10 Watt, mainly for marking (of metals, wood and composites), to a very high power of tens of kilowatts used in industrial applications e.g. welding, soldering (low and high temperatures), drilling, cutting and heat treatment. The wavelength of CO_2 lasers are in the mid-IR region characterised by heat generation, making the laser a good source of heat required in thermal or heat-related applications [1- 7].

CO_2 laser micromachining has opened up new applications in microtechnology, especially in the microvia formation required for current PCB architecture. The CO_2 laser has been extensively used in via drilling, offering both efficiency and cost-effectiveness. Unlike mechanical drilling, CO_2 laser machining is a non-contact process which depends significantly on the thermal, and to some extent, on optical and chemical properties of the materials to be processed [6]. Undoubtedly, owing to its wavelength in the mid-IR and, of course, its photon energy, CO_2 laser ablation is a photothermal process in nature. As such, application of CO_2 lasers is favoured in processes where heat generation is not an issue of concern rather a merit, for example in soldering.

Only lately, new applications – besides the aforementioned areas – of CO_2 have begun to emerge. For instance, Chen, et al [8] has used a pulsed CO_2 laser to inscribe Arabic numerals on eggs aimed to replace, or at least to circumvent the potential chemical hazards that might accompany the current ink printing method of bar-coding consumable products while Williams, et al [9] used a similar system, i.e. a TEM_{00} pulsed CO_2 laser by Coherent

Inc., to machine various channels, of widths between 1 mm and 1.4 mm, in ceramic materials, namely aluminium oxide and aluminium nitride. Furthermore, Chung et al [10 - 11] reported the use of a CO_2 laser for etching holes in silicon, which naturally does not absorb an IR laser beam – this, according to the authors, was unprecedented. The etching of the silicon was achieved by placing pure silicon on top of a glass material which was then irradiated by a beam from a high power CO_2 laser source with the evidence of etching demonstrated from the top through to the glass.

Reports [12 - 14] are now available on the use of a CO_2 laser for optical waveguide fabrications based on changing the refractive-index of the materials. In these investigations [12 - 14], the RI of the region adjacent to the ablated site was reduced by an order that was typical of the difference in clad-core refractive indices required for the containment of light by TIR. This process was photothermal and the region of the reduced index was the area affected by the heat diffused from the irradiated site, which was not sufficient enough to cause any etching; that is to say, it was the HAZ which represented the cladding in this scheme.

The CO_2 laser-material interaction is photothermal (or a photothermally-dominated process) because the photon energy of any laser or laser system is calculated using $= h\lambda$, it thus follows that the photon energy (1.88 x 10^{-20} J or 0.1 eV) emitted by a CO_2 laser at 10.6 µm is far smaller than the chemical bond energies of typical polymers (e.g. C-C single bond) usually in the range of 3 – 10 eV. It is therefore obvious that micromachining in this case cannot be achieved by direct chemical bond-breaking as is the case with a UV laser source (i.e. a photochemical process); rather, it takes place by thermal processes. In order to successfully laser-ablate polymer waveguides using this class of laser, careful optimisation of the system parameters is therefore essential to minimise thermal damage that could result in a large HAZ and possible losses in any resulting waveguide.

4.3   Experimental Setup

The CO_2 laser used is a commercially available air-cooled SYNRAD series-48 IR laser source, with a fundamental wavelength of 10.6 µm, using WinMark Pro® software to control the experimental parameters such as power and speed of laser scanning. It operates in the CW operation mode with a Gaussian TEM_{00} beam profile and a maximum power of 10 Watts with output specified as a percentage of maximum power. The maximum

scanning speed achievable is 3000 mm/s; it has a beam divergence of approximately 4 mR. The circular beam diameter (or spot size) is fixed at 300 µm, but the system, through software control, allows the ablation of any width larger than this to be made by passing the beam over an area multiple times to cover the required width.

Figure 4.1 is a schematic diagram of the experimental setup used for the results presented in this chapter and chapter 7; for this, the sample was usually placed on the workpiece, which was stationary, while the laser beam was used to irradiate the area of interest to form the desired structures. The laser scanning was achieved by moving-mirrors placed on a high speed optical scanner forming the beam path; the mirrors move back and forth in a way that it converts schematic drawings from the CAD software into the structure and then onto the processing sample at the ablation site. Because the optical components are generally light objects, this type of design provides a very high processing speed compared to both moving laser and moving workpiece [15]. It should be noted here that, since the laser processing on this system was achieved through scanning – where the sample was stationary with the laser beam moved to ablate the drawn patterns – it was impractical to measure powers at the workpiece using the available power meter. Thus, all powers reported on this system were the laser output power values given by the software.
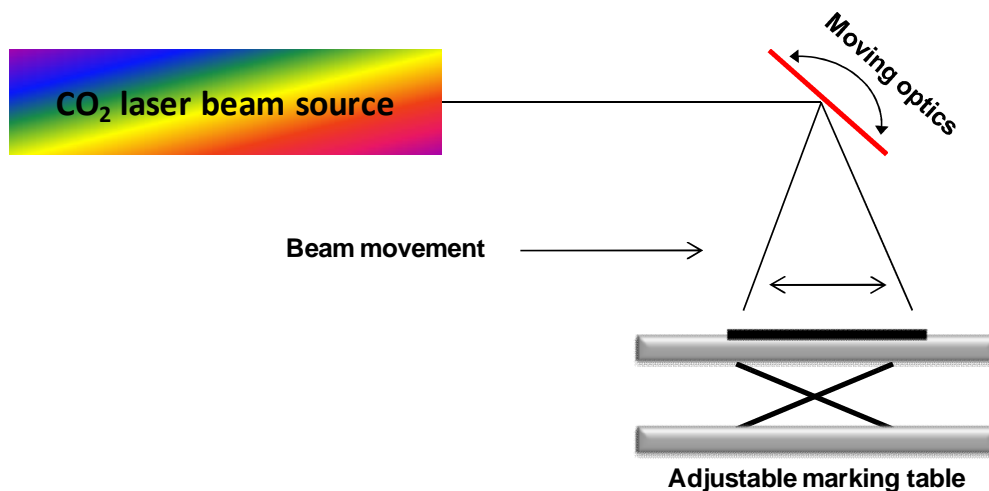
Figure 4-1: Schematic diagram of an experimental setup employed for laser ablation process using CW TEM_{00} Gaussian beam intensity profile.

This laser system was designed for marking and simple cutting. However, its possible application in the laser ablation of optical polymer waveguides was considered here, which

was preceded with a feasibility study. The results of this study are reported here and the fabrication of optical waveguides using this laser is detailed in chapter 7.

4.4   Experimental Results and Discussion

4.4.1   *Laser micromachining trial – feasibility study*

Due to the lack of literature reporting the use of this class of laser on optical polymer, an initial feasibility study was considered necessary. During this study, a wide range of parameters were covered, with powers varying from 1 to 9 Watts and a scanning speed range of 20 mm/s – 500 mm/s. Table 4.1 shows the experimental parameters employed to machine channels in two different materials, namely Truemode™ and PMMA at various power-speed combinations. In each case, the polymer sample was placed on a stationary stage with the CO_2 laser beam kept at 300 µm diameter, at the desired parameters, and which was then passed over the sample to create a straight line or channel.

Table 4-1: Parameters used for laser micromachining of PMMA and Truemode™ polymers during the initial trial.

Track No	Power (Watt)	Scanning Speed (mm/s)
1	9	500
2	9	200
3	9	100
4	9	50
5	9	20
6	8	50
7	7	50
8	6	50
9	5	50
10	4	50
11	3	50
12	2	50
13	1	50

In this experiment, a TEM_{00} Gaussian beam profile was used, resulting in a cylindrical-like channel when the beam was translated across the surface. Figure 4.2 is an SEM image showing a three-dimensional view of the channel made in a Truemode™ optical polymer at an input power of 9 Watt and scanning speed of 200 mm/s. It is obvious from figure 4.2 that, due to the Gaussian nature of the beam profile coupled with the fact that the beam is circular, the depth of ablation was not the same across the track width; this is because the power intensity was not even across the profile. This phenomenon made it difficult to

predict the depth of ablation, which is essential for optical waveguide fabrication in order to make sure that etching is done beyond the core layer, but not into the FR4 layer. It should be noted here that the spots/lines that appears on the channel in figure 4.2 are likely to be debris deposited, during and/or after ablation, since the sample in this case was not subjected to post-ablation treatment.
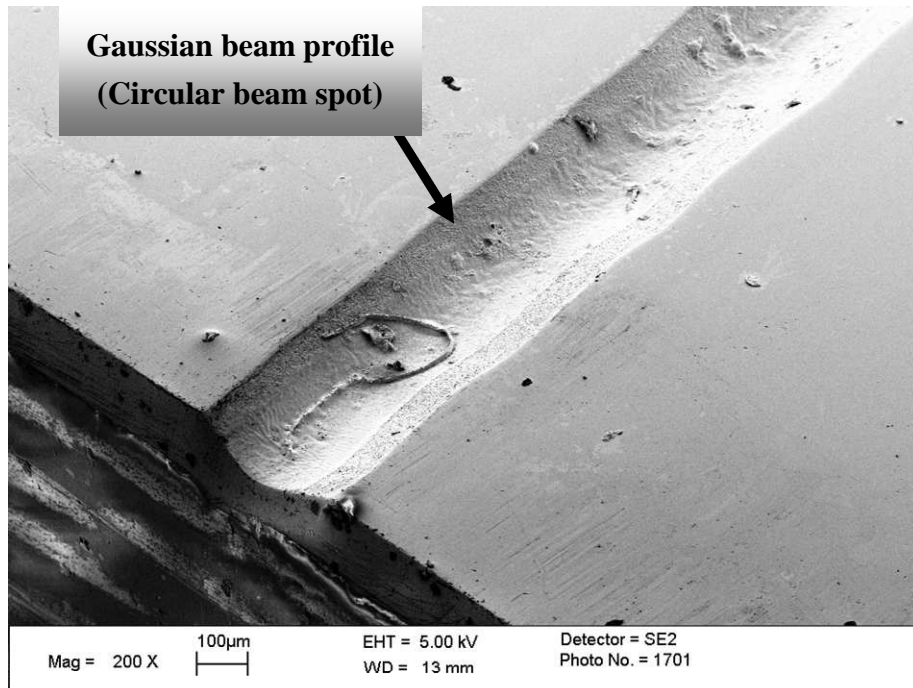
Figure 4-2: Cylindrical-like ablated profile resulting from the TEM_{00} mode CW beam for a structure machined in Truemode™ optical polymer at input power of 9 Watt and scanning speed of 200 mm/s.

While ablating at high powers and low speeds, a charring-like effect (with smoke emanating occasionally) at the ablation zones was observed – an indication of a thermal process. It was also noticed that the channels machined had different widths depending on both the power input and scanning speed. Figure 4.3 shows SEM images of various channels machined in Truemode™ with tracks having different widths even though the same beam size of 300 µm was used in each case. For instance, consider the case of a track machined at an input power of 9 Watt and scanning speed of 500 mm/s using a 300 µm spot size (figure 4.3 a) where the resulting channel width was only about one-third of the laser beam size; which could be due to power density variation.

In addition, it was also observed that the channel had wavy edges (figure 4.3a); this could

be due to the circular profile of the beam coupled with the fact that the machining was carried out at a relatively high speed. In fact such was also the case when a PMMA polymer sample was machined at the same input power of 9 Watt but with a much low speed of 20 mm/s as evident in figure 4.4, with the circular beam profile apparent at the end of the track. Analysis of the surface profile using Flash™200 showed variations in track width (figure 4.5). It was found that the resulting track width could be as small as 100 µm with a maximum width of about 500 µm achievable at high power and low speed. The track width having a width larger than the beam spot size could be a result of many factors but most likely is the power density and thermal effect of the ablation mechanism.
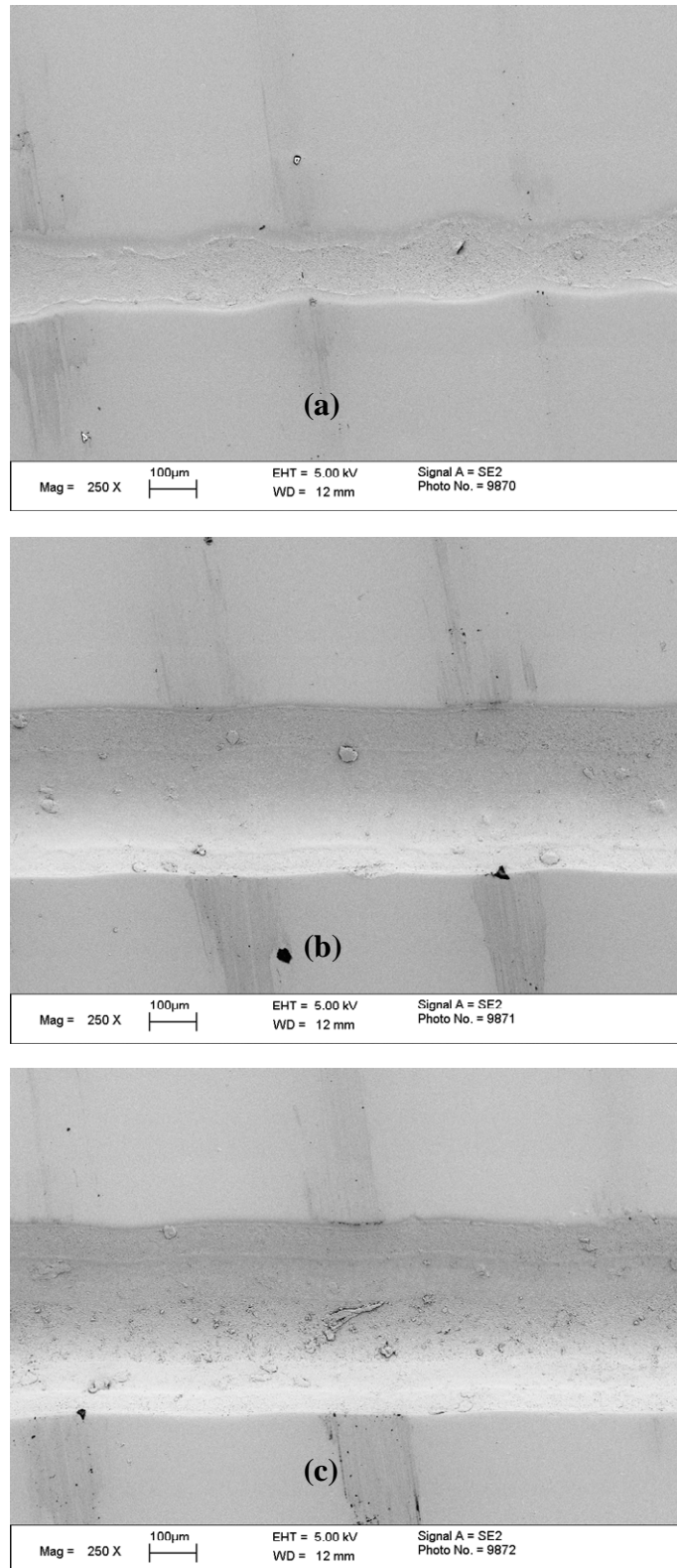
Figure 4-3: SEM images of various channels machined in Truemode™ showing variation in ablated track widths at different parameter combinations using the same beam size of 300 µm (a) 9 Watt and 500 mm/s, (b) 9 Watt and 200 mm/s, and (c) 9 Watt and 100 mm/s.
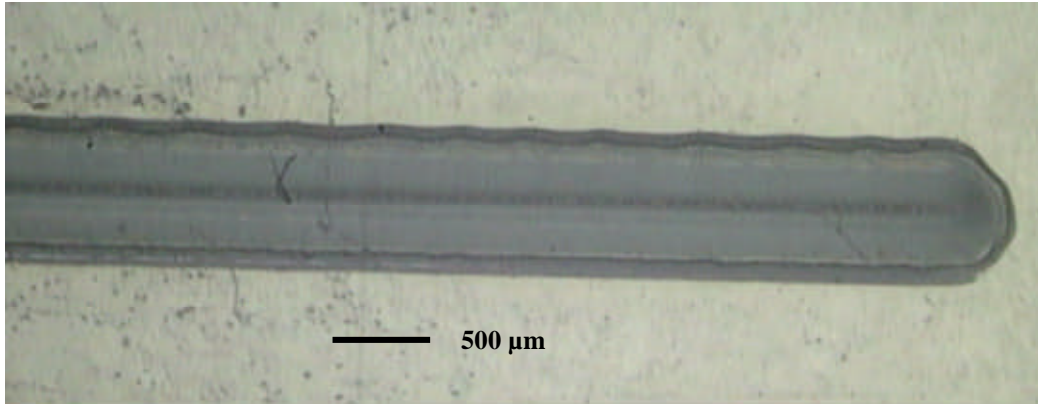
Figure 4-4: A figure showing a PMMA polymer machined at 20 mm/s and 9 Watt using a 300 µm circular beam profile.

Since machining on this system is a photothermal process achieved by scanning the beam, it implies that, for example, a scanning speed of 100 mm/s at 1 Watt of energy would likely produce the same effect as that done at 200 mm/s and 2 Watt or 100 mm/s at 1 Watt but with two passes, all other parameters being equal. It is on this premise that the author considers that laser ablation using this CW CO_2 laser, taking into cognizance the fact that only the power and speed could be altered, could be achieved by calculating what could be called a 'Scanning Power Density (SPD)', obtained by dividing power with speed, measured in Watt per Millimetre per Second (Watt/mm/s) or Joule per Millimetre (J/mm) (Equation 4.1). Therefore, it is possible to plot the relationship between the parameters used, represented as SPD, against the widths of ablated channels as shown in figure 4.6. From this, it is evident that the track width varies with increase in the power density; however this increase gradually reduces as the values of SPD becomes higher. In addition, a plot of SPD against the depth of ablation, shown in figure 4.7, indicates a linear relationship between the two quantities. This is because as the power density is increased so is the absolute beam intensity across the profile, which means that more power would be available at points, especially at the region close to the edge of the Gaussian profile where no ablation would have occurred if low power density were to be used.

$$'Scanning\ power\ density\ (SPD)' = \frac{Power\ (Watt)}{Speed\ (mm/s)} = \frac{Energy}{Length}(J/mm) \qquad (4.1)$$
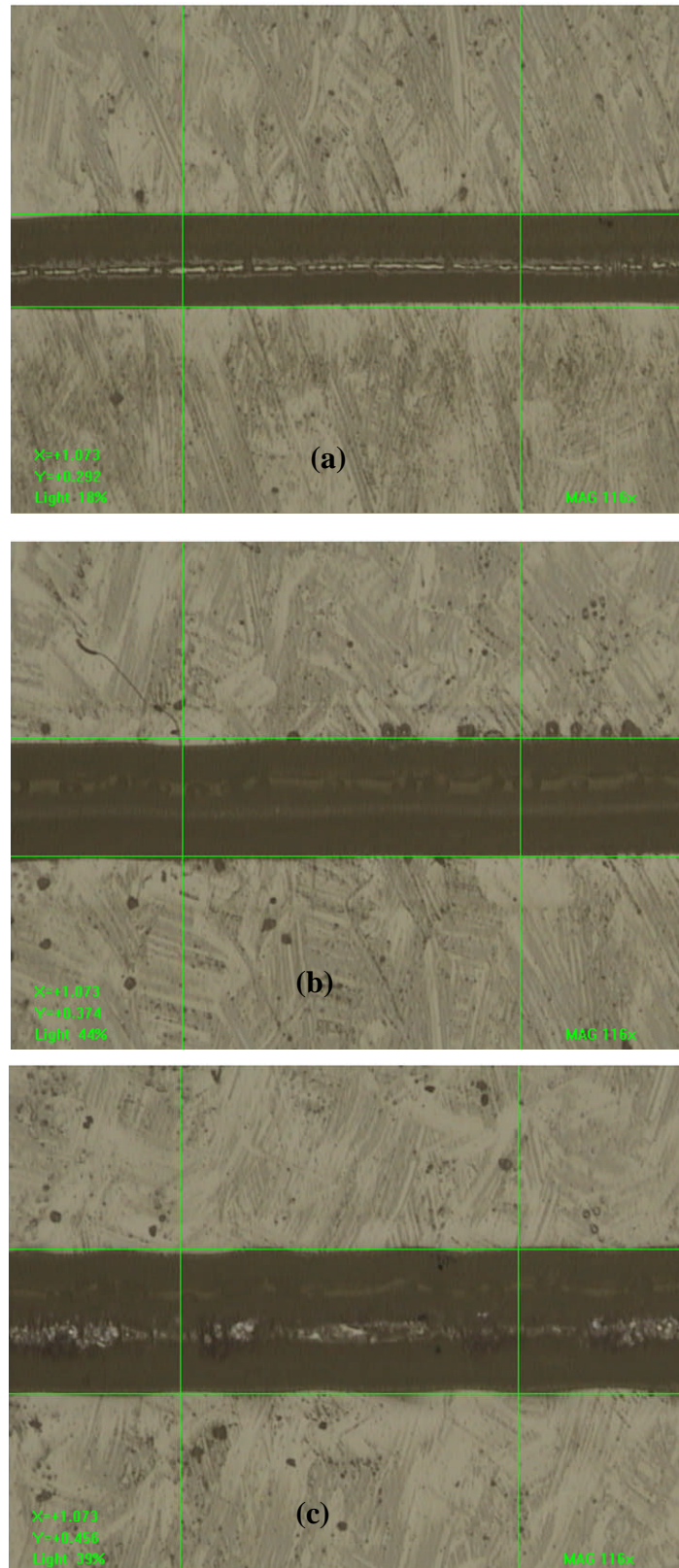
Figure 4-5: Surface profile of various channels machined in Truemode™ showing variation in ablated track widths at different parameter combination using the same beam size of 300 µm (a) 9 Watt and 100 mm/s, (b) 9 Watt and 50 mm/s, and (c) 9 Watt and 20 mm/s.
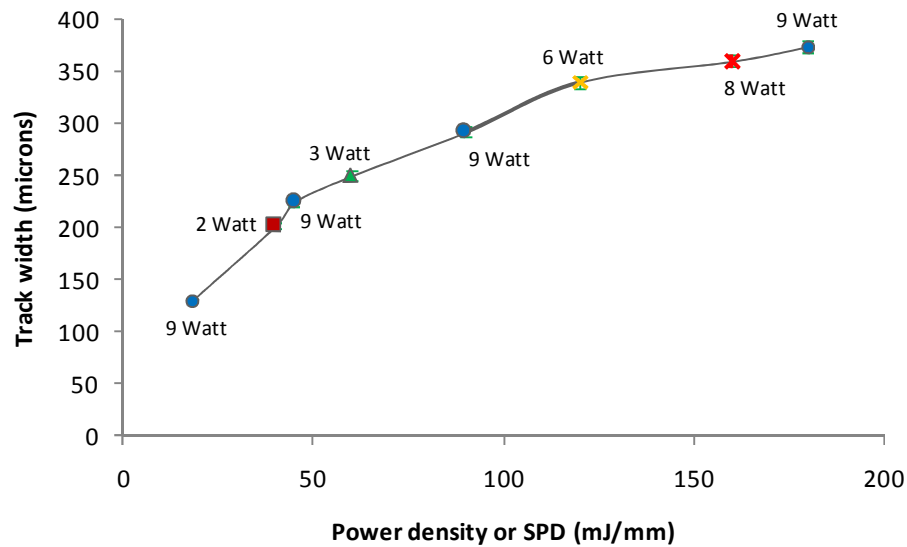
Figure 4-6: A graph showing the relationship between the SPD and the resulting ablated track width for a given beam size of 300 µm.
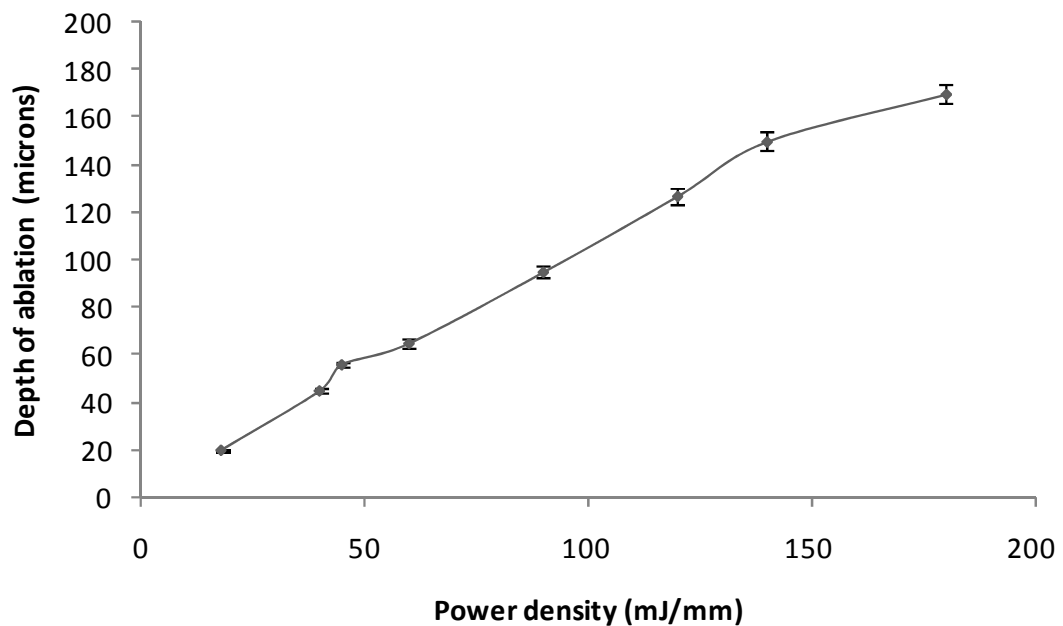
Figure 4-7: Graphical representation of the effect of power density on the depth of ablation for micromachining carried out on Truemode™ optical polymer.

Finally, and indeed on a very important note, is the HAZ effect of this process. Since it is a thermal or at least a thermally-dominated process, the effect of HAZ cannot be ruled out, rather it should be minimised. Figure 4.8 shows the cross-section of three different structures machined in a PMMA polymer with obvious thermal effect, on the sides of the tracks which might have changed the RI of the adjacent region by softening the polymer

material used, i.e. PMMA. The thermal effect seen on both sides of the structures in figure 4.8 is similar to that shown in [14, 16] where the refractive indices of the materials were altered. However, in [14], the side modifications were purposely intended such that a RI change would be introduced in the region in order to make the region act as a clad layer thus forming a waveguide. It should be noted here that such obvious HAZ effect was not observed for machined structures in Truemode™ polymer most likely due to being a better beam absorber (of the two) at this wavelength; nevertheless, this does not mean that machining in this case was a HAZ-free process.
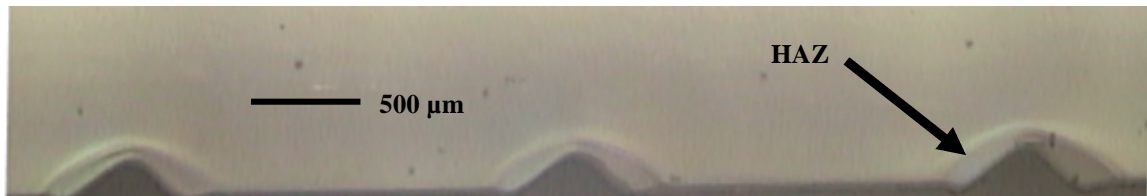
Figure 4-8: Machined channels in PMMA polymer showing the thermal effect on the sides of ablated tracks. The parameters used from the left: 9 Watt and 50 mm/s; 9 Watt and 20 mm/s; and 8 Watt and 50 mm/s.

4.4.2   Laser micromachining – effect of speed and power

Having conducted the feasibility study in the midst of a wide range of parameters, the subsequent experiment(s) was more focused in narrowing down the operating window and assessing the effect of the two main parameters, namely input power and scanning speed. In this case, the polymers used were Truemode™ and polysiloxane (OE4140 and OE 4141). Similar to the initial trial, channels were machined in these two polymers using a fixed beam spot size of 300 µm at the desired parameters.

Since high powers at 7 – 9 Watts and low speeds at 50 mm/s or less were found to cause a large HAZ in the first trial, as described above, 5 Watt was taken as the upper limit for operating power while a minimum scanning speed of 100 mm/s was used. The micromachining was therefore carried out in two phases; one at varying powers of 1 – 5 Watts keeping the scanning speed constant and the other at varying speed between 100 mm/s and 400 mm/s with the power kept constant. This, in effect, maintained the power density (or SPD) applied in every case in the range of ~ 10 mJ/mm to 50 mJ/mm; unlike in the first trial where as high as 450 mJ/mm was employed with a parameter combination of 9 Watt – 20 mm/s (Table 4.1).

It was observed that a change in any of the two main variable parameters affects the quality of the ablated channels. Figure 4.9 shows top views of a series of channels machined in a polysiloxane-based photopolymer at a fixed input laser power of 5 Watt and varying scanning speed between 150 mm/s and 400 mm/s. This corresponds to a change in the scanning power density with a minimum SPD of 12.5 mJ/mm employed at 400 mm/s and a maximum SPD of 33.3 mJ/mm at 150 mm/s. It is evident from figure 4.9 that an increase in the scanning speed from 150 mm/s to 400 mm/s which corresponds to a decrease in SPD from 33.3 mJ/mm to 12.5 mJ/mm, at a fixed output power of 5 Watt dramatically improved the quality of ablation on a polysiloxane-based polymer. For example, the structure machined at 5 Watt and 150 mm/s, i.e. SPD 33.3 mJ/mm (figure 4.9 a), resulted in a great amount of debris deposited at the ablation site, however, at a higher scanning speed of 250 mm/s and lower SPD of 20 mJ/mm, the debris deposition was reduced. Figures 4.9 c and 4.9 d resulted in very clean ablated structures with no apparent debris deposition at the site of the processing. However, as expected, these clean structures ablated at lower SPD resulted in smaller track widths compared with those at higher power densities.
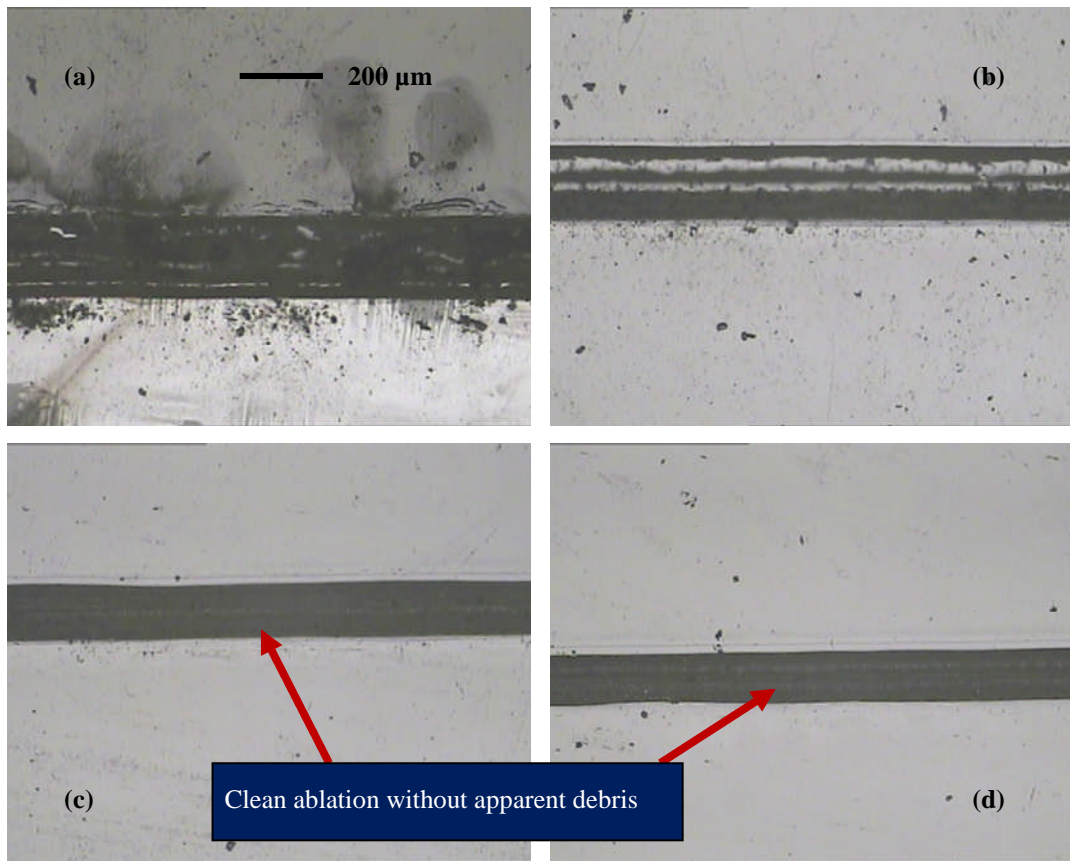
Figure 4-9: Effects of varying scanning speed at a fixed input power of 5 Watt on the quality of ablation on polysiloxane (OE4140 and OE 4141) polymer using CW CO_2 laser showing (a) 150 mm/s scanning speed (SPD = 33.3 mJ/mm), (b) 250 mm/s scanning speed (SPD = 20 mJ/mm), (c) 350 mm/s scanning speed (SPD = 14.3 mJ/mm), and (d) 400 mm/s scanning speed (SPD = 12.5 mJ/mm).

In figure 4.10, images of two channels structured at a fixed scanning power of 150 mm/s but different power are presented. Although, there is evidence of debris deposition in both situations, however, it was milder at a lower power of 4 Watt (figure 4.10 b) where lower SPD of 26.7 mJ/mm was utilised. It can therefore be argued that SPD values, which combine the effects of the two changeable parameters used on the system, can be used as a guide of ablation quality (as demonstrated in the tables 4.2 and 4.3). This allows for a wide range of combinations between power and scanning speed to be made for an optimisation of the process and subsequent reduction to the HAZ. Tables 4.2 and 4.3 present optical microscope images of machined structures in Truemode™ and polysiloxane polymers respectively at various parameter combinations arranged in increasing order of SPD values. For polysiloxane-based photopolymer (table 4.3),

minimum debris deposition was achieved when samples were machined at low SPD values of 12.5 mJ/mm up to about 17 mJ/mm. However, at higher SPDs ≥ 20 mJ/mm, it could be observed that the debris deposition became more apparent.

It was also observed during the course of the investigation that, at a constant scanning speed of 100 mm/s and 1 Watt, i.e. SPD of 10 mJ/mm, there was no evidence of ablation or a structure being created in Truemode™ polymer. At SPD value of 12 mJ/mm (table 4.2), there is evidence of ablation although it appears to produce a shallow depth, but as the SPD values increased the ablated structure improved without apparent debris deposited at either side of the ablated tracks, however, at much higher SPDs ≥ 40 mJ/mm there appears to be some thermal effect on the sides of the machined structures.
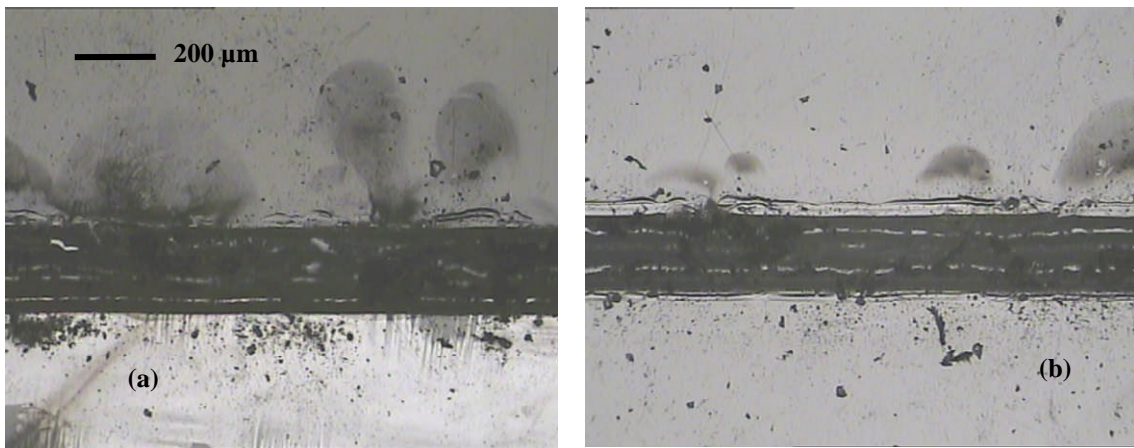
Figure 4-10: Images showing the samples machined in polysiloxane (OE4140 and OE 4141) at fixed scanning speed of 150 mm/s but different input laser power : (a) 5 Watt (SPD = 33.3 mJ/mm), and (b) 4 Watt (SPD = 26.7 mJ/mm).

Table 4-2: Table showing optical microscope images of structures machined in Truemode™ polymer with parameters used and corresponding SPD values.
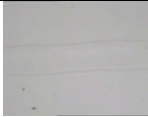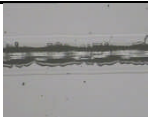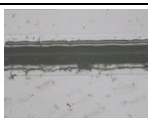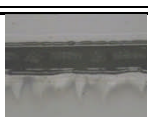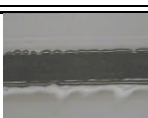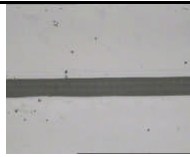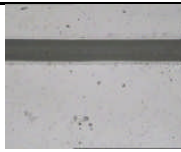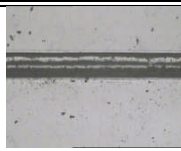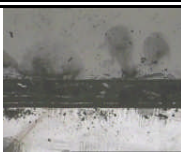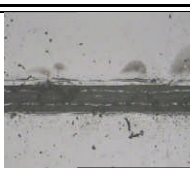
Power (Watt)	Speed (mm/s)	SPD (mJ/mm)	Machined Structure
3	250	12	
3	200	15	
3	150	20	
3	100	30	
4	100	40	
5	100	50	
6	100	60	

Table 4-3: Table showing optical microscope images of structures machined in polysiloxane (OE4140 and OE 4141) with parameters used and corresponding SPD values.

Power (Watt)	Speed (mm/s)	SPD (mJ/mm)	Machined Structure
5	400	12.5	
5	350	14.3	
5	300	16.7	
5	250	20	
4	150	26.7	
3	100	30	

Undoubtedly, the surface quality of the ablated profile is essential for a good performance of an optical waveguide; the desirable roughness or smoothness is still subject to further research, nevertheless, this needs to be kept as fine as possible. Figure 4.11 shows the

surface and wall of an ablated channel in a Truemode™ sample at SPD value of 45 mJ/mm which indicates a fairly smooth surface, with no apparent thermal damage. Although no quantitative value of the smoothness of these surfaces could be obtained due to the dimensional constraints of the structures, this is of an improved quality, in terms of the debris deposition at the ablation zone, to that reported in [16]. Qi, et al [16] concluded that the surface of a CO_2 laser micromachined polycarbonate was rough, but an Excimer laser could be used to polish the surface; a similar observation was made by the authors of [9] for the micromachining carried out on ceramics. Further work is needed to quantify the roughness and its effect in respect to various applications.
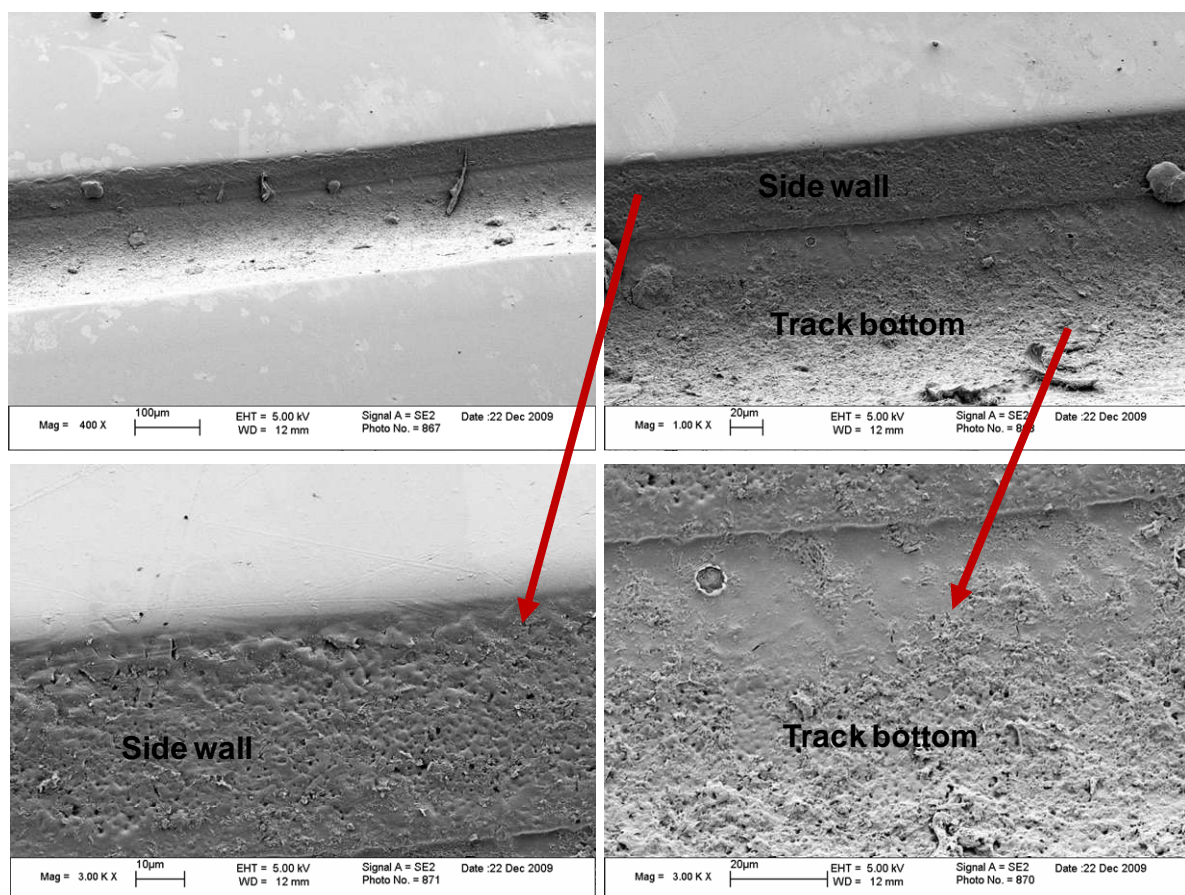
Figure 4-11: Field Emission Gun Scanning Electron Microscope (FEGSEM) images of a sample machined in Truemode™ optical polymer at input power of 9 Watt and scanning speed of 200 mm/s (SPD = 45 mJ/mm) to visually examine the quality of the surfaces (i.e. roughness of the ablation).

4.5 Discussion

As pointed out earlier in this chapter, although the CO_2 laser is the most widely used gas laser it is mainly employed where heat generation and photothermal mechanism are desirable, if not essential, for processing such as in welding, drilling, soldering and cutting. However, since its invention over four decades ago when its key usage was (and still is) in the aforementioned areas, the CO_2 laser system design has also witnessed significant changes mainly in power, and beam delivery and quality, for this reason and many other needs, research is underway to explore other possible applications especially in microfabrication since the laser in question offers a very competitive processing speed.

The lack of literature reporting the use of the CO_2 laser for optical polymer waveguide fabrication posed some challenges to the study conducted and reported in this chapter. The SYNRAD series-48 IR laser (section 4.3) used for this study was actually designed for processes such as marking, engraving, etc. where the Gaussian and circular beam shape was not an issue; however, this is of concern for the application under consideration. This is evident in the SEM images of an ablated channel structure in Truemode™ optical polymer where the depth of ablation was not the same across the track having a Gaussian profile shape. The shape of the ablated structure was considered to be as a result of a combined-effect of the Gaussian profile of the beam and its circular shape. Consequently, the depth of any ablated channel varied from a minimum value at the edges to a maximum value at the centre of the structure.

One possible way of overcoming this is by taking the depth at a point in the middle of the ablated profile, i.e. neither at the edge nor at the centre, when estimating the expected depth of ablation. This idea is akin to taking the beam waist of a Gaussian profile at a point where the beam intensity has fallen to $1/e^2$ (~13.5 %) of the beam at the centre; that is to say, the working depth should be taken as equal to 86.5 % of the centre depth value. This was quite useful during waveguide fabrication since in every case ablation was guaranteed to reach the lower cladding, thus ensuring a successful waveguide fabrication. On the other hand, the choice of taking the maximum depth, i.e. the value at the centre of the structure, as the working value could sometimes result in a situation whereby the centre part of a given track, for a particular set of parameter values, reached the FR4 substrate or the centre was not ablated into the lower cladding while other parts were not; neither was desirable. It was therefore essential that process optimisation was employed if this challenge was to be

overcome, and this was part of the objectives of this study.

The analysis of the ablated tracks showed that the resulting channels could have widths different from the beam spot size of 300 µm; either narrower or wider (figures 4.3 and 4.5). Figure 4.12 shows a schematic diagram of the 300 µm beam profile and the distribution of the intensity which is a maximum along the centre. An arbitrary horizontal line is drawn across the beam profile to indicate the ablation threshold; this means that only the power density below the threshold line can cause effective ablation while the part of the beam profile above this line is insufficient to result in etching in the sample. Therefore, the channel would have a width shorter than the beam spot size as indicated by the red double arrow line in figure 4.12. In other words, only a fraction of the beam, located at points in the centre, carries sufficient power density or intensity which is above the ablation threshold for the polymer.
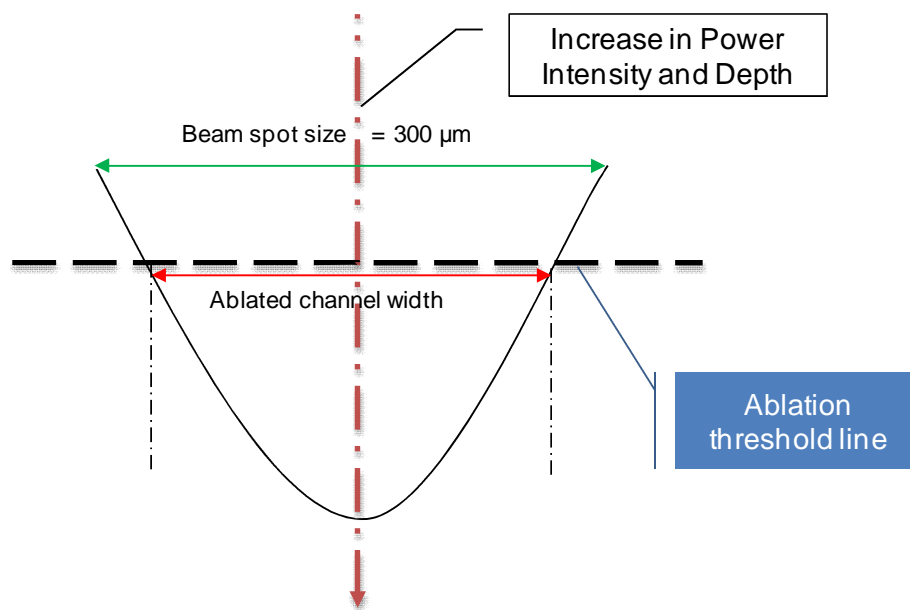
Figure 4-12: Schematic diagram of the CO_2 laser beam profile showing how the power intensity and power threshold affect the width of ablated channels.

The observation that the resulting track width was larger than the beam diameter can be explained if the thermal effect of the mechanism is taken into consideration. In this case, it can be said that, the combined effect of high power and low speed gave rise to a very high power density at the ablation zone, this in effect caused a high thermal agitation and temperature at the ablation site which was capable of melting and vaporizing the adjacent

region to the actual beam size thus producing a larger track width. Other factors might also be responsible; for instance, Crafer and Oakley [15] argued that, in a moving optics design, the spot size at the workpiece is governed by the diameter of the beam incident on the lens which can vary as the optics moves. This, according to [15] can also have an effect on the power density and beam quality produced at the workpiece. Having said this, since the tracks were machined with varying parameters, it is difficult to make a direct correlation between the parameters used and the resulting channel size. However, this may explain the "rippled" effect observed in some of the machined structures.

Although the effect of HAZ was much pronounced when ablating PMMA polymer samples (figure 4.8), this does not mean that other polymers – Truemode™ and polysiloxane – are not prone to thermal effects. In fact, what could be an explanation for this difference in behaviour might be because while PMMA is a thermoplastic polymer, both Truemode™ and polysiloxane are thermosetting and elastomeric materials respectively which could affect the way the materials react to the thermal effect of the laser beam. It can be observed from the SEM images of the ablated samples (figures 4.2, 4.3 and 4.11) that a line, in most cases, runs along the ablated structure, it is thought to be due to (i.e. occurring at) the interface between the core and the clad layer of the sample, though no evidence either in the literature or during this study could be obtained to support this.

4.6   Summary and Conclusion

IR CW CO_2 (at 10.6 µm wavelength) laser micromachining of optical polymer was considered; the laser output beam was Gaussian with a fixed circular beam size of 300 µm, which resulted in a cylindrical-like profile in the ablated structures. Due to the lack of literature report on the use of this class of laser on optical polymer, a feasibility study was thus conducted on both PMMA and Truemode™. Two system parameters, power and scanning, were not fixed. While input power could be changed between 1 Watt and 10 Watt, scanning speeds between 1 mm/s and 3000 mm/s was possible. Initially, 90 percent of the available power ranges (1 – 9 Watt) and speed ranging from 20 mm/s to 500 mm/s was utilised; this was done in order to identify the relevant operating windows for this polymer since such information was not readily available in the public domain.

Following the initial trial, subsequent investigation was centred on changing the power and scanning speed in order to optimise the process; in those cases, Truemode™ and

polysiloxane-based photopolymers were employed. It was observed that, for this process, the effect of changes in one parameter at a fixed value of the other depended on the value of the fixed parameter. In other words, increasing the scanning speed at a fixed input power can either improve or mar the quality of ablation depending on the value of the power used. This is because, the combination of the two factors – power and speed – determines the effective power or power density at the ablation zone, and since the beam wavelength would restrict the photon energy to a value < 0.1 eV – much lower than the bond-energies typical polymers required for bond scission in a photochemical mechanism – the process can therefore be viewed as purely athermal. Therefore, the author proposed that 'Scanning Power Density (SPD)', obtained by dividing power with speed measured in Joule per millimetre, be used as a basis of achieving a qualitative fabrication mechanism since 2 Watt at scanning speed of 200 mm/s would provide the same effective power or power density as 1 Watt at 100 mm/s. It is believed that this derived parameter (i.e. SPD) would have the same effect as fluence (energy per unit area) in pulsed lasers.

A plot of SPD against the depth of ablation was found to be relatively linear with an SPD value of 50 mJ/mm resulting in 60 microns depth of ablation, which was adequate to ablate through the core into the lower cladding of a typical multimode waveguide. Additionally, the ablated tracks were found to have varying widths, which the author considered to be another proof that the laser micromachining at this wavelength is a photothermally-dominated, if not a pure photothermal, process. HAZ effect was equally studied; this was found to be much pronounced in PMMA which was thought to be due to its low absorption and its being a thermoplastic material. Debris deposition and thermal effect was observed to be relatively significant at SPDs above 60 mJ/mm and 30 mJ/mm for Truemode™ and polysiloxane respectively. As a result, SPD values below 20 mJ/mm were found to give clean ablated structures with minimum or no debris deposition at the ablation site for polysiloxane-based polymer; for Truemode™, values between 15 mJ/mm and 50 mJ/mm were considered optimum.

References

1. Ion, J. C. in *Laser processing of engineering materials: principles, procedure and industrial application* 556 (Elsevier Butterworth-Heinemann, Oxford, 2005).

2. Gower, M. C. Industrial applications of laser micromachining. *Optics Express* 7, 56-67 (2000).

3. Powell, J. in *CO2 laser cutting* (Springer, Berlin, 1998).

4. Gillner, A. Laser applications in microtechnology. *Journal of materials processing technology.* 167, 494 (2006).

5. Meijer,J. Laser beam machining (LBM), state of the art and new opportunities. *Journal of materials processing technology.* 149, 2-17(2004).

6. Dubey, K.A and Yadava, V. Laser beam machining – a review. International journal of machine tools and manufacture. 48, 609-628 (2008)

7. Steen, W. M. in *Laser material processing* (Springer, London, 2003).

8. Chen, M. Laser coding on the eggshell using pulsed-laser marking system. *Journal of materials processing technology.* 209, 737 (2009).

9. Williams, O, Williams, M., Liu, C., Webb, P. and Firth, P. Laser micromachining of polycrystalline alumina and aluminium nitride to enable compact optoelectronic interconnects. EPTC 11th Electronics Packaging Technology Conference, Singapore, 9th-11th December 2009, pp. 920-925.

10. Chung, C. K., Wu, M. Y., Hsiao, E. J. and Sung, Y. C. Etching behaviour of silicon using CO_2 laser in Proceedings of the 2nd IEEE International Conference on Nano/Micro Engineered and Molecular Systems, Thailand, 2007.

11. Chung, C. K., Wu, M. Y., Wu, J. C., Sung, Y. C. and Huang, G. R. Silicon micromachining by CO_2 laser in Proceedings of the 1st IEEE International Conference on Nano/Micro Engineered and Molecular Systems, China, 2006.

12. Treanton, V., et al. Engineering of waveguides and other micro-structures in dielectrics. Proceedings of the SPIE, Photonics North 2006, Vol. 6343, 634312(2006).

13. Terui, H. and Kobayashi, M. Fabrication of channel optical waveguide using CO2 laser. *Electron. Lett.* 15, 79-80 (1979).

14. Ozcan, L. C. Fabrication of buried waveguides in planar silica films using a direct CW laser writing technique. *Journal of non-crystalline solids.* 354, 4833 (2008).

15. R. Crafer and P.J. Oakley, Laser Processing in Manufacturing. London : Chapman

and Hall, 1993, pp.292.

16. Qi, H, et al. Micromachining of microchannel on the polycarbonate substrate with CO2 laser direct-writing. *Journal of optics and lasers in engineering.* (2008).

5   UV Nd:YAG Laser System Characterisation

5.1   Introduction

In this chapter, results of the feasibility and laser system characterisation carried out using a UV Nd:YAG laser hosted by Stevenage Circuits Limited – an industrial partner to the OPCB consortium – are presented. The chapter starts by explaining the UV Nd:YAG laser micromachining in general and its potential application in the fabrication of optical polymer waveguides in particular. The results section is divided into two sets of experiments: those carried out as part of the feasibility study undertaken to investigate the potential of this class of laser for the proposed application and those aimed at understanding the effects of various laser system parameters.

5.2   Nd:YAG Laser Micromachining

Laser drilling of microvias in printed circuit boards for high density interconnects has been a dominant technology in PCB manufacturing [1 - 4]. The carbon dioxide laser, described in the previous chapter, is the foremost candidate in laser drilling and offers a tremendous improvement, in terms of speed and quality, over the traditional mechanical hole drilling. However, the kerf – the width of the machined hole – obtained with CO_2 is only in the range of 100 – 200 µm, which is a major constraint in today's need for small-size high density multi-layer PCB circuits for opto-electronic and photonic devices [3, 5]. In addition, copper (a conducting layer in PCB assembly) naturally reflects light at about 10 µm [1] wavelength which also makes the CO_2 laser less suitable for drilling of buried or through holes in multi-layer PCBs. These challenges were overcome with the introduction of the Neodymium-doped Yttrium Aluminium Garnet (Nd:YAG) laser that offers, among other benefits, a smaller spot size and a wavelength (or wavelengths) [6, 7] that are readily absorbed by copper. However, this is not to say that Nd:YAG lasers have overhauled CO_2 in the PCB industry, as for blind hole drilling, the CO_2 laser is the most suitable laser as it terminates at the dielectric material–copper layer interface without causing damage to the copper pad [1].

Nd:YAG is a solid-state laser optically pumped by flash lamps, continuous gas discharge lamps or near-infrared diode lasers with a fundamental wavelength of 1064 nm; they operate in both pulsed and continuous mode. With recent improvements, it is now

possible to operate this type of laser in the visible region, i.e. at 533 nm wavelength, known as frequency-doubled (second harmonic) Nd:YAG and at various wavelengths in the ultraviolet region of the electromagnetic spectrum, namely 355 nm, 266 nm and 213 nm, called frequency-tripled (third harmonic), frequency-quadrupled (fourth harmonic) and frequency-quintupled (fifth harmonic) respectively, which are all collectively referred to as UV Nd:YAG lasers. These solid-state lasers, when pumped with semiconductor/diode lasers, are commonly referred to as Diode-Pumped Solid-State lasers (DPSS) [6 - 8].

5.3   UV Nd:YAG Laser Ablation of Polymer Waveguides

Excimer laser ablation of polymers, typically at 193 nm (of ArF) and 248nm (of KrF), has been repeatedly reported in the literature [9 - 13]. Excimer micromachining has also been used for other applications, including via drilling in PCBs and still remains part of some PCB laser drilling operations [1]. However, its speed and running cost are some of the reasons for its comparatively low acceptance today in the PCB manufacturing industry [2, 4, 14, and 15]. In the aforementioned technology, high quality micromachining, sometimes referred to as 'cold ablation', is thought to be due to the UV absorption sensitivity (including an affinity of these polymers to these UV wavelengths) on the one hand, and the short pulse time of the Excimer laser in the range of 15 – 30 ns on the other. Going by these assumptions, the current UV Nd:YAG lasers which offer both features, could therefore be adapted for the same technology. In spite of these potential advantages offered by the UV Nd:YAG lasers, there has been less attention towards their use in polymer waveguide fabrication except in [16] where a waveguide fabrication was performed at 1 mm/s, for which both energy and frequency were observed to have an impact on the smoothness of the waveguide side wall but required optimization although the optimised values used were not stated. Steenberge, et.al [16] further wrote that both photothermal and photochemical processes were present during the fabrication, due to the high wavelength of UV Nd:YAG compared to KrF Excimer laser, and was also said to have an impact on the smoothness of the waveguide side wall; although, waveguide losses were yet to be performed and the values of wall roughness were not stated. For the aforementioned points, the author considered its investigation not only as a necessity, but also as a requirement and contribution to the ongoing drive in the deployment of OI.

5.4   Experimental Set-up

The principal UV Nd:YAG laser used in this project was a diode-pumped frequency-tripled UV Nd:YAG laser system manufactured by Electro Scientific Industries (ESI). It is an ESI model 5200 UV µVia Drill, which operates at a wavelength of 355 nm (i.e. near ultraviolet) with 60 ns pulsewidth, power and PRF of up to 3 Watt and 20 kHz respectively. For this system setup, it was impractical to measure the power at the workpiece due to certain restrictions hence the average input powers were usually referred to whenever power was mentioned unless otherwise stated. In addition, since the laser used pulsed operation mode, the energy per pulse (mJ) can be obtained by dividing the average power (Watt) by the PRF (kHz). The author of this thesis conducted a test on the beam stability (figure 5.1); it shows the beam stability of 2.33 % over a period of 10 minutes. This is more or less in the order of the quoted long term stability of 2.5 % by the manufacturer [17] – an indication of a satisfactory beam profile used for the experiments.

The beam intensity profile was Gaussian with a fixed beam diameter of 25 µm, primarily designed for drilling holes in PCB materials. Therefore, etching a track of dimensions greater than 25 µm wide required the beam passes to be overlapped; for this, a value in microns for beam overlapping, less than the size of the original spot size was inserted into the system software which then calculated the optimum pattern by which the required track width was to be filled. For the results of the experiments presented here, the value of the beam overlap was maintained at a fixed value of 5 µm. The depth measurement was carried out using the Flash™200 optical measuring device; for this, the samples were diced, potted and polished such that the measurement could be obtained by looking at the cross-section profiles of the ablated structures. In each case, measurement was taken at three or more points along the track length to ascertain the deviation of the data obtained.
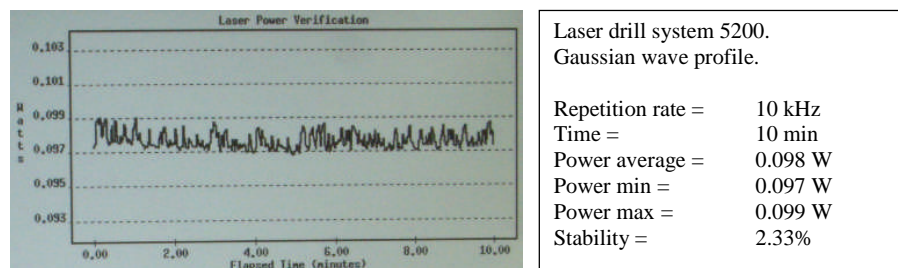
Figure 5-1: Power versus time curve for 5200 laser drill system (courtesy of Stevenage Circuits Limited).

5.5   Feasibility Study – Initial Laser Machining

The initial trial was largely focused on the laser-matter interaction vis-a-vis laser beam absorption and the possibility of using this class of laser for Truemode™ photopolymer albeit the same laser has been reportedly used for other polymers [2, 4]. The first laser micromachining trial was conducted on two different polymers, namely PMMA and Truemode™ using the host fabrication settings for processing PCB materials at high speed $\geq$ 100 mm/s and powers $\geq$ 1 Watt. The results showed a very poor absorption of the beam (which led to a non-clear line/track pattern marred with black spots and very dark patches like re-solidified molten material) especially with regard to PMMA; an unexpected result since the ablation of both polymers had been successfully demonstrated in the literature using Excimer laser(s) and, to some extent, on UV Nd:YAG. Incorrect parameters were thought to be the cause. In addition, the low absorption coefficient of PMMA, < 10 cm^{-1} at 351 nm [18] may have led to such a pronounced effect. For this reason, further trials were scheduled.

In the second trial, a range of parameter combinations (at much lower power and speed) were considered to machine Truemode™ as follows: (i) translation stage velocity between 5 mm/s and 100 mm/s, (ii) power between 0.1 Watt and 0.5 Watt, and (iii) pulse repetition rate between 10 kHz and 20 kHz. In addition, for each experimental value, a set of three tracks, 50 µm, 75 µm and 100 µm wide, were made; this was achieved by beam overlap. Figure 5.2 shows cross-sections through machined samples from this trial in which the laser beam was passed once or twice over the structures; in figure 5.2a the three structures were machined at 5 mm/s, 20 kHz and 0.1 Watt and shows that the depth varied proportionally to the width of the track from 50 µm to 100 µm looking from left to right. The variation in the ablation depth when compared with the track width in this process could be a result of the fact that the number of 25 µm fixed beam spots needed to form any desired width increases as the width enhances, this stepped-up the beam intensity delivered to a given area and thus the depth of ablation as shown later in section 5.6 where the effect of changing the track width with depth of ablation is presented. In figure 5.2b however, the parameters were different: the speed and power were doubled to 10 mm/s and 0.2 Watt respectively, while the repetition rate was the same as that used for the structures in figure 5.2a. The increase in speed and power led to a greater depth of ablation.

During this investigation an unusual effect was observed (figure 5.2c) when the structures were ablated at the same setting as that of figure 5.2a with the exception that 0.2 Watt input power was applied as opposed to the former. This led to a greater depth of ablation, closer to, but not reaching the clad/FR4 interface. However, despite this, a "discontinuity" was observed directly below the machined area at this interface. This was observed at other parameters (figures 5.2b and 5.2d) indicated in the solid circular blue line. There could be many possible interpretations for this 'abnormality'. One could argue that it was possibly due to the parameter change from 0.1 Watt to 0.2 Watt since this trend did not occur in the former. However, it still occurred when the same parameters used in figure 5.2a were used for structures in figure 5.2d except for a change in the number of passes from 1 to 2 which should only relate to the depth of ablation.

A close examination (of the figures) revealed that the effect occurred only when the micromachining was close to the lower cladding-FR4 substrate interface, which might suggest that the phenomenon may be largely due to the difference in the optical property of the materials, most especially the absorption coefficient and etch rate. The etch rate difference would then mean more pulses or higher beam intensity requirement at this interface (since etch rate in FR4 is obviously expected to be lower than that of Truemode™ polymer) and thus a possible thermal or similar damage at this region.

Chung, et al [19] observed, as discussed in chapter three, that putting a glass substrate below a silicon material caused the latter to absorb the 10.6 µm wavelength of the CO_2 laser; a similar situation could be attributed to this case. Although this might not be an issue of concern for the waveguide fabrication technique since for this method (as previously explained in chapter 3) ablation is not intended and in fact not recommended to reach the FR4, nevertheless further research is needed to explore the possible cause(s) not only in this case but also for that of silicon as admitted by the authors of [19].

It is also worthwhile to note that the ablated structures in figure 5.2d have different shapes compared to corresponding images in figures 5.2a, 5.2b and 5.2c; this could be due to the fact that all were, with the exception of the former (i.e. figure 5.2d) machined at one pass. It could be argued that during the first laser beam pass, the profiles in figure 5.2d would have produced similar shapes as the others, however, when the second beam pass was carried out on this, it further etched the tip of the profile formed during the first pass and thus broadened the profile of the ablated structures as evidently seen in figure 5.2d.
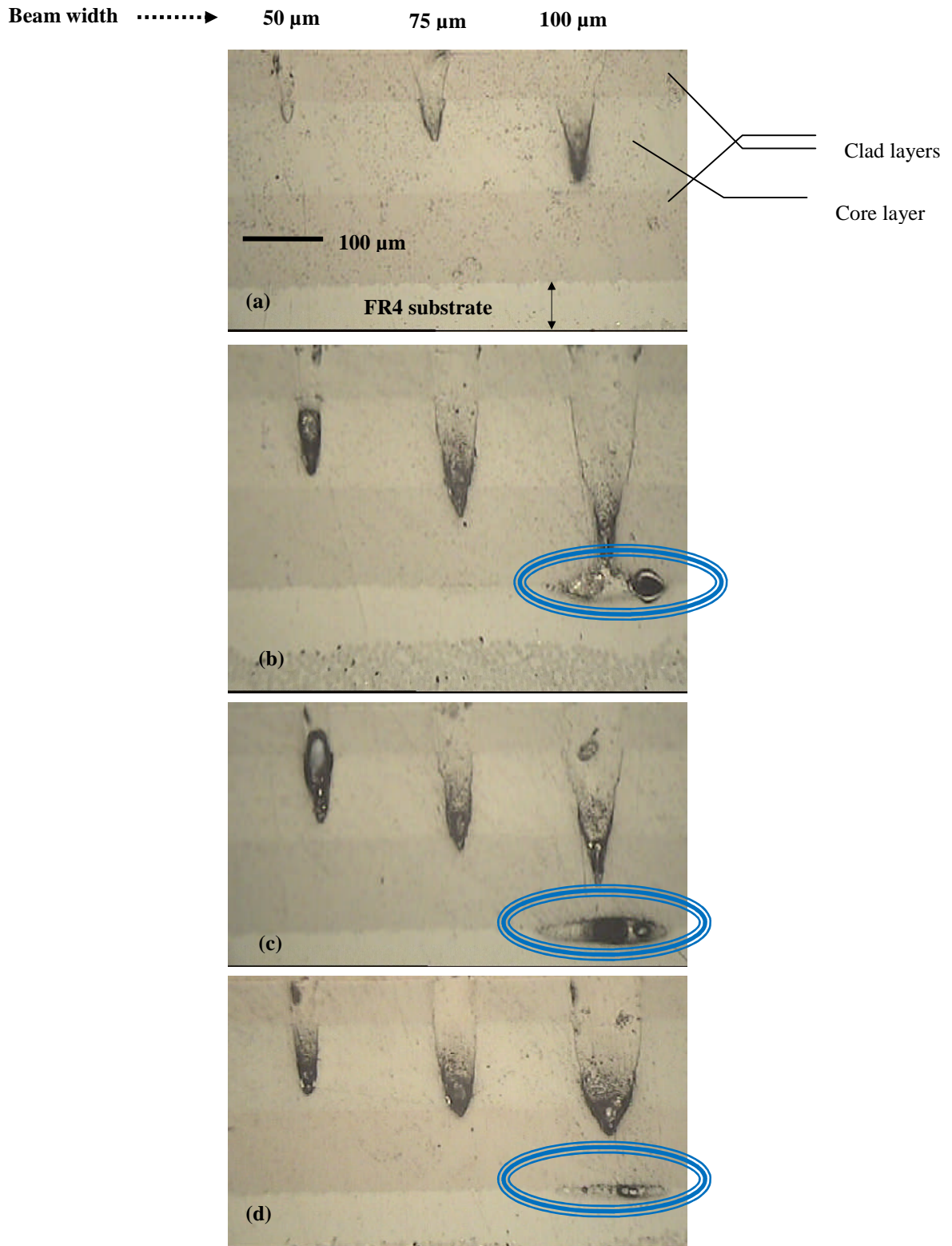
Figure 5-2: (a) 5 mm/s, 20 kHz, 0.1 Watt and a single pass; (b) 10 mm/s, 20 kHz, 0.2 Watt and a single pass; (c) 5 mm/s, 20 kHz, 0.2 Watt and a single pass; and (d) 5 mm/s, 20 kHz , 0.1 Watt and 2 number of passes.

The following points sum up the results of the feasibility study carried out: (i) that the Truemode™ optical polymer used in this research absorbs at 355 nm UV Nd:YAG wavelength provided that an appropriate laser parameter is used, (ii) that velocity, power, PRF, number of passes and track width (and beam overlap) on the laser used are the salient factors that affect the depth of ablation and thus require further investigation, and (iii) that ablation at relatively high speed above 30 mm/s is not suitable and similarly relatively high power above 0.3 Watt is too thermally-damaging for the material – the basis of the choice of the 'operating window' used during the laser characterisation.

5.6   Laser System Characterisation

As with Excimer laser micromachining, UV Nd:YAG ablation is governed by certain controllable experimental parameters – the basis of investigation in this section. Effects of the laser power, PRF, translational stage velocity, number of passes, and effective linewidth on the depth of ablation were studied. In each case, all factors were kept constant with the exception of the one under investigation and the setting was used to ablate 75 µm wide 50 mm long channels. The fact that there was no, as far as it is known to the author at the time of writing this thesis, public information showing the relationship between the aforementioned factors and the depth of ablation for Truemode™ polymer coupled with the fact that experimental results in relation to other polymers using the same 355 nm UV Nd:YAG laser cannot be easily used taking into consideration the difference in absorption coefficients of the polymers, established the importance of this investigation.

5.6.1   Power

In this set of four experiments, all factors were fixed while power was increased at an interval of 0.05 Watt from 0.1 Watt to 0.25 Watt. Figures 5.3 and 5.4 show the cross-section and plan views respectively of the four different channels machined at 0.1 Watt, 0.15 Watt, 0.2 Watt and 0.25 Watt input power; these correspond to input pulse energies of 0.01 mJ, 0.015 mJ, 0.02 mJ and 0.025 mJ respectively. It is obvious from the cross-sectional view of the ablated structures shown in figure 5.3 that an increase in power resulted in an increase in the amount of material removed with minimum and maximum etch achieved at 0.1 Watt (figure 5.3 a) and 0.25 Watt (figure 5.3 d) respectively; the ablated channels at these settings (with power varying) produced straight edges as shown in

figure 5.4. Since the energy/power could not be obtained at the workpiece, it followed that these values would be the basis of analysis in this case rather than the commonly used fluence; however, both are directly related. That is to say, fluence is equal to the energy divided by the beam or spot size.
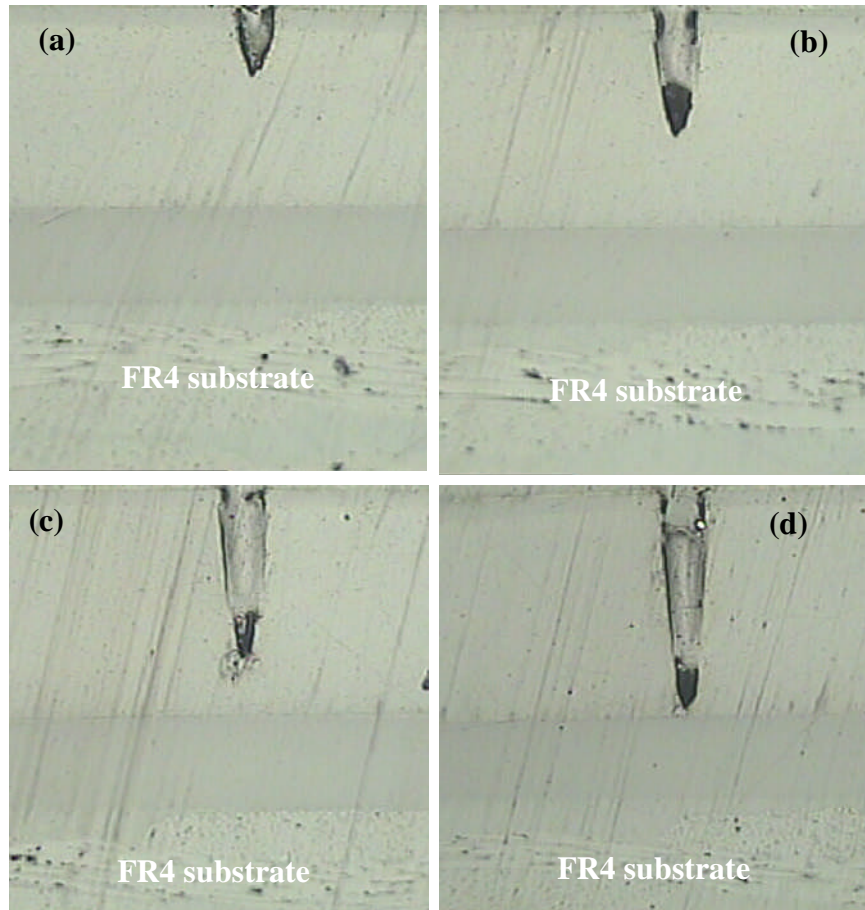
Figure 5-3: Cross-section of structures machined in Truemode™ optical polymer at 10 kHz, 10 mm/s, 75 µm linewidth and six passes but varying input power (a) 0.1 Watt, (b) 0.15 Watt, (c) 0.2 Watt, and (d) 0.25 Watt.
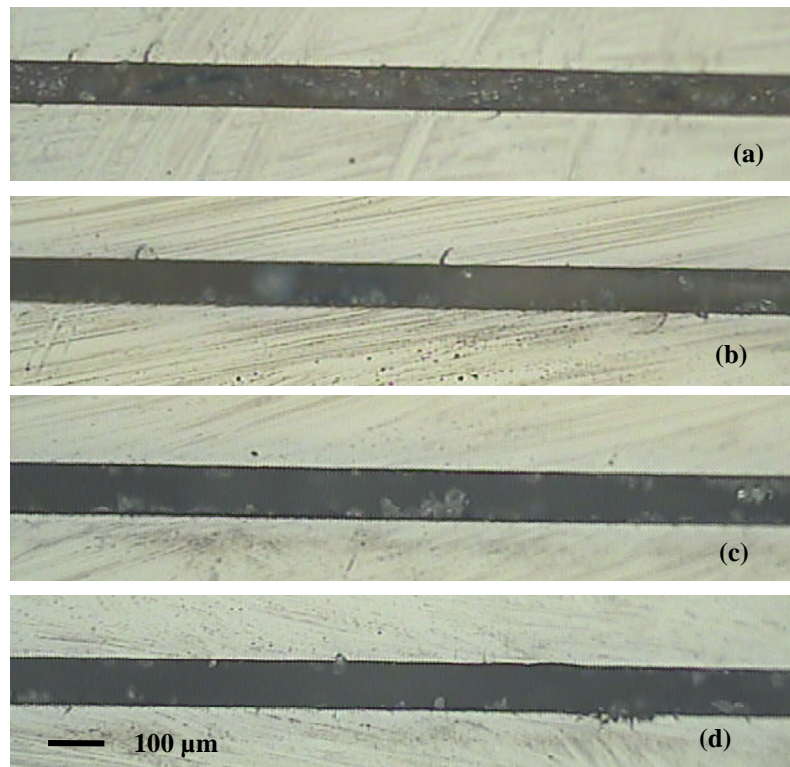
Figure 5-4:   Plan view of structures machined in Truemode™ optical polymer at 10 kHz, 10 mm/s, 75 µm linewidth and six passes but varying input power (a) 0.1 Watt, (b) 0.15 Watt, (c) 0.2 Watt, and (d) 0.25 Watt.

The graph shown in figure 5.5 is the plot of the relationship between the input power and the depth of ablation which indicates a direct proportionality between the two factors as expected; that it to say, increase in power caused a corresponding increase in the total depth of ablation. It was obvious that laser power played a major role in the amount of material removed.

The ablation (power) threshold at 10 kHz and 15 mm/s can be obtained by extrapolating the graph in figure 5.5, which is about 0.08 Watt. The estimated threshold here suggests that the ablation of Truemode™ using this system ought to be carried out at a value equal or greater than 0.08 Watt or at $\geq$ 0.008 mJ/pulse. This is because, an average power of 0.1 Watt at 10 kHz is the same as that of 0.2 Watt at 20 kHz as each produces a 0.01 mJ/pulse of energy. In addition, the operating power should be maintained only a little above the power threshold, say between 0.1Watt - 0.2Watt (i.e. 0.01 – 0.02 mJ/pulse) for this case, to avoid the dominance of photothermal processes over photochemical as per the general recommendation in laser ablation of polymers. This supports the observation made during the initial trials where ablating at high power of 0.5Watt produced poor results which could

be as a result of the fact that the power used then was well above the ablation threshold.

As previously affirmed, the modelling of laser-matter interaction cannot be generally taken/used, however, a curve fitting (represented by the green dotted line in figure 5.5) provided a mathematical means of representing/interpreting the behaviour of the process as shown in equation 5.1, where D is the depth of ablation in microns and p, the input power in Watt. A similar graph showing the relationship between the power and the depth of ablation is plotted in figure 5.6 with the horizontal axis (or x-axis) representing the ratio of the input laser power and the estimated power threshold denoted as p and p_t respectively. The ablation power threshold, p_t, used is that obtained by extrapolating the graph in figure 5.5 as earlier mentioned which is 0.08 Watt. This graph (figure 5.6) is identical in shape to that of figure 5.5 since the former is obtained from the latter with the introduction of ablation threshold. Furthermore, the resulting equations (equations 5.1 and 5.2) are similar with each having an R^2 of 0.9982 and the coefficient of the logarithmic term in both equations is also equal with a value of 488.54.

$$D = 488.54 \, ln \, (p) + \, 1214.8 \qquad (5.1)$$

$$D = 488.54 \, ln \, (^p/_{p_t}) - \, 19.102 \qquad (5.2)$$
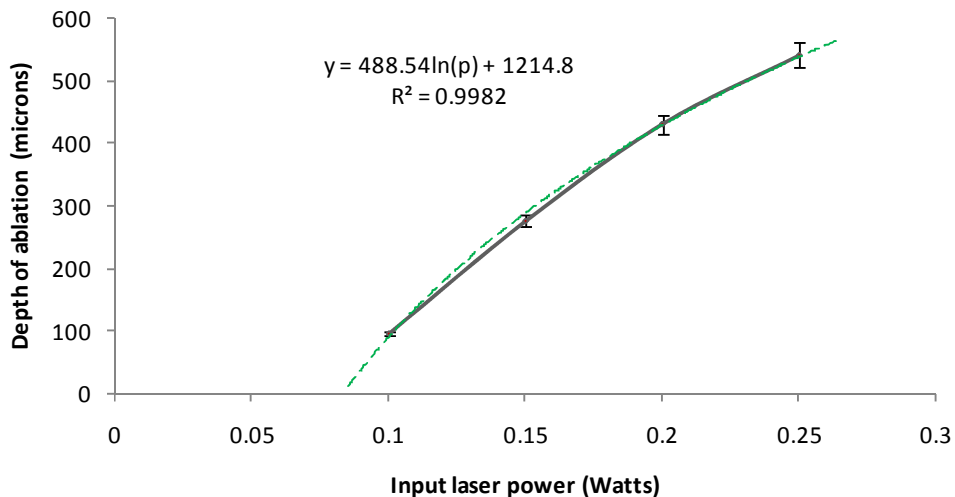
Figure 5-5: Graphical representation of the effect of power on the depth of ablation at 15 mm/s translation speed 10 kHz and scanning at six times.

$$y = 488.54\ln(p/p_t) - 19.102$$
$$R^2 = 0.9982$$
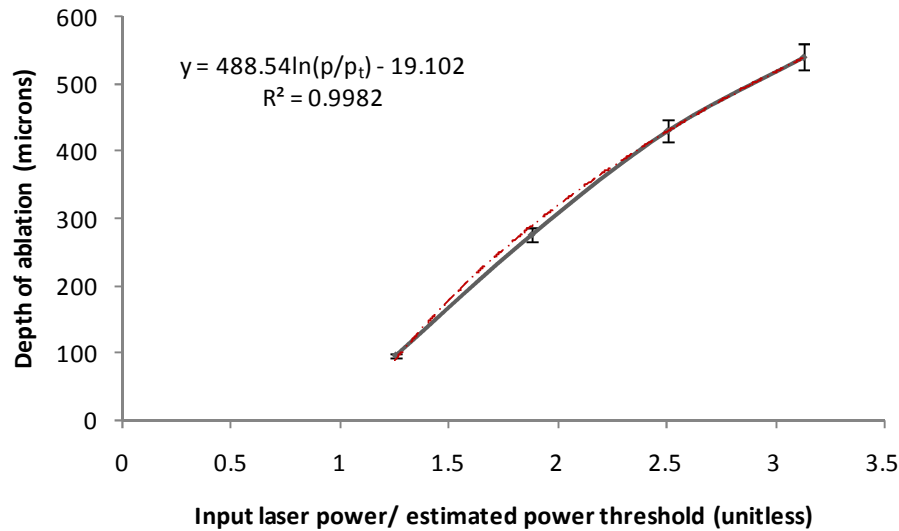
Figure 5-6: Graphical representation of the effect of (input power / estimated power threshold) on the depth of ablation at 15 mm/s translation speed 10 kHz and scanning at six times.

5.6.2 Pulse repetition frequency (PRF)

Reports have indicated different behaviours – depending on the laser wavelength and material absorption – with regard to the effect of the pulse repetition rate/frequency (PRF/PRR) on the depth of ablation. To investigate the relevance of PRF (or PRR), all other experimental parameters, namely: laser power, translation stage speed and number of scans (or passes), were kept constant at 0.1 Watt, 5 mm/s and 4 passes respectively with the exception of PRF, which was increased at intervals of 5 kHz between 5 kHz and 20 kHz.

Figure 5.7 shows the cross-section of the four different channels ablated by changing the frequency from 5 kHz to 20 kHz while figure 5.8 is the plan view of the same set of channels. The plot of PRF against the depth of ablation is shown in figure 5.9; this indicates a decrease in ablation depth from 5 kHz to 15 kHz, thereafter, an increase is noticed from 15 kHz to 20 kHz.

In the first three instances, i.e. from 5 kHz to 15 kHz, where there was a decrease in the depth of ablation as the repetition rate increased, it could be argued that the depth decrease was due to the fact that though more pulses per area were released per second at higher frequencies, the energy per pulse was reduced. This is because, since the average power of the laser remained constant at 0.1 Watt, the energy per pulse, which is equal to the average

power, divided by the PRF, decreased. In other words, both the PRF and energy per pulse played their individual role at this instance. A sudden rise in the depth of ablation at 20 kHz, which has the least pulse energy, though unusual, can only be explained by considering the 'effectiveness' of this high PRF. That is to say, at high PRF, though the energy per pulse is low, the fact that more pulses were used per area could mean that some of the pulses were not photochemically used to ablate the material. These unused pulses effectively contributed to a photothermal process or part of the ablation mechanism and thus enhanced (or increased) the absolute depth of ablation. Having said this, the matter is more complex than this especially when it involves changes in PRF.
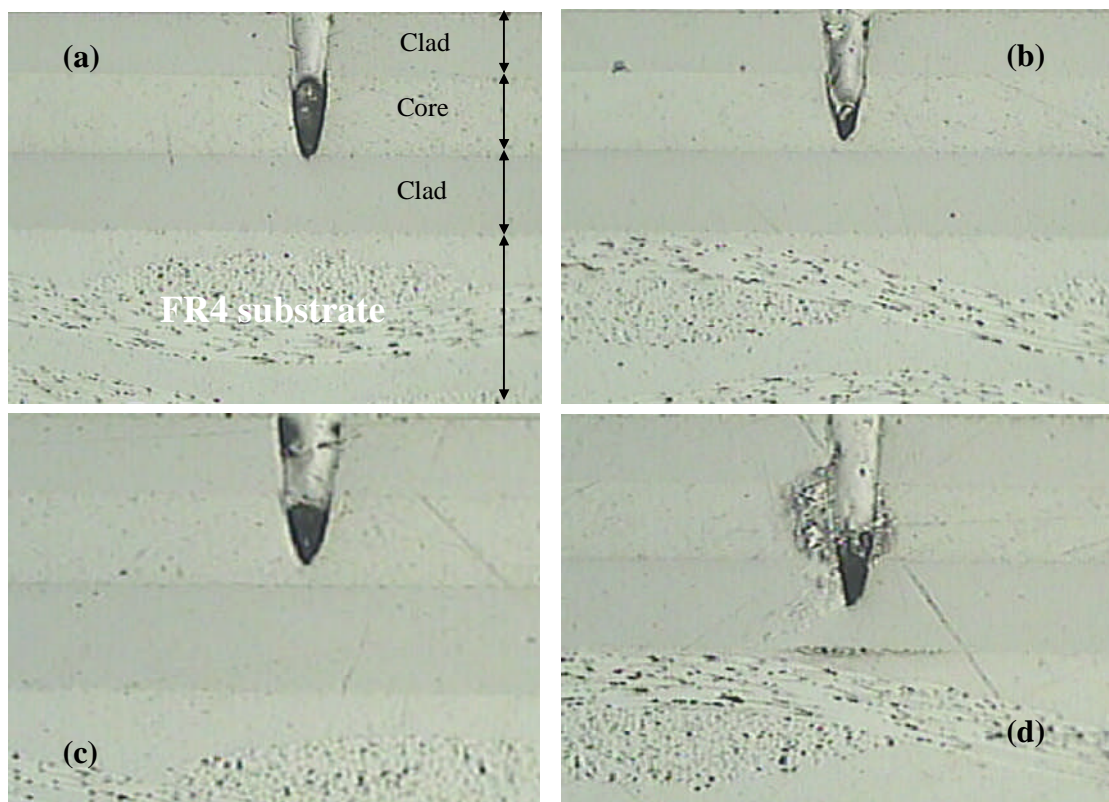
Figure 5-7:   Cross-section of structures machined in Truemode™ optical polymer at 0.1 Watt, 5 mm/s and four passes but varying PRF: (a) 5 kHz, (b) 10 kHz, (c) 15 kHz, and (d) 20 kHz.
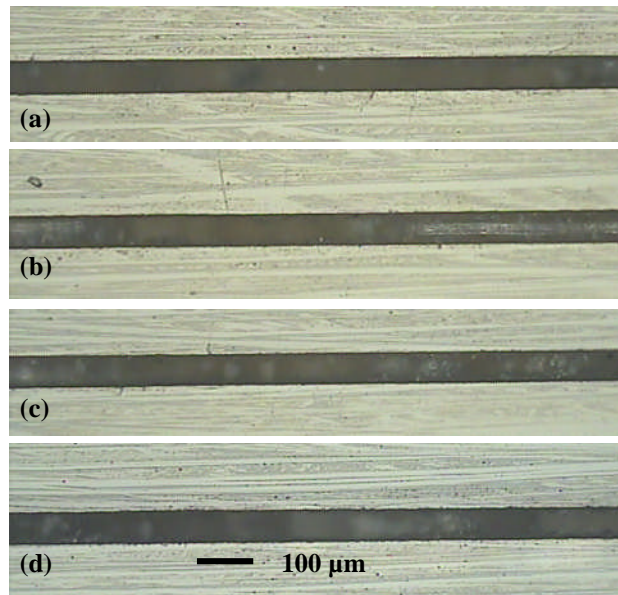
Figure 5-8: Plan view of structures machined in Truemode™ optical polymer at 0.1 W, 5 mm/s and four passes but varying PRF (a) 5 kHz, (b) 10 kHz, (c) 15 kHz, and (d) 20 kHz.
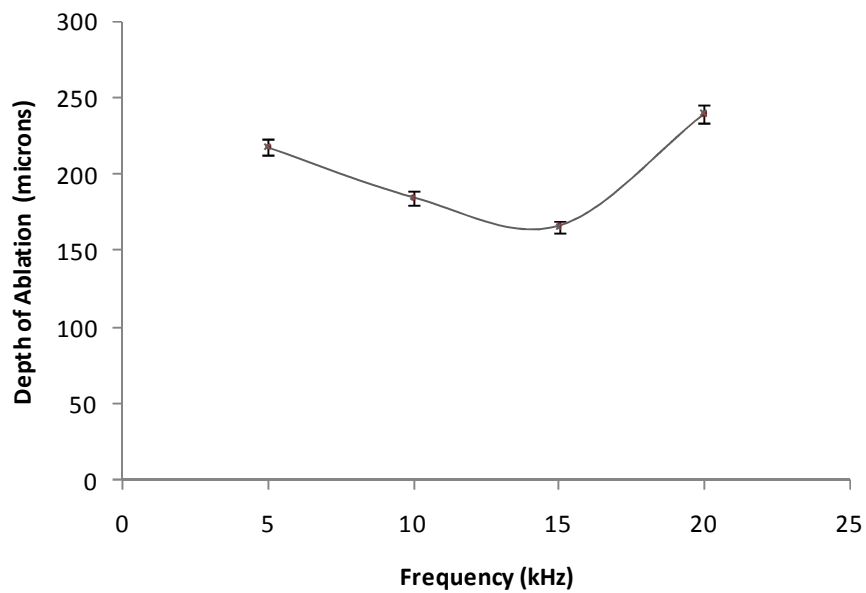
Figure 5-9: Graphical representation of the effect of PRF on the depth of ablation at a constant power of 0.1Watt, and a translational stage speed of 5mm/s showing the depth of ablation against PRF.

5.6.3   Velocity

The two main relevance of the scanning speed or velocity of the beam across the surface during laser ablation, are first, its contribution to the power/energy density available at the point of ablation and secondly, its influence on the smoothness of the ablation, especially the edges. In this investigation, laser ablation was carried out keeping all experimental factors – power, PRF and number of passes – fixed at 0.1 Watt, 5 kHz and two passes respectively, with the exception of the velocity of the translation stage, which was increased at an interval of 5 mm/s between 5 mm/s and 20 mm/s. It is obvious from figure 5.10, which shows the ablation depth as a function of speed, that the depth of ablation was inversely proportional to the speed of the translation stage, i.e. more material was removed at low speed due to more pulses reaching the material at this instance. However, the slope of the curve was steeper between 5 mm/s and ~ 10 mm/s than towards the 20 mm/s speed.

The plan views of the ablated channels shown in figure 5.11 imply that the lower the speed the better is the edge 'finish' with ablation at 5mm/s speed giving the smoothest finish of all. This effect/observation was expected (since the process was carried out with an appropriate parameter combination for the given material) because, at low speed, the laser pulses could overlap much better than at a high speed and it is also in line with the general recommendation for laser ablation of polymers. Therefore, low speeds, ~ 5 mm/s, of ablation were used during the optical waveguide fabrication.
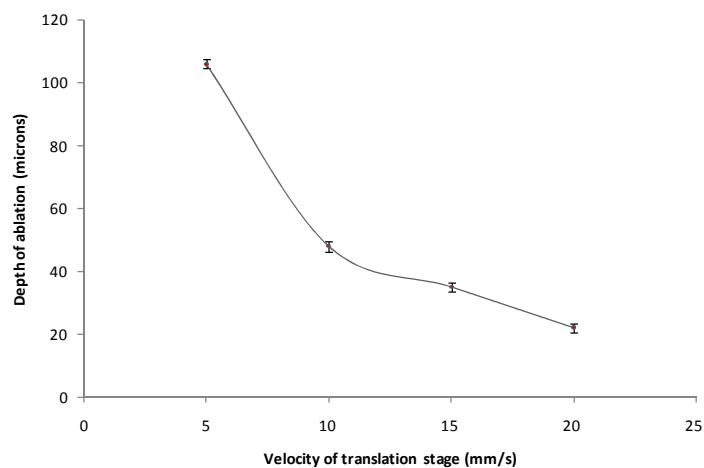
Figure 5-10:   Graphical representation of the effect of velocity on the depth of ablation at 0.1 Watt, 5 kHz and 2 passes.
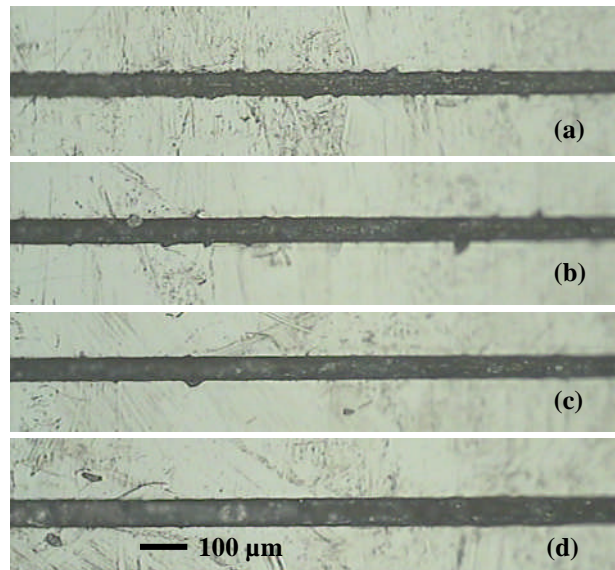
Figure 5-11: Optical microscope images showing structures machined in Truemode™ optical polymer at 0.1 Watt, 5 kHz, 75 µm linewidth and two passes but varying speed: (a) 20 mm/s, (b) 15 mm/s, (c) 10 mm/s, and (d) 5 mm/s.

5.6.4   Number of passes

For this experiment, input laser power, PRF and velocity of the translation stage were held constant at 0.2 Watt, 15 kHz and 15 mm/s respectively while the number of passes was varied. Figure 5.12 is the plot of the number of times the polymer material was laser-scanned against the depth of ablation; this showed an increase in the ablation depth as the number of passes increased. The ablation depth did not exactly correspond to the increase in the number of passes; that is to say, the ablation depth for four passes was not exactly twice that of two passes. A possible explanation for this could be that, the 'effective' pulses reaching the material at the ablation zone is reduced in subsequent scans as there will be some debris deposition from the preceding scan that needs to be removed using a portion of the incoming pulses of the current scan. Alternatively, the increasing depth of the hole makes it harder for the ablated material to be ejected clearly, such that some remains. This result is useful as it means that the incident energy was efficient in removing the material in multiple passes such that the input power, for example, could be halved and 2-passes used as an alternative. By and large, reducing the operating power and/or power density for multiple passes could minimise the dominance of photothermal processes and HAZ.
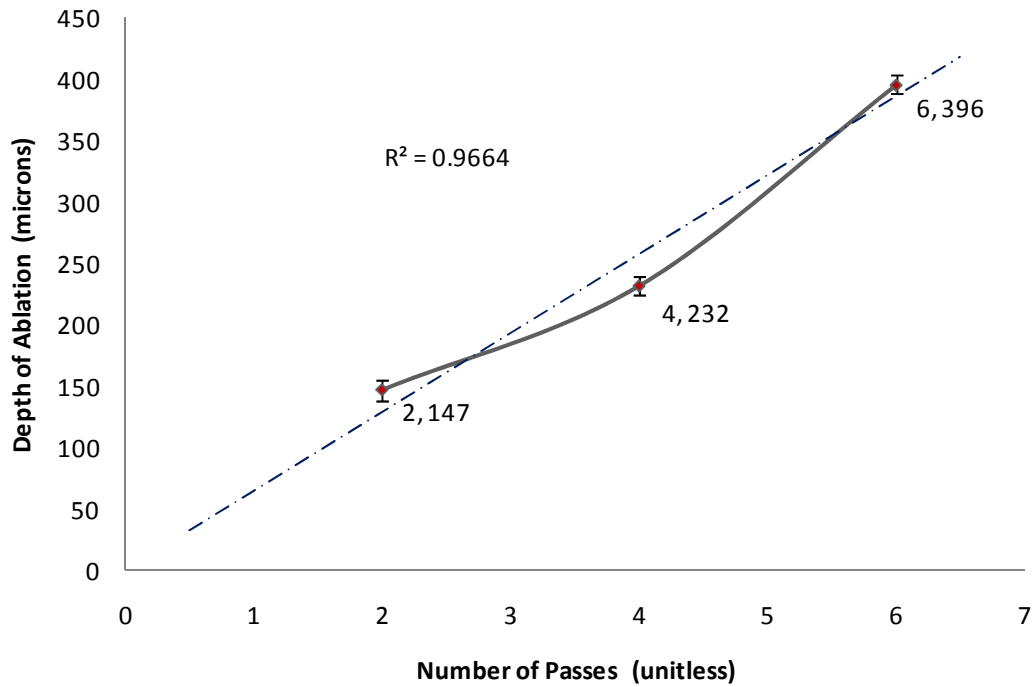
Figure 5-12: Graphical representation of the effect of passes/scans on the depth of ablation at constant power of 0.2Watt, 15 kHz and 15 mm/s.

5.6.5 Line width

The UV Nd:YAG laser system described in section 5.4 has a beam size fixed at 25 μm which means that only 25 μm wide features could be created in a single pass. To achieve other feature sizes, for instance 70 μm wide tracks, the beams are overlapped using a computer program, which fills the desired feature size, hence making it easy to create any desired beam size from 25 μm upwards. The effect of change in the 'effective beam size' on the amount of material that could be removed was investigated at a constant power of 0.1 Watt, 5 kHz PRF, 5 mm/s and one pass with 'effective beam size' varied from 30 μm to 100 μm. The plot of 'effective beam size' against the depth of ablation (figure 5.13) indicates a linear relationship between the two quantities up to a width value of 80 μm, thereafter any increment in width did not have much effect on the quantity of material removed.
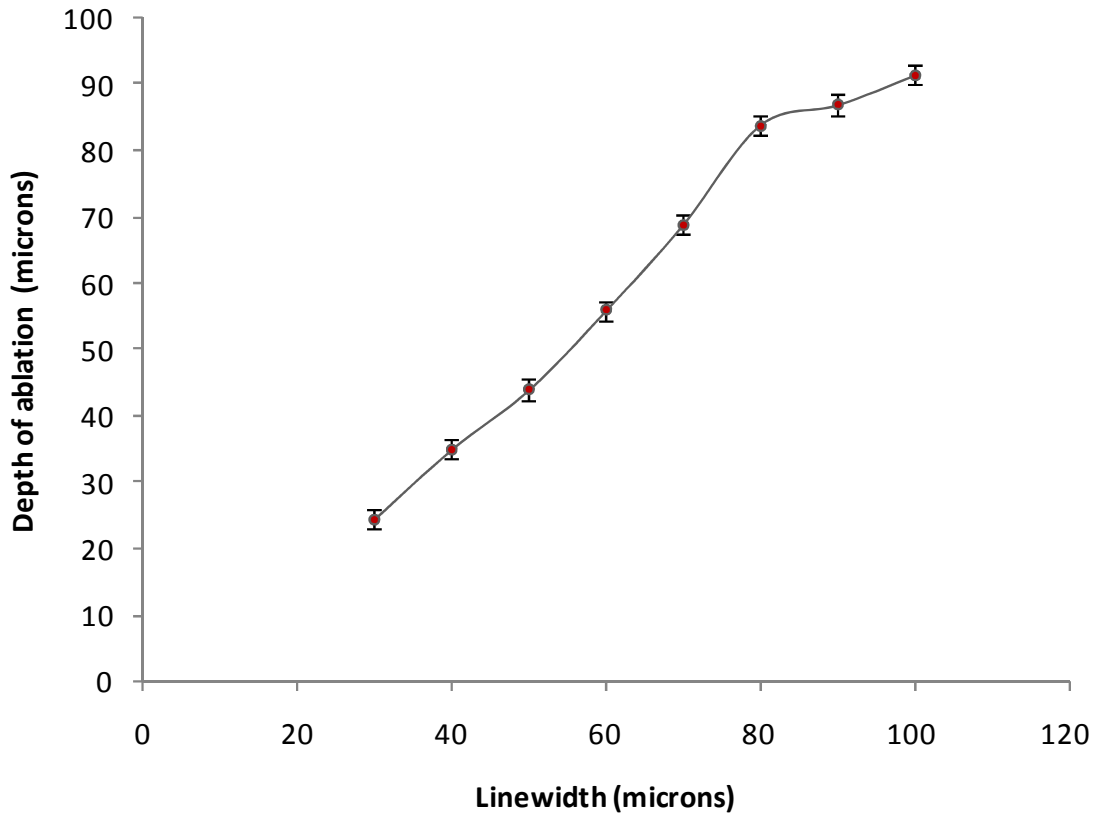
Figure 5-13: Graphical representation of the effect of ablated line width on the depth of ablation at constant power of 0.1Watt, 5 kHz, 5 mm/s and one repetition.

5.7   Discussion

The laser ablation of polymeric or other materials is, without doubt, a complex mechanism. That is why in most cases, it is better that an explanation is made specific to a process under investigation. It is however understood from the results of the laser system characterisation carried out in this study (section 5.6) that the factors considered – velocity, power, number of passes and effective beam size – each had an effect on the ablation of Truemode™ polymer for the settings used. These factors are related to the power or power density available at the ablation zone; for example, two passes means doubling the power at the workpiece compared to a single pass though the effectiveness and efficiency of the second pass might be lower. Similarly, an increase in processing speed (i.e. stage speed) means that the number of pulses reaching the material to be machined is reduced in the same proportion, which in turn leads to a decrease in the ablation depth since less energy or power is expended on the material.

Steenberge et al. [16] observed that due to the high wavelength of UV Nd:YAG compared to Excimer lasers, the photothermal process cannot be ignored for ablation (of ORMOCER) at this wavelength. Winco, et al. also concluded in [4] that due to an apparent melting effect during the ablation of polyimide at 355 nm, the mechanism has a photothermal contribution. The regression line (equation 5.1) obtained from the graph of the relationship between the power and depth of ablation has two terms/parts. The first part, 488.54 ln(p), can be regarded as a photochemical contribution to the ablation mechanism since it is a function of fluence (or power) with a coefficient not equal to zero. The second term of this equation is a constant term with a value of 1214.8 which can be viewed as a photothermal effect of the process; however, since the value of this constant part cannot be approximated to zero relative to the first part in this equation, it is therefore logical to conclude that both photochemical and photothermal mechanisms were responsible for the laser ablation of Truemode™ polymer at 355 nm wavelength using UV Nd:YAG laser. This is similar in form with the Srinivasan-Smrtic-Babu (SSB)'s mathematical representation of laser ablation process – with two terms each representing photothermal and photochemical – which is favoured by the author of this thesis. The fact that the coefficient of R^2 is very close to 1, for this case 0.9982, implies that the equation is a close representation of the behaviour. It is worthwhile mentioning at this point that an attempt was made to fit the curve with other 'models' such as linear and exponential models but the R^2 values obtained were lower than that of a logarithmic function; for example, the R^2 for linear and exponential fittings were 0.9889 and 0.9641 respectively. Although, these values also showed a high degree of correlation since they are very close to unity, nevertheless, the logarithmic function still offer a better degree of confidence.

Having said this, the following should however be noted about equation 5.1 : (i) the 'p' in this equation is the input power and not the fluence/fluence threshold (f/f_{th}) as it is the case in the two models discussed in chapter two, (ii) since natural logarithm of zero, i.e. ln (0), is a mathematical error, it follows that the equation is not valid at an input power of zero, (iii) the fact that the two commonly cited models are valid provided that fluence is greater than the ablation threshold means that values below the threshold cannot be directly substituted for the model, and (iv) since ln (p) for $0 < p < 1$ is negative; then the depth of ablation (D) would always be less than the constant part of this equation for the range of power input considered. By and large, it appears that equation 5.2 conforms more to the SSB's model for laser ablation since the p/p_t value was used in plotting the graph in figure 5.6 which

produced the equation; however, unlike with the SSB's model (and equation 5.1) the 'photothermal' or constant term in equation 5.2 carries a negative sign which can be viewed as an 'anti-photothermal'.

Since ablation rate or depth is largely dependent on the fluence or power density used, provided the ablation threshold is reached, this explains the main reason why the graphs obtained for velocity, power, linewidth and number of passes bore a direct relationship with the depth of ablation. In other words, increase in one of these factors resulted in a corresponding increase in the depth of ablation for Truemode™ polymer machined at 355 nm using UV Nd:YAG.

However, a careful assessment of the graph showing the relationship between the change in Pulse Repetition Rate (PRR) and the depth of ablation showed that there are two distinctive regions (figure 5.9), both of which require different interpretations. Further to what has been said earlier, two possible explanations for this behaviour are given below.

i.   In the first region, where the slope is negative, incident pulses which were in excess of the absorption rate of the polymer (i.e. Truemode™) were directly converted to heat energy, which increased the temperature of the ablated material but not quite enough to result in photothermal ablation. The continuous increment in the number of incident pulses eventually resulted in the photothermal threshold being reached and ablation at this stage was not only photochemical but also photothermal, thus speeding up the ablation rate [20].

ii. It could also be that frequency has no direct effect on the quantity of ablation at this frequency range as some authors have reported [20] for Excimer laser ablation of polymers with high absorption coefficients, namely: PC, PET, PI and PS. It could also be that specific frequencies perform optimally at particular combinations with other parameters. In other words, the effect of frequency is determined and influenced by a combination of other factors. In addition, the fact that the pulse energy released from this laser varies with frequency also compounded the trend observed in this study.

5.8   Summary and Conclusion

355 nm diode-pumped third harmonic UV Nd:YAG laser was used to machine structures

in Truemode™ polymer; the laser is a standard drilling machine - ESI model 5200 UV µVia Drill – hosted by a PCB manufacturer and an industrial partner to the consortium within which this PhD research was conducted. This made it a worthwhile investigation since it demonstrated the potential of using a single system for the definition of both electrical and optical channels. The pulse mode, short wavelength and pulse duration (60 ns) are some the key attractions to this laser which the author believes can allow it to complement and/or compete well with the Excimer laser for this application. The power and pulse repetition frequency of up to 3 Watt and 20 kHz respectively were possible; the beam was Gaussian with a fixed size of 25 microns but beam overlapping was possible to create wider dimensions.

The initial trial was largely focused on the laser-matter interaction vis-a-vis laser beam absorption and the possibility of using this class of laser for Truemode™ photopolymer micromachining; this was carried out using the host fabrication settings for processing PCB materials at high speed ≥ 100 mm/s and powers ≥ 1 Watt. The results showed a very poor absorption of the beam. The power used was reduced to $0.1 - 0.5$ Watt in the subsequent trial; similarly, the translation speed was kept below 100 mm/s to improve on the quantity of the ablated tracks in the initial trial. For this case, the results were of much better quality than when high power and speeds were used; this proved the suitability of the laser and served as the basis of operating windows for the system characterisation.

Therefore the effect of power (0.1 Watt to 0.25 Watt), PRF (5 kHz and 20 kHz), velocity (5 mm/s and 20 mm/s), number of passes (2 – 6) and line width (30 µm to 100 µm) on the depth of ablation were studied. These chosen parameters were observed to have direct link with the power or power density at the workpiece. In each case, all factors were kept constant with the exception of the one under investigation and the setting was used to ablate 75 µm wide 50 mm long channels. This represents an important investigation since such study, in relation to Truemode™, has not been reported before. Regression analysis was used in each case to explain the relationship between the variables studied and the depth of ablation. The depth achieved were found to be within the range required for ablating multimode core layer thickness (> 10 µm) through to the lower cladding in order to form a waveguide; for example, at 10 mm/s, 10 kHz, 6 passes and 0.2 Watt, the ablated depth was ~430 µm; this would give an average of ~70 µm/pass, which is enough for fabricating a multimode waveguide. Reducing the velocity to 5 mm/s can result in

doubling the depth of ablation. The author observed that velocity below 10 mm/s, power at < 0.15 Watt, PRF at <15 kHz and single pass would provide minimum thermal effect while still capable of etching through to the lower cladding.

The author observed that the relationship between the change in PRR and the depth of ablation showed two distinctive regions which require for both photothermal and photochemical interpretations of the mechanism. Having analysed the various behaviours, the author concludes that both photochemical and photothermal mechanisms were responsible for the laser ablation of Truemode™ polymer at 355 nm wavelength using UV Nd:YAG laser.

References

1. Gower, M. C. Industrial applications of laser micromachining. *Optics Express* 7, 56-67 (2000).

2. Yung, K. C., Zeng, D. W. and Yue, T. M. XPS investigation of Upilex-S polyimide ablated by 355 nm Nd:YAG laser irradiation. *Appl. Surf. Sci.* 173, 193-202 (2001).

3. Holden, H. T. The developing technologies of integrated optical waveguides in printed circuits. Circuit World 29, 42-50+9 (2003).

4. Winco, K.C. Yung, J.S. Liu, H.C. Man. Experimental investigation of 355nm Nd:YAG laser ablation of RCC in PCB . Circuit World 25, 13 -17 (1999).

5. Li, J. and Ananthasuresh, G. K. A quality study on the Excimer laser micromachining of electro-thermal-compliant micro devices. *Journal of micromechanics and micro engineering: structures, devices, and systems.* 11, 38-47 (2001).

6. Ion, J. C. in Laser processing of engineering materials: principles, procedure and industrial application 556 (Elsevier Butterworth-Heinemann, Oxford, 2005).

7. Steen, W. M. in Laser material processing (Springer, London, 2003).

8. Bityurin, N. Studies on laser ablation of polymers, Annu. Rep. Prog. Chem., Sect. C: Phys. Chem., 2005, 101, 216 – 247

9. Van Steenberge, G., Geerinck, P., Van Put, S. and Van Daele, P. Integration of multimode waveguides and micromirror couplers in printed circuit boards using laser ablation. *Proceedings of the SPIE - The International Society for Optical Engineering* 5454, 75-84 (2004).

10. Rumsby, P. T. and Gower, M. C. Excimer laser projector for microelectronics applications. *Proc SPIE Int Soc Opt Eng* 1598, 36-45 (1991).

11. Van Steenberge, G. et al. Laser ablation of parallel optical interconnects waveguides. IEEE Photonics Technology Letters 18, 1106-1108 (2006).

12. Thomas, D.W., Foulkes-Williams, C., Rumsby, P.T., and Gower, M.C. Surface modification of polymers and ceramics induced Excimer laser radiation, in Laser Ablation of Electronics Materials, Basic Mechanisms and Applications, 1992.

13. Harvey, E. C., Remnant, J. L., Rumsby, P. T. and Gower, M. C. Microstructuring by Excimer laser. *Proc SPIE Int Soc Opt Eng* 2639, 266-277 (1995).

14. Guillong, M., Horn, I., and Günther, D. Capabilities of a homogenized 266nm Nd:YAG laser ablation system for LA-ICP-MS. *J. Anal. At. Spectrom.,* 2002, 17, 8 - 14,

15. Zeng, D. W., Yung, K. C. and Xie, C. S. UV Nd:YAG laser ablation of copper: chemical states in both crater and halo studied by XPS. *Appl. Surf. Sci.* 217, 170-180 (2003).

16. Van Steenberge, G. et al. MT-compatible laser-ablated interconnections for optical printed circuit boards. J. Lightwave Technol. 22, 2083-90 (2004).

17. ESI 5200 Laser μvia Drill data sheet:
http://www.stevenagecircuits.co.uk/downloads/5200.pdf

18. Liu, Y. S., Cole, H. S. and Guida, R. Laser ablation of polymers for high-density interconnect. *Microelectronic Engineering. Vol. 20* 20, 15-29 (1993).

19. Chung, C. K., Wu, M. Y., Hsiao, E. J. and Sung, Y. C. Etching behaviour of silicon using CO_2 laser in Proceedings of the 2nd IEEE International Conference on Nano/Micro Engineered and Molecular Systems, Thailand, 2007.

20. Illy, E. K., Piper, J. A., Brown, D. J. W. and Withford, M. J. Enhanced polymer ablation rates using high-repetition-rate ultraviolet lasers. *IEEE Journal on Selected Topics in Quantum Electronics* 5, 1543-1548 (1999).

6   EXCIMER LASER SYSTEM CHARACTERISATION

6.1   Introduction

As with the last two chapters, this chapter also focuses on laser system characterisation; however, unlike other lasers, no feasibility study preceded the experimentation in the current case as the Excimer laser beam is believed to be strongly absorbed by most polymers and thus considered to be a viable technique for qualitative ablation.

6.2   Excimer Laser Ablation

Since its introduction into the market in 1977, with its first commercial available product from Lamda Physik called EMG 500, the Excimer laser has turned out to be a multi-purpose, multi-featured laser operating over a wide range of energy with increasing market shares in industrial and medical applications [1]. Although other lasers such as YAG and CO_2 lasers are also extensively used in HDI technology, when it comes to 'fine' finish micro- and nano-fabrication, especially of sensitive electronics or biomedical materials, the Excimer laser ablation is indispensable. This is largely due to its wavelength, pulse duration, and of course, its pulse energy allowing for what is generally termed as a 'cold ablation' process. The safety concern associated with the use of hazardous gases in the Excimer laser has been technically and considerably addressed with the emergence of technology such as HaloSafe making it comparatively cost effective and user-friendly [1].

The Excimer laser also excels the others in its ability to 'mask-project' patterns on to a sample. A minimal HAZ is another merit of Excimer laser over others, i.e. those operating in the visible and infrared regions of the electromagnetic spectrum; this minimal HAZ is argued to be due to its short interaction between the laser beam and the material. In addition, the short pulse duration of the Excimer is also a contributing factor; nevertheless, today, picosecond and femtosecond lasers are now available, designed to further reduce the HAZ and these class of lasers are also characterised with higher etch rate and lower ablation thresholds.

These aforementioned features of the Excimer laser have attracted and favoured its use not only for polymers [2, 3] but also other materials such as ceramics [4], glasses [5] and silicon [6] which are hard to machine. Besides, Excimer lasers are now used for surface

modification of various materials; Pleging, et al [7] has used Excimer at fluences below the ablation threshold to fabricate single mode optical waveguides in PMMA similar to that employed using CO_2 laser in [8]. Thomas, et al [9] also used an Excimer laser to effect changes to the chemical structures of materials (polymer and ceramic) with potential application in enhanced material adhesion and surface wettability among others.

6.3   Experimental Set-up

The Excimer laser used for the experiments presented in this chapter and chapters 7 and 8 is a 7000 Series Exitech Krypton Fluoride (KrF) laser operating at 248 nm wavelength with 20 ns pulse length schematically shown in figure 6.1. The system operates in both energy and voltage modes with values ranging from 0 – 250 mJ/pulse and 17 - 24 kV respectively; the operating energy was obtained with the aid of an energy meter placed at the workpiece. The output energy can be manipulated by an attenuator controlled by Aerotech Unidex-500 (U500) software. The system has a Charged-Coupled Device (CCD) camera for viewing samples placed on a XYZθ stage, with an aligner camera for focus setting. To define the size and shape of the beam spot at the workpiece the beam is passed through a mask which is then focused at the sample through a changeable projection lens (currently 10 times reduction, with 10.0 J/cm^2 achievable at the workpiece). This enables various shapes (square, circular, etc.) of beam spots to be used simply by changing the shape of the mask. Some of the main components of the system setup are described:
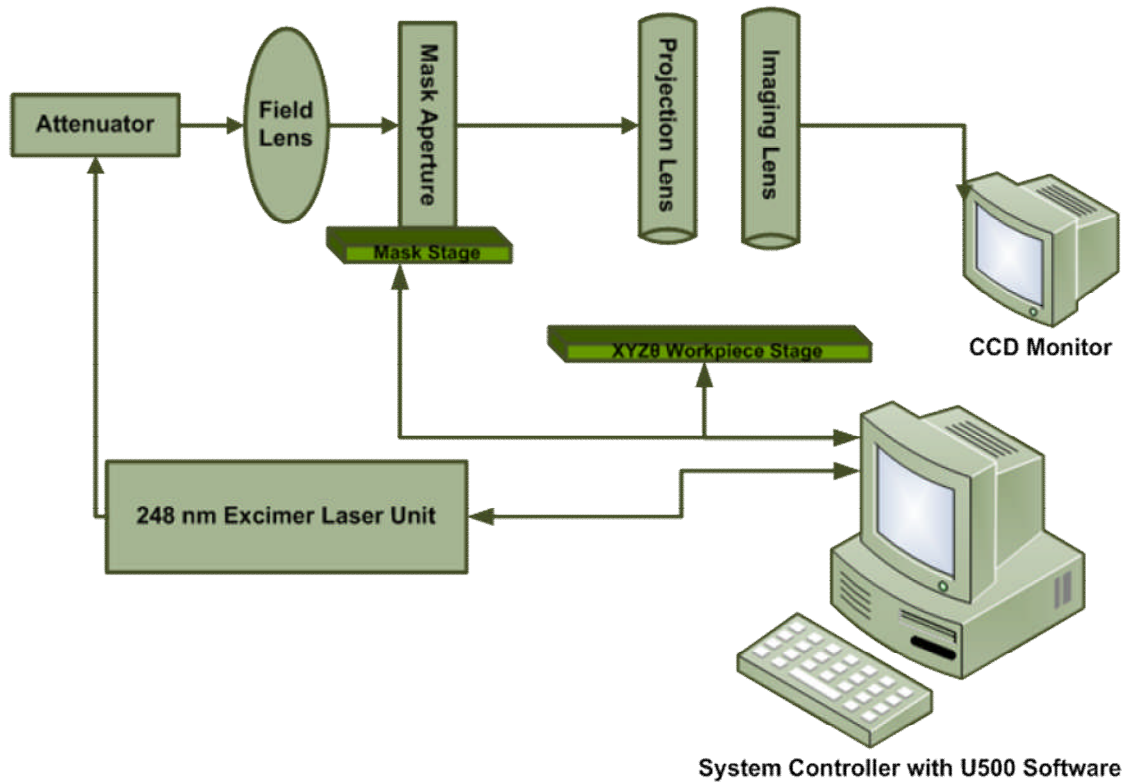
Figure 6-1: Schematic diagram of 7000 Series Exitech Krypton Fluoride (KrF) laser system setup showing various key components of the experimental setup.

1. Attenuator

The attenuator is the first optical component in the beam delivery system controlled using U500 software commands; it is an essential component because it allows the fluence to be controlled such that low fluence in the range required for the polymer(s) under investigation can be obtained from the high energy of the exit beam. Its value varies from 0.01 to 0.95 though this does not translate to a linear increase in output fluence.

2. Lenses

The number of lenses used in the beam delivery depends on the application; here, two different lenses are utilised in the beam delivery path to achieve different goals:

  a. Field Lens: Situated between the attenuator and mask; it is employed to redirect the beam onto the aperture or mask after having travelled a relatively long distance along the beam path.

  b. Projection Lens: This allows high-resolution images of the mask to be cast

onto the substrate with options of either 4 or 10 times demagnification thus permitting high fluences to be accomplished over a relatively small area on the substrate.

3. Projection Masks

Mask projection is an essential and unique feature of Excimer laser micromachining as it allows multiple and various patterns to be made on samples without needing to alter the beam shape. The mask can be made from a number of different alloys and metals such as thin chrome (on a quartz substrate), brass or stainless steel sheet. It is important that the mask used cannot be damaged at the working energy/power densities, for example, in a situation whereby fluences above 100 mJ/cm^2 are to be used, a mask made of chrome cannot be used because its damage threshold is at about this fluence [10].

 Although, one can argue that energy is wasted using the mask projection technique because a high proportion of the beam, depending on the ratio of the mask to the beam size, is wasted, its advantages (e.g. multiple complex patterning, increase in fluence by demagnifying factor of the projection lens, etc.) surpasses its demerits. For a simple and less sensitive process, such as in microvia fabrication, a mask with a desired pattern can be placed in contact or close to the polymer sample [11]. While other lasers – CO_2 and Nd:YAG – can be useful for mass production due to their high speeds, mask projection in the Excimer laser makes it easy for the patterning of complex shapes at a relatively high speed since the pattern can be made on the mask and replicated easily on the sample. In this current setup, both stationary and dynamic mask patterning is possible with the aid of a vertical – horizontal translation stage having a travel range of about 250 mm in each direction [Table 6.1]. This is an added advantage for the replication of a large complex pattern.

In this study, square masks made of brass were extensively used such as the one shown in figure 6.2 this is of 5 mm square (approx.). In general, a disadvantage of mask projection, especially in-house made, is the fact that the edge roughness of the mask could also be introduced into the machined profile though at a demagnified size due to the projection lens that is put in place. However, the combined effect of pulse overlap and the workpiece dragging would greatly improve the edge finish.
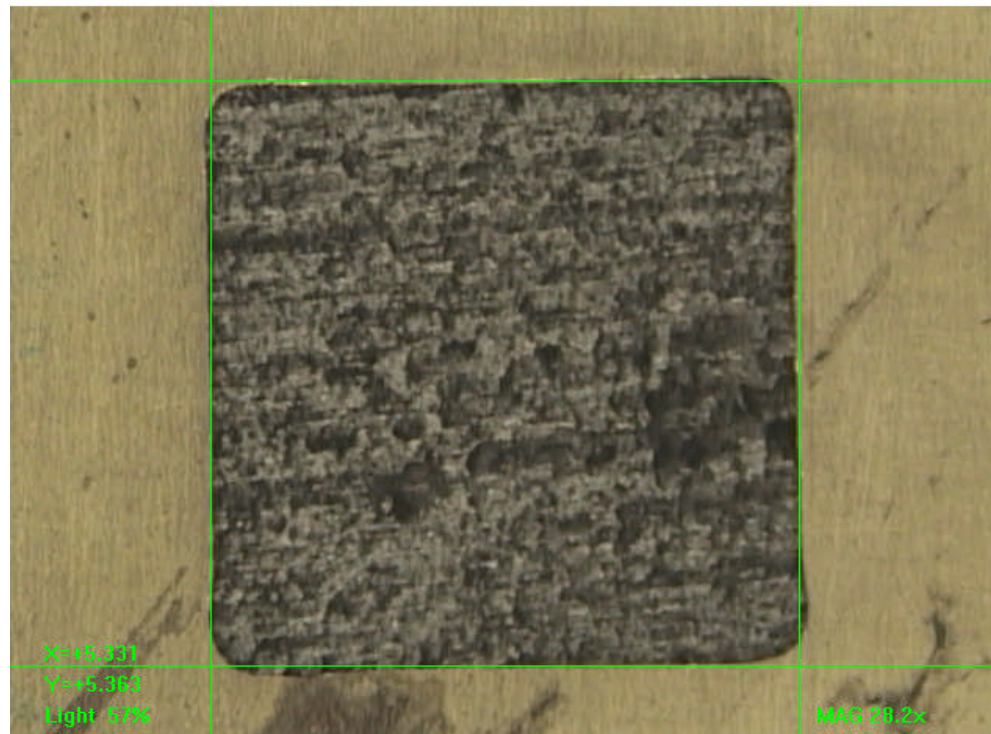
Figure 6-2: An example of in-house manufactured mask ~ 5 mm^2 etched in brass used for beam projection in Excimer laser experiments.

4. Controller

The system was controlled using U500 software. This was used to send commands to control, among other things, laser firing, the attenuator, x-y axis of the masks and XYZθ stage. The commands were programmed either in PSO, and/or RS-274 ('G' and 'M' Codes).

5. Axes

There were seven different axis terminals including attenuator that could be controlled from the U500 software having different travel ranges and recommended velocities. Table 6.1 is the list of the seven different axes with their associated board and axis identifier/label. Therefore, with such stages, there are four different approaches that can be potentially used to ablate samples, based on the permutation of the two scenarios; they are (i) static-mask moving-stage ablation, (ii) scanning-mask static-stage ablation, (iii) static-mask moving-stage ablation, and (iv) synchronised (i.e. scanning-mask moving-stage) ablation.

Table 6-1: Specifications of various axes used in the Excimer laser system setup for the fabrication of optical waveguides.

Board	Axis	Usage	Range
1	X	Workpiece Left/Right	0 – 200 mm
1	Y	Workpiece Forward/Back	0 – 200 mm
1	Z	Mask Horizontal Direction	0 – 250 mm
1	U	Mask Vertical Direction	0 – 250 mm
2	X	Attenuator	0 – 0.95
2	Y	Workpiece Rotation	$0 – 360^{\circ}$
2	Z	Workpiece Elevator	0 – 10 mm

6.4   System Parameter Test and Calculation

This section describes the calculation and various tests performed for optimising the ablation process during this study.

6.4.1   Workpiece translation stage

Serial or workpiece dragging machining utilises a static mask projection containing an aperture – square, rectangular or otherwise – to shape the Excimer beam which was used to ablate tracks, waveguides and mirrors. In this case, the workpiece is moved in x- or y-directions while the laser beam was turned on to serially write a channel on the workpiece. The shape of the aperture will determine the shape of the channel cut in the material. The velocity of the workpiece stage, both X and Y, is obtained by using equation 6.1 below.

$$Velocity = {LR}/{N} \qquad (6.1)$$

Where L is the length of the beam, R is the pulse repetition rate and N is the required laser pulses per area. This implies that the 'dragging' stage velocity is directly proportional to both PRF and beam length (along the direction of stage motion) and inversely proportional to the number of pulses per area required.

6.4.2   Focus position

The position of the projection lens determines the exact demagnification and the focus position of the machining system; it also affects the fluence and thus the ablation rate. To find the correct focus position of the imaging lens, a U500 program was run to machine a series of marks on a sample at different workpiece elevator (z-axis) positions. Figure 6.3 shows a series of holes machined in Truemode™ polymer using a ~ 5 x 5 mm^2 mask with a 10x demagnification lens by varying the relative position of the sample (at the workpiece placed on the stage) and the projection lens. The plot of the resulting dimensions at various positions is also shown in figure 6.4.

Analysis of the experimental results showed that, for the Truemode™ polymer used in this test, ablation occurred over a range of focus position; even though the focus position determines the demagnification of the beam hitting the sample at the workpiece, there was no significant change in shape dimension (with shape preserved in most cases) within 200 µm (above or below) when working in the proximity of the theoretical (i.e. expected) focus position. This is particularly useful for many reasons : (i) the spin coating is relatively non-uniform coupled with the fact that the sample could not be made perfectly flat on the stage, therefore a slight change in the sample height relative to the projection lens during ablation of a channel means the beam dimension will remain constant, and (ii) the combined thickness of both the lower cladding and the core layers is within 200 microns, so ablating from the top, does not result in any dimensional change as ablation progresses down into the material. If otherwise is the case, it might cause serious shape deformation in terms of tapering either positive (v-shape like profile) or negative (Λ-shape like profile) tapers.

For a 5.300 mm x 5.377 mm square mask (as per the measurement shown in figure 6.2) using a 10 x demagnification lens, the structure at the workpiece should be 0.530 mm x 0.538 mm (to three decimal places) which is similar to that shown in figure 6.3 b. Nevertheless, structures at ±0.100 mm^2 (e.g. figure 6.3c) of the aforementioned estimated dimension were also found to be of good quality. It should be noted however that, ablated profiles at other focus positions, far from the 'assumed' focus were either of poor quality and/or deformed structures.
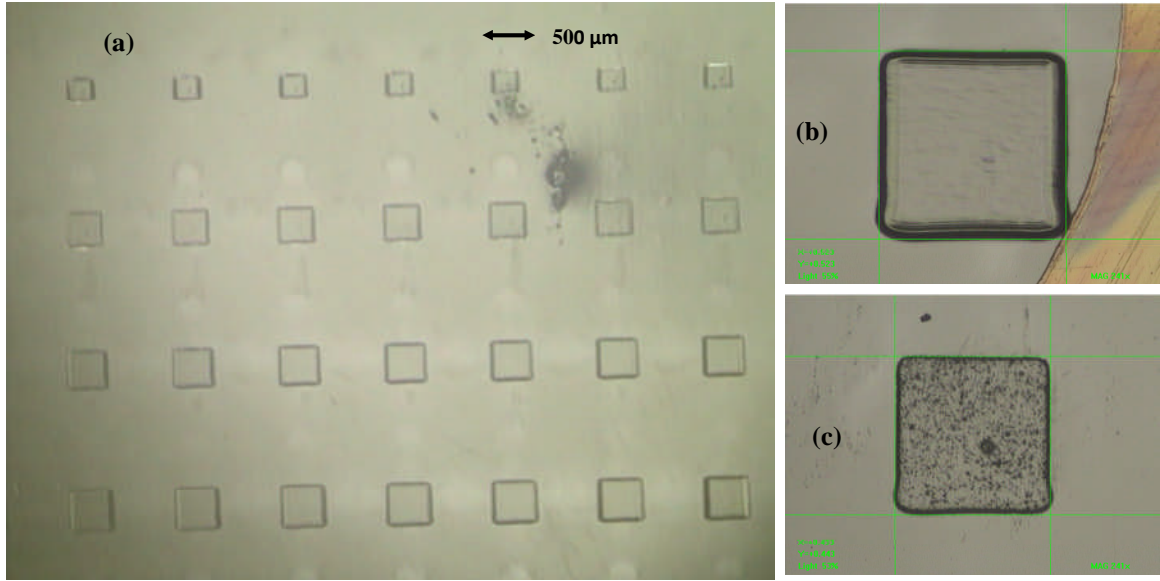
Figure 6-3: Effect of focus position on feature beam dimension at workpiece for ~5 x 5 mm^2 mask aperture (a) structures machined at various position of Z-axis of the stage, (b) structure showing about x10 demagnified replica of the mask used, and (c) structure of good quality not exactly 10 x demagnified machined at other position of Z-axis.
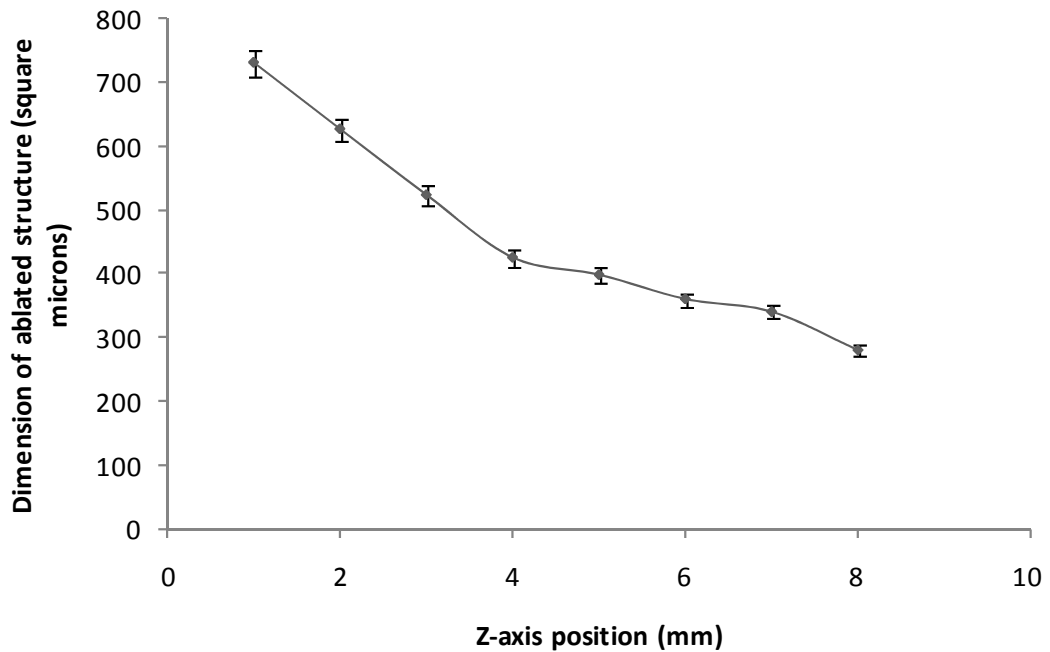
Figure 6-4: A plot of z-axis position against the dimension (area) of ablated structures in Truemode™ polymer using Excimer laser.

6.4.3   Mask feature position

Homogenisation is done by breaking the beam into multiple components, typically using a number of lenses, which is then reconstructed at a predefined position generally at the aperture or mask. By doing this, the spatial inhomogeneities in the laser beam intensity are reduced; this technique helps the quality of the ablation such as in reducing the tapering as previously mentioned in chapter 2. Since the laser system used in this study was not equipped with either beam shaper or homogenizer, the beam intensity distribution was not to be uniform guaranteed and this could have an effect on the depth profile. Furthermore, given that the position of the mask used in relation to the beam profile could not be measured, inappropriate positioning of the mask stage in relation to the output beam from the field lens could result in sampling, for example, the worst region of inhomogeneity of the beam intensity distribution.

To minimise the effect this could cause, a test of optimum position was carried out. The assessment was made by first locating the mask central position manually; the mask translation stage was then moved at a step of 0.5 mm in the U-direction (vertical) and 1 mm in the Z-direction (horizontal) at a time. Figure 6.5 shows machined profiles obtained from various channels ablated by simply moving the mask position in either direction. The images were taken by using the Talysurf CLI measuring system to scan the ablated channels perpendicular to the length of the structures. The majority of the profiles (figure 6.5) were either slanting left to right, however, there was a position where the obtained profile was symmetric about the centre of the shape (figure 6.5f). Although the profile obtained at this 'optimum' mask position was tapered, this can however be reduced by proper selection of the machining parameters vis-à-vis the fluence and number of pulses as demonstrated in figure 6.6 b.

(a)

(b)

(c)

(d)

(e)

Maximum depth	2.52 µm
Mean depth	1.77 µm
Width	0.072 mm

(f)

Maximum depth	2.56 µm
Mean depth	2.07 µm
Width	0.105 mm

(g)

Maximum depth	2.25 µm
Mean depth	1.99 µm
Width	0.083 mm

(h)

Maximum depth	3.07 µm
Mean depth	2.23 µm
Width	0.069 mm
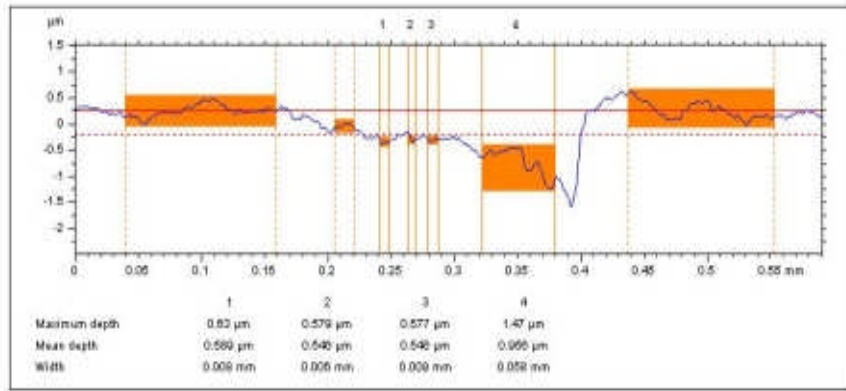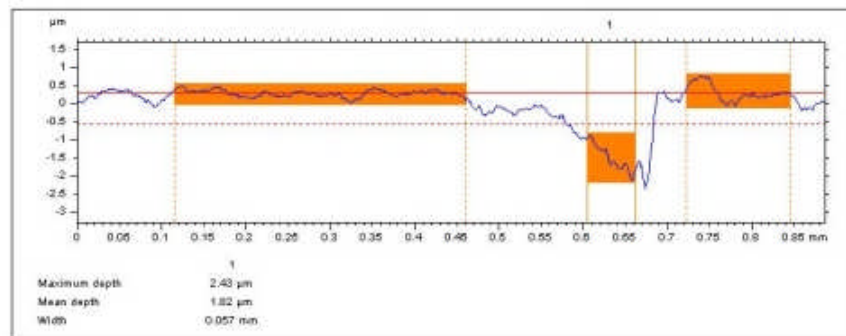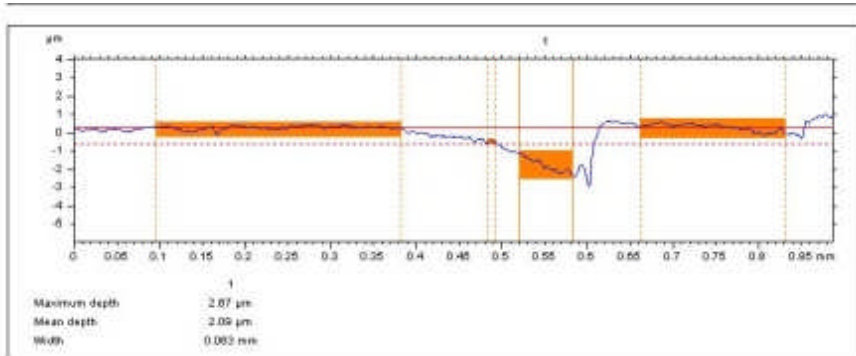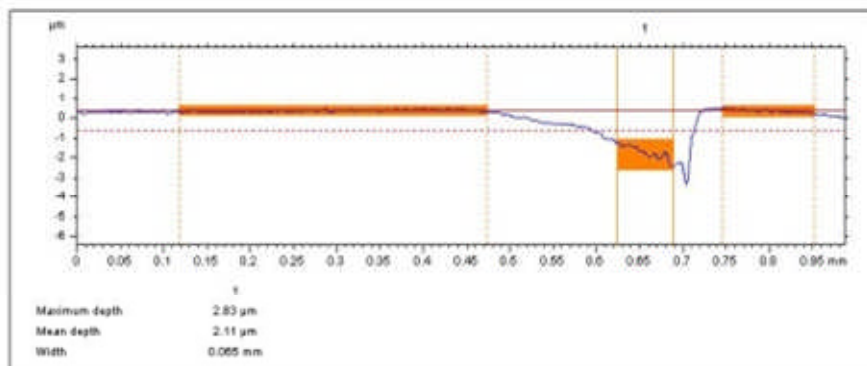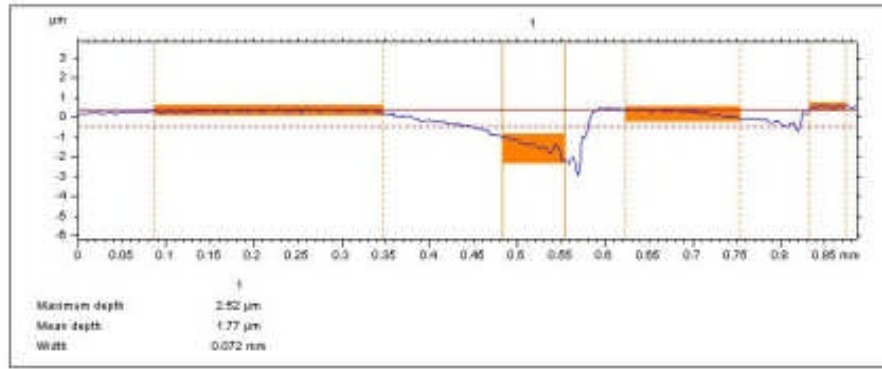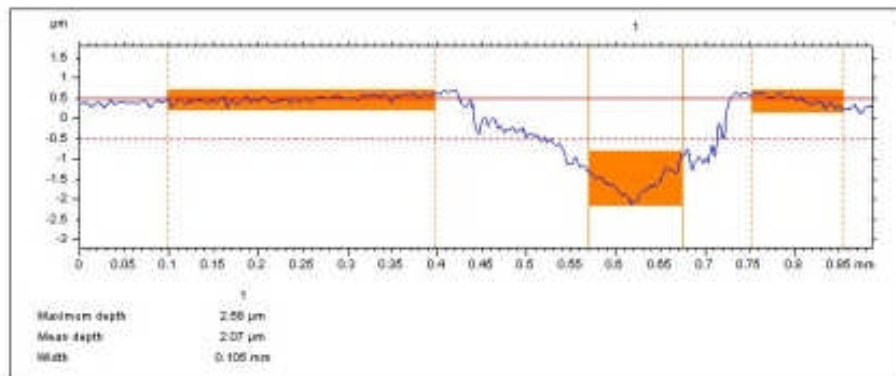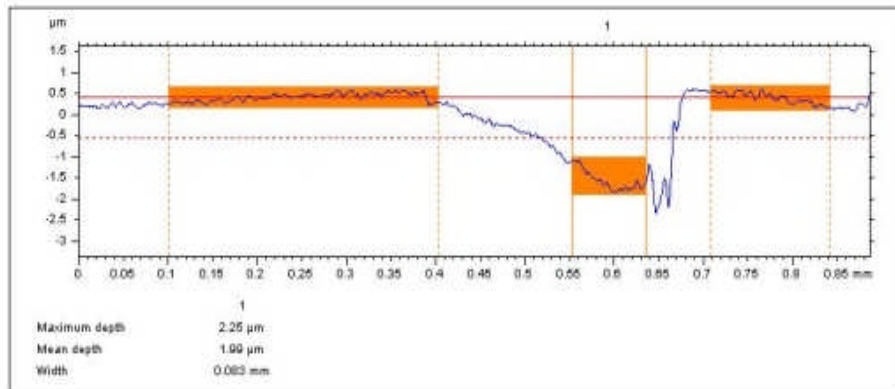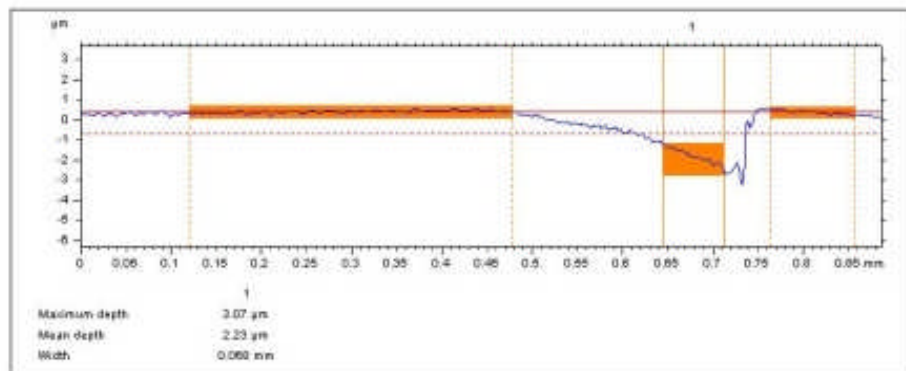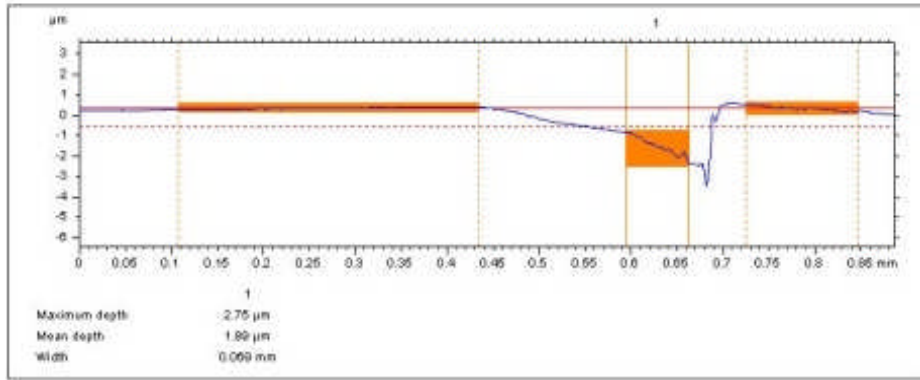
(i)

Figure 6-5: Optimising the position of mask in order to obtain an optimum position of symmetry done by moving the mask stage by 0.5 mm in U- and Z-directions (a) position of (u, z) = (182, 142), (b) position of (u, z) = (183,142), (c) position of (u, z) = (184,142) (d) Position of (u, z) = (185,142), (e) Position of (u, z) = (186,142), (f) position of (u, z) = (184, 141), (g) position of (u, z) = (184,141.5), (h) position of (u, z) = (184,142), and (i) position of (u, z) = (184,142.5).
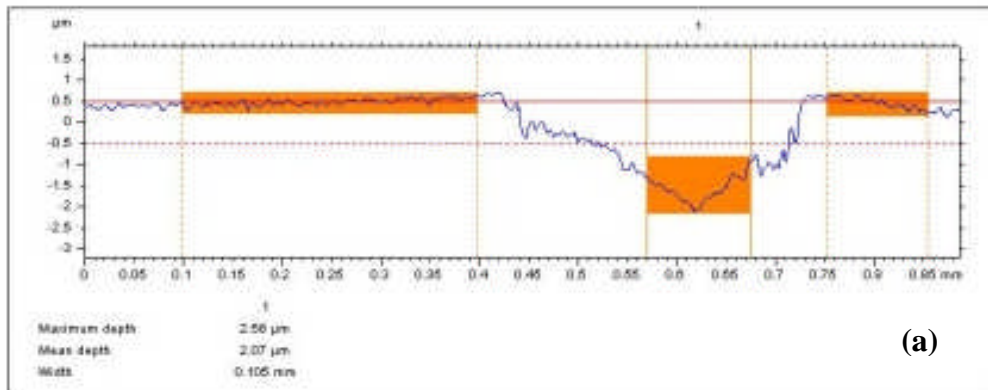
(a)
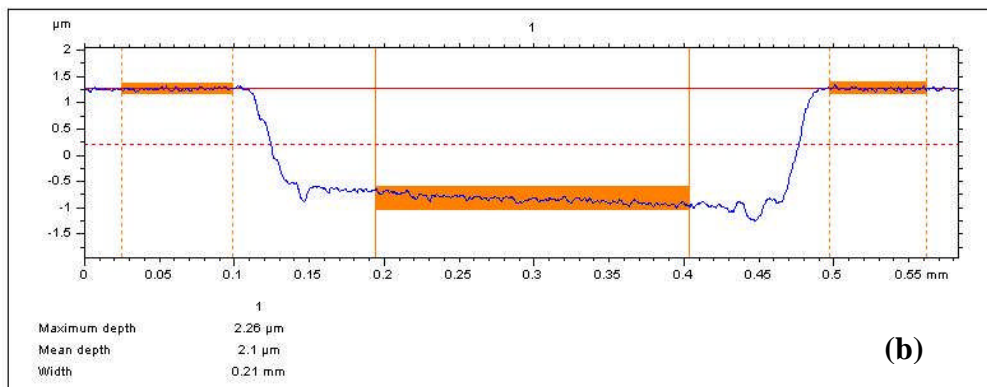
(b)

Figure 6-6: Optimising the effect of tapering by changing the fluence at 10 Hz (a) Fluence = 30mJ/cm^2 and 10 shots per point, and (b) Fluence = 200 mJ/cm^2 and 1 shot per point.

6.5   Laser System Characterisation

Although there is information in the literature detailing the effect of certain experimental parameters such as fluence, pulse repetition rate, pulse duration and wavelength, in relation to the etch rate of different materials, most importantly polymers such as PMMA, PC, PI, PET and PS among others, nonetheless, new materials require characterisation. For this reason, experiments were conducted to determine the effect of various machining parameters – fluence, number of shots per point, speed and number of passes - on Truemode™ polymer.

In this study, a series of tracks, 30 or 40 mm long, were machined at different values – either in an increasing or decreasing order of magnitude – to examine the effect of the parameter under investigation. Figure 6.7 shows a schematic diagram of an experimental design typically used showing the variation of the number of pulses used between 1 and 10 shots per point. This shows a ten-channel design grouped into two with a space of 3 mm between the adjacent channels and 10 mm between the groups. This design served three main purposes; first, it facilitated the analysis process especially when potting was required since a group of five ablated tracks spaced at 3 mm could be easily mounted without much difficulty, secondly the spacing used made it more straightforward such that data required for a particular effect study could be accommodated on a typical sample of 60 x 60 mm^2 commonly used in this research and finally, since the process was meant for a waveguide fabrication, ablating tracks instead of holes was a suitable choice.
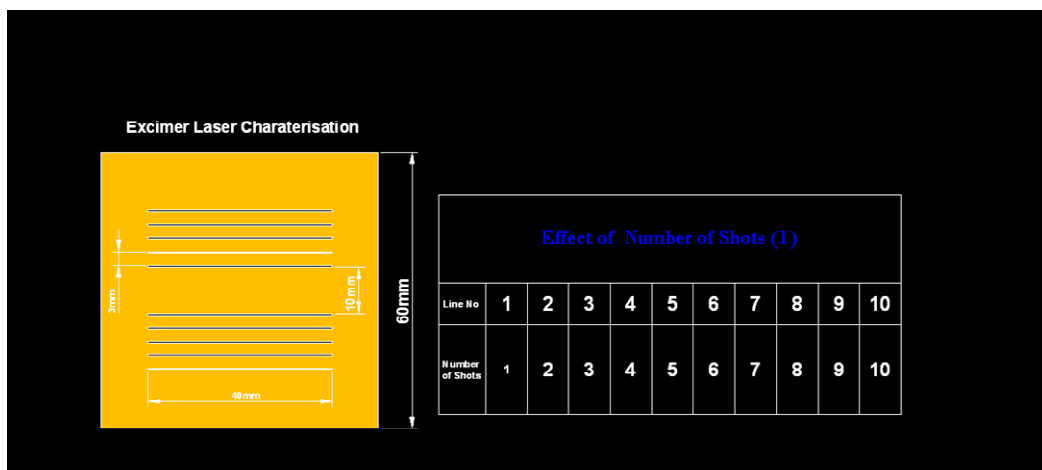
Figure 6-7: A schematic diagram showing an experimental design used for Excimer laser system characterisation.

6.5.1   Fluence

Fluence is the energy density obtainable from a laser or a laser system usually measured at the workpiece; it is expressed in either energy per area (i.e. J/cm^2) or power per area (i.e. Watt/cm^2) for pulsed and CW lasers respectively. It is an important parameter that has been studied and reported widely in relation to the laser-matter interaction and most importantly when determining the etch rate for materials. Furthermore, it is the fluence threshold that matters the most for any ablation process; unfortunately, the value of this fluence threshold (or ablation threshold as it is commonly referred to) varies from material to material and from laser to laser which also necessitated this investigation.

To study the fluence, the attenuator was utilised to adjust the fluence between ~ 0.025 J/cm^2 and 0.25 J/cm^2 while keeping the input energy constant. The PRF, beam length and number of pulses were also fixed at 10 Hz, 100 µm and 10 pulses per area respectively with stage moving at 6 mm/min (as per equation 6.1). Figure 6.8 is a plot of the fluence against the ablated depth. In this graph, the total ablation depths were divided by the number of pulses received by a particular area, i.e. 10, to obtain the ablation depth per pulse or etch rate in microns/pulse. The graph shows a relatively linear relationship between the fluence and etch rate for the chosen fluences in the range of ~ 0.025 J/cm^2 – 0.25 J/cm^2. Up to about 0.15 J/cm^2, the direct proportionality between the etch rate and the fluence was quite high with little deviation from the regression line shown in dotted green. The etch rates at fluences of 30 mJ/cm^2; 86 mJ/cm^2, 169 mJ/cm^2 and 280 mJ/cm^2 were 0.252 µm/pulse, 0.797 µm/pulse, 1.79 µm/pulse and 2.5 µm/pulse respectively.

The ablation threshold could be obtained by extrapolating the best fit line which was around 0.02 J/cm^2; this agrees with the range cited for polymers [12]. To mathematically represent the relationship between the fluence and etch rate, the regression line was utilised; this produced equation 6.2 with R^2 of 0.9958 showing a high degree of correlation.

$$y = 13.945x - 14.992x^2 - 0.2186 \qquad\qquad (6.2)$$

where y = etch rate in microns, and x = fluence in J/cm^2
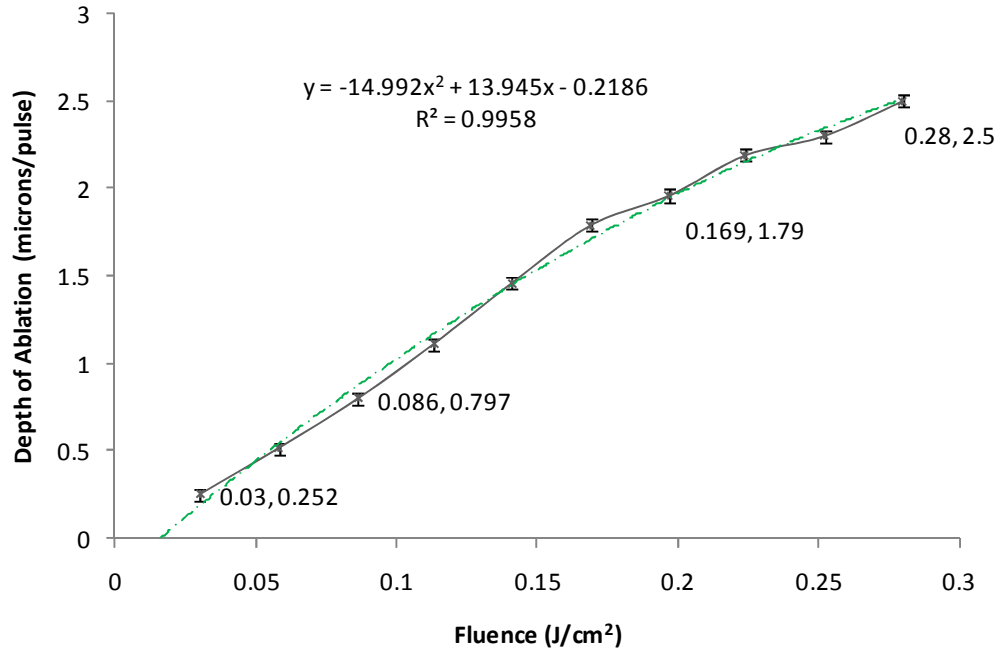
Figure 6-8: Relationship between fluence and the etch rate
of ablation of Truemode™ polymer at 100 µm beam length
and 10 Hz.

6.5.2   *Number of pulses or shots*

Similar to fluence, the effect of the number of pulses or shots impinging on a particular
point needs to also be considered. This is because, knowing the etch rate, the number of
pulses released can be controlled to meet the depth of ablation required. In fact, this can be
done in a sequence such that when the desired depth is not reached more pulses can be sent
to etch more from the material. Figure 6.9 shows the plan view of tracks machined in
Truemode™ at a constant fluence of 86 mJ/cm^2, beam length of 100 µm and frequency of
20 Hz; the number of pulses per area was however varied as shown (figure 6.10). Since the
velocity of the translation stage is inversely proportional to the number of pulses delivered
to a point, keeping other factors constant, an increase in the number of pulses from 1- 10
shots per point corresponds to a decrease in the stage velocity from 120 mm/min to 12
mm/min. This implies that this variation in pulse number does not only have an effect on
the depth of ablation but also on the pulse (or beam) overlap during the ablation process as
evident in the structures shown in figure 6.9 where the beam overlap improved as the shots
increased.

In figure 6.10, the relationship between the total depth of ablation and the number of shots
is plotted which indicates an increase in the ablation for any corresponding rise in the pulses

as expected. Although the graph is not perfectly linear, nonetheless, an average etch rate can still be obtained by taking the slope of the best fit line. The slope is thus calculated to be 0.801 µm/pulse using the two points shown on the graph. This value agrees with the etch rate obtained in the earlier study on the effect of fluence which gives an etch rate of 0.797 µm/pulse at the same fluence of 86 mJ/cm^2, but at half the PRF of 10 Hz.
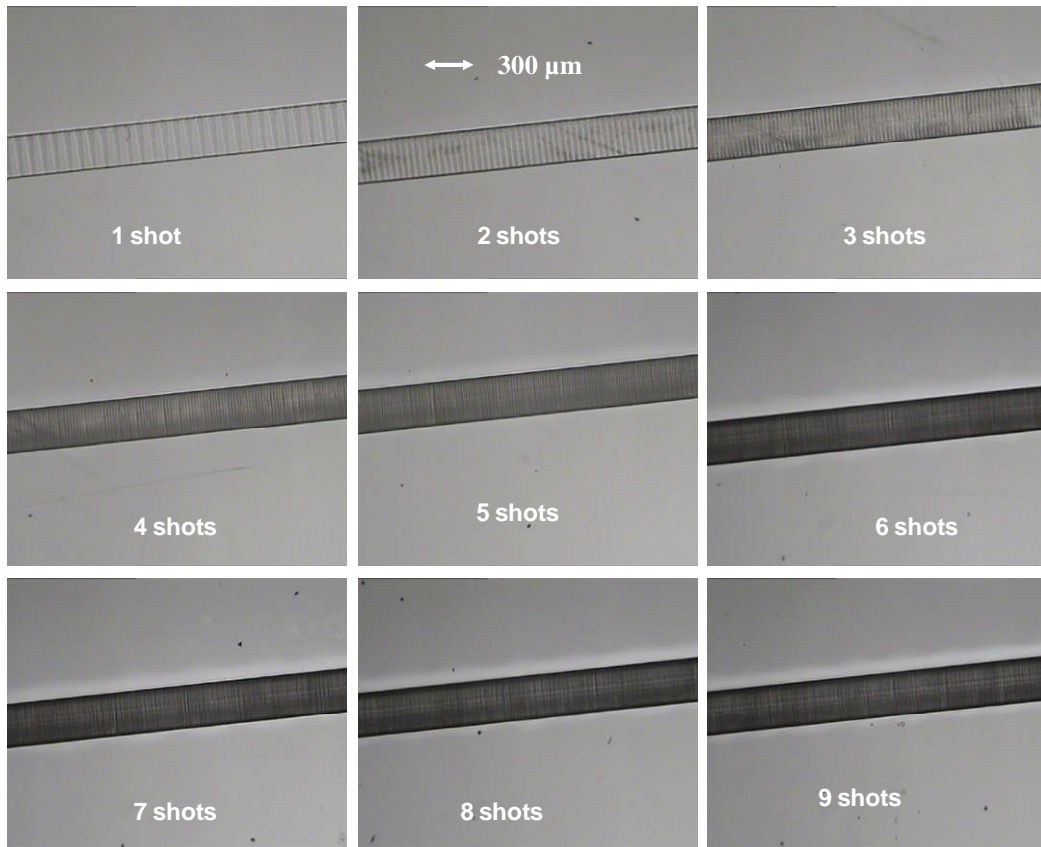
Figure 6-9: Optical microscope images showing structures machined in Truemode™ optical polymer at a constant fluence of 86 mJ/cm^2, a beam length of 100 µm and a pulse frequency of 20 Hz but with a varying number of applied pulses from 1 to 9 shots per point.
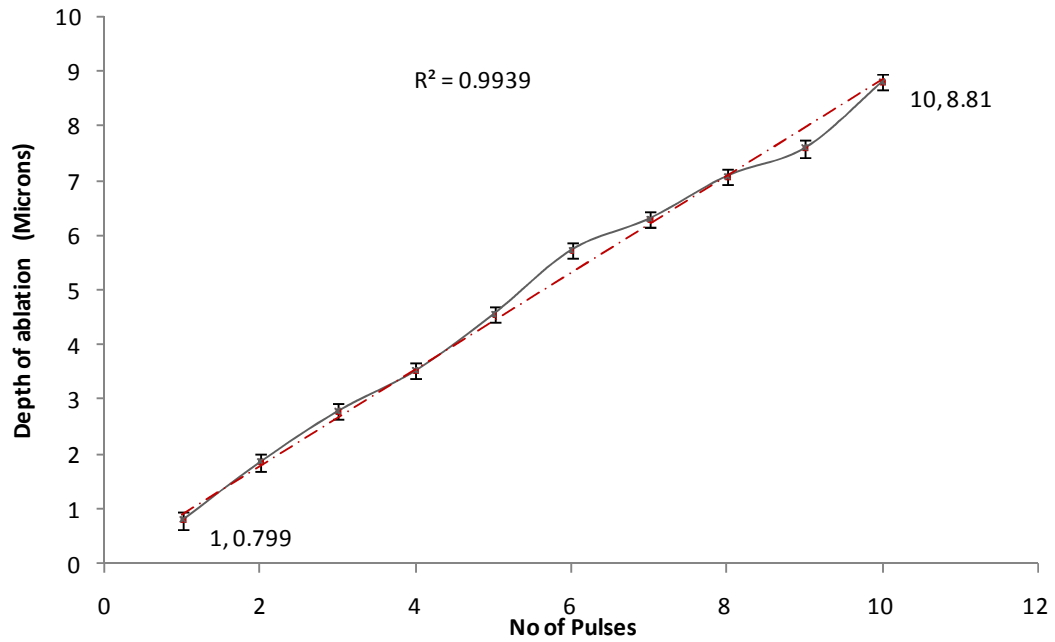
Figure 6-10: Relationship between the number of pulses/shots per point and the etch rate of ablation of Truemode™ polymer at 86 mJ/cm^2 and 20 Hz.

6.5.3 No of passes

The effect of the number of passes (of the laser across the surface) was also investigated at a constant fluence of 86 mJ/cm^2, beam length of 100 µm and a single shot per point. Figure 6.11 shows the surface view of the structures machined which also indicated an increase in the effective energy reaching the sample at the ablated zone indicated by the increase in the darkening of the profile; this was also observed with the naked eye, i.e. without the aid of a microscope. It was observed that, as the number of passes increased, there was an indication of a HAZ on the sides of the ablated channels. Equally important to note is the fact that the stage translation velocity used was 120 mm/min to obtain one shot per location and, this was responsible for the poor beam overlap. The graph of the relation between the number of passes and the total depth of ablation is plotted in figure 6.12; this indicates, as expected, an increase in the ablated depth for a corresponding increase in the number of scans.
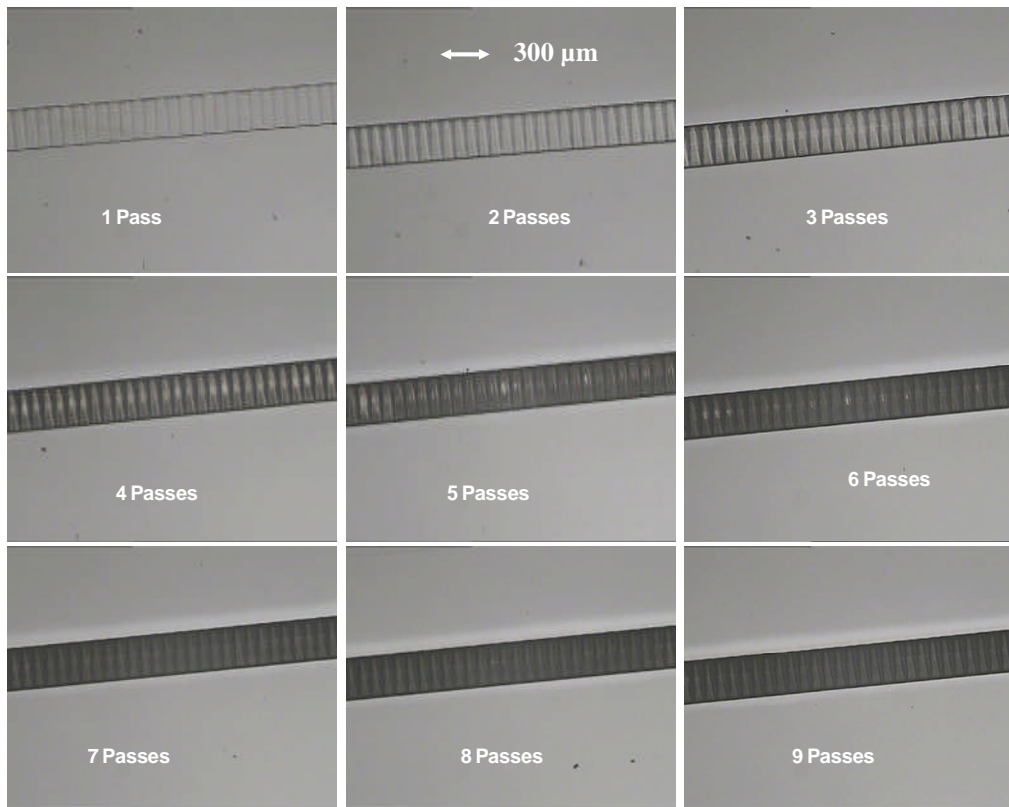
Figure 6-11: Optical microscope images of structures machined in Truemode™ polymer at a constant fluence of 86 mJ/cm^2, a beam length of 100 µm, a single shot per point but with varying number of passes.
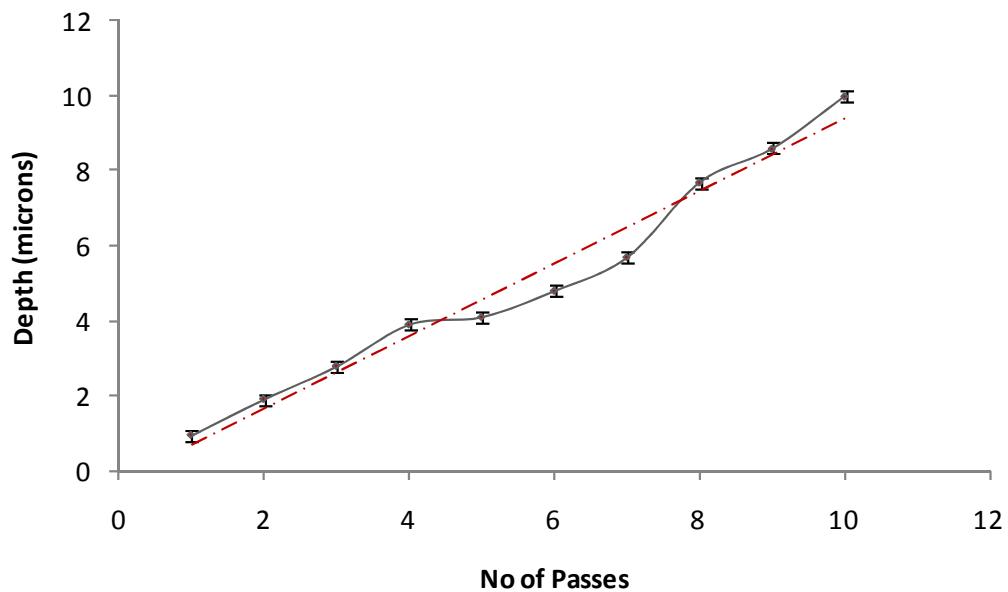
Figure 6-12: Relationship between the number of passes and the etch rate of ablation of Truemode™ polymer at constant fluence of 86 mJ/cm^2, 20 Hz 'reprate',100 microns beam length, 120 mm/min and a single shot per location but a varying no of passes.

6.6   Discussion

Excimer laser ablation of polymeric materials continues to gain momentum due to the quality of the process and the expanding applications of polymers both for engineering and medicine. This is a cornerstone for the rapid increase in the study of its interaction with matter; while some investigations focus on material modification (e.g. below ablation thresholds) others centre on the system optimisation through parameter optimisation. As for the latter, fluence and number of pulses used during laser ablation are key factors of investigation. This is because, these two parameters are directly related to the etch rate during micromachining. Nevertheless, factors such as PRF have also been studied; however, reports have shown different effects of this quantity on the depth of ablation. For example, Pfleging, et al [7] observed that while PI showed no apparent ablation depth variation as a result of change in the PRF, an increase in the etch rate was noticed for the ablation of PC at elevated pulse repetition rates of 10 Hz using 248 nm KrF. They argued that for a photochemically-dominated process, not only is a short pulsewidth required but a low pulse repetition rate is also essential. The authors of [13] observed an increase in the depth of ablation of PC only for the range of reprate between 1 Hz – 5 Hz, further increase in pulse frequency caused no change in the etch rate of PC. As tracks were machined in an ABS sample, a gradual increase in the ablation depth was noticed for frequencies between 1 Hz – 20 Hz but any increase beyond this upper limit caused a corresponding decrease in the ablation rate for the same polymer; this was said to be due to a cumulative heat effect. The thermal conductivity of PC is 0.19 – 0.22 W/mK while that of ABS is 0.17 W/mK [13]; the quoted thermal conductivity of Truemode™ is within the same range having a value of 0.21 W/mK [14]; this suggests that Truemode™ polymer, like PC, might show no dependence on the frequency at values above 5 Hz. The author supports the observation that PRF at above 5 Hz might not have an effect on highly absorbing polymers because, for independent the two experiments carried out at varying fluence and number of pulses (figure 6.8 and figure 6.10 respectively), the etch rate at 86 mJ/cm^2 was ~0.8 µm/pulse. While the former (figure 6.8) was conducted at PRF of 10 Hz, the latter (figure 6.10) was carried out at higher PRF of 20 Hz suggesting that, between this range of values, i.e. 10 – 20 Hz, etch rate is independent on the operating PRF.

It also mentioned in [3] that for polymers with high absorption coefficient like PC, PET,

PI and PS, reprate in the range of 20 – 150 Hz had no significant effect on the ablation, while a polymer such as PMMA, with low absorption coefficient showed a change in the ablation at the operating frequency due to thermal effects. Having said this, the fact that the frequency in the case of the system used in this study related to the speed implies that its effect can only be explained in the context of other associated factors; therefore, system optimisation at low speed and frequency could be the best practice for a photochemically-dominated mechanism.

The effects of fluence and number of pulses have always been subjects of study; an increase in either fluence or number of pulses with corresponding increase in the depth of ablation was usually observed. While some results showed linear relation others have shown exponential correlation between the quantities. The plot of number of pulses against fluence (figure 6.10) obtained here has a linear profile similar to that shown for ABS in [13] at 0.54 J/cm^2 and 40 Hz. Equally, a linear relation between fluence and ablation depth was observed for PC at fluences between 74 mJ/cm^2 – 1000 mJ/cm^2 which was said to obey Beer's proposition [7]. The author also noticed a linear relationship up to a fluence of about 0.15 J/cm^2 for the ablation of Truemode™ polymer (figure 6.8). The equation of the regression line drawn for the graph obtained for the range of fluence considered is a second degree polynomial expression which is neither similar to the Beer's law nor to Srinivasan-Smrtic-Babu (SSB) model; however, this gives the highest correlation (R^2 value of 0.9958) between the two the quantities. By and large, the relationship between these two parameters, i.e. fluence and etch rate, is complex and rather specific to a chosen polymer.

6.7   Summary and Conclusion

Laser ablation of Truemode™ using 248 nm KrF Excimer laser was presented; the Excimer laser used is a 7000 Series Exitech with 20 ns pulse length; energy up to 250 mJ/pulse are possible but this could further be reduced using an attenuator placed along the beam delivery path. The system was integrated with two stages each for moving the mask and XYZθ workpiece stage; a fluence value of up to 10.0 J/cm^2 was achievable at the workpiece using a 10x demagnification.

The investigation carried out here was based on the effect of various salient system parameters – fluence, number of pulses and number of passes – on the etch rate. For the

system configuration, the velocity of translation stage was obtained using the relationship, V = LR/N, where L, R and N are the beam length, PRF and number of pulses respectively; this is why its effect was not considered in this study since it is directly related to the other parameters investigated.

For fluence effect, fluence between ~ 0.025 J/cm^2 and 0.25 J/cm^2 was used while keeping PRF, beam length and number of pulses fixed at 10 Hz, 100 microns and 10 pulses per area respectively with workpiece stage moving at 6 mm/min. The etch rate was found to vary with fluence; etch rates of 0.252 µm/pulse (minimum) and 2.5 µm/pulse (maximum) at fluences of 30 mJ/cm^2 and 280 mJ/cm^2 respectively were achieved for this setting. The ablation threshold for Truemode™ polymer was estimated to be ~ 20 mJ/cm^2, this agrees with the thresholds reported for polymers. Although beam homogeniser was not employed, the tapering effect – an inherent problem of the process – of the ablated profile was minimized by a careful selection of mask position and experimental parameters with a near-vertical profile obtained at an operating fluence of 200 mJ/cm^2 when a single pulse was used; this is one of the key achievements of this study.

The effect of fluence on the etch rate was found to be suitably represented using a quadratic expression rather than the logarithmic relationship used in Beer's Law, though this does not suggest that the process is not photochemically-dominated. Although, the etch rate increased as the operating fluence was increased, it is usually believed that a moderate fluence should be used for laser ablation of polymers to ensure the dominance of photochemical mechanism and for an optimum quality; the author thus considered the use of fluence at ~ 100 mJ/cm^2 as a good practice for laser ablation of Truemode™ polymer especially when high number of pulses, above 30 shots, was employed.

The relationship between the number of pulses and etch rate at 86 mJ/cm^2 and 20 Hz is relatively linear with etch rate of 0.801 µm/pulse obtained; this agrees with the value obtained when fluence was varied – an indication of the reliability and consistency of the results. Literature report has shown different behaviours of PRF in relation to ablation but this could not be established in this study as the PRF on this system is a function of other factors such as the speed of the translation. Conclusively, a moderately low fluence (< 120 mJ/cm^2) and speed (< 6 mm/min) with an appropriate number of pulses and passes were found to be a good practice during the laser ablation of Truemode™ polymer.

Reference

1. Basting, D. *et al.* History and future prospects of Excimer laser technology. *RIKEN Review*, 14-22 (2002).

2. Wei, M. -. and Yang, H. Cumulative Heat Effect in Excimer Laser Ablation of Polymer PC and ABS. *Int J Adv Manuf Technol* 21, 1029-1034 (2003).

3. Chen, Y., Naessens, K., Baets, R., Liao, Y. and Tseng, A. Ablation of transparent materials using Excimer lasers for photonic applications. *Optical Review* 12, 427-441 (2005).

4. Ihlemann, J., Excimer laser micro machining of inorganic dielectric. *Applied Surface Science* 106 (1996) 282-286

5. Chen, Y., Ma, K., Zhou, J. G. and Tseng, A. A. Excimer laser ablation of glass-based arrayed microstructures for biomedical, mechanical, and optical applications. *J. Laser Appl.* 17, 38-46 (2005).

6. Li, J. and Ananthasuresh, G. K. A quality study on the Excimer laser micromachining of electro-thermal-compliant micro devices. *Journal of micromechanics and micro engineering: structures, devices, and systems.* 11, 38-47 (2001).

7. Pfleging, W. Excimer laser material processing – state of the art and new approaches in microsystem technology *Proc of SPIE* Vol 6107 (2006)

8. Ozcan, L. C. Fabrication of buried waveguides in planar silica films using a direct CW laser writing technique. *Journal of non-crystalline solids.* 354, 4833 (2008).

9. Thomas, D.W., Foulkes-Williams, C., Rumsby, P.T., and Gower, M.C. Surface modification of polymers and ceramics induced Excimer laser radiation, in *Laser Ablation of Electronics Materials, Basic Mechanisms and Applications,* 1992.

10. Rizvi, N. H. Production of novel 3D microstructures using Excimer laser mask projection techniques. *Proc SPIE Int Soc Opt Eng* 3680, 546-552 (1999).

11. Liu, Y.S., Cole, H.S., Guida, R. Laser ablation of polymers for high-density interconnect. *Microelectronic Engineering* 20 (1993) 15-29

12. R. Crafer and P.J. Oakley, Laser Processing in Manufacturing. London : Chapman and Hall, 1993, pp.292

13. Wei, M.-K. and Yang, H. Cumulative Heat Effect in Excimer Laser Ablation of Polymer PC and ABS. *Int J Adv Manuf Technol* 21, 1029-1034 (2003).

14. Material Data Sheet [Accessed October 2008] : Available from : http://www.exxelis.com/products/Truemode-datasheet-f.pdf

7   FABRICATION OF WAVEGUIDES

7.1   Introduction

The last three chapters have focused on the laser investigations carried out to understand the possibility of laser micromachining using three key lasers used in the PCB manufacturing industry, i.e. CO_2, UV Nd:YAG and Excimer lasers, and to further explore the effects of various system parameters on the ablation depths. However, in this chapter, the result of the polymer waveguide fabrication using the aforementioned lasers are presented and a compare-contrast analysis given. The chapter also provides information on the wall roughness assessment of the waveguides carried out in an attempt to improve the quality of the resulting structures in terms of the achievable losses.

7.2   Waveguide fabrication and measurement

Laser ablation of polymer waveguides were carried out separately on the three laser systems described in the previous chapters. For each of the lasers, a series of waveguides were made by varying key parameters, i.e. fluence, power, PRF and speed. The method of fabrication followed the process route described in section 3.4 with laser machining of the optical polymer layers of clad and core on an FR4 substrate, which was thereafter covered with another layer of cladding material.

Single-layer optical waveguides were considered in this research; thus the optical layer part consisted of a lower clad layer, a core layer and the upper cladding layer. The upper cladding layer was, as mentioned above, only deposited after the fabrication of the waveguide. For a single waveguide, two grooves were made with the spacing between the two equal to the width of the indented waveguide. For two or more adjacent waveguides, the number of grooves required was equal to $(n + 1)$, where n is the number of adjacent waveguides. Once the fabrication exercise was accomplished, the samples were then analysed using a Flash™200 optical device mainly to detect the presence of a 'continuous' waveguide; this was achieved by passing white light through one end of the guide for possible detection at the other end. Thereafter, the samples were ready for loss measurement which was carried out at UCL.

For the loss measurement of the waveguides carried out at UCL, a 850 nm multimode

(MM) VCSEL was used as input or light source which was coupled to a 10 m 50/125 step index multimode fibre for light launching. The power measured at the fibre output was usually set at 0 ± 0.1 dBm. A 70 µm circular pin hole PD was used to monitor the output power emerging from the waveguide channel. Both the PD and the MM VCSEL were mounted on a 3-axis motorized translation stage. The position of the PD was usually fixed at the maximum output considered to be a zero point and the VCSEL was scanned horizontally to 280 microns on both sides (i.e. from -280 to 280 µm with a scan step size of 0.5 microns). Alternatively, the position of the VCSEL was fixed at the maximum output point while the PD was scanned horizontally. This method gives the total loss (insertion loss), i.e. Total loss = Propagation loss*Waveguide length + Coupling loss.

Often for loss measurement, a "cut-back" method is employed which entails a cut-measure – cut-measure exercise to be carried out on a waveguide sample. This cut-back approach is useful for two main reasons, first, by recording the loss for several different waveguide lengths, the average coupling loss can be estimated and the propagation loss determined. Secondly, if there are defects along the waveguide path which could potentially cause high loss, the cutting exercise reveals these anomalies by a sudden improvement in loss when the defective section is removed. Unfortunately, the loss measurement results provided for the samples here are the total waveguide loss; therefore propagation losses are calculated based on the coupling loss obtained from other measurements carried out on the same system. The coupling loss obtained by UCL from other waveguide measurements carried out during the OPCB project was ~4.5 dB; this is used throughout this chapter.

7.3 CO_2 Laser Ablation of Optical Polymer Waveguide

CO_2 laser has been known for the drilling of vias, cutting and welding among other applications; the literature survey shows, at the time of writing, no or little attention in fabricating optical waveguides with this class of laser. Following the feasibility study and subsequent laser machining as detailed in chapter four, it is evident that such a class of laser can now be used to machine Truemode™ polymer and may therefore be capable of fabricating waveguides.

A series of waveguides were made mainly to look at the effect of machining power and speed on optical propagation loss. These were achieved by considering various speeds in the range from 80 to 120 mm/s and powers between 3 and 5 Watt; these correspond to SPD

values between 30 mJ/mm and 50 mJ/mm. For these range of SPD values, as detailed in chapter 4, the expected depth of ablation was approximately between 30 µm and 60 µm which guaranteed the waveguide fabrication at these settings to machine the core layer (and, in other cases, into the lower cladding layer) of the samples used. However, the maximum achievable width of the ablated channels at these parameters would be ~ 250 µm, therefore the resulting waveguides would, at all times, be greater than the estimated width that was input into the design, i.e. the spacing in microns between two consecutive ablated channels.

Figure 7.1 shows an optical microscope image of three adjacent waveguides machined in acrylate Truemode™ polymer processed at input power of 4 Watt and speed of 100 mm/s. For this, a 300 µm circular beam with a Gaussian profile was utilised. As shown in chapter 4, it is evident from this picture that the shape of the resulting waveguides was trapezoidal in nature due to the curved profile of the machined groove. This shape might be an issue for signal propagation thus further study is required in this regard. In figure 7.2, optical microscope images of samples with different numbers of waveguides with varying 'OD' are shown machined in Truemode™ polymer at power and speed of 4 Watt and 100 mm/s respectively. There was no apparent damage observed, possibly due to thermal accumulation resulting from the individual channels that made up the number of guides shown in figure 7.2 even though the mechanism was photothermal in nature. As a result, and for the purpose of quantifying the uncertainties in the waveguide measurement, the insertion losses reported for this laser class were those obtained by measuring losses in five identical adjacent waveguides.
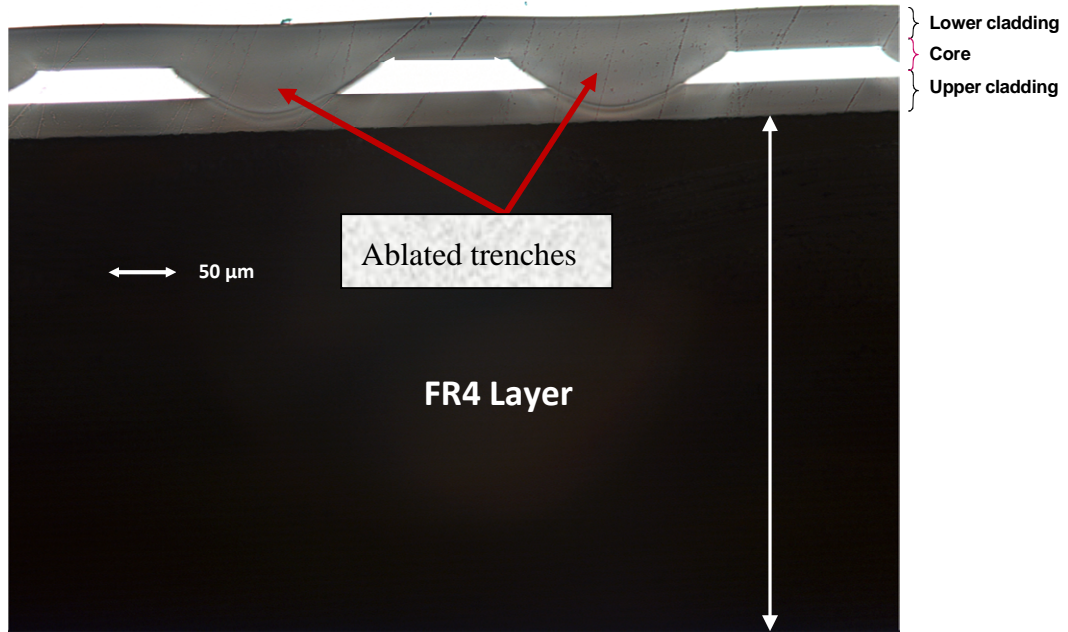
Figure 7-1: An optical microscope image of three adjacent waveguides fabricated at input power of 4.0 Watt and speed of 100 mm/s using the CO_2 laser in Truemode™ acrylate photopolymer.
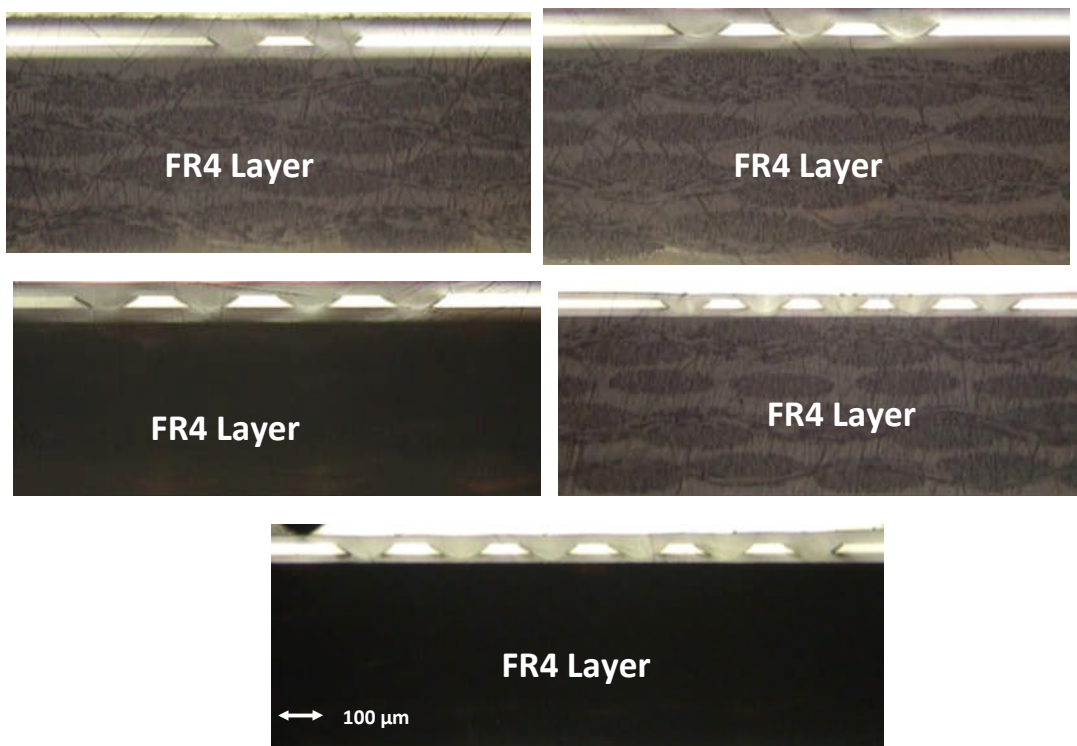
Figure 7-2: Optical microscope waveguide images showing varying degree of OD machined at an input power of 4.0 Watt and speed of 100 mm/s using the CO_2 laser in Truemode™ acrylate photopolymer.

For the purpose of loss measurement, the effect of two factors, namely power and translation speed, were investigated. In the first instance, the power was fixed at 3.5 Watt with speed varying between 70 mm/s and 90 mm/s; while on the other hand, the speed was kept constant at 100 mm/s whilst the power changed between 3 Watt and 5 Watt. In each case the length of the fabricated waveguides was 50 mm with five adjacent waveguides utilised and the mean values of their losses taken. Figure 7.3 is a plot of insertion loss against the variable parameters. With varying power (figure 7.3a) the insertion loss showed a minimum value at 4 Watt; on the other hand, with changing speed (figure 7.3b), the insertion loss showed only a small variation with a maximum at 80 mm/s. In both cases (figures 7.3a and 7.3b), the variation in insertion losses can be attributed to either changes in power or speed which also corresponds to the changes in the SPD values. However, since the SPD value also determines the ablated track width as presented in chapter 4, it thus follows that this can also be a contributing factor to the loss variation but further research is required in this area.

From these results and the fact that there is no linearity in relation between these quantities, it appears that the optimum operating parameters would have to be deduced by either choosing the setting which gives the minimum propagation loss and improve on this or by extending the range of parameter combinations. In this case, the least insertion loss of 10.7 dB was achieved at 100 mm/s and 4 Watt; the estimated propagation loss was 1.3 dB/cm for an assumed coupling loss of 4.5 dB.
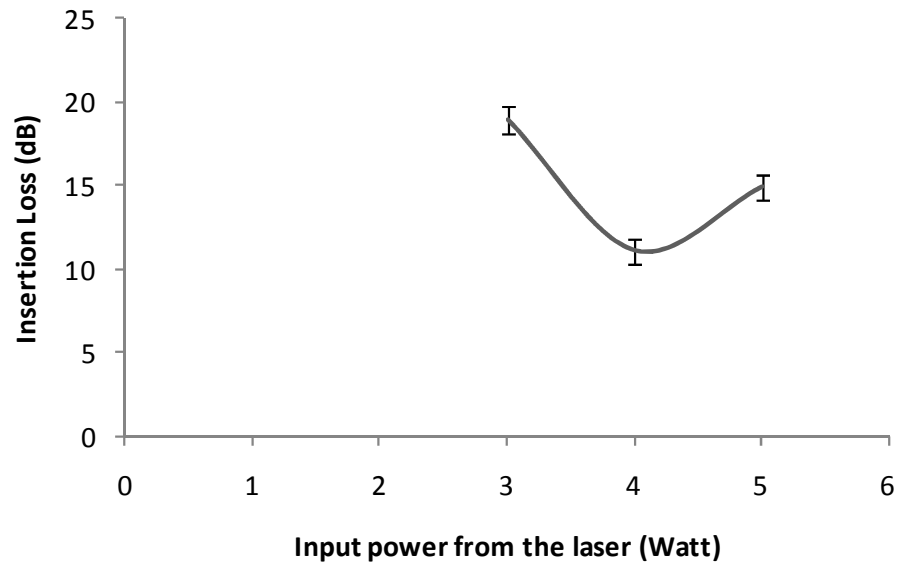
(a)
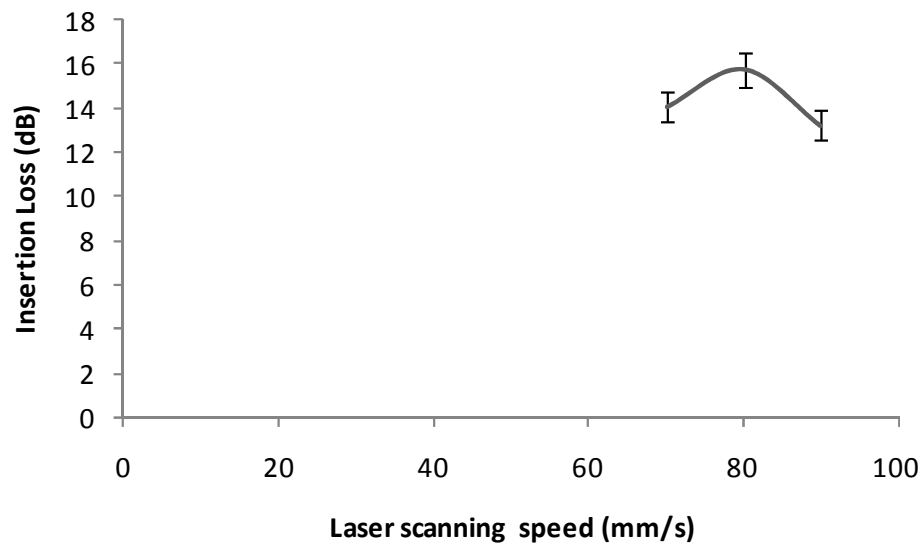
(b)

Figure 7-3: Optical loss measurement carried out on samples from CO_2 laser machining showing relationship between (a) input power and insertion loss, and (b) scanning speed and insertion loss.

7.4 UV Nd:YAG Laser Ablation of Optical Polymer Waveguides

The UV Nd:YAG laser system characterisation was carried out using the ESI 5200 model laser as described in chapter 5, however, two models of UV Nd:YAG, namely 5200 and Flex 5330, were used for the fabrication of optical waveguides reported in this section as the latter system became available and offered some alternative features. Table 7.1 compares the key features of the two models while figure 7.4 shows plots of the beam

stability test made on the two lasers. By and large, the two models operated at the same wavelength, their fundamental difference lies in the fact that the Flex 5330 model has an additional feature such as a beam shaper and beam expander. While the beam shaper made it possible to obtain both Gaussian and top-hat profiles at the workpiece; the beam expander of the Flex 5330 was useful where tracks of different widths were to be made without the need for beam overlapping as was the case with the fixed beam size of the 5200 model laser.

Table 7-1: Table showing features of two different models of UV Nd:YAG used for laser machining and optical waveguide fabrication on Truemode™ polymer.

Parameter / Model	ESI Model 5200	ESI Flex 5330
Wavelength (nm)	355	355
Beam profile	Gaussian	Gaussian and top-hat
Frequency (kHz)	20 (max.)	70 (max.)
Spot size (µm)	25 (fixed)	53 – 123 (changeable)
Power (Watt)	Up to 2.5 (approx.)	Up to 3.3 (approx.)
Pulse width (ns)	30	60
Stability	2.33 %	3.29 % (top-hat)
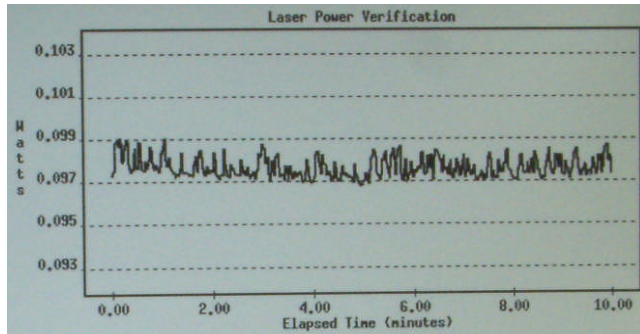
Laser drill system 5200. Gaussian wave profile.	
Repetition rate =	10 kHz
Time =	10 min
Power average =	0.098 W
Power min =	0.097 W
Power max =	0.099 W
Stability =	2.33%
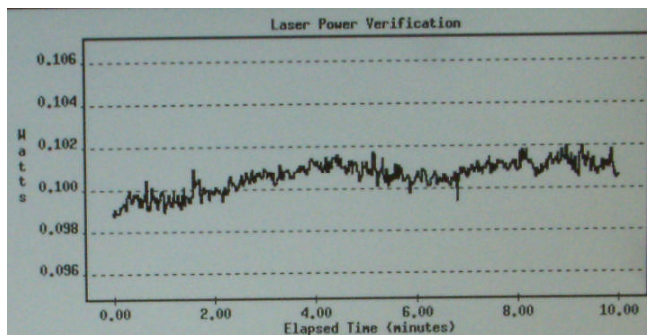
Laser drill system 5330 Flex. Flat-top wave profile.	
Repetition rate =	10 kHz
Time =	10 min
Power average =	0.101 W
Power min =	0.099 W
Power max =	0.102 W
Stability =	3.29%

Figure 7-4: Power versus Time curve for laser drill systems: (a) 5200 model Gaussian profile, and (b) 5330 flex model, top-hat profile (courtesy of Stevenage Circuit Limited).

Figure 7.5a shows the image of a single multimode waveguide of 45 µm x 45 µm and 60 mm long; this was machined using the ESI 5200 model and the structure was made by ablating ~200 µm wide grooves in Truemode™ polymer with a Gaussian beam profile. However, in figure 7.5b, the Flex 5330 model was employed to fabricate a ~ 70 µm x 80 µm, 30 mm long multimode waveguide using the top-hat beam profile by machining 50 µm wide grooves. In both cases, the waveguides were detected using Flash™200 to establish that there was no significant channel deformation with the potential to cause discontinuity along the channels. Qualitatively, there was no apparent improvement offered by the top-hat over the Gaussian beam profile, but this does not, in any way, conclude that the propagation loss would be the same for both.
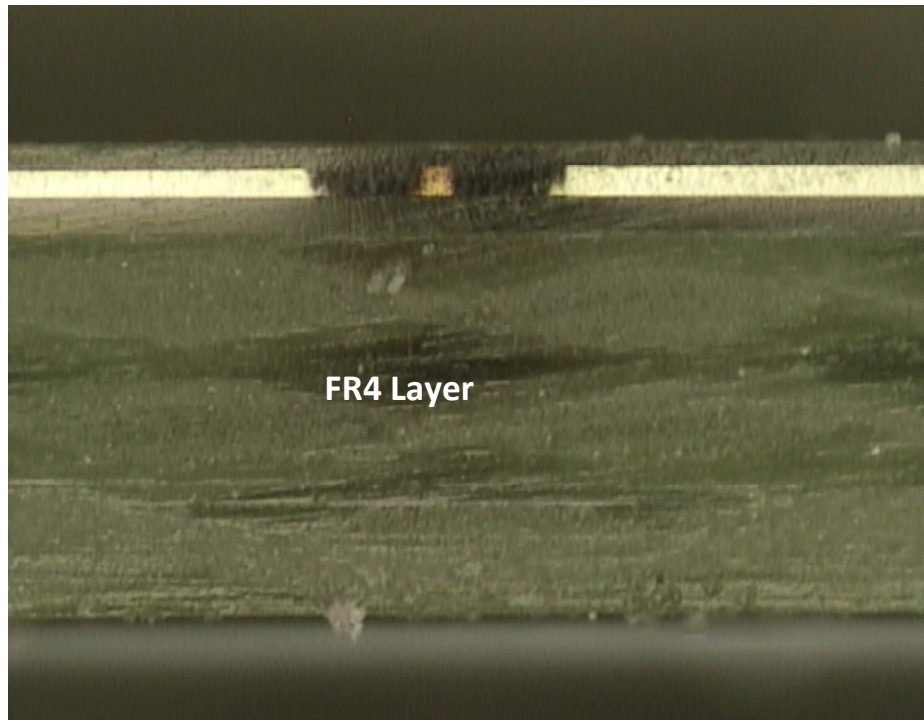
(a)
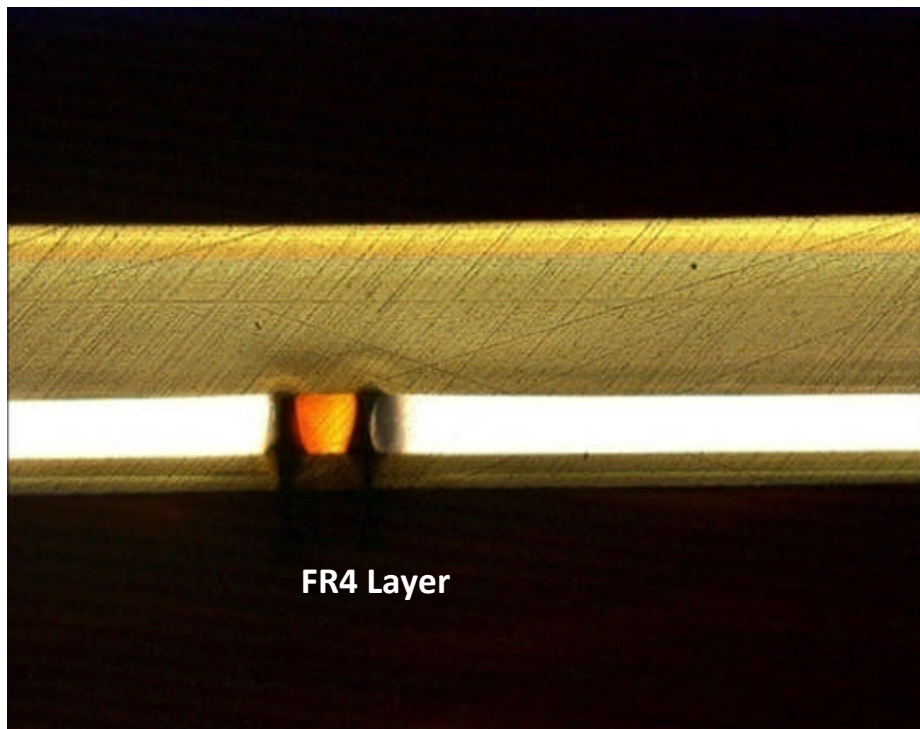
(b)

Figure 7-5: (a) Waveguide of 45 µm x 45 µm made on Truemode™ optical polymer using the 5200 model UV Nd:YAG laser system at 5 mm/s, 5 kHz and 0.1 Watt, and (b) Optical microscope image of a cross-section through a Truemode™ polymer waveguide of ~70 µm x 80 µm ablated using the Flex 5330 model laser system with top hat beam at 2 mm/s, 10 kHz and 0.1 Watt.

Having demonstrated the viability of polymer waveguide fabrication on both systems especially on Flex5330 on which a detailed characterisation was not performed; subsequent experiments were centred on studying the effects of the laser system variables on the optical loss achievable. That is to say, to fabricate waveguides with one variable changing while other factors were fixed in order to understand how this variable contributed to the propagation loss. It would have been desirable, with the results of such a study, to quantify the effect of the beam intensity profile, Gaussian from 5200 and 'top-hat' from Flex 5330, in relation to loss. Unfortunately, such a design could not be accomplished with the Flex 5330 owing to some challenges faced during the exercise as follows.

1. Figure 7.6 highlights some anomalies (a form of discontinuity in the tracks) encountered while ablating samples on the 'top-hat' profile of the Flex 5330 model which appeared in different degrees and with different shape. This could to be due to the absorption and/or beam stability as observed for 5200 model during the initial laser micromachining as described in chapter 5. However, unlike with the 5200 model, the anomaly was in the core layer (or between core-clad layers rather than at the clad-FR4 interface). The cause of this unusual phenomenon could not be identified but it was observed that system maintenance/service was duly required for this system. Following the maintenance, it appeared that the problem was only partially solved as the phenomenon still occurred albeit in a random manner.

2. In contrast to the stable beam profile shown earlier in this chapter for the 'top-hat' profile, a beam profile stability measurement was carried out for the Gaussian beam profile of the Flex 5330 as shown in figure 7.7. The result indicated poor beam stability (25.58%) over the duration of the 10 minutes examined; this is about an order of magnitude higher than that obtained for the 'top-hat' profile. Thus, comparison in this situation, between the two profiles was not possible as this would reveal not only the beam profile contribution but also the beam stability.

For the above mentioned factors, it was thus concluded that the problem seemed to be a random system error and any subsequent fabrication could not be carried out on both models for profile comparison but were carried out only on the 5200 model. Hence, loss measurement reported here for UV Nd:YAG was those obtained from samples fabricated using the 5200 model only.
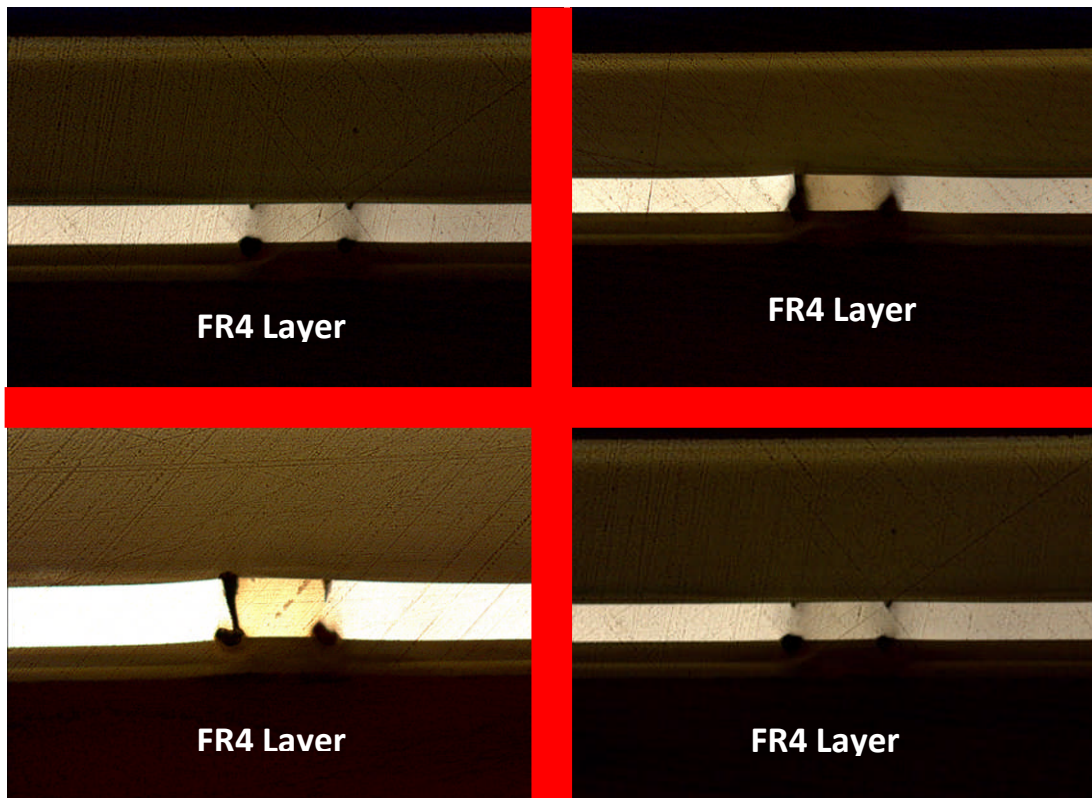
Figure 7-6: Figures showing some of the potential challenges with waveguide fabrication using UV Nd:YAG laser possibly due to the absorption of the beam.
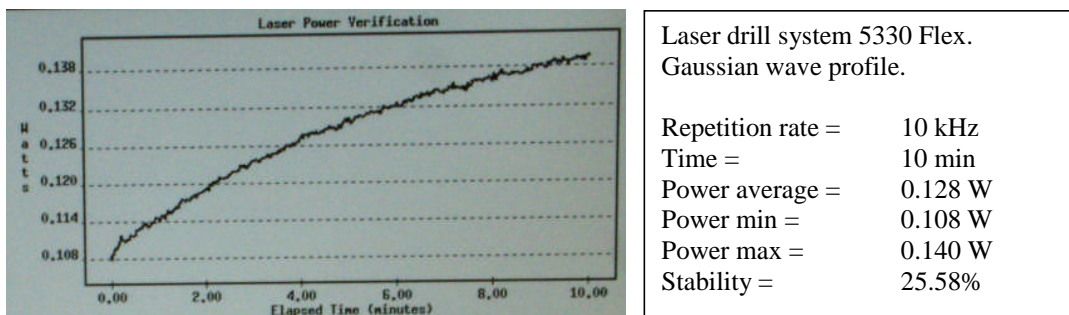
Figure 7-7: Power versus Time curve for the Gaussian beam profile of 5330 Flex laser drill system (courtesy of Stevenage Circuit Limited).

With the 5200 model of the system (and for the purpose of loss measurement), the effect of varying power and frequency from 0.11 Watt to 0.13 Watt and 8 kHz to 12 kHz respectively were considered while keeping the translation speed and number of passes constant at 5 mm/s and 1 scan in all cases. Additionally, the ablated channel of ~200 µm wide was used for all the samples with a spacing of 50 µm left between the channels to

represent the waveguides; a single waveguide (i.e. with OD of one) was used in all cases.

The experimental/operating values were chosen following the laser system characterisation result presented in chapter 5; for example, the PRF was kept within the range 5 kHz – 15 kHz, where its relationship with the depth of ablation was linearly proportional which also corresponds to the pulse energy variation at a fixed operating power as detailed in section 5.6.2 . The input power and translation speed were maintained at minimum possible values, i.e. below 0.15 Watt and 5 mm/s respectively, in line with the general recommendation for qualitative laser ablation of polymer materials. The minimum input power helped in reducing the thermal damage that could result from the photothermal contribution to the process while the low scanning ensured optimum pulse overlap and smooth edged finish.

With power change, the PRF, translation stage speed and number of passes were kept fixed at 5 kHz, 5 mm/s and 1 scan; with varying frequency, input power was maintained at 0.12 Watt and the number of passes and the speed of the translation were both fixed at 5 mm/s and 1 scan. In all cases, the length of the fabricated waveguides was 40 mm. Figure 7.8a is the plot of PRF against insertion loss and figure7.8b is the plot of power against the insertion loss.

 In the first set of the results of this study (figure 7.8a), for an increase in PRF from 8 kHz to 12 kHz there appears to be a slight decrease in the insertion loss of the waveguide. There is little explanation to be offered as to why it is the case, however, a possible interpretation of the effect is that, perhaps, at high frequency, the stability and intensity distribution of the laser beam was improved. As a result of this improvement in the beam quality, the ablated profile became better; however this account cannot be substantiated at this stage. In addition, since the energy per pulse at constant average laser power decreases as the PRF increases, it thus follows that the decrease in the insertion loss in this case corresponds to lowering the pulse energy used during the ablation process; this means that, for the range of parameters considered, the minimum insertion loss was achieved at 0.1 Watt, corresponding to 0.01 mJ/pulse obtained by dividing the input power with operating PRF, i.e. 0.12 Watt / 12 kHz.

For the change in power shown in figure 7.8b, an increase in laser input power caused a corresponding increase in the loss for the range of values considered in this study. This trend of relation between the power and loss could be due to the thermal damage that might

have been caused by the excessive power. In addition, it could be argued that the excess power input has caused some changes in the material characteristic such as RI which might affect the containment of light in the core by TIR thus contributing to the optical loss along the waveguide channel.

 In this study, the minimum insertion loss was 10.2 dB obtained independently at (i) 5mm/s, 5 kHz and 0.11 Watt, and (ii) 5 mm/s, 12 kHz and 0.12 Watt. Assuming a coupling loss of 4.5 dB, the propagation loss at this minimum insertion loss is 1.4 dB/cm. In figure 7.8c, a plot of energy per pulse against the insertion losses is presented; the pulse energies used in this case were those calculated from figures 7.8a and 7.8b assuming the fact that energy/pulse (mJ) is equal to input power (Watt) divided by the PRF (kHz) as previously asserted. However, a close observation of the relationship between the two quantities shown in figure 7.8c does not reveal a defined correlation between the calculated pulse energies and the resulting insertion losses. There is a possibility that the pulse energy for this system cannot be obtained, in some cases, by dividing the input power with the operating PRF. More also, it is possible that the achievable losses are subject to the experimental settings.
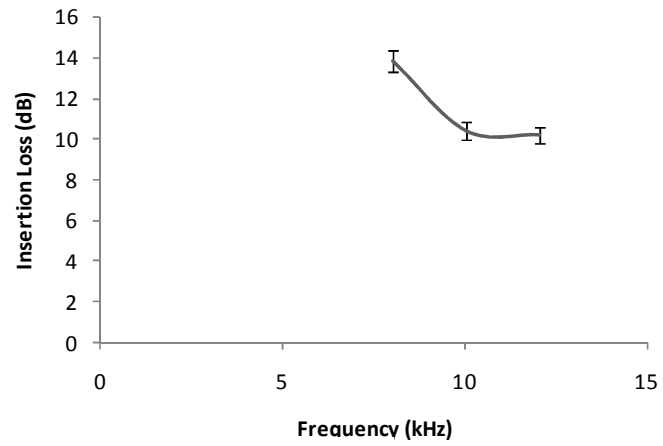
(a)
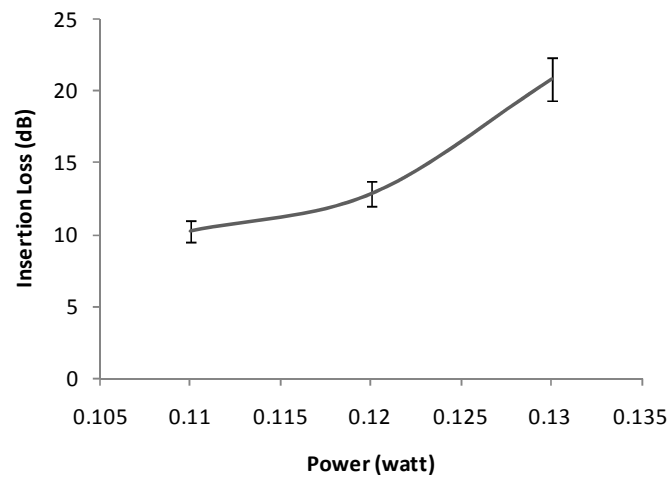
(b)
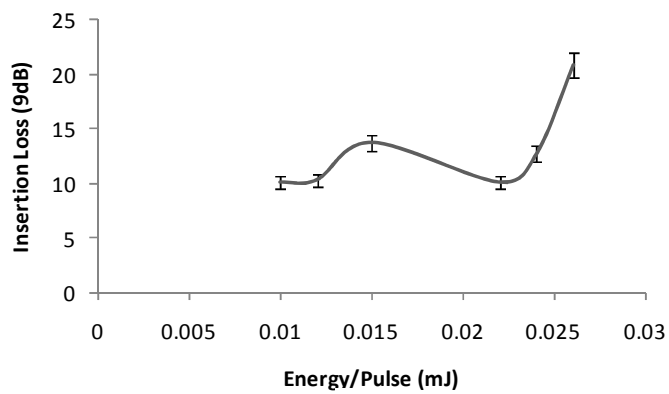
(c)

Figure 7-8: Optical loss measurement carried out on samples from UV Nd:YAG showing relationship between (a) input power and insertion loss, (b) frequency and insertion loss, and (c) calculated pulse energy and insertion loss.

7.5   KrF Excimer Laser Ablation of Optical Polymer Waveguide

The capability of Excimer coupled with its photochemical interaction with polymer material in particular, as already explained, allows for different structures to be made. Figure 7.9 shows a cross-section of a 50 µm x 35 µm multimode waveguide in Truemode™ polymer machined at 100 mJ/cm^2, 35 shots per point, 25 Hz and a single pass.
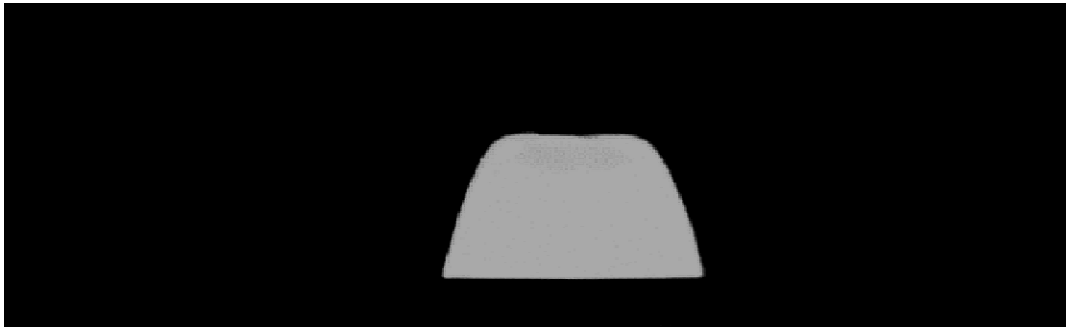
Figure 7-9: Excimer laser ablation of optical waveguide showing cross-section of a 50 µm x 35 µm multimode waveguide in Truemode™.

Having successfully produced a waveguide on Truemode™ optical polymer, further experiments were conducted to investigate among others the effects of OD on the propagation loss. For this, the feedrate used was between 3.00 mm/min and 4.00 mm/min; both the number of pulses and PRF were maintained at the range between 40 and 50 shots per point and 22 Hz and 30 Hz respectively in order to keep the feedrate at the aforementioned range since they are all related by an equation as described in chapter 6 and also to ensure that the etching was carried out beyond the core layer based on the fact the total ablation depth is a function of the number of shots per area as presented in section 6.5.2. A fluence of ~ 100 mJ/cm^2 was used in all cases except where the effect of fluence was the subject of investigation; it is equally important to mention that an OD of three (for the purpose of loss measurement exercise) was used with the exception of where this factor was investigated, in that case, the OD varied from one up to eight adjacent waveguides. In each case, the laser beam was passed over the sample once using a 100 µm beam length.

Figure 7.10 shows images of waveguides, at various OD taken using the FEGSEM while figure 7.11 shows optical microscope images of similar structures. In figure 7.12,

FEGSEM images of four waveguides made at different fluence are shown; close visual examination of the structures does not reveal any significant difference and/or definite pattern of improvement in terms of quality, i.e. roughness, in the waveguides fabricated at this varying fluence. This observation was further substantiated by the insertion losses obtained at varying fluence.
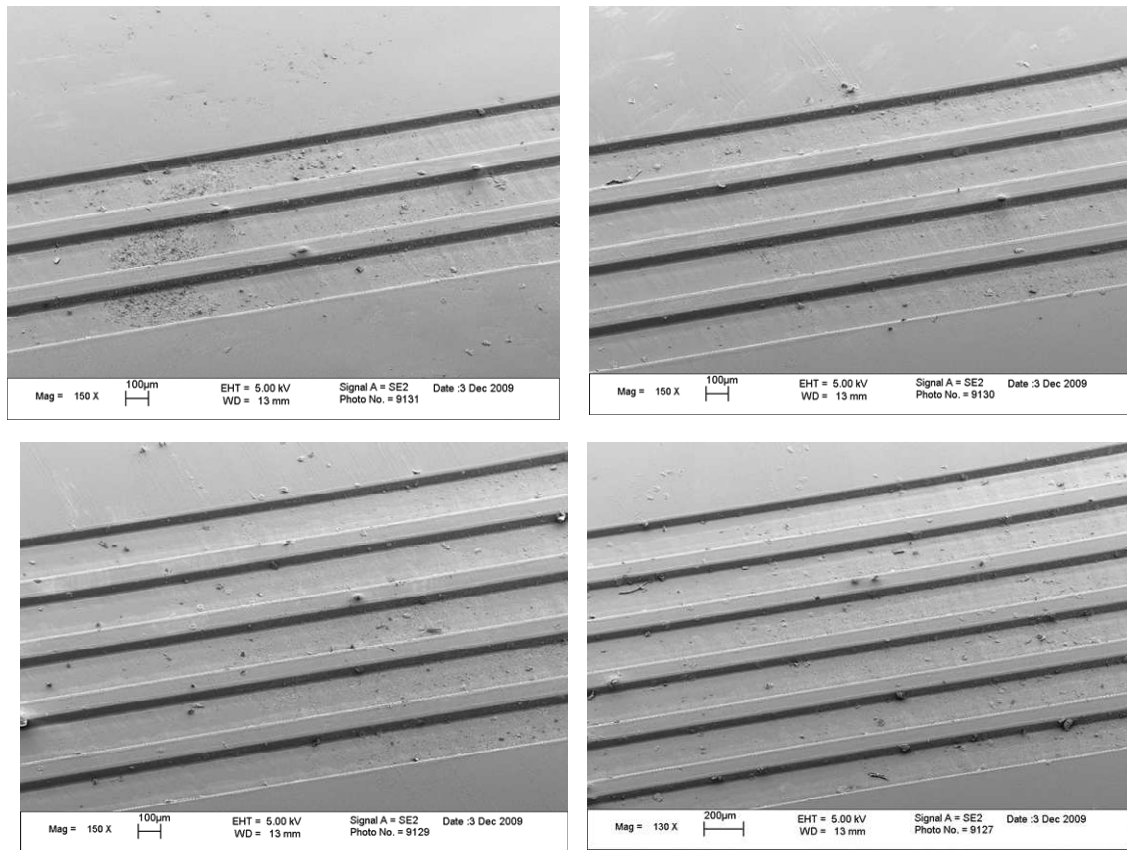
Figure 7-10: FEGSEM images of optical waveguide fabrication showing different number of adjacent waveguides, i.e. different OD in Truemode™ polymer machined at 100 mJ/cm^2, 50 shots per point, 3.6 mm/min, 30 Hz and a single pass.
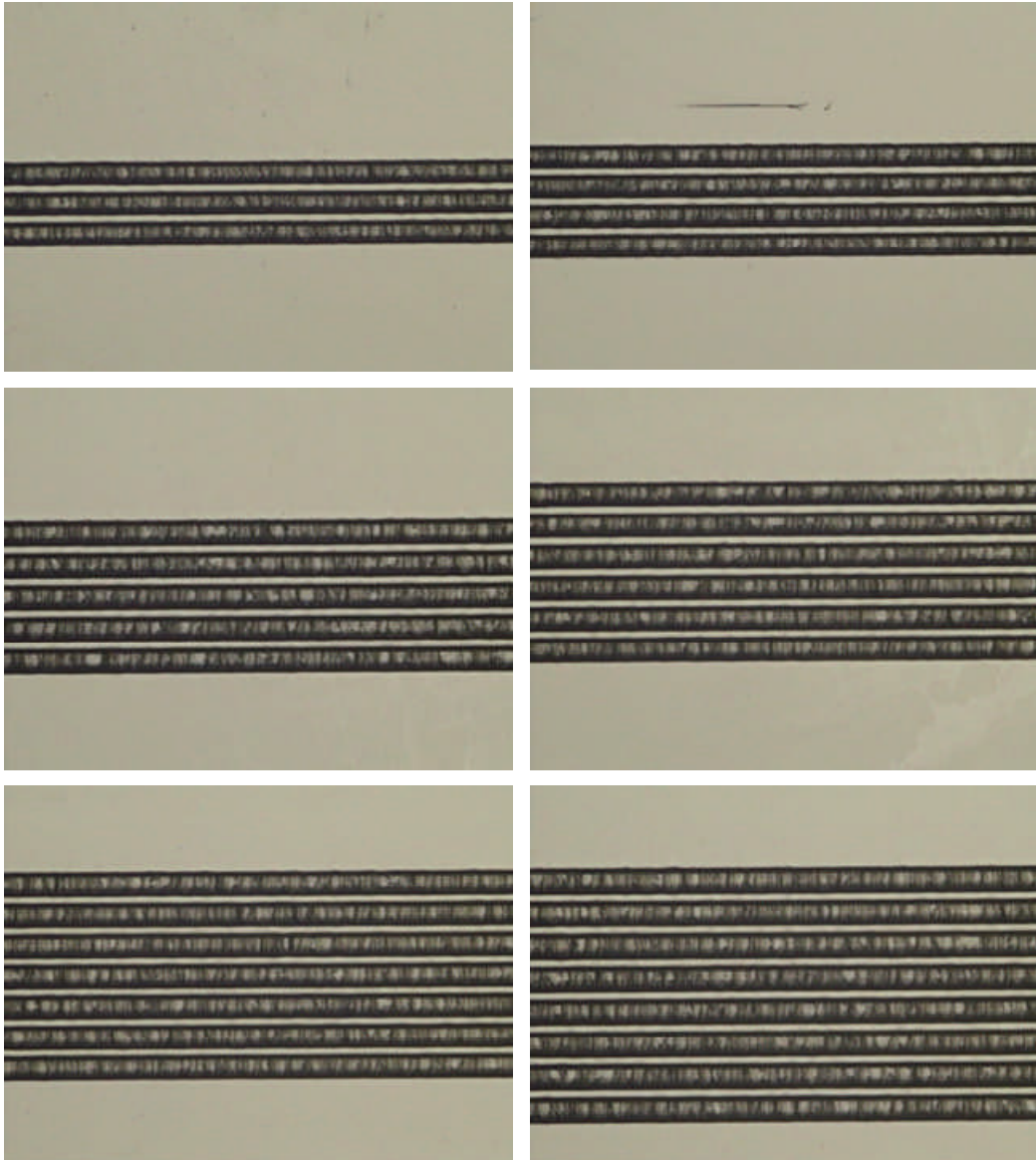
Figure 7-11: Optical microscope images of optical waveguide fabrication showing different numbers of adjacent waveguides, i.e. different OD in Truemode™ polymer machined at 100 mJ/cm^2, 45 shots per point, 3.3 mm/min, 25 Hz and a single pass.
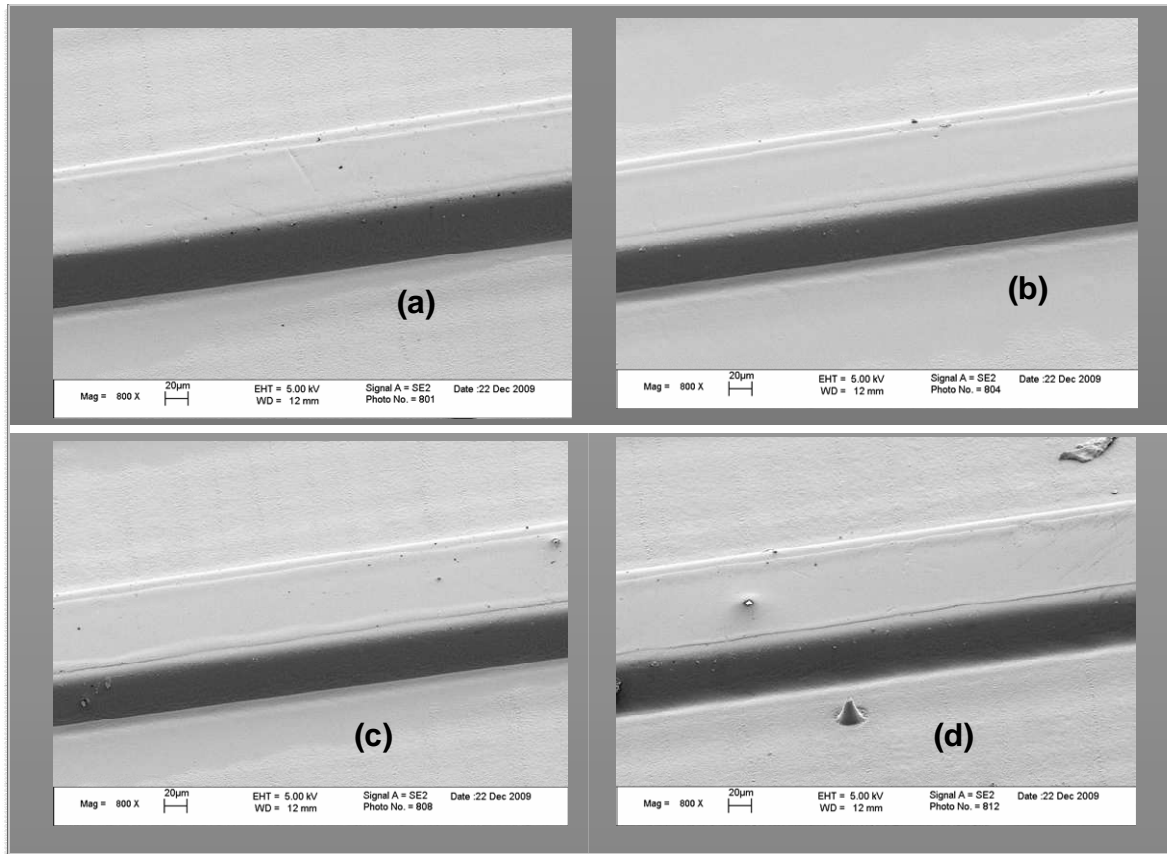
Figure 7-12: Samples machined at 30 Hz, 50 shots per point and 3.6 mm/min with different fluences of (a) 80 mJ/cm^2, (b) 90 mJ/cm^2, (c) 100 mJ/cm^2, and (d) 110 mJ/cm^2.

Finally, a 90 degree cross-over waveguide was tried (figure 7.13). The sample was structured by ablating four L-like shapes forming the four quadrants of figure 7.13a in turn. Each L-shape or quadrant was carried out by moving either x- or y-axis of the workpiece stage keeping the other stationary while the laser beam was turned on; on reaching the junction of the L-shape the axis motion was reversed. That is to say, the stationary axis became the moving axis and vice versa. It is possible to 'cross' the waveguides at angles other than 90 degree for example 60 degree; however in this case, the quadrants would not be L-like shapes rather V-like shapes and a square mask (beam spot) would not be very suitable or difficult to machine this.
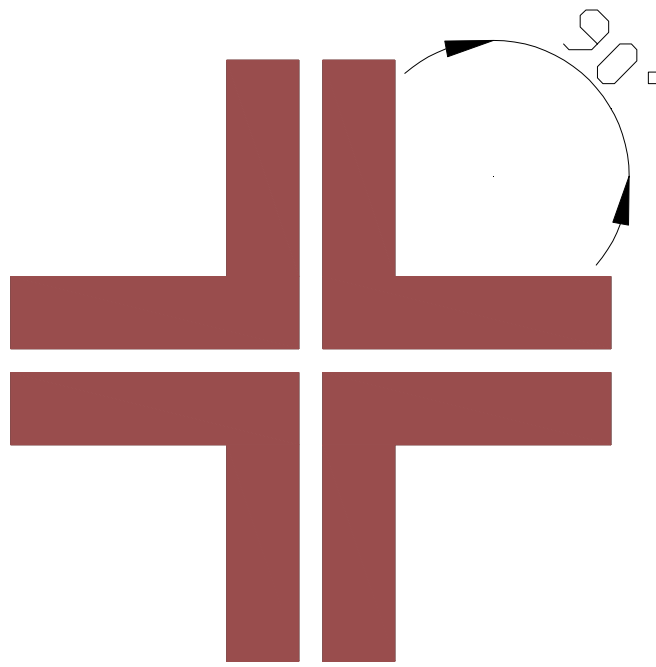
(a)
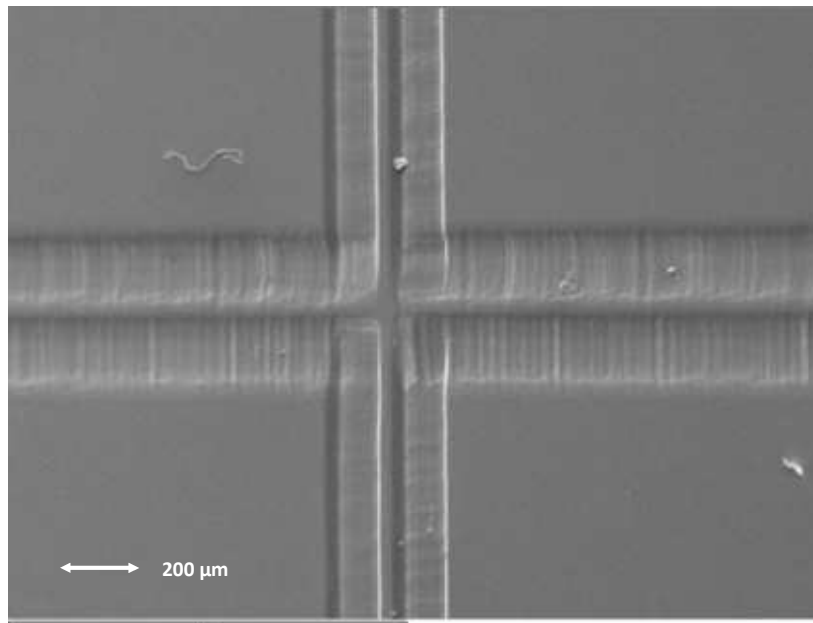
(b)

Figure 7-13: Waveguides crossed over at 90 degree to each other machined at 100 mJ/cm^2, 45 shots per point, 3.3 mm/min, 25 Hz and a single pass showing (a) a schematic diagram, and (b) an SEM image of an initial trial.

For the purpose of loss measurement, the effects of four different parameters were considered and varied in each case study while keeping other system parameters constant; the varying factors were: the fluence, the speed/frequency, the waveguide width and the

OD. The length of the waveguide in each case was 45 mm. The plots of the effects of the changing parameters on optical loss (figure 7.14) show that there is no direct pattern or deduction that can be drawn between the optical loss and each of the variables for the settings applied in this study; in other words, these parameters have no direct relation to the optical loss achievable.

The minimum insertion loss obtained was about 22 dB at 45 shots, 25 Hz pulse reprate, 3.3 mm/min and 100 mJ/cm^2. Again, assuming a 4.5 dB coupling loss, the propagation loss at this setting is 3.9 dB/cm. This is quite high, even higher than those from the other systems considered where relatively high losses could be expected. Unfortunately, the literature survey conducted showed no such investigation being reported. In fact, the vast majority of reports available only show the optical propagation loss achieved without detailing the parameters at which they were achieved. Therefore, it is likely that parameter optimisation is the key to low-loss fabrication.
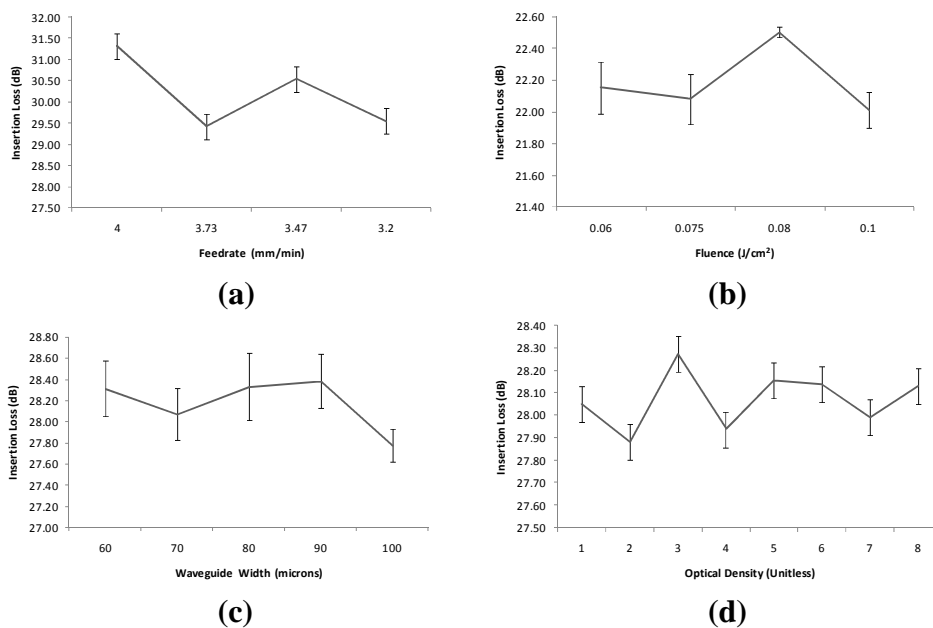
Figure 7-14: Optical loss measurement carried out on samples from Excimer laser showing the relationship between (a) feedrate and insertion loss for a sample machined at constant 100 mJ/cm^2 and 45 shots per point (b) OD and insertion loss for a sample machined at constant 100 mJ/cm^2, 45 shots per point and 30 Hz (c) fluence and insertion for a sample machined at constant 45 shots per point, 3.3 mm/min and 25 Hz, and (d) waveguide width and insertion for a sample machined at constant 100 mJ/cm^2, 45 shots per point, 3.3 mm/min and 25 Hz.

7.6   Wall Roughness Assessment

The optical losses obtained for the waveguides under this study were relatively high. Although, insertion loss from UV Nd:YAG and CO_2 lasers are promising and thus tolerable since they are still at an early stage in the development of the process, those obtained on Excimer were, indeed, high and might satisfy the optical budget currently on the roadmap unless if optical amplification is used. It is difficult, at this stage, to identify what was responsible for these high losses because there are numerous potential factors which are either due to the fabrication process or/and defects in the waveguides.

Defects in waveguides can be: (i) those due to impurities, i.e. particles; this can cause absorption and Rayleigh scattering, (ii) bubbles in the guides, and (iii) quality of the interface, i.e. wall surface roughness. Working in a clean room environment is a key way to eliminate or minimise the effect of (i) and partly (ii) but this was not available during this research. The wall roughness is another factor that can play a substantial role in losses but measuring this proved to be difficult due to the geometry of the waveguides. This is because, for the dimension of the current waveguides (less than 100 µm), it is impractical to use the currently available optical measuring devices to obtain data from the wall of such waveguides; attempts were made using facilities at Loughborough University and BAE Systems (an industrial partner to the OPCB consortium) but such effort was futile as no data was obtained (figure 7.15).
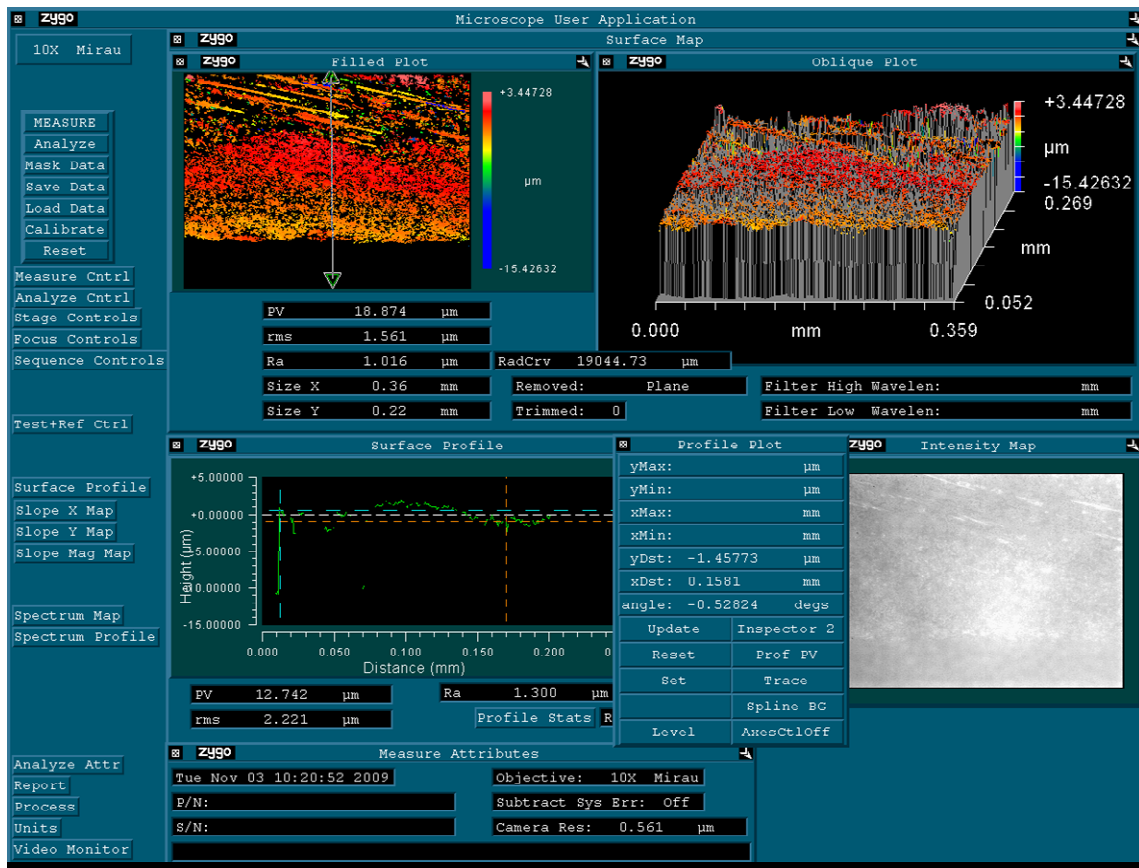
Figure 7-15: Wall roughness measurement trial with insufficient data/signal from the target surface.

However, to circumvent this difficulty of not obtaining data from the walls of a waveguide using the available measuring systems, a new approach of waveguide fabrication was considered. In this method, waveguides were made at the very edge of the sample such that a waveguide sample could be mounted with its wall facing the (lens of the) measuring devices (Zygo or Talysurf). Both the exercises – fabricating the sample at the edge and measuring such waveguide – were not easy and time consuming. In both cases, alignment was a major issue. Figure 7.16 shows images of some of the attempts made in patterning waveguides at the edge of the samples for the purpose of a wall roughness assessment. Figure 7.17 is the result of a measurement carried out at BAE Systems on a waveguide placed at the edge of the sample following this new approach; the sample used was fabricated at 45 shots, 25 Hz, 4 passes and 100 mJ/cm^2. This gave a wall roughness, Ra of ~ 650 nm. Similarly, a roughness measurement was trialled using Talysurf CLI measuring device at Loughborough University on a similar waveguide machined with two passes; the result (figure 7.18) gave a Ra of ~ 260 nm. For this purpose, the sample was usually turned upside down with the wall of the ablated trench facing the incoming light from the optical

device such that the light could be scanned along the length of the track, then moved a 5 microns step along a direction perpendicular to the length of the wall. This was done so that reliable signal could be obtained from the surface of the wall as schematically shown in figure 7.19.

Furthermore, the bottom surface roughness of the trench was also assessed and found to be 30 nm Ra using AFM (figure 7.20). Although this value does indicate a relatively smooth ablation further work is still required in this area to know what the acceptable Ra for any optical waveguide is and how it is linked to any loss. It is also crucial that the real contribution to the loss is identified from among the three possibilities mentioned earlier (section 7.6).
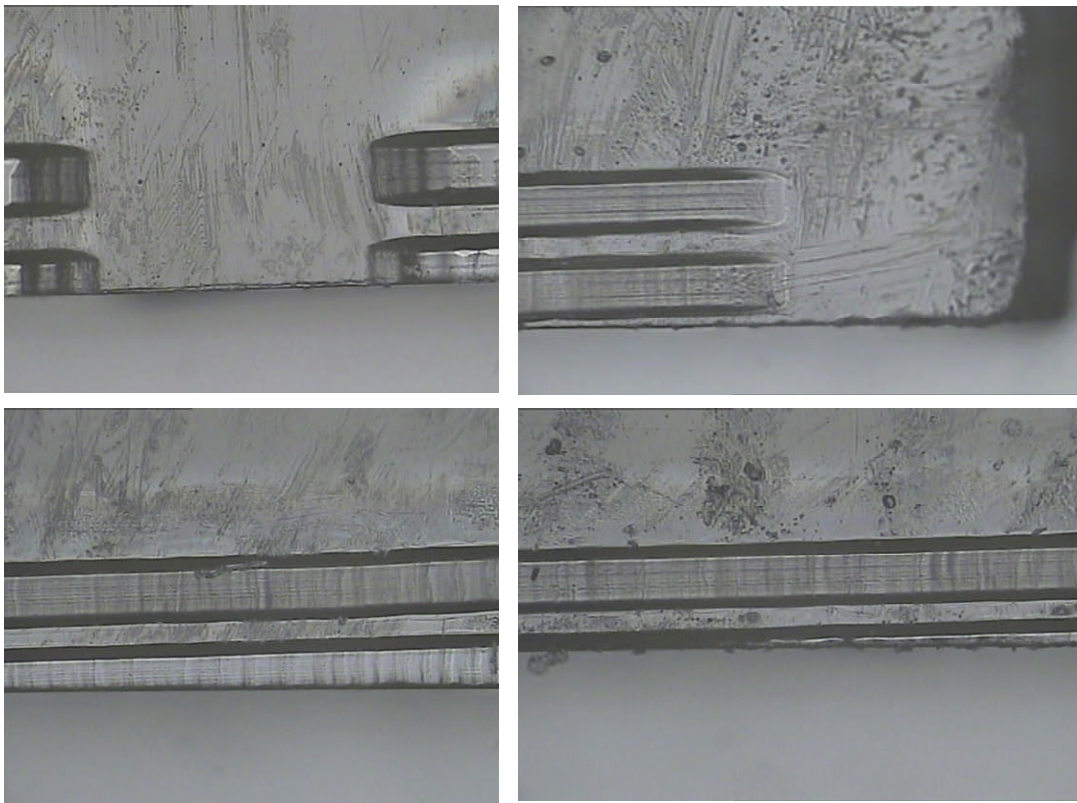
Figure 7-16: Optical microscope images of samples machined at constant 100 mJ/cm^2, 45 shots per point and 25 Hz showing surface view of some of the attempts made in patterning waveguides at the edge of samples for the purpose of wall roughness assessment.
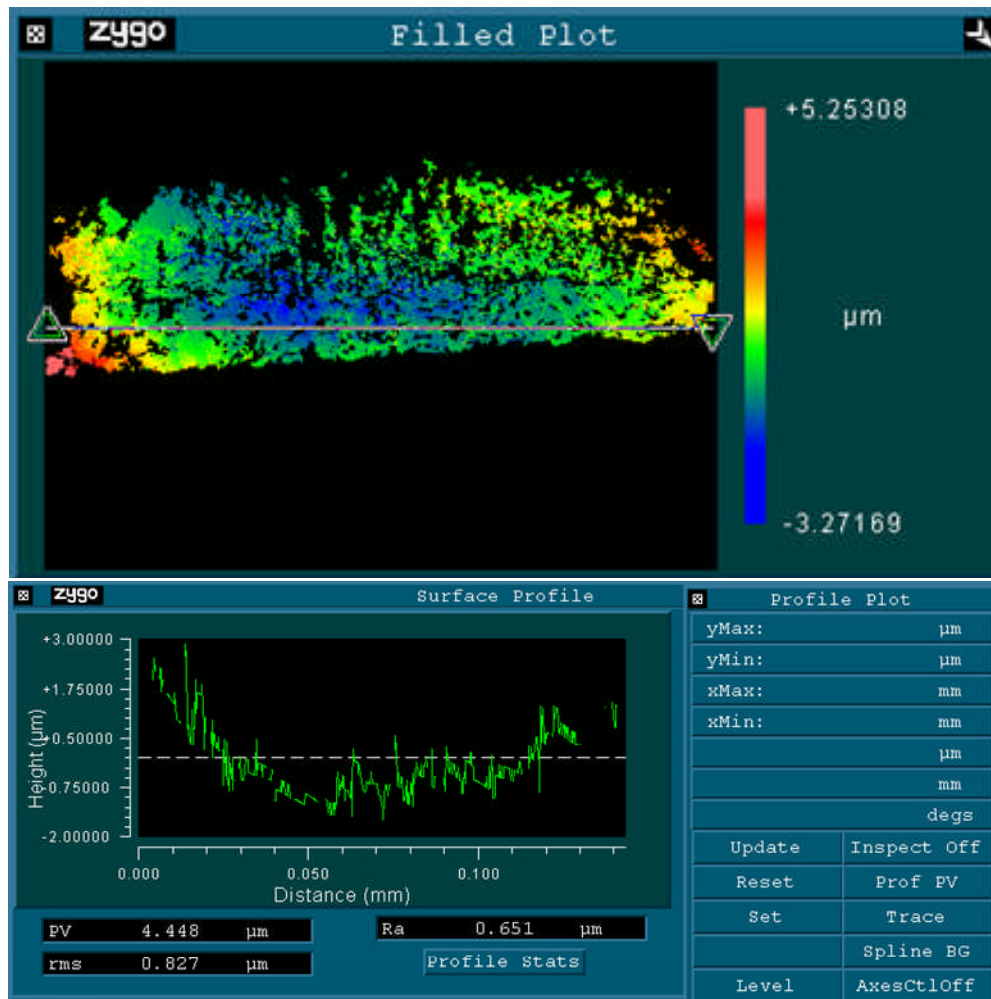
Figure 7-17: Wall roughness measurement of a waveguide fabricated using Excimer at 100 mJ/cm^2, 45 shots, four passes and 25 Hz.
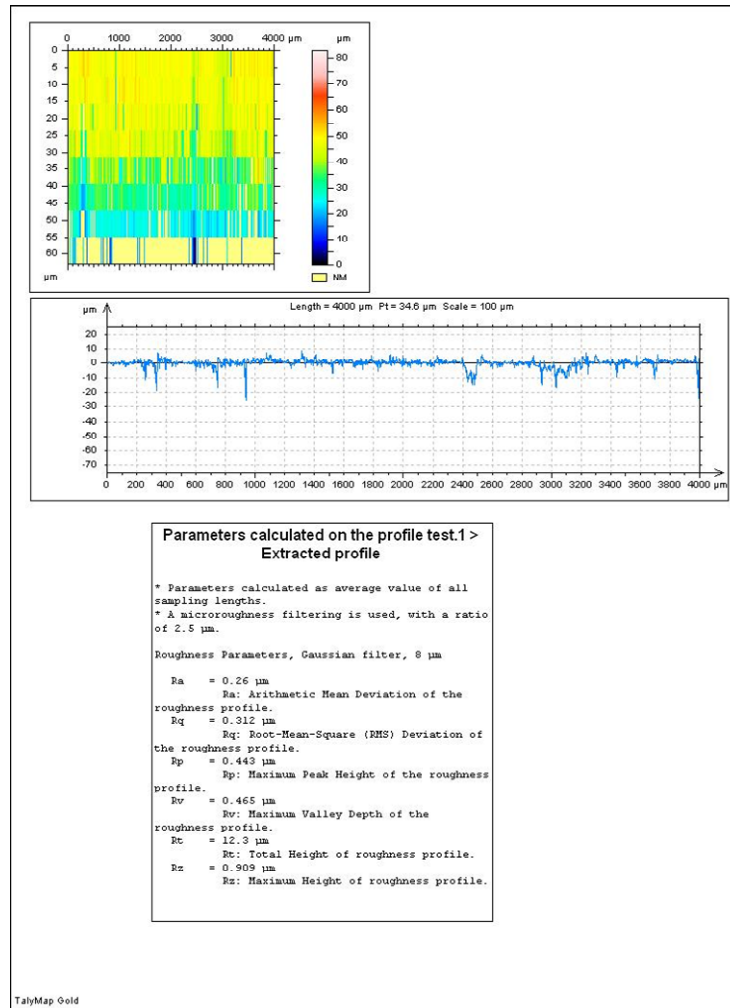
Figure 7-18: Talysurf CLI wall roughness measurement of a waveguide fabricated using Excimer at 100 mJ/cm^2, 45 shots per point, two passes and 25 Hz.
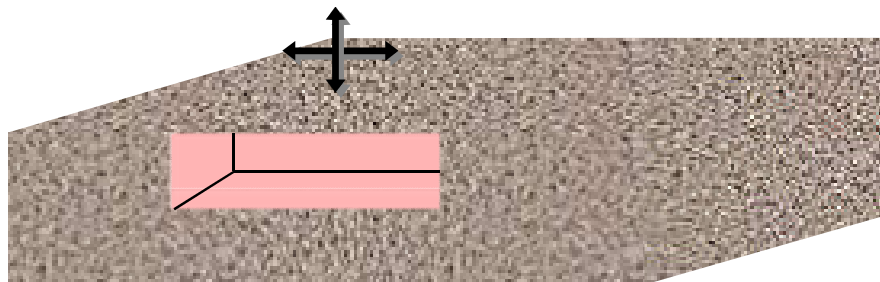
Figure 7-19: Schematic diagram showing the scanning process of the wall surface of ablated trenches machined in Truemode™ optical polymer in order to assess its roughness.
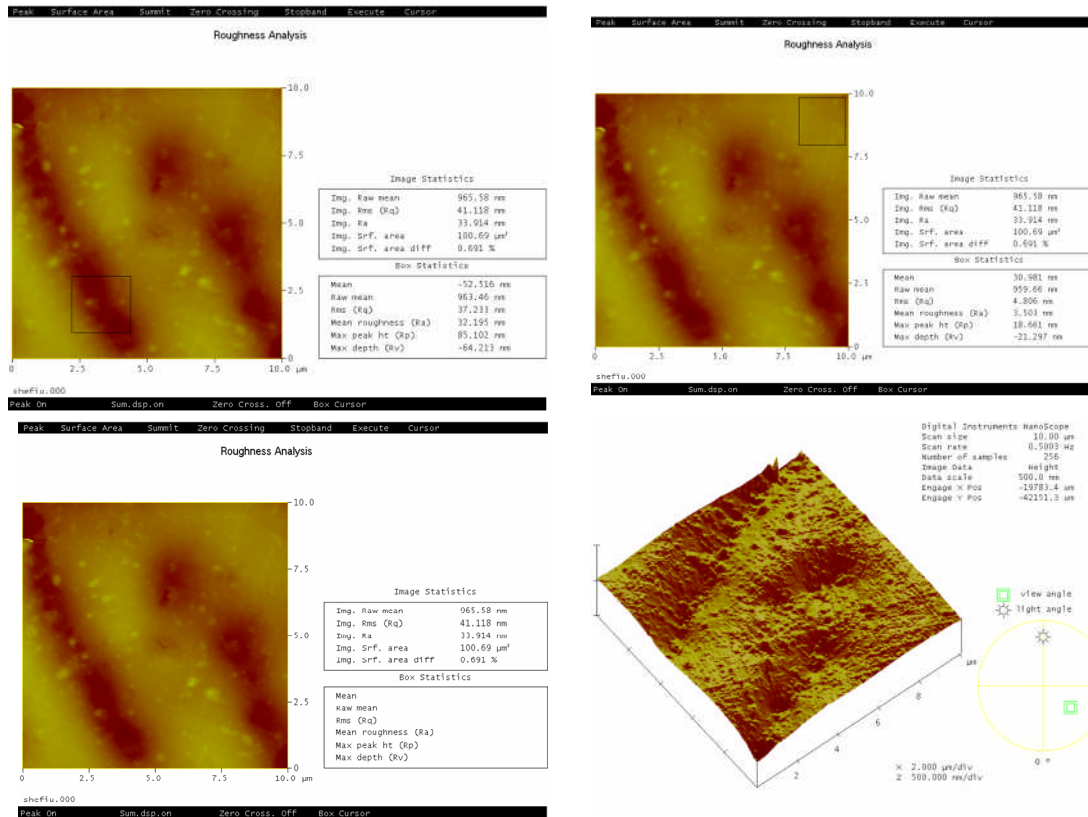
Figure 7-20: AFM roughness measurement of the bottom of a trench fabricated using Excimer at 100 mJ/cm^2, 45 shots per point, two passes and 25 Hz.

To conclude on this study (i.e. wall roughness assessment), FEGSEM images of the bottom and the wall of a waveguide machined at 100 mJ/cm^2, 50 shots, 30 Hz and one pass were examined as shown in figure 7.21. It is evident from these images that the roughness (wall and bottom) of the waveguide is of good quality agreeing with previous measurements; however, a quantitative analysis would be desirable so that the process can be optimised in line with this.
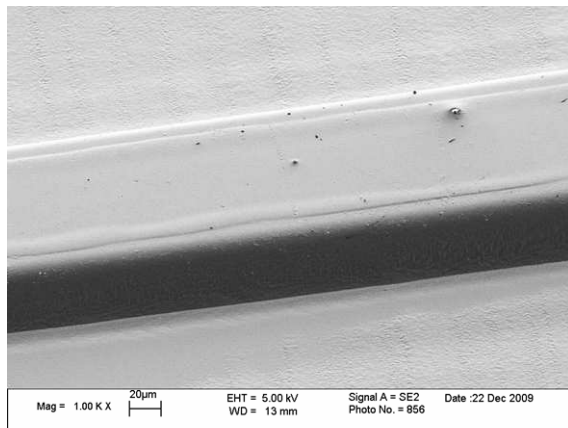
(a)
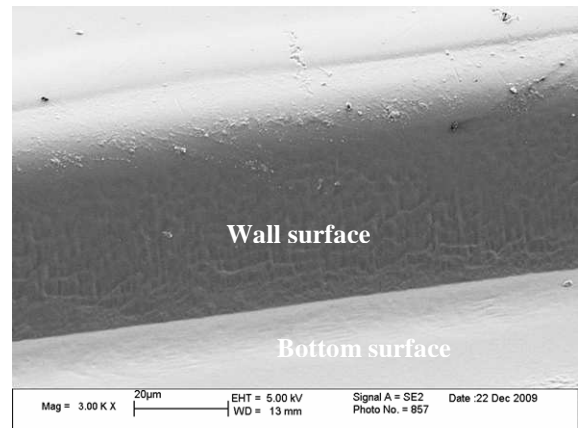
(b)
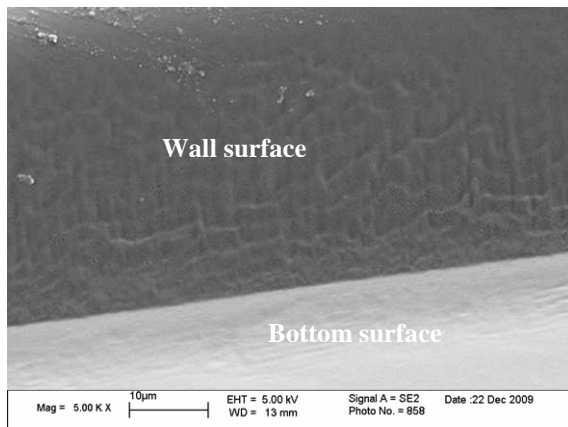
(c)
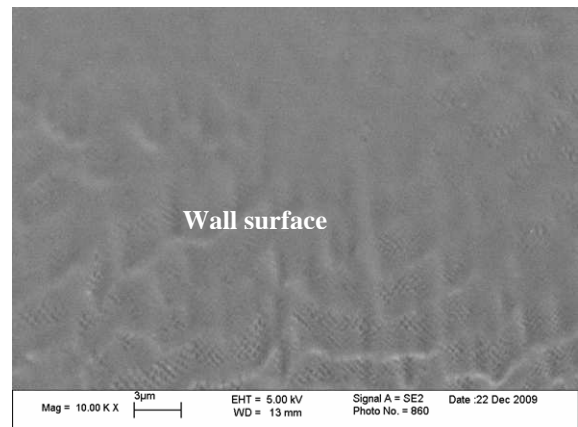
(d)
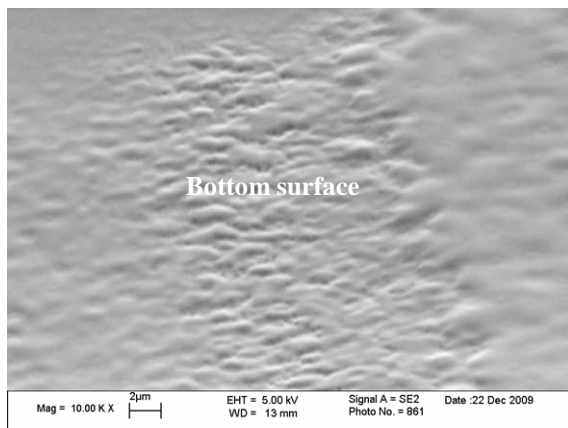
(e)
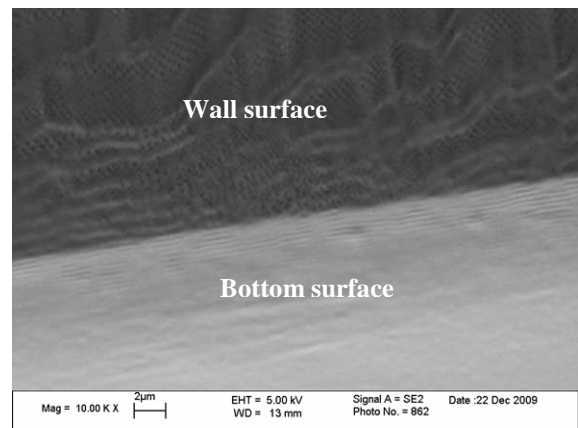
(f)

Figure 7-21: FEGSEM images of a sample machined at 30 Hz, 50 shots and 3.6 mm/min and 100 mJ/cm^2 to visually investigate the waveguide quality showing (a) single waveguide (b) wall and bottom surfaces (c) wall and bottom surfaces (d) wall surface (e) bottom surface, and (f) wall and bottom surfaces .

7.7   Discussion

Reports have shown different values for the waveguide propagation loss depending mainly on the materials and the fabrication process used; Lim, et al [1] put the values in the range of 0.05 – 0.6 dB/cm. The author of [2] compiled a table of optical waveguide polymers, their manufacturers, fabrication techniques and optical losses at three wavelengths, namely 840 nm, 1,300 nm and 1, 550 nm. At a datacom wavelength of 840 nm, the loss is in the range of 0.01 dB/cm – 0.8 dB/cm, however at telecom wavelengths the upper limit was much higher, for instance at 1,550 nm, the loss varied between 0.07 dB/cm – 1.7 dB/cm. Equally important is the compilation made by Eldada in [3], the author covered more processes and polymer candidates than those available in [2]. The losses reported in the former table varied between as low as < 0.01 dB/cm at 840 nm for a single mode waveguide in a halogenated acrylate polymer to as high as 5.0 dB/cm at 1,300 nm telecom wavelength. Propagation loss of 0.24 dB/cm was recorded for a single mode waveguide in Polyetherimide at 830 nm using laser ablation; for the same laser ablation of a single mode waveguide in an acrylate polymer though at 1550 nm, the propagation loss of 0.8 dB/cm was quoted.

Furthermore, researchers at IMEC-TFCG of Ghent University, Belgium, have repeatedly reported laser ablation of optical polymer waveguides in ORMOCER and Truemode™ polymers using an Excimer laser at 248 nm wavelength [4 -6]. In [4] for example, Excimer laser ablation of multimode waveguide in Truemode™ polymer was demonstrated but no information was given on the loss achieved. An average propagation loss of 0.13 dB/cm at 850 nm was given in [5] for a multimode waveguide patterned in an acrylate polymer using 248 nm Excimer laser, however, it is not clear if this was a Truemode™ acrylate polymer. In the same article, 355 nm UV Nd:YAG was said to have been trialled but it was limited by dimension such that waveguide structures of 50 x 50 μm^2 could not be achieved, however, it was argued in [5] that UV Nd:YAG laser offered an excellent surface quality for small structured waveguide and thus has a potential for single mode waveguide fabrication. In addition, no literature report is available for the CO_2 laser ablation of optical waveguide in Truemode™ polymer. Therefore, it can be understood that at the point of writing this thesis, there are no available quoted values (of propagation loss) for laser ablation of multimode waveguide in Truemode™ polymer using either 355 nm UV:YAG or 10.6 μm CO_2 lasers.

The estimated propagation losses obtained in this study for multimode waveguides in Truemode™ acrylate polymer are 1.3 dB/cm, 1.4 dB/cm and 3.9 dB/cm for CO_2, UV Nd:YAG and Excimer lasers respectively. For both CO_2 and Nd:YAG lasers, this is quite acceptable considering the range quoted in the literature coupled with the fact that there was no precedent for the two lasers upon which a benchmark could be set. However, the loss with the Excimer laser was much higher than expected despite the fact it is presumed to be the one providing the highest quality of ablation among the three lasers used. Table 7.2 summarises waveguide fabrication using CO_2, UV Nd:YAG and Excimer lasers. Since the three systems operate at different wavelengths, different process, i.e. photochemical / photothermal, and with many other differences, it is thus difficult to make a thorough comparison between them in terms of their suitability for this technology. However, what is paramount here is to demonstrate the possibility of employing these laser candidates for the optical waveguide fabrication thus facilitating its deployment into the targeted industry and markets. Having said this, there are three fundamental deductions or conclusions from the fabrication point of view that can be made from the three systems, they are:

1. Excimer is considered to be the most capable of the three in patterning structures especially in photopolymers with the finest ablation quality due to the dominance of a photochemical behaviour. It is therefore logical to conclude that the highest loss obtained using this class of laser compared to the two others does not in any way negate the general assumption of the Excimer rather it points to the fact that the loss measurement exercise and good fabrication practice, i.e. in a clean room, should be the objectives of further research.

2. CO_2 laser has the highest processing speed which can, in turn, mean that it is relatively the cheapest of the three; this is followed by UV Nd:YAG while Excimer is the slowest and most expensive of the three, both in maintenance and production-wise.

3. Although, for Excimer and CO_2 lasers, three to five adjacent waveguides were fabricated at each parameter setting in order to average the losses obtained. This approach is still not satisfactory in revealing any contaminant that can result in high insertion loss; it is therefore recommended that the cut-method approach should be the primary objective of any further measurement exercise if comparison is to be precisely made among the laser candidates.

Table 7-2: Key properties of the three systems used in the
fabrication of optical waveguides.

Property	CO_2	UV Nd:YAG	Excimer
Wavelength	10.6 µm (IR)	355 nm (UV). Other wavelengths available	248 nm (UV). Other wavelengths available
Beam–polymer interaction	Photothermal	Photothermal-photochemical	Photochemical
Processing speed	Very high (e.g. ~100 mm/s)	Moderately high (~10 mm/s)	Low (~3 mm/min)
Mask projection	No	No	Yes
Power measurement	Not possible / difficult at the workpiece for the setup used	Not possible / difficult at the workpiece for the setup used	Energy measured at the workpiece and fluence calculated.
PCB process	Widely used	Widely used	Used for complex and sensitive applications
Mode of operation	CW common but pulsed also available	CW common in IR wavelengths but pulsed Q-switched are common in UV harmonics	Mostly in pulsed mode
Roughness	Not measured but relatively smooth (microscope/SME images)	Not measured but relatively smooth (microscope/SME images)	Very smooth: 260 nm Ra (Wall surface) and 30 nm Ra (Bottom surface)
Total insertion loss (dB)	10.7 (for 50 mm long waveguide)	10.2 (for 40 mm long waveguide)	22 (for 45 mm long waveguide)
Estimated Propagation Loss (dB/cm)	1.3	1.4	3.9

7.8   Summary and Conclusion

Laser ablation of optical polymer waveguides carried out using three different separate

lasers, namely, 248 nm Excimer, 355 nm UV Nd:YAG and 10.6 µm CO_2, was presented

in this chapter. Laser ablation was chosen, among the potential candidate techniques,

because of its current usage in the drilling of microvias on PCB and equally because of its capability. The choice of 355 nm UV Nd:YAG and 10.6 µm CO_2 lasers was primarily based on their processing and relative cost effectiveness when compared to an Excimer laser, thus facilitating the deployment of OI.

For each of the lasers, a series of single-layer waveguides were made by varying key parameters, i.e. fluence, power, pulse repetition frequency and speed. Fabricated waveguides were then examined for continuity using Flash™200 optical device; this was achieved by passing white light through one end of the guide for possible detection at the other end. The loss measurement of the waveguides was carried out at UCL using a 850 nm MM VCSEL which was coupled to a 10 m 50/125 step index multimode fibre for light launching; a 70 µm circular pin hole PD was used for light detection at the exit of the waveguide. Cut-method was not employed here; hence the total insertion loss was presented and propagation estimated using a coupling loss ~4.5 dB obtained from other waveguide measurements carried out during the OPCB project.

For CO_2 laser, the effect of input power (3 and 5 Watt) and scanning speed (70 to 100 mm/s) – corresponding to SPD values between 30 mJ/mm and 50 mJ/mm – on optical propagation loss were considered; in each case the length of the fabricated waveguides was 50 mm with five adjacent waveguides. Plots of the varied quantities against the insertion loss did not indicate a strong relationship between them; the least insertion loss of 10.7 dB however was achieved at 100 mm/s and 4 Watt, which gave an estimated propagation loss of 1.3 dB/cm. Similar study was undertaken on UV Nd:YAG at varying power and frequency from 0.11 Watt to 0.13 Watt and 8 kHz to 12 kHz respectively at fixed values of 5 mm/s and 1 scan. It was observed that, for an increase in PRF from 8 kHz to 12 kHz, and decrease in input power between 0.11 – 0.13 Watt, there appears to be a slight decrease in the insertion loss for values considered in this study. A minimum insertion loss of 10.2 dB, corresponding to a propagation loss of 1.4 dB/cm, was obtained for 40 mm waveguide.

The effect of varying the speed/frequency, fluence, waveguide width and optical density on the insertion loss was considered on Excimer laser for 45 mm long five adjacent waveguides. No direct pattern or deduction could be drawn from the graphs of relationship between these parameters and the measured insertion loss. The minimum insertion loss obtained was about 22 dB at 45 shots, 25 Hz pulse reprate, 3.3 mm/min and

100 mJ/cm^2 corresponding to the propagation loss of 3.9 dB/cm at this setting. Due to this unexpected high loss, waveguide quality assessment was carried out. The results of this exercise indicate Ra values of 260 nm (wall roughness) and 30 nm (surface roughness) for a waveguide sample machined at 100 mJ/cm^2, 45 shots per point, two passes and 25 Hz. These Ra values are indication of the good quality of the fabricated waveguides. It was however surprising, despite this quality, to note that the loss values from the Excimer laser samples were higher than even those from both UV Nd:YAG and IR CO_2 – a condition that was unexpected based on the machining qualities of these instruments; therefore, this suggests that there are more areas to investigate to fully understand the loss characteristics and its causes.

Although the insertion losses obtained here are relatively high considering the optical power budget, however, optical power amplification might be necessary for a realistic OI on PCBs. Nevertheless, the ability to successfully demonstrate that such process can be accomplished on both UV Nd:YAG and CO_2 is a key to a low-cost production route since both lasers are currently used for high volume PCB production while loss improvement should be considered in the future.

Debris and contaminants are an area for greater control in the future. The solution to this is by working, for example, in a clean environment. By and large, the investigations conducted (presented in this chapter) have demonstrated the potential of many more laser candidates that can be used for the fabrication of optical waveguides thus broadening the tools available and strengthening its deployment. It follows from this research that, for example, femtosecond Ti-Sapphire, which is expected to produce a cleaner ablation than nanosecond Excimer due to its shorter pulse duration, is a potential candidate.

Reference

1. Teck, G. L. *et al*. Demonstration of direct coupled optical/electrical circuit board. *IEEE Transactions on Advanced Packaging* 32, 509-16 (2009).

2. Holden, H. T. The developing technologies of integrated optical waveguides in printed circuits. *Circuit World* 29, 42-50 (2003).

3. Eldada, L. Polymer integrated optics: Promise vs. practicality. *Proc SPIE Int Soc Opt Eng* 4642, 11-22 (2002).

4. Hendrickx, N. *et al*. Laser ablation as enabling technology for the structuring of optical multilayer structures. *Journal of Physics: Conference Series* 59, 118-21 (2007).

5. Van Steenberge, G ; Hendrickx, N ; Geerinck, P ; Bosman, E ; Van Put, S ; VAN DAELE, P; Development of a technology for fabricating low cost parallel optical interconnects. *Proceedings of SPIE Photonics Europe Conference* 2006 - 2006 - (Vol. 6185) p. 618507-1-618507-8

6. Van Steenberge, G. *et al*. MT-compatible laser-ablated interconnections for optical printed circuit boards. *J. Lightwave Technol.* 22, 2083-90 (2004).

8   INTEGRATED MIRROR FABRICATION

8.1   Introduction

Optical signals on PCBs need to be routed to different parts of a device, such as between the boards of a backplane, if OI is to be fully utilised. Various proposals have been made on how to direct signals out of the plane of the board in a 3D fashion; they include 45-degree ended optical connection rods, microlens, 90°-bent fibre connectors, 45^{0}-ended blocks, 45°-ended I-shape waveguides, optical coupler and microprism. These aforementioned concepts of out-of-plane coupling use blade cutting, laser ablation, dicing or RIE with each having its pros and cons. [1 – 6]. To improve the coupling efficiency, Lee, et al [7] proposed a curved micro-mirror instead of the flat 45-degree commonly utilised.

Even though the 3D out-of-plane coupling scheme is gaining momentum, there is no doubt that in-plane routing of optical signals is needed. A typical system architecture would require routing of signals not only from one layer to the other, i.e. 3D coupling, but also within a layer 2D coupling; the latter would be extremely important if optical interconnect is extended to the board (and even chip) level as the various roadmaps have laid down this possibility. This is the drive that is 'fuelling' the research into this technique.

This chapter is dedicated to the novel fabrication of in-plane mirrors that would allow the redirection of optical signals within the plane of the board. The laser ablation approach was chosen to fabricate the 2D mirror in line with a technique presented by Lim, et al [1] and Misselbrook [3] for 3D out-of-plane coupling. In addition, since 2D in-plane coupling would mostly be useful at the board level where OI deployment is expected to reach in the next decade as argued by Savage in [8] for chip-to-chip communication, the introduction of any additional micro-optical component at this level of integration could face serious challenges including alignment problems.

8.2   2D Mirror Formation for in-plane Coupling

Figure 8.1 is a schematic diagram of the 2D in-plane mirror fabrication, as conceptualised by the author of this thesis, which can be used to couple light between multiple numbers of chips or other components in the same layer. With this design, an effective turning angle of zero, 90-degree and multiples of 90-degrees are possible. For this fabrication, laser ablation

was chosen because, in addition to what has been previously mentioned, it also allows for both the waveguide and the mirrors to be fabricated using a single process on the same system, i.e. Excimer laser.
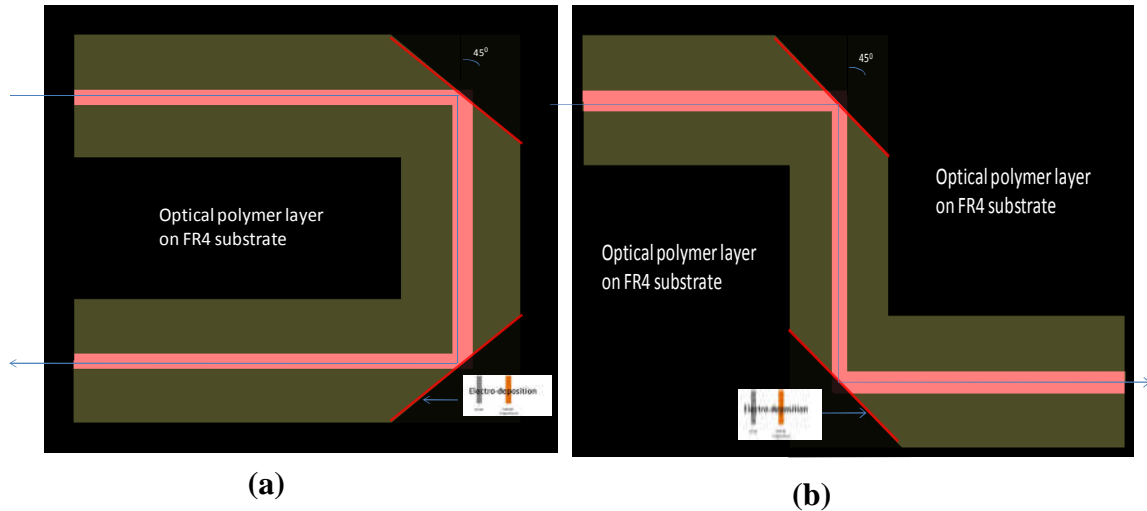
<div style="text-align:center">(a)   (b)</div>

Figure 8-1: Proposed 2D in-plane scheme showing (a) 45-degree in-plane coupling mirror design with 180-degree effective turning angle, and (b) 45-degree in-plane coupling mirror design with zero-degree effective turning angle.

Since the ablated mirror was to be coated and this coating would be made by electro-deposition as discussed in the next section, the samples used for this experiment consisted of a copper pad or layer on the FR4 substrate obtained from Stevenage Circuits Limited. This was followed by the deposition of the optical layer, i.e. lower cladding and core, as per the procedure discussed in section 3.4.

Based on the laser system setup used for the fabrication of the waveguide and the mirrors reported here, the process involved a number of stages carried out sequentially as depicted in the schematic diagram of figure 8.2. For simplicity, the stages can be grouped into two phases / steps.
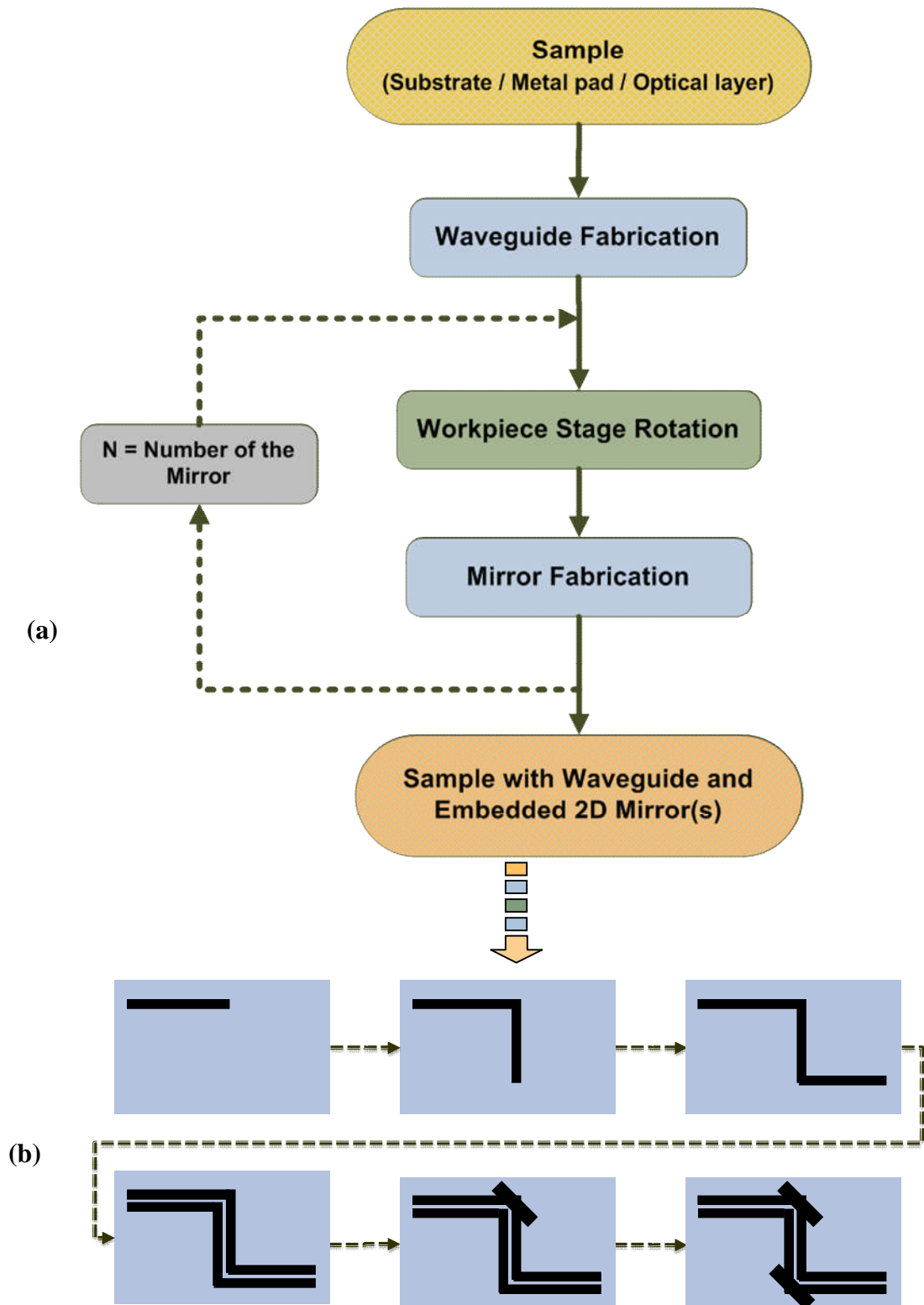
Figure 8-2: Schematic diagram showing the stages involved in the 2D in-plane coupling mirror fabrication: (a)process flow diagram; and (b) plan view of the sample showing the laser ablation path.

1. Phase One

In the first phase, the waveguide structures were fabricated in such a way that the copper layer was not exposed; in other words, the ablation was done through the core into the lower cladding layer and not beyond. This phase is similar in every respect to the waveguide fabrication discussed in chapter seven, however, unlike the case of the straight waveguides previously discussed, the waveguides here consisted of multiple straight tracks which were joined together to form a single structure. For example, for the zero turning angle scheme (figure 8.1b), the waveguide consisted of three straight tracks or channels; the first and the last tracks were parallel to each other while the second channel was perpendicular to them. To ablate this structure, the workpiece stage was moved in such a way that positioned the three channels sequentially; that is to say, the x-axis was moved while the y-axis was stationary to create the first track at the desired length, then the x-axis was maintained stationary while the y-axis was moved along the pattern to join the second arm of the waveguide with the first; finally, the y-axis became stationary while the x-axis was moved to complete the first part/structure of the waveguide. Once this was accomplished, the second part of the waveguide was machined in the same way as for the first part.

As with the straight waveguides, the second structure was created such that a space, dimensionally equal to the required waveguide, was left between the two structures. Moreover, since the waveguide was made up of vertical and horizontal lines joined together, the 'offset' – space left between the two channels that sandwich a waveguide – was required in both directions in this design. Figure 8.3 is an optical microscope image indicating the accomplishment of the first phase of this process; in this image, a waveguide with zero-effective turning angle was fabricated as shown. Integrated mirror fabrication was carried out in the next stage of the manufacturing process.
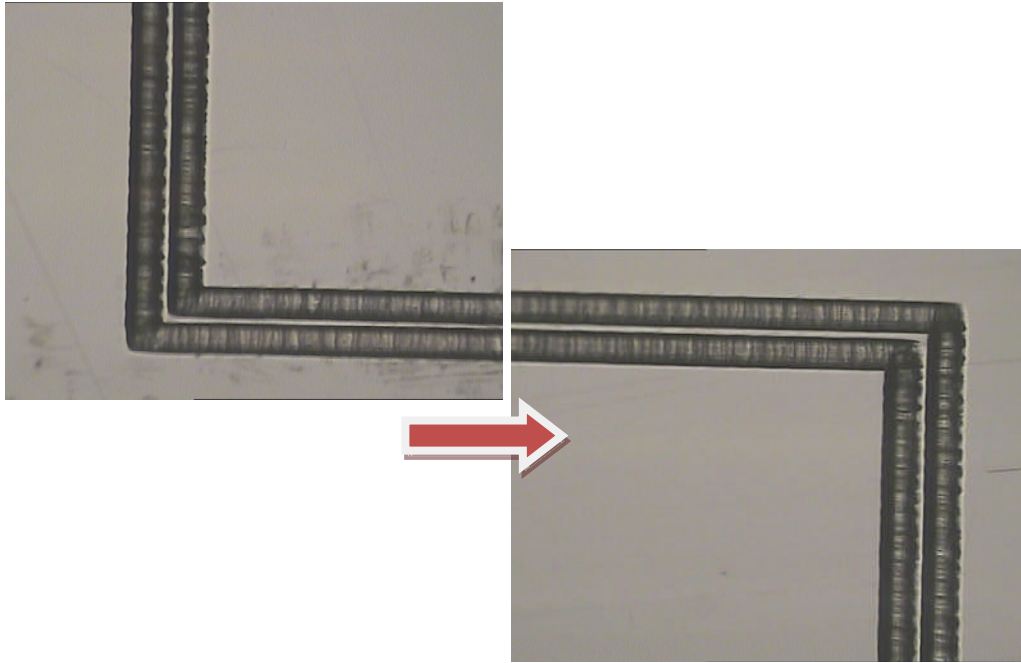
Figure 8-3: Image of the first stage of a 2D in-plane mirror fabrication process showing the initial waveguide formation.

2. Phase Two

The second phase involved ablating the mirror structures on the waveguide created in phase one (figure 8.3). To ablate the mirror in this phase, the workpiece stage was rotated by 45-degree either clock-wise or anticlockwise depending on the mirror required to be micromachined. The corners where the mirrors are required were first located by moving the sample under the imaging lens and viewing it using the CCD monitor incorporated with the system. Once the mirror point was located, a straight line, tangential to this corner, was ablated using appropriate parameters such that the copper layer would be exposed; this was typically done by passing the laser beam over the track a number of times. The sample was then viewed, using the CCD monitor, to examine the ablated structure and then the laser was passed over the track again if required. This exercise required that the x-y position used was recorded such that the ablation could be continuously done on the same line when needed.

Alignment was problematic with this process due to the system setup, which required that many trials were conducted in order to appropriately place the mirror at the corners of the waveguides. Figure 8.4 is an example of an issue that occurred if the offset was wrongly

calculated/estimated probably during the process of adding the coordinates; as could be seen, this possible error marred all the work carried out in phase one. An easier procedure would have been to make a mask with patterns containing both the waveguide and the mirror such that it would be projected onto this sample but this would not be cost effective and would be time consuming from the research point of view but certainly it is a suitable method for large scale production. Alternatively, an aperture/mask with square or rectangular features could be made so that some are parallel to the direction of beam travel while others inclined at 45-degree angle – an approach considered by the author. The former could be used for the waveguide while the latter is used for the mirror; this eliminates the problem of having to turn the stage and the hurdles of calculating the coordinates.
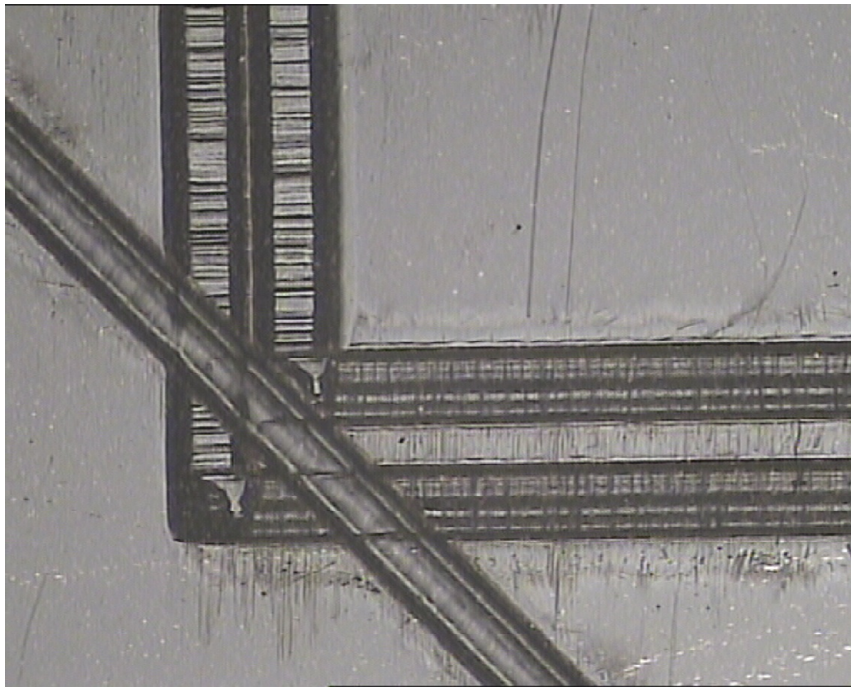
Figure 8-4: Images showing mirror overlapping the fabricated waveguide due to error in offset estimation.

Since the mask design proposed could not be incorporated and the offset calculation inevitable, thus, apart from the great care required during the offset determination and calculation, a further step was taken by the author to avoid waveguide-mirror overlap. This additional move was to ablate a first track a little far away from the estimated coordinate of the mirror point at a very low fluence. The sample would then be brought under the CCD monitor for viewing; if the point was as desired then the overlapped tracks were then

ablated until the required coordinate was reached. Figure 8.5 shows such a concept where the 45-degree in-plane mirror was made by overlapping three tracks. Having said this, great care, though time consuming and inefficient, was the best practice taking into consideration the limitation of the system setup.
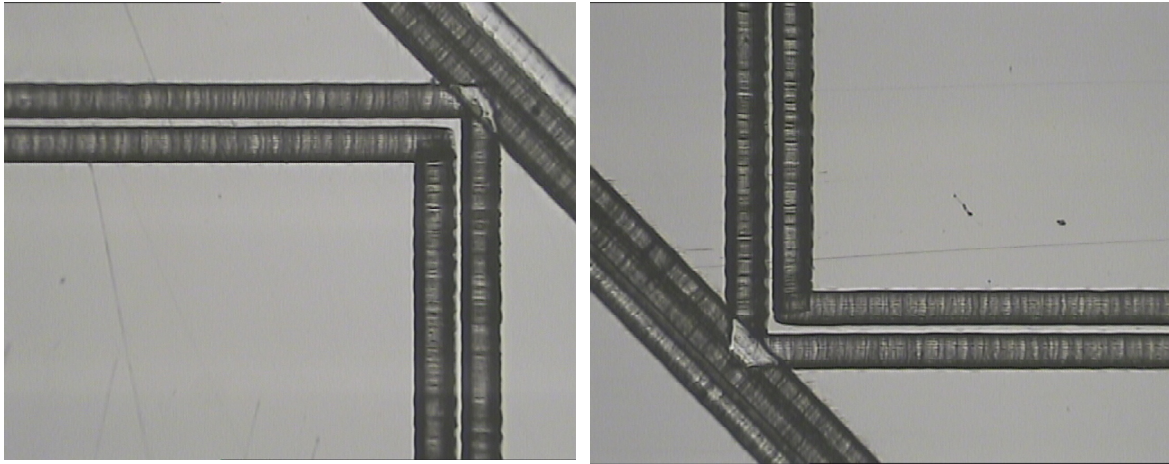
Figure 8-5: Optical microscope images showing waveguides and zero-degree effective turning angle scheme of a 45-degree in-plane coupling mirror fabricated using Excimer laser machined at 25 Hz, 45 shots per point and ~100 mJ/cm^2.

Figure 8.6 shows a waveguide with embedded mirror where a single short track was employed with the mirror structure having a dimension of ~ 0.2 mm x 1.5 mm. This meant that the ablated feature required to be filled was much smaller compared to when overlapped and longer tracks were used. The obvious advantage in this smaller dimension is its relative cost effectiveness since less material (copper or nickel) would be required and the deposition time would be greatly reduced. The waveguide was fabricated at ~ 100 mJ/cm^2, 20 Hz, 40 shots per point, 3 mm/min and at a single pass; the mirror was however carried out at the same parameter setting but the number of passes was ten instead of only once used for the waveguide.
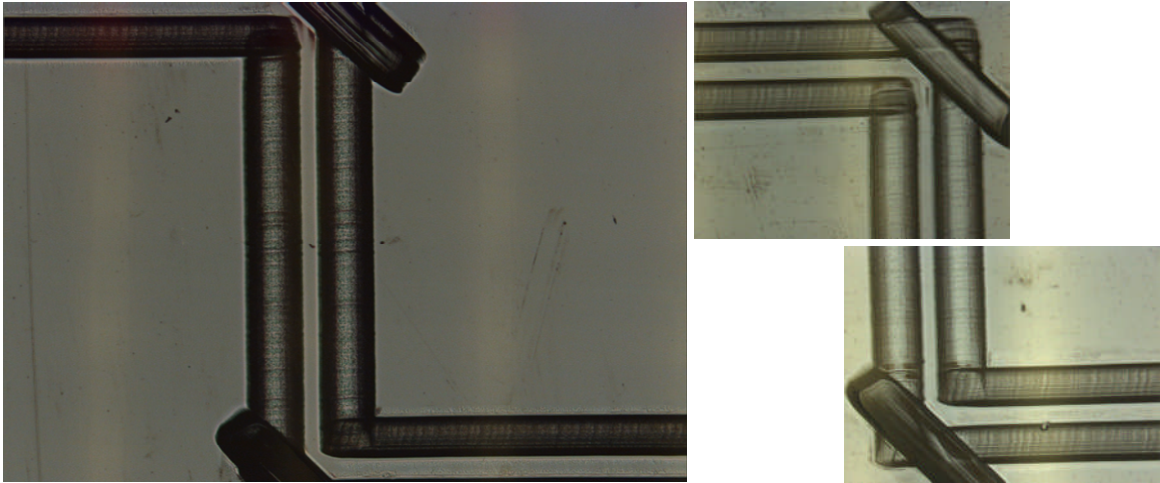
Figure 8-6: Images showing waveguides and zero-degree effective turning angle scheme of a 45-degree in-plane coupling mirror fabricated using Excimer laser. The waveguide was fabricated at ~ 100 mJ/cm^2, 20 Hz, 40 shots per point, 3 mm/min and at a single pass; the mirror was however carried out at the same setting but the number of passes was ten instead of a single pass as used for the waveguide.

8.3   Metal deposition

For 3D out-of-plane mirrors, different methods of metallisation have been used as shown in figure 8.7, which can also be applied to the 2D systems used here. Coupling light in and out of the waveguides could be achieved by relying on the air/vacuum RI which is capable of causing TIR (figure 8.7a) at this interface as used in [1], but this can be difficult in a real application because (i) a vacuum is not guaranteed in a typical electronic assembly, (ii) components are not immune from contamination, e.g. grease or moisture, which could alter the RI, (iii) air content and temperature is a subject of the environmental condition, and (iv) air RI is guaranteed to be constant. These aforementioned constrains, could have effect on the coupling efficiency.
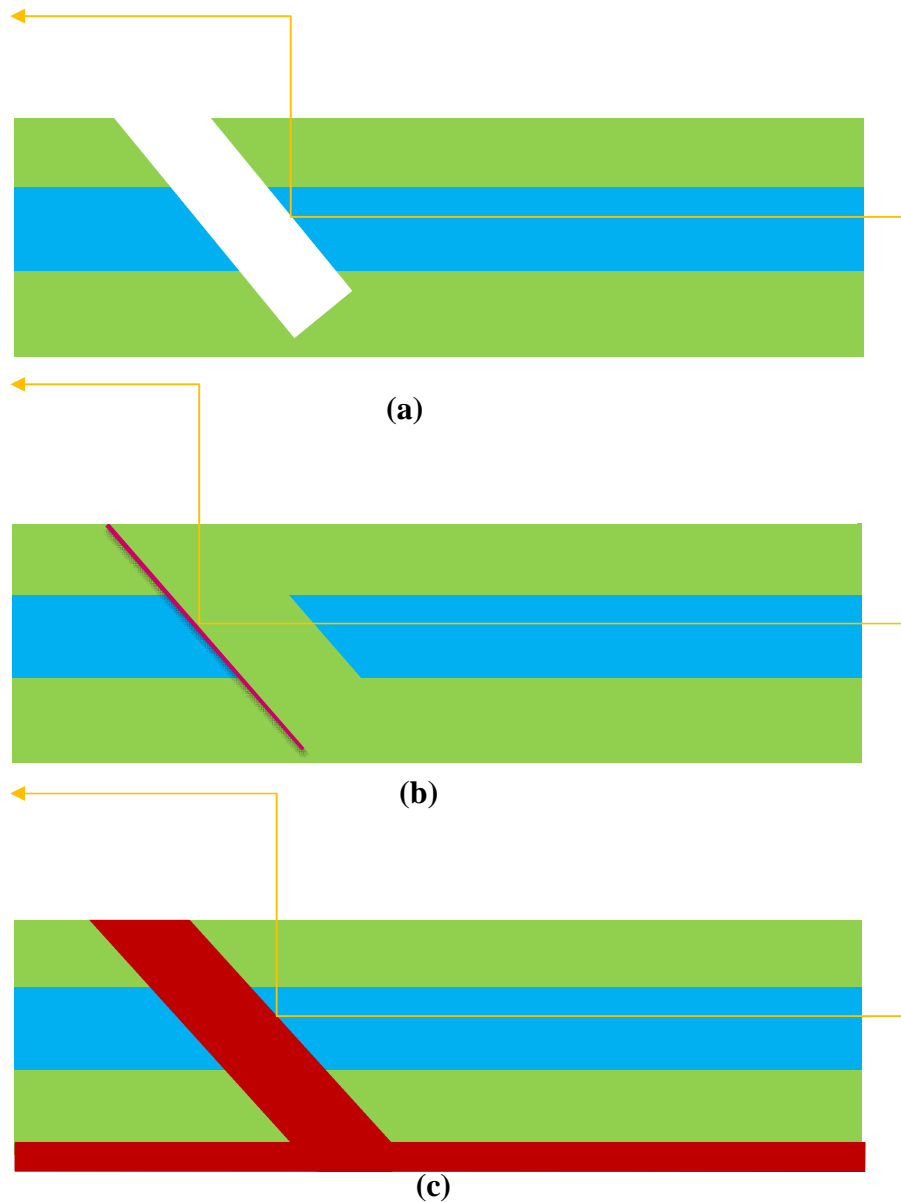
Figure 8-7: 3D mirror fabrication schemes (a) TIR is used
to deflect incoming signal out of the waveguide at the
waveguide-air interface (b) light is coupled from a metal
deposited at the surface of the mirror trench which is then
filled with cladding material after metallisation, and (c) 3D
coupling of incoming signal achieved by filling the ablated
trench with a metal using electrodeposition.

For these reasons, end facets of mirrors are coated with metal to improve the reflectivity
and for a good surface finish (figures 8.7b and 8.78c). This type of deposition technique
depends largely on the sample to be coated and adhesion among other things, for example,
Glebov, A. L. et al [7] used sputtering to deposit a thin layer of gold (Au) on the surface of
the mirror before filling the trench with upper cladding; a similar process was used for a
laser ablated mirror [2]. Misselbrook, P.J. [3] backfilled the trench of a laser ablated mirror

used to terminate a photolithographically-made waveguide using electrodeposition; in this case a copper pad was considered.

In this research, two different types of metal depositions were considered both were similar to figure 8.7c, with electrodeposition and electroless plating used. The filling of the ablated trench was the objective rather than the surface coating of the mirror. Filling of the trench is considered more suitable than surface coating because the processes involved in achieving the latter such as sputtering and chemical vapour deposition (CVD) can also coat the adjacent waveguides which have no upper cladding.

8.3.1   Electroplating

Electroplating is a well-known technique of coating conducting surfaces with metals. The process setup utilises an anode and cathode submerged in an electrolytic solution containing the ions of the metal to be deposited. The waveguide sample containing the mirror which is to be plated was made into the cathode by exposing a small part of the metal layer at the edge of the part which was then clipped to the negative terminal of a DC electric power supply, while the anode was connected to the positive terminal. During this process, the copper anions from the anode are dissolved into the electrolyte (an acidic solution containing copper(II) sulphate ($CuSO_4$)) solution to replenish the metal ions that are attracted to the cathode - in this case the mirror – in order to coat its copper pad thus building up the thickness of the trench. Current density and time of plating determines the thickness of coating but other factors such as air bubbles in the trench and chemical reaction can also affect the rate of deposition thus, an optimum parameter needs to be determined for each process.

Figure 8.8 shows an optical microscope image of an electrodeposited copper feature in the ablated mirror carried out during the trial which took about 2 hours. No delamination occurred between the optical layer and the substrate (copper on FR4). Initially, the 45-degree trench to be used for 2D mirror was made big about 0.3 mm x 3 mm to avoid air bubble entrapment, it was thereafter decided that the mirror be made much smaller.

Figure 8-8: An image of a 45-degree 2D in-plane mirror
filled with copper using electroplating.

8.3.2   Electroless plating

Electroless plating is a type of electrochemical but does not require an electric power
supply. The type of metal used in this process forms the basis of its naming; for example, in
electroless copper plating, copper is the metal to be deposited. Here, Nickel was chosen as
the metal because it was easy to monitor the formation of the Nickel deposit on the mirror
visually since a copper pad was used and Nickel has a different colour. One of the benefits
of this process, in addition to its cost effectiveness as argued by Shacham-Diamand, et al in
[9], is that the geometry of the sample to be plated is not an issue.

An initial trial was conducted to investigate the possibility of using this technique and to
determine the plating rate; this was carried out with three different samples:

i.   a sample of FR4 with a layer of copper, and

ii.   a similar sample to (i) above but spun coated with clad and core of
Truemode™ polymer, and

iii. a sample similar to (ii) but with a small hole made from the core to the

copper layer to simulate a mirror. This was made to act like a typical mirror so as to confirm the possibility of selectively coating the actual mirror part, which is the only part exposed to the copper layer. In all cases neither waveguide nor mirror was patterned in it.

With the first sample, after its immersion in the solution for 40 minutes, it was removed and examined. It was noticed that the nickel evenly deposited only on the surface of the copper with no deposit on the FR4 side suggesting that the process can selectively plate on the exposed metal part. With the second sample, after about half an hour, no Nickel metal appeared on the photopolymer (i.e. core layer of Truemode™) of the sample but traces of nickel were also found on the FR4 side around an engraved mark. This trace of deposits on the engraved part can only be explained by assuming that the engraved part exposed the copper layer underneath.

The third sample was left immersed in the solution for about an hour; examination showed an occurrence of plating only on the pierced hole on the side of the Truemode™ polymer and nowhere else. This was easy to detect due to the silvery white or brownish-like colour of the nickel deposit.

Figure 8.9 shows the result of this trial with copper pad being coated with Nickel; the profile obtained across the deposit showed that the Nickel coat was not uniform across the substrate but this was more likely due to the fact that the substrate used was not flat. From this analysis, the maximum thickness of the coating was found to be around 18 microns. This means that the rate of coating is approximately 25 microns/hour; this is within the range quoted in the literature [10].
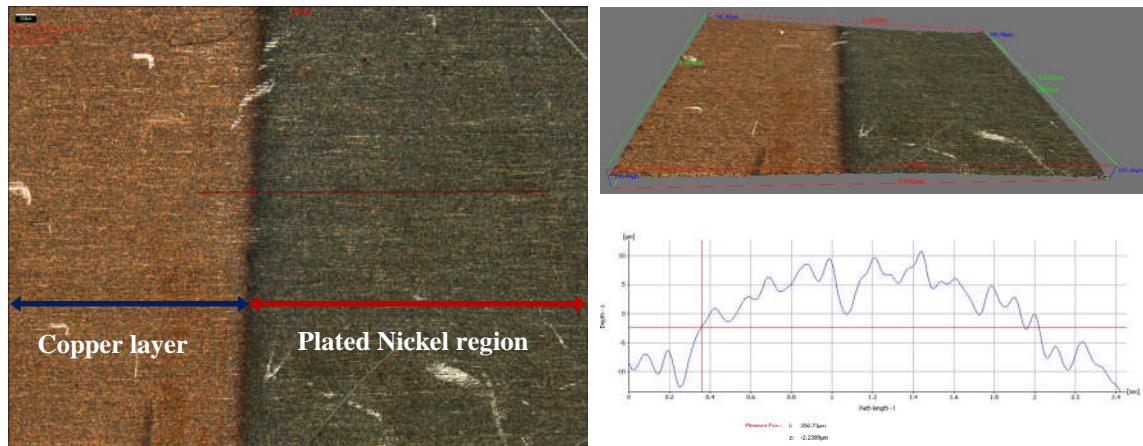
(a)

(b)

Figure 8-9: Figure showing an initial trial to investigate the possibility of coating an embedded in-plane mirror using electroless nickel technique; the trial was made on a FR4-copper layer: (a) plan view showing a region with plated Nickel on copper, and (b) depth profile of the plated Nickel region.

Having successfully tried electroless Nickel plating, samples with waveguide and mirrors were made. The samples were prepared in such a way that a thin layer of upper cladding was used. This scheme was utilised so that plating could be done assuming the minimum estimated plating rate to ensure that (i) the mirror is fully filled, and (ii) any resulting over filling due to using minimum plating would not 'coat' the waveguide. This method, in addition, can minimise possible contamination on the part of the waveguide especially as discussed in chapter two. Although the deposition was successfully achieved by this technique, unfortunately, the adhesion between the optical layer and the copper especially had been weakened and peeled off soon after the process. In the future, adhesion promoter might be needed to circumvent this problem.

8.4 Summary and Conclusion

While attention has been dedicated to out-of-plane coupling of signals, in the chapter, a novel 2D in-plane mirror fabrication was presented which is required for routing signals between components on a plane. This is because such a scheme would be particularly important if OI is extended to board-level. The laser ablation approach was chosen to fabricate the 2D mirror as this has also been used for 3D out-of-plane coupling. In addition, it allows for the definition of waveguides and the mirror to be done using a single process thus benefiting from accuracy, minimum alignment problem and small size since the introduction of new components, such as lens, would not be required. The 45-degree

coupling considered in this work allows an effective turning (or signal re-direction) angle of zero to be achieved using two mirror at 45-degree to the waveguides but, a 90-degree and multiples of 90-degrees are possible with as many mirrors as necessary.

The ablated mirror was coated, by backfilling the ablated mirror trench with a metal, using both electroplating and electroless plating. For this reason, the samples used for this study consisted of a copper pad or layer on the FR4 substrate which was followed by the deposition of the optical layer, i.e. lower cladding and core. A complete structure of waveguides and two 45-degree embedded mirrors was demonstrated with the mirrors having a dimension of ~ 0.2 mm x 1.5 mm; the mirror was fabricated at ~ 100 mJ/cm^2, 20 Hz, 40 shots per point, 3 mm/min and at ten number of passes while the waveguide was carried out at the same parameter setting but at a single pass in lieu of the ten passes used for the mirrors.

The loss due to the mirror was not assessed in this research due to the lossy nature of the waveguides fabricated using Excimer laser, it is therefore recommended that such a measurement be made a priority after the main cause of losses in the waveguides is or are identified and corrected. With this approach, a separate waveguide can be made alongside the waveguide containing the mirror; the former can then be used as a reference for which losses due to the mirror can be obtained. Alternatively, this 2D coupling technique could be applied to prepare mirrors in waveguides made by other methods such as photolithography.

Backfilling of the trench was considered to allow for efficient coupling and thus low loss but there were certain challenges to this process which needs to be considered in any future work. Some of these problems were to do with the sample preparation while others are related to the plating technique, albeit there are some due to both. Apart from the fact that the deposition rate is relatively slow, about 25 µm/hour for the initial trial, it is also precisely defined depending on the wide range of changes in parameters such as the activator used, concentration of activation, activation time and even temperature [10]. In addition, the small size of the mirror can cause bubbles to be trapped in the structure and thus affecting either the plating process to continue and/or the uniformity of the final plated material. This can be overcome by sample preparation and process optimisation.

Reference

1. Teck, G. L. *et al*. Demonstration of direct coupled optical/electrical circuit board. *IEEE Transactions on Advanced Packaging* 32, 509-16 (2009).

2. Van Steenberge, G. *et al*. MT-compatible laser-ablated interconnections for optical printed circuit boards. *J. Lightwave Technol.* 22, 2083-90 (2004).

3. Misselbrook, P. Novel manufacture of Out-of-Plane Optical Interconnects to Enable Low-Cost OECB substrates. *Wolfson School of Mechanical and Manufacturing Engineering, Loughborough University*, PhD Thesis (2006).

4. Cho, M. H. High-coupling-efficiency optical interconnection using a 90-bent fibre array connector in optical printed circuit boards. *IEEE Photonics Technology Letters* 17, 690-692 (2005).

5. Byung, S. R. *et al*. PCB-compatible optical interconnection using 45 deg -ended connection rods and via-holed waveguides. *J. Lightwave Technol.* 22, 2128-34 (2004).

6. M. H. Cho, S. H. Hwang, H. S. Cho, and H.-H. Park, "High-coupling efficiency optical interconnection using a 90 -bent fibre block connector in optical printed circuit boards," *IEEE Photon. Technol. Lett.*, vol. 17, no. 3, pp. 690–692, Mar. 2005.

7. Glebov, A. L., Yokouchi, K., Roman, J. and Lee, M. G. Optical interconnect modules with fully integrated reflector mirrors. *IEEE Photonics Technology Letters* 17, 1540-1542 (2005).

8. Savage, N. Linking with light. *IEEE Spectrum* 39, 32-36 (2002).

9. Y. Shacham-Diamand, S. Lopatin, Electrochim. Acta 44 (1999) 3639.

10. Rohan, J. F., O'Riordan, G. and Boardman, J. Selective electroless nickel deposition on copper as a final barrier/bonding layer material for microelectronics applications. *Appl. Surf. Sci.* 185, 289-4, (2002).

9 CONCLUSION AND FUTURE WORKS

9.1 Summary and Conclusion

In this thesis, laser ablation of optical polymer to fabricate waveguides has been successfully demonstrated; the ablation was carried out using three different lasers, namely, Excimer, UV Nd:YAG and CO_2 lasers, thus providing opportunities for rapid deployment of OI to the PCB manufacture industry. In addition, a novel in-plane coupling mirror fabrication using Excimer laser ablation was demonstrated which was considered to be vital for communication between chips at board-level.

Although there are literature information detailing the effect of certain experimental parameters such as fluence, pulse repetition rate, pulse duration and wavelength among others, in relation to the etch rate of different materials as asserted in the chapters on laser system characterisation, the machining of new materials requires new data to be obtained. In fact various models are available to try to model the laser-matter interaction in a mathematical way, but these cannot be taken universally as they fail to be applicable in many scenarios. For this reason, experimental optimisation appears to be the logical way forward at this stage of the research thus requiring material-system characterisation to be conducted for each case and thus formed an integral achievement of this thesis.

Among the polymers investigated, PMMA seems to be the only candidate that has been mostly considered for laser ablation. This research has therefore, provided information on how another commonly used photopolymer i.e. Truemode™ behaves in relation to the aforementioned factors. This study conducted during laser system characterisation revealed that, while Beer's and SSB's models can be used as a reference in explaining some behaviour, this is not universal thus requiring that a different model (i.e. a mathematical representation based on a regressive analysis) be formed to interpret other relations where these models cannot hold. This study was able to conclude that a photothermal-photochemical phenomenon is more likely to be used to explain the effect of the laser on the polymer during laser ablation, most particularly that of UV Nd:YAG.

The CW CO_2 laser micromachining of the optical polymers was understood to be governed by the SPD calculated using the input power and scanning speed. While polysiloxane-based polymer ablation gave clean structures at SPD values between 12 mJ/mm and 20 mJ/mm,

the laser ablation of Truemode™ polymer was found to better at the range between 15 mJ/mm and 50 mJ/mm. Laser ablation of Truemode™ polymer at 355 nm using Nd:YAG laser was considered to be a photochemical-photothermal process thus favouring Srinivasan-Smrtic-Babu (SSB) explanation; it was found that input power below 0.15 Watt at 5 mm/s – 10 mm/s speed and a frequency of 5 kHz – 10 kHz is an effective operating condition. The depth of ablation was also found to increase linearly proportional to an increase in the number of laser scans; however, a single scan was considered optimum and sufficient to obtain the required depth of ablation during optical waveguide. Ablation threshold of ~ 0.02 J/cm^2 was obtained for Excimer laser ablation of Truemode™ polymer at 248 nm wavelength which agrees with the thresholds reported for polymers. The tapering effect is a major issue in Excimer laser ablation but this was overcome by a careful selection of mask position and experimental parameters with a near-vertical profile obtained at an operating fluence of 200 mJ/cm^2 when a single pulse was used. The etch rates was found to vary with fluence; a value of 0.252 µm/pulse and 2.5 µm/pulse were achieved at 30 mJ/cm^2 and 280 mJ/cm^2 respectively; however, a moderately low fluence above the threshold, typically ~100 mJ/cm^2 mJ/cm, was chosen as optimum operating condition in order to avoid thermal damage.

9.1.1 Optical waveguide fabrication

The fabrication of single-layer optical waveguides has been demonstrated; laser ablation was chosen here first, from its cost effectiveness point of view and secondly, because the equipment is currently being used in the PCB industry. The Excimer laser is costly to maintain on the one hand and the safety concern associated with its use, which requires some strict procedures of operation and handling is a major cause of reluctance to its use in laser ablation of PCB materials in general and of photopolymer in particular. These barriers would not allow the technique to be highly welcome at this stage even though the technology, OI, is unavoidable with the current state of copper bottlenecks. Nevertheless, the use of Excimer at a later stage in this deployment loop or circle would become necessary, if not inevitable, as this would be more suitable for fabrication of more complex structures such as mirrors and may be assisted by the future integration of sensitive and/or biomedical devices into PCBs.

The research reported here has managed to answer the two potential primary concerns of PCB manufacturers by showing the possibility of using the existing lasers, namely UV

Nd:YAG and CO_2 lasers. An estimated propagation loss of 1.3 dB/cm, 1.4 dB/cm and 3.9 dB/cm were obtained for CO_2, Nd:YAG and Excimer laser ablated waveguides respectively; while the loss for Excimer-based waveguides were considered too high for the optical power budget, those for CO_2 and Nd:YAG laser ablated waveguides were highly encouraging considering the fact that they are new. It is hoped that, in the future, the process can be optimised to reduce the losses to < 1 dB/cm.

9.1.2   In-plane mirror fabrication

As previously asserted the typical system architecture would require the routing of signal not only from one layer to the other, i.e. 3D coupling, but also within a layer. Chip-to-chip interconnection is currently under development and that requires in-plane routing of signals for which the integrated mirrors such as the one demonstrated here, where no additional component is required, are a suitable option. A novel 2D in-plane mirror using laser ablation was successfully demonstrated in this research; this utilised a 45-degree fabrication method with zero-degree effective turning angle for coupling the signals. An advantage of the laser ablation technique is that both the waveguide and the mirror can be fabricated at the same time which means less possibility for contamination.

The ablated mirror trenches created were backfilled with metals. Having considered the two forms of electrodeposition, namely electroless and electrolytic plating to fill the mirror trenches, it is fair to say that although the two are suitable for the process, electroless was easier; with electroless plating, there was no need to make an electrical connection to a copper pad thereby simplifying the sample preparation, experimental design and processing. Having said that, this idea is still in its premature stage and more research would dictate the way forward

9.2   Future Work

9.2.1   Loss improvement:

The findings in this research are fundamental inputs that could help in the rapid deployment of the technology to the targeted industry at a relatively affordable cost. It provides, among other things, a means of having a choice of tools in carrying out the tasks such that laser choice can be made in line with complexity and the geometry of the waveguides required. However, to meet the optical power budget, low-loss waveguides – a highly essential

requirement – were not met in this research. Therefore, it is anticipated that further research should be focused on improving the optical loss. The following are some of the areas where efforts should be exerted:

1. Clean room: Working in a clean environment should be the first and foremost benchmark to be set for improving the loss. This is because, as repeatedly mentioned, the Rayleigh loss is mainly as a result of some particles in the path of the signal. These particles could be a product of either the process, such as debris from the ablation or contaminants from the environment or during the post ablation handling of the samples. Loss due to debris formation can be mitigated using optimum parameters or applying one of the approaches already proposed as detailed in chapter two. However, the extrinsic contamination can only be minimised by working in a clean environment. It is also recommended that post-ablation handling and processes, i.e. measurement and analysis, should be set or carried out as quickly as possible so that the potential volume of contamination can be greatly reduced.

2. Curved mirror: Although, loss measurement has not been carried out, it is opined that the use of a curved mirror might increase the efficiency of the coupling. Unlike in the case of 3D out-of-plane coupling mirrors where the coupling is between a VCSEL and a waveguide and from waveguide to a PD, the coupling for in-plane mirror is between a section of a waveguide to another, thus, there is no need for the mirror to be angled out of the plane. However, there could still be multiple reflections at this junction if the incident signal from an arm of the waveguide is not properly coupled into the adjacent perpendicular waveguide arm; and this could be reduced by the use of a curved mirror that has been shown to help with 3D coupling efficiency.

9.2.2   *System comparison (Excimer, UV Nd:YAG and CO_2 lasers)*

PCB manufacturers would be interested to know what the merits and demerits are of each candidate proposed, unfortunately, this could only be subjectively made in the context of this research primarily due to the difference in the system setup. For instance, it is obvious from this research that CO_2 laser processing of optical waveguides is the fastest among the three candidates investigated, but the arising question is that (i) was this high speed achieved at the expense of optical loss, and (ii) is there any relationship between optical loss and scanning speed such that a processing speed on a particular laser, e.g. CO_2, can be used to obtain an

equivalent or same loss on a different laser. Therefore, a study would be essential to answer some of these puzzles and to provide a means of a subjective compare-contrast mechanism.

In addition to the aforementioned recommendations, and in order to be able to make a logical comparison, it is recommended that additional features and/or modification of the existing systems should be made in the following manner:

1. Excimer: A beam homogeniser should be integrated into the system to allow for a more uniform beam intensity at the workpiece; a mask pattern should be designed in such a way that different shapes of mirror for example, can be made without needing to create a complex program for moving the workpiece stage. On a practical level, for more efficient machining and registration of features, a more sophisticated control system would need to be established, with provision for alignment features. This is especially important for mirror fabrication such that a waveguide made, for example, using photolithography can be brought for mirror fabrication using laser ablation. Furthermore, the system could be customised so that two, or even three, lasers can be housed in a single assembly which would be ideal from a production point of view where straight guides could be prepared rapidly with one type of laser, e.g. CO_2, with the mirrors then added by the more accurate Excimer.

2. UV Nd:YAG and CO_2: A low energy YAG and CO_2 laser should be tried since laser ablation of polymers is better at low energy. The system setup to be used should allow that energy /power at the workpiece can be measured using an energy meter; this would make it easier to compare losses against fluence. Since the laser used in this research is mainly designed for processing PCB materials as in the case of the UV Nd:YAG or simple marking and cutting as with CO_2, the beam stability might not be a primary issue of concern in those applications, but this is not the case with optical waveguide fabrication where fine micro features are demanded. Therefore, stability of the system is vital and that should be taken into consideration in any future research. A system configuration such as that of the Flex 5330, where both Gaussian and Top-hat beam profiles are possible, should be used. Even though, waveguides were achieved using both profiles, there are no reports on whether the profile affects the loss, so such system would enable a good comparison.

9.2.3 Roughness assessment

The roughness of the base of ablated channels of the waveguides were visually examined and evaluated using a non-contact measuring technique; this gave a low Ra even below 30 nm, however, the wall roughness of the channels is also required to be known in order to correlate the effect of this on the loss. Obviously, a rougher surface would empirically mean a lossy waveguide but this needs to be established experimentally. Attempts were made to assess the wall roughness of the waveguides made, but this proved unsuccessful despite the consultations made with experts at for instance, the National Physical Laboratory (NPL), UK. The major barrier to this study, i.e. wall roughness measurement, was due to the geometry of the waveguides obtained using this technique; this requires that waveguide samples are made very close to the edge of the substrate so that light from an interferometer can be used – this exercise was tedious and the measurement obtained in this manner was not highly reliable. Therefore, extra effort is expected to be made or spent in this study, preferably by non-contact mechanism, and to correlate the values to the losses in waveguides.

9.2.4 Mirror characterisation

Mirror characterisation is required to be able to ascertain the effectiveness of its coupling capability; further to this, a comparison should be made between air and metal as reflectors. Still more areas where further research should be undertaken are the study of the effects of a curved mirror on achievable optical loss as suggested above. These, indeed, are some of the areas of study that this thesis has created for researchers to investigate.